

# Methodology for the prediction of the strength of naturally aged glass based on surface flaw characterization

Irene Sofokleous





# Methodology for the prediction of the strength of naturally aged glass based on surface flaw characterization

by

Irene Sofokleous

to obtain the degree of Master of Science in Civil Engineering  
at the Delft University of Technology,  
to be defended publicly on Friday September 30, 2022 at 14:00.

Student number: 5265304  
Project duration: November 15, 2021 – September 30, 2022  
Thesis committee: Prof. dr. ir. M. Overend, TU Delft, chair, supervisor  
Ir. E. H. J. ten Brincke, ABT b.v., supervisor  
Dr. ir. F. A. Veer, TU Delft  
Ir. C. Noteboom, TU Delft

An electronic version of this thesis is available at <http://repository.tudelft.nl/>.



# Acknowledgements

This thesis marks the end of my master's degree at TU Delft and I would like express my sincere appreciation to the people and organizations which made that possible.

I would like to express my deep gratitude to the members of my committee, for their valuable input and their encouraging words over the last couple of months. It is a pleasure to thank my chair professor and academic supervisor, Prof. Mauro Overend for his guidance and support through each stage of this project. I am grateful to Dr.ir. Fred Veer, who supervised the experimental part of this research, shared his experience in fracture mechanics and glass and answered with patience my countless questions. Special thanks to Ir. Chris Noteboom, whose inspirational lectures about structural glass at TU Delft motivated me to dive into this field and he supported me with his knowledge and innovative ideas from the first day until the completion of this project. I would also like to acknowledge ABT B.V. for their contribution to my thesis and especially Ir. Erwin ten Brincke, my company supervisor and source of inspiration for finding the topic of my thesis. His enthusiasm, his detailed feedback from the perspective of a professional engineer and his expertise in structural glass were invaluable to me and to this project.

I would also like to express my gratitude to the Structural Design & Building Engineering department of TU Delft for the financial support. I am grateful to Prof. Christian Louter for his kind advice and feedback at crucial moments of my research. I would also like to thank Dr. Kyriaki Corinna Datsiou for generously taking time out of her schedule to share her knowledge and experience with fracture statistics and in general with structural glass.

This thesis would have not been the same without the contribution from Innowep GmbH, who believed in the importance of this research, and they provided me with Traceit<sup>®</sup>. Special thanks to Julian Schary and Bastian Göbel for the great hosting at Innowep in Germany, and for the training on the use of Traceit<sup>®</sup>.

I would like to thank Scheldebouw B.V. for providing me with the weathered glass for the experiments and Hermans Groep for the processing and the transportation of the glass specimens. I would also like to thank Versteeg Zichtbaar in Glas, for providing me with the specimens of new glass for the experiments. I am grateful to the staff of the Faculty of Architecture, and especially to Hans and Bos, for their practical support during the experimental part of the research. I would also like to thank Kendeas for his kind help during the transportation of the glass specimens and the experiments.

On a personal note, I am grateful to my dear parents Andreas and Kalli for their endless trust and love, to my brother Sofoklis who always kept me motivated and confident and to my sister Stalo, for being the most supportive sister. Last but definitely not least, I am forever thankful to my friends in Cyprus who believe in me and they are always by my side.

*Irene Sofokleous  
Delft, September 2022*



# Abstract

Flat glass is a material which is used extensively in almost all the buildings, mainly as infill for windows or facade panels. However, neither glass production nor its recycling are sustainable processes, as both incorporate the use of gas furnaces, which produce high amounts of CO<sub>2</sub> emissions. Thus, the reuse of glass seems the only way to minimize the environmental impact of this material.

The greatest challenge in the safe reuse of glass elements lies in the assessment of their strength after several years of use. This strength is reduced, compared to the inert strength, due to the damage ("defects") that the environment inevitably introduces into the glass surface. According to the Linear Elastic Fracture Mechanics (LEFM), one of the defects in a stressed brittle material, which in this case is glass, will initiate the failure. Therefore, in order to assess the residual strength of weathered glass, it is essential to quantify it in terms of defects. The aim of this thesis is to develop the understanding on the performance of weathered glass, and to propose a methodology for the prediction of its residual strength, based on its surface defects.

The examined material is a 55-year-old annealed glass, which was used as facade elements in a building in the Hague, in the Netherlands. The X-Ray Fluorescence analysis showed that the composition of this glass meets the common float glass recipe but no tin residues were found on its surface.

This research firstly, focuses on the detection and characterization of the defects on the examined weathered glass. Both sides of glass were examined through non-destructive tests with the mobile optical profilometer Traceit® and the digital microscope Keyence VHX 7000. These tests revealed that the weathering induced mainly dense pits, digs and fine linear scratches on the surface exposed to the outside environment (external surface). The depth of these defects, as measured with Traceit®, ranged from 19 μm to 161 μm, which is aligned with the depths reported in literature, which range from 20 μm to 200 μm (Schula et al., 2013). The internal surface had occasionally some large defects which were probably man-made defects. Overall, Traceit® showed a potential for detecting and measuring the defects on weathered glass, whereas with the used microscope it was not possible to measure the defects nor to scan larger surfaces.

Subsequently, 90 specimens of weathered glass were subjected to Coaxial Double Ring tests, with either the external or the internal surface in tension, to assess the effect of weathering on strength. The specimens were of two different dimensions and they were loaded with two different rings to investigate the "size effect". In addition, 81 similar specimens of new glass were tested, with either the tin or the air side in tension, and they were used as a reference. These tests showed that the strength of the 55-year-old glass ranged from 22,9 MPa to 138,2 MPa, whereas that of new glass ranged from 38,3 MPa to 219,2 MPa. In particular, the average strength of the internal surface of the small weathered specimens was 53% higher than the external, but no major difference was observed in the tests of the large specimens. Furthermore, the average failure stress of the air side of new glass was approximately 45% higher than that of the tin side, while in literature that difference was characterised as marginal. Finally, although the size effect was clearly observed in the tests on new glass and in those on the internal surface of weathered glass, the strength of the external surface was found independent of the size of the loaded area. This implies that the defects on this surface are similar and uniformly distributed, so the probability of encountering a critical flaw is equal regardless the size of the loaded area.

Fracture statistics were used to derive the design strength of the glass of each testing series. Among three probability distributions, the Weibull distribution was found to describe the strength data of glass better. However, for low probabilities of failure, the data did not fit well to the Weibull distribution and thus, the resulted design strength values are probably very conservative.

The information collected during the non-destructive tests, namely the size and the shape of the defects found on the surface of weathered glass, was used for the identification of the critical defect which will

initiate failure. At this step, the assumption that the largest defect will be the critical one was made. Then, the theory of LEFM was used to relate the size of the found critical defect to the failure stress, through the critical stress intensity factor  $K_{IC}$  and the geometry factor  $Y$ . The predicted values for the failure stresses were analysed with fracture statistics and compared to the actual failure stresses of weathered glass, as emerged from the Coaxial Double Ring tests. In this way, the accuracy of the predictions was evaluated.

The effectiveness of the methodology for the detection of the critical flaw was evaluated through post-fracture analysis. This analysis showed that the critical defect was successfully detected in the 23% of the examined specimens. This suggests that the visually largest defect on a glass element could be the critical one. Furthermore, even if most of the specimens did not failed at the measured defect, the average predicted failure stress differ by less than 9% from the average actual failure stress. This outcome suggests that the defects induced by weathering on the glass surface are similar. Thus, a defect which was identified as critical for one specimen but eventually it was not, it was probably very similar to the critical defect of another specimen.

To conclude, this thesis examines and proposes a novel methodology for the prediction of the glass strength, based on LEFM, applied to defects found on the surface of naturally aged glass. If the defects on the glass surface are studied according to this methodology, a good estimation of the average failure stress can be obtained. For lower probabilities of failure the methodology gives conservative estimations, so it has a potential for use in design applications. Overall, the defects on the surface of glass, and especially their size and geometry, appear to have the greatest effect on the strength of weathered glass so far. Further experimental investigation on the parameters which affect the strength of weathered glass should be carried out, as well as further research on the automation of the proposed methodology, which is expected to increase its effectiveness and efficiency.

# Contents

<b>Acknowledgements</b>	<b>iii</b>
<b>Abstract</b>	<b>v</b>
<b>Contents</b>	<b>vii</b>
<b>List of Tables</b>	<b>ix</b>
<b>List of Figures</b>	<b>xi</b>
<b>Nomenclature</b>	<b>xv</b>
<b>1 Introduction</b>	<b>1</b>
1.1 Motivation . . . . .	1
1.2 Problem statement . . . . .	2
<b>2 Research design</b>	<b>3</b>
2.1 Main objectives . . . . .	3
2.2 Research question . . . . .	3
2.3 Methodology . . . . .	3
2.4 Limitations . . . . .	4
2.5 Research outline . . . . .	4
<b>3 Theoretical background</b>	<b>5</b>
3.1 Introduction . . . . .	5
3.2 Strength of glass . . . . .	5
3.2.1 Characteristic strength . . . . .	5
3.2.2 Actual strength . . . . .	6
3.3 Defect Characterization . . . . .	6
3.4 Fracture mechanics . . . . .	8
3.4.1 Stress Intensity Factor . . . . .	8
3.4.2 Static fatigue . . . . .	8
3.5 Experimental methods for determining the strength of glass . . . . .	10
3.5.1 Destructive tests on glass . . . . .	10
3.5.2 Tests on large glass panels . . . . .	11
3.6 Fracture statistics . . . . .	11
3.6.1 Probability distribution functions . . . . .	12
3.6.2 Weibull probability distribution function . . . . .	12
3.6.3 Prediction of glass strength . . . . .	15
3.7 Non-Destructive Tests . . . . .	16
3.7.1 Equipment used in research . . . . .	17
3.7.2 Selection of equipment . . . . .	20
3.8 Conclusions . . . . .	22
<b>4 Experimental investigation</b>	<b>25</b>
4.1 Introduction . . . . .	25
4.2 Test specimens . . . . .	25
4.3 Test methods . . . . .	29
4.3.1 Microscopy examination before the CDR tests . . . . .	29
4.3.2 Coaxial Double Ring tests . . . . .	30
4.3.3 Microscopy examination after the CDR tests . . . . .	33
4.4 Test results . . . . .	35
4.4.1 Results of Keyence digital microscope VHX7000 . . . . .	35

4.4.2	Results of Traceit® . . . . .	36
4.4.3	Flaw characterization . . . . .	40
4.4.4	Results of the CDR tests . . . . .	44
4.4.5	Results of the microscopy examination after the CDR tests . . . . .	49
4.5	Correlation of flaw size and failure stress . . . . .	51
4.6	Discussion . . . . .	53
<b>5</b>	<b>Failure analysis</b>	<b>55</b>
5.1	Introduction . . . . .	55
5.2	Fractographic analysis . . . . .	55
5.3	Statistical processing of the results . . . . .	57
5.3.1	Weibull parameter estimation . . . . .	59
5.3.2	Normal and Lognormal probability distributions . . . . .	61
5.3.3	Goodness of fit of the three probability distribution functions . . . . .	61
5.4	The tin-air side effect . . . . .	63
5.5	The effect of weathering . . . . .	64
5.6	The size effect . . . . .	65
5.6.1	The Weibull theory for the size effect . . . . .	70
5.6.2	Design and characteristic strength of glass . . . . .	70
5.7	Discussion . . . . .	73
<b>6</b>	<b>Prediction of glass strength</b>	<b>77</b>
6.1	Introduction . . . . .	77
6.2	Methodology . . . . .	77
6.2.1	Assumptions for the development of the methodology . . . . .	78
6.2.2	Examined specimens . . . . .	78
6.3	Stress intensity factor formula . . . . .	79
6.4	Evaluation of the methodology . . . . .	81
6.4.1	Non-destructive detection of the critical flaw . . . . .	81
6.4.2	Prediction of failure stress . . . . .	82
6.4.3	Predicted design and characteristic strength . . . . .	86
6.4.4	Reverse prediction process . . . . .	86
6.5	Discussion . . . . .	88
<b>7</b>	<b>Conclusions</b>	<b>91</b>
7.1	Introduction . . . . .	91
7.2	Conclusions . . . . .	91
7.2.1	Conclusions . . . . .	91
7.2.2	Findings . . . . .	92
7.3	Future work . . . . .	94
7.3.1	Recommendations for practice . . . . .	94
7.3.2	Recommendations for further research . . . . .	95
	<b>References</b>	<b>97</b>
<b>A</b>	<b>Chemical analysis</b>	<b>101</b>
<b>B</b>	<b>Specimens dimensions</b>	<b>103</b>
<b>C</b>	<b>Traceit reliability study</b>	<b>109</b>
<b>D</b>	<b>Results of the CDR tests</b>	<b>111</b>
<b>E</b>	<b>Normal and Lognormal probability plots</b>	<b>117</b>
<b>F</b>	<b>Strength data of new glass (without FEA correction)</b>	<b>121</b>
<b>G</b>	<b>Design strength according to ASTM</b>	<b>125</b>
<b>H</b>	<b>Error in the predictions</b>	<b>127</b>

# List of Tables

3.1	Overview of the design methods for the calculation of the design strength of glass . . . .	15
3.2	Overview of the equipment used in research for defect detection in glass. . . . .	18
3.3	Matrix for scanning equipment selection based on multiple criteria. . . . .	21
4.1	Overview of the specimens number and dimensions of each testing series. . . . .	28
4.2	Verification of specimen and ring dimensions according to ASTM C1499-09 (2013). . . .	39
4.3	Depth of the critical defects on each specimen, as measured with Traceit®. . . . .	40
4.4	Summary of the CDR test results on weathered glass. . . . .	45
4.5	Average failure stresses of specimens scored from the same panel. . . . .	45
4.6	Summary of the CDR test results on new glass. . . . .	47
5.1	Number of valid and invalid tests based on the location of the fracture origin. . . . .	56
5.2	Comparison of computational and manual Weibull parameter estimation methods for weathered glass. . . . .	60
5.3	Comparison of computational and manual Weibull parameter estimation methods for new glass. . . . .	61
6.1	Evaluation of critical flaw detection method. . . . .	81
6.2	Average actual and predicted failure stresses for $K_{IC}=0,75 MPa m^{0,5}$ and $Y = 1,12$ or $0,713$ . . . . .	86
6.3	Comparison of the flaw depths as measured with Traceit® and as calculated based on the actual failure stresses. . . . .	88
A.1	Chemical composition of the examined new and weathered (old) glass (wt%). . . . .	102
B.1	Dimensions of the specimens of series NA-1a (Weathered glass). . . . .	104
B.2	Dimensions of the specimens of series NA-1b (Weathered glass). . . . .	104
B.3	Dimensions of the specimens of series NA-2a (Weathered glass). . . . .	105
B.4	Dimensions of the specimens of series NA-2b (Weathered glass). . . . .	105
B.5	Dimensions of the specimens of series AR-1a (As received glass). . . . .	106
B.6	Dimensions of the specimens of series AR-1b (As received glass). . . . .	106
B.7	Dimensions of the specimens of series AR-2a (As received glass). . . . .	107
B.8	Dimensions of the specimens of series AR-2b (As received glass). . . . .	107
D.1	Results of the CDR tests for the series NA-1a (250x250x10mm, external surface). . . .	112
D.2	Results of the CDR tests for the series NA-1b (250x250x10mm, internal surface). . . .	112
D.3	Results of the CDR tests for the series NA-2a (450x450x10mm, internal surface). . . .	113
D.4	Results of the CDR tests for the series NA-2b (450x450x10mm, external surface). . . .	113
D.5	Results of the CDR tests for the series AR-1a (250x250x10mm, tin side). . . . .	114
D.6	Results of the CDR tests for the series AR-1b (250x250x10mm, air side). . . . .	114
D.7	Results of the CDR tests for the series AR-2a (450x450x10mm, tin side). . . . .	115
D.8	Results of the CDR tests for the series AR-2b (450x450x10mm, air side). . . . .	115
H.1	Error between predicted and actual failure stress for each specimen for series NA-1a (250x250x10mm, external), for $K_{IC}=0,75 MPa m^{0,5}$ and $Y=1,12$ . . . . .	128
H.2	Error between predicted and actual failure stress for each specimen for series NA-2b (450x450x10mm, external), for $K_{IC}=0,75 MPa m^{0,5}$ and $Y=1,12$ . . . . .	129
H.3	Error between predicted and actual failure stress for each specimen for series NA-1a (250x250x10mm, external), for $K_{IC}=0,75 MPa m^{0,5}$ and $Y=1,12$ or $Y=0,713$ . . . . .	130

H.4 Error between predicted and actual failure stress for each specimen for series NA-2b (450x450x10mm, external), for $K_{IC}=0,75 \text{ MPa } m^{0,5}$ and $Y=1,12$ or $Y=0,713$ . . . . .	131
---	-----

# List of Figures

1.1	The linear process of the current use of glass . . . . .	1
1.2	The new circular process of use and reuse of glass . . . . .	2
1.3	The initial idea-concept of this thesis project (sketch by Erwin ten Brincke). . . . .	2
3.1	Images of several types of defects in glass. . . . .	7
3.2	Three failure modes, mode I (opening mode), mode II (sliding mode) and mode III (tearing mode) (LINDQVIST, 2013). . . . .	8
3.3	Inert strength of a single crack as a function of its depth by Haldimann, 2006. . . . .	9
3.4	Section View and Perspective View of Basic Fixturing and Test Specimen for Equibiaxial Testing (ASTMC1499-09, 2013). . . . .	10
3.5	Front view of dynamic glass testing rig showing the 2.35m diameter piston behind the opening where the glass will be installed (Dalglish and Taylor, 1990). . . . .	11
3.6	Front view with tempered glass panel in place (All the wires are from the strain gages). (Johar, 1981). . . . .	11
3.7	Goodness of fit for all data series fitted to a Weibull, a Normal and a Lognormal distribution (Datsiou and Overend, 2018). . . . .	12
3.8	Relative strength of annealed glass with variation in surface area (dotted lines represent weathered glass) from Overend et al. (2007). . . . .	14
3.9	Design strength as a function of the loaded area, according to the European and Dutch standards, for a four-sided supported plate under wind load with duration 5 seconds (For annealed float glass with as cut edges). . . . .	16
3.10	Configuration of retroreflective scanner for simultaneous detection of body glass defects and coating defects (Holmes, 1997). . . . .	17
3.11	Optical microscope image of the external surface of weathered glass (Zammit and Overend, 2010). . . . .	19
3.12	3D surface map of the external surface of weathered glass (Zammit and Overend, 2010). . . . .	19
3.13	The influence of the viewpoint on visual detectability: inwards view, high viewpoint (top); inwards view, low viewpoint (bottom) (Haldimann, 2006). . . . .	20
3.14	Digital Microscope Keyence VHX7000 (Faculty of Architecture, TU Delft) . . . . .	21
3.15	The monitor of the digital microscope Keyence VHX700 . . . . .	21
3.16	Traceit® mobile 3D profilometer (Innowep GmbH, n.d.). . . . .	22
3.17	Working principle: measuring head with three white lights (Innowep GmbH, n.d.). . . . .	22
4.1	Location of the building from which the examined glass was removed. . . . .	26
4.2	The office building at Koningskade 4, the Hauge. . . . .	26
4.3	Detail of the facade of the examined building at Koningskade 4, provided by Scheldebouw B.V. . . . .	27
4.4	Cutting process of the large specimens at Hermans factory. . . . .	28
4.5	Image of the glass specimen cleaned with alcohol (left part) and uncleaned (right part), as captured with Keyence VHX7000. . . . .	30
4.6	Experimental setup with Traceit® . . . . .	31
4.7	Screenshot of the main interface of Traceit® software. . . . .	31
4.8	Process of measuring the depth and the width of flaws with Traceit®. . . . .	32
4.9	Sketches of the CDR testing setup. . . . .	34
4.10	Materials testing machine Zwick Z100 at the Faculty of 3ME, TU Delft. . . . .	35
4.11	Experimental setup for the CDR tests on the large specimens. . . . .	35
4.12	Experimental setup for the CDR tests on the small specimens. . . . .	36
4.13	Small specimen after fracture in a CDR setup. . . . .	36
4.14	Micrograph of the 50-year-old tested glass, taken with the Keyence VHX7000. . . . .	37

4.15	Microscopic images of the two sides of one specimen at a magnification of 200x. . . . .	37
4.16	Example of an image taken with the default top lighting option of Traceit® . . . . .	38
4.17	Example of an image taken with the transmitted lighting option of Traceit® . . . . .	38
4.18	The "visual impression" image after the edit in Paint.Net. . . . .	38
4.19	The "visual impression" image after histogram equalization. . . . .	38
4.20	Traceit® positions during the reliability study. . . . .	41
4.21	The three examined defects on the same specimen, as captured by Traceit®. The green line indicates the location of the measurement along the defects. . . . .	41
4.22	Micrograph of 20-year-old weathered float glass. (Overend and Zammit, 2012). . . . .	42
4.23	Images of several types of defects as captured with Traceit®, after processing. The images show an area of 5mm by 5mm of the glass specimens. . . . .	43
4.24	Force-Displacement curves of the tested specimens . . . . .	44
4.25	Finite element model of the small specimens in Abaqus SIMULIA (2022). . . . .	46
4.26	Finite element model of the large specimens in Abaqus SIMULIA (2022). . . . .	47
4.27	Maximum principal tensile stresses according to ASTM C1499-09 (2013) ("Analytical") and to the FEA models for the non-linear calculation. . . . .	48
4.28	Microscopic images of the fracture pattern of specimen 1.2 (NA-1a). . . . .	49
4.29	Microscopic images of the probably critical flaw of specimen 1.2 at magnification x200. . . . .	50
4.30	Microscopic images of the probably critical flaw of specimen 1.1 at magnification x200. . . . .	50
4.31	Microscopic images of "beach marks", below the surface of glass . . . . .	50
4.32	Half-penny crack (Overend et al., 2007). . . . .	51
4.33	Critical defect of the specimen of series NA-1a which failed at the lower stress ( $\sigma_f=37,1$ MPa). . . . .	52
4.34	Critical defect of the specimen of series NA-1a which failed at the highest stress ( $\sigma_f=88,9$ MPa). . . . .	52
5.1	Examples of specimens which broke inside, just below and outside the loading ring. . . . .	56
5.2	Examples of specimens which broke outside the loading ring - invalid tests. . . . .	56
5.3	Fracture patterns of specimens . . . . .	57
5.4	Specimen with not detectable fracture origin ( $F_{break}=36960N$ ). . . . .	58
5.5	Specimens with probably more than one fracture origins ( $F_{break}=27080N$ and $30047N$ , respectively). . . . .	58
5.6	Normalised strength data of weathered glass fitted to the Weibull probability distribution function. . . . .	62
5.7	Normalised strength data of as received glass fitted to the Weibull probability distribution function. . . . .	62
5.8	Goodness of fit of the test data to the three probability distributions, compared to the chosen level of significance $\alpha=0,05$ . . . . .	64
5.9	Micrographs of the air and tin sides of new glass at magnification x200. . . . .	65
5.10	The effect of tin side on the strength of the specimens of new, as received glass. . . . .	66
5.11	Comparison of the strength of weathered and new, as received glass. . . . .	67
5.12	The size effect on the strength of the new glass specimens. . . . .	68
5.13	The size effect on the strength of the weathered glass specimens. . . . .	69
5.14	Weibull plots for the actual and the estimated strength of the larger specimens of weathered glass, for several $\lambda$ . . . . .	71
5.15	Weibull plots for the actual and the estimated strength of the larger specimens of new glass, for several $\lambda$ . . . . .	72
5.16	Loaded area in the CDR test. . . . .	73
5.17	Theoretical design strength and design strength according to EN1990:2002 (2005) of the tested specimens (for $P_f=0,0012$ and load duration 5 seconds). . . . .	74
5.18	Theoretical and experimental characteristic strength of the tested specimens (for $P_f=0,05$ ). . . . .	74
6.1	Specimens with the deepest defects marked on their surface. . . . .	79
6.2	The calculated dependencies of the bending strength of glass plates subject to the depth of semi-elliptical surface micro-crack in a fracture focus (Rodichev and Veer, 2010). . . . .	80
6.3	Flaw characteristics (Haldimann, 2006). . . . .	80

6.4	Specimens which broke at the detected "critical flaw". . . . .	82
6.5	Failure stress of a surface crack as a function of stress duration by Overend and Zammit (2012). . . . .	83
6.6	Weibull plots of the actual and predicted failure stresses for the specimens tested with the external surface in tension, for $K_{IC} = 0,75 \text{ MPa } m^{0,5}$ and $Y=1,12$ . . . . .	84
6.7	Weibull plots of the actual and predicted failure stresses for the specimens tested with the external surface, in tension for $K_{IC} 0,75 \text{ MPa } m^{0,5}$ and $Y=1,12$ or $Y=0,713$ . . . . .	85
6.8	Weibull plots of the average actual and predicted failure stresses tested with the external surface in tension. . . . .	87
6.9	Goodness of fit of the predicted failure stresses to the three probability distribution functions. . . . .	88
6.10	Actual and predicted design strength (for $P_f=0,0012$ and load duration 5 seconds) of the series NA-1a, along with the design strength according to the Dutch and the European standards. . . . .	88
6.11	Results of previous application of Traceit <sup>®</sup> for the prediction of the strength of artificially scratched glass (Kwan, n.d.) . . . . .	89
C.1	Plots of the ten measurements for the three examined defects. . . . .	110
E.1	Normalised strength data of weathered glass fitted to the Normal probability distribution function. . . . .	118
E.2	Normalised strength data of weathered glass fitted to the Lognormal probability distribution function. . . . .	118
E.3	Normalised strength data of as received glass fitted to the Normal probability distribution function. . . . .	119
E.4	Normalised strength data of as received glass fitted to the Lognormal probability distribution function. . . . .	119
F.1	Normalised strength data of as received glass fitted to the Weibull probability distribution function. - data not corrected with FEA. . . . .	122
F.2	Theoretical design strength and design strength according to EN1990:2002 (2005) of the tested specimens (for $P_f=0,0012$ and load duration 5 seconds) - data not corrected with FEA. . . . .	122
F.3	Theoretical and experimental characteristic strength of the tested specimens (for $P_f=0,05$ ) - data not corrected with FEA. . . . .	123
G.1	Theoretical design strength and design strength according to ASTM-E1300 (1997) of the tested specimens (for $P_f=0,008$ and load duration 5 seconds). . . . .	126



# Nomenclature

## Abbreviations

Abbreviation	Definition
AD	Anderson Darling goodness of fit test
AR	As Received glass
CDF	Cumulative Distribution Function
CDR	Coaxial Double Ring test
DHM	Digital Holographic Microscope
FEA	Finite Element Analysis
FEM	Finite Element Model
FF	Fail to Find (Chapter 6)
IR	Inside the loading Ring (Chapter 5)
LEFM	Linear Elastic Fracture Mechanics
LR	At the Loading Ring (Chapter 5)
MLE	Maximum Likelihood Estimation
NA	Naturally Aged glass
ND	Not Detected (Chapter 6)
NDT	Non-Destructive Test
OR	Outside the loading Ring (Chapter 5)
SEM	Scanning Electron Microscope
SIF	Stress Intensity Factor
WLR	Weighted Least squares Regression
XRF	X-Ray Fluorescence analysis

## Greek symbols

Symbol	Definition
$\alpha$	Level of significance for the AD test
$\beta$	Shape factor of the Weibull distribution
$\gamma_m$	Material factor
$E$	Young's modulus
$\theta$	Scale factor of the Weibull distribution
$\lambda_A$	Size effect factor (area)
$\lambda_l$	Size effect factor (edge, hole)
$\nu$	Poisson's ratio
$\sigma$	Tensile stress, normal to crack's plane
$\sigma_{eq,1s}$	Equivalent failure stress for reference time 1 second
$\sigma_f$	Failure stress
$\sigma_{f,eq}$	Equivalent failure stress
$\sigma_{predicted} (\sigma_{pred})$	Predicted failure stress

## Latin symbols

Symbol	Definition
$f_{g;k}$	Characteristic strength
$A$	Surface area
$a$	Crack length
$c$	Flaw size
$D$	Diameter of a circle that expresses the characteristic size of a plate
$d$	Flaw depth (measured with Traceit®)
$D_L$	Diameter of the loading ring
$D_S$	Diameter of the supporting ring
$E_i$	Probability estimator
$F$	Failure load
$f_{mt,u,d}$	Design strength
$h$	Thickness at the middle of glass specimen
$k$	Effective area for bending under out-of-load loads
$k_A$	Size effect factor (area)
$k_e, k_{ed}$	Factor for the edge quality of glass
$K_I$	Stress intensity factor for mode $I$ crack propagation
$K_{IC}$	Critical stress intensity factor for mode $I$ crack propagation
$k_{mod}$	Modification factor for the load duration
$k_{sp}$	Factor for the surface treatment of glass
$l$	Length of specimen's edges
$n$	Stress corrosion constant
$p_{AD}$	Observed significance level for the AD test
$P_f$	Probability of failure
$R_d$	Design resistance
$R_M$	Consequence class
$t_f$	Failure time
$t_{ref}$	Reference time for equivalent failure stress
$v$	Crack velocity
$v_o$	Crack velocity parameter
$W_i$	Weight function of the WLR method
$Y$	Geometry or shape factor

# Introduction

## 1.1. Motivation

The construction industry has detrimental influence on the challenges that the environment currently faces. More specifically, 50% of the extracted raw material is attributed to construction activities, while 35% of the European waste is generated by the construction industry (Commission, 2011). This contradiction between the resource depletion and the increase in landfill waste generates concerns about the current construction practices and underlines the need of greater material efficiency. On these grounds, the main responsibility of engineers towards the society and the planet, should be to take drastic actions which will lead to a sustainable built environment.

Float glass is a material which is used extensively for more than sixty years in the building industry, mainly as infill for windows or facade panels. Lately, modern architecture promotes the use of float glass also for structural elements but still the facades remain the most common application of glass. Currently, most of the buildings undergo renovations and the existing glass elements are discarded because they do not meet the latest energy performance requirements. Therefore, the glass waste increases and concurrently, the need for production of new glass grows.

The production process of glass incorporates gas furnaces, for the melting of the raw material at high temperatures, which produce high amounts of CO<sub>2</sub> emissions. Similarly, the recycling of glass, which requires the melting of the old product, is also a non-sustainable process. Thus, the reuse of glass seems the only sustainable alternative of glass applications. To achieve that, the so-called linear model of "take-make-use-dispose" must be abandoned, and a circular model of glass use must be introduced (see Figures 1.1 and 1.2). In this model a new service-life is assigned to old glass panels, which can be reused for the manufacturing of new windows that comply with the current standards.

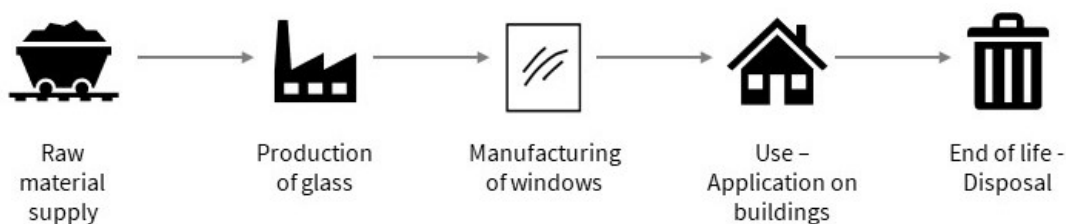


Figure 1.1: The linear process of the current use of glass

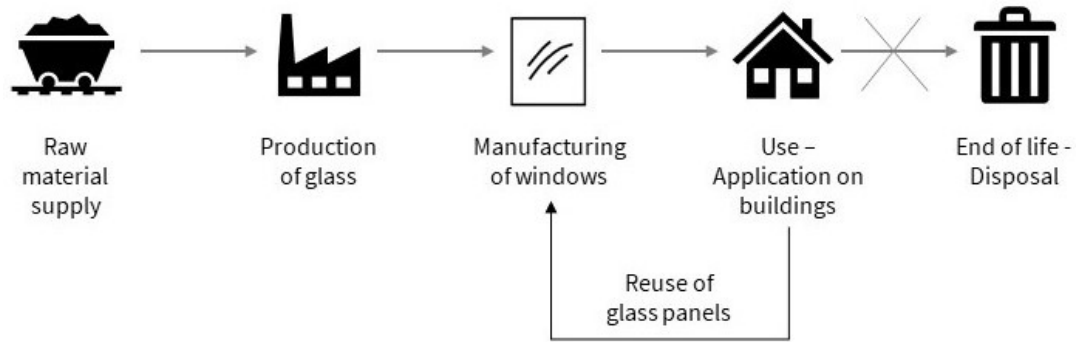


Figure 1.2: The new circular process of use and reuse of glass

## 1.2. Problem statement

The greatest challenge in the reuse of glass is the estimation of its strength after several years of use. Unlike other materials, the strength of glass is not a material property but it is governed by the surface, edge and volume defects of the material. The distribution of these defects inside the material is unknown, and there is no direct relation among them and the glass strength. For that reason, the brittle failure of glass could originate from locations which do not necessarily coincide with the location of maximum stress, due to the random existence of defects inside the material. As a result, engineers interpret the strength of glass by means of destructive tests and fracture statistics, aiming to tackle these uncertainties.

After several years of exposure to the natural environment, the existing defects on glass grow and new defects are induced naturally or during the processing, transportation, use phase etc. The growth and increase of these defects affect its performance and lead to a dynamic strength reduction over the service life of the glass elements. This phenomenon has been explained well in literature based on theory of Linear Elastic Fracture Mechanics and experimentally, based on destructive tests.

The ultimate goal of this research is to assess the strength of weathered <sup>1</sup> glass based on non-destructive examination of its surface, which does not limit its possibilities for reuse. Therefore, the correlation between the surface defects of weathered glass and its surface strength must be further investigated. Inspiration of that research was the concept of strength prediction based on surface scanning for re-using glass elements, proposed by Erwin ten Brincke, engineering consultant and associate partner at ABT b.v., one of the committee members of this thesis project (see Figure 1.3).

<sup>1</sup>The term "weathered" or "naturally aged" glass stands for glass which has been in use for several years.

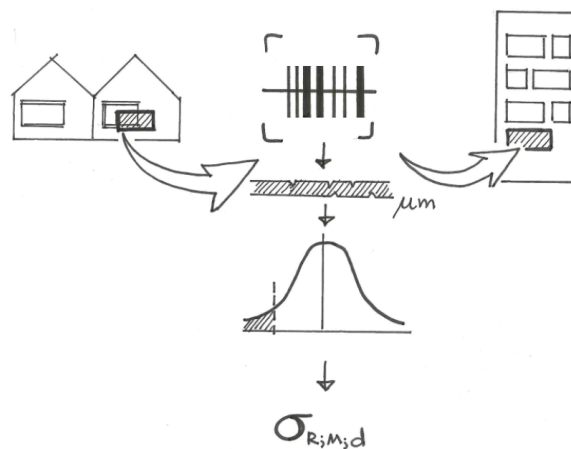


Figure 1.3: The initial idea-concept of this thesis project (sketch by Erwin ten Brincke).

# 2

## Research design

### 2.1. Main objectives

The objective of this thesis is the development of a methodology for the prediction of the strength of naturally aged glass, based on its surface flaws. The aim is to quantify the residual surface strength of weathered annealed glass in terms of flaws, which are introduced over its service life as a facade element. To achieve that, non-destructive tests for defect detection and characterization will lead to the prediction of the theoretical strength of glass. Then, this strength will be compared to the actual strength, as will emerge from destructive experimental investigation. A post-failure fractographic analysis will reveal the actual governing flaw. The novelty of this research lies on the methodology itself and the incorporated equipment, which normally has completely different applications. Finally, through this research, the size effect on the strength of weathered glass will be also investigated, since it is essential for scaling this methodology up, from a small test specimen to a window panel.

### 2.2. Research question

The main research question of this thesis project is:

*How can the strength of weathered glass be predicted based on its surface flaws and the theory of Linear Elastic Fracture Mechanics (LEFM)?*

The sub-questions are:

- How can the defects on the surface of glass be identified and measured?
- What type of defects can be found on the surface of naturally aged glass?
- Which one of the surface defects will initiate the fracture?
- How does the size of the loaded area influence the strength of weathered glass?
- How do the flaws induced by weathering on the surface of glass affect its strength?

### 2.3. Methodology

The methods used in this thesis include both non-destructive and destructive experimental investigation. The tested specimens are small-scale glass plates, of two different dimensions, scored out of larger facade panels which have been in use for almost 55 years. In addition, similar specimens of new glass will be tested to derive a reference value for the strength of new glass. The specimens will be subjected to equibiaxial field of stresses, in a Coaxial Double Ring (CDR) setup, for the derivation of the surface bending strength. A sufficient amount of experimental data will be collected to obtain

statistically meaningful values for the surface strength of the new and weathered glass, taken from a particular building.

A microscopy study will be performed both before and after the bending tests on the weathered specimens to assess first, the surface condition of glass and then, the identify the fracture origin of the specimens. Scanning equipment which is available in the laboratories of TU Delft will be used for defect detection. In addition, the Traceit<sup>®</sup> mobile optical profilometer is provided by Innowep GmbH for use in this research.

## 2.4. Limitations

The undertaken research focuses on the strength of weathered glass and its surface defects. In order to reach the ultimate goal of re-using existing glass elements, additional relevant topics must be investigated, which are excluded from this research. Therefore, the limitations of this project are the following:

- The examined material is soda-lime silica annealed glass. This type of glass is chosen as the most representative of the glass elements that are currently discarded from buildings. In more recent applications, it is more likely to find strengthened glass. This type of glass imposes even more complications in the correlation of the strength and the defects, due to the layer of residual stresses. Therefore, the simplest version of glass is chosen for the testing and evaluation of the effectiveness of the proposed methodology.
- For the same reason, the performance of weathered laminated glass is not addressed in this research. When this type of glass is examined, one should considered apart from the aging of the glass surface, the aging of the interlayer.
- According to the providing company, the examined old glass is "ordinary float glass". However, when it comes to buildings built more than 50 years ago, it is not certain that the glass was produced on a tin bath. For instance, until the 1960s, the standard used product was drawn sheet glass (Feldmann et al., 2014). Although the production method might affect the performance of glass, only float glass is included in this investigation.
- The non-destructive examination focuses only on the surface defects of glass. However, glass has also edge and volume defects which are not in the scope of this project because the aim is to study the effect of weathering, which is more likely to induce surface defects than internal or edge defects.

## 2.5. Research outline

This thesis is organised in seven chapters. **Chapter 1** motivates the relevance of the topic and highlights the existing problem. **Chapter 2** presents the structure of this research, the main objectives, methods and limitations. The theoretical background of this study along with the knowledge gap are presented in **Chapter 3**, based on the state-of-the art literature review. The review focuses on the defects of glass, the LEFM theory, the testing methods and the fracture statistics. Furthermore, the non-destructive tests are introduced and the equipment used before is reviewed.

The experimental investigations are described in **Chapter 4**. The tested specimens, the testing methods and the methodology for detecting the flaws on the glass surface are elaborated. Subsequently, the results of the tests are presented. The types of defects found on the surface of the examined weathered glass along with their dimensions are also reported. In **Chapter 5**, the statistical analysis of the experimental results is presented. Furthermore, the strength of the old and the new glass of this research are compared to the design strength proposed in the European and Dutch standards. The proposed methodology for the prediction of the strength of weathered glass along with its evaluation is presented in **Chapter 6**. Finally, in **Chapter 7**, all the findings of this research are summarised and conclusions are drawn. Recommendations for practice and for further research are proposed in that chapter.

# 3

## Theoretical background

### 3.1. Introduction

In this chapter, the basic knowledge on glass strength, defects and failure is presented. The aim is to introduce the influence of the glass defects on the strength of glass and on the dynamic reduction of the latter over its service life. Thus, Sections 3.2 and 3.3 review the strength of glass according to the current standards and the several types of glass defects, respectively. The failure of glass due to the existence and the sub-critical growth of defects on its surface are discussed on the basis of fracture mechanics in Sections 3.4 and 3.4.2.

This chapter introduces also the methods for both non-destructive and destructive testing on glass, which are useful for the validation of the theoretical strength of glass. The experimental methods for the determination of the bending strength of glass according to the European and the American standards are presented in Section 3.5. Section 3.6 reviews the probability distribution methods which are used for the processing of the experimental results and it introduces the phenomenon of "size effect". Finally, the non-destructive testing methods and the required equipment are reviewed in Section 3.7.

### 3.2. Strength of glass

Glass is a brittle material whose failure is not preceded by any warning sign. Due to this behavior and the increasing use of it as a structural material, the exact value of its strength is required. However, glass is a material which does not have an intrinsic strength, constant over its service life. Unfavorably, its strength depends strongly on various parameters which differ per glass application, such as the loading condition and the existence of material defects. Therefore, the determination of its strength has never been a straight forward process.

#### 3.2.1. Characteristic strength

The theoretical strength of glass is calculated as the energy that is required for the detachment of its atoms, and it is approximately 32 GPa (Shelby, 2020). Over the transition from theory to practice this value decreases dramatically, mainly due to the existence of defects, resulting in a practical strength orders of magnitude smaller than the theoretical one, namely between 30 to 100 MPa (Schula et al., 2013). The draft European standards suggest a characteristic value for the bending strength of annealed glass equal to  $f_{g,k}=45$  MPa which leads to an even lower design value (prCEN/TC250-1, 2018).

The most common way to increase the strength of glass is through the tempering process. The glass is heated and then rapidly cooled by air jets (quenching), creating a significant temperature difference between the inner and the outer parts of it. The effectiveness of this treatment lies on the prevention of

the development of new cracks, by introducing a layer of residual compressive stresses on the glass surface. The characteristic strength of this type of glass, according to the draft European standards, equals to  $f_{g,k}=70$  and 120 MPa for heat and thermally toughened glass, respectively (prCEN/TC250-1, 2018).

Annealed, heat strengthened and fully toughened, all types of glasses suffer from strength degradation over their service life, due to the phenomenon of static fatigue <sup>1</sup>. Although this reduction in the long-term strength of glass has been proven experimentally, it is still complex to calculate. The current codes and standards for glass (prCEN/TC250-1, 2018; NEN2608, 2014) do not include any information about the strength of weathered glass. The provided information covers the testing, design and application of new glass in buildings.

### 3.2.2. Actual strength

Veer (2007) conducted experiments over a seven-year-period, with more than 450 specimens of glass, of several thicknesses and edge processing, and a maximum strength of 100,2 MPa was reported for flat annealed glass plates. Experiments have been also conducted on artificially aged annealed glass and an average strength of 42,8 MPa was found (Kwan, n.d.). More recently, Datsiou and Overend (2017b) studied the strength of fully and chemically toughened artificially aged glass. The results indicated that the fully tempered aged glass had the highest strength, equal to 138,4 MPa while those of the chemically toughened and annealed glass were 63,7 and 38,6 MPa, respectively. Despite the broad ongoing research in this field, there is lack of information regarding the strength of naturally aged glass. Such information can be found in the study of Datsiou and Overend (2017a) where a maximum strength of 75,8 MPa was reported for a 20-year old flat annealed glass. Although other studies reported considerably lower strength values for weathered glass, this value allows the consideration of re-using concepts for glass elements.

### 3.3. Defect Characterization

In 1920, Griffith identified the link between the discontinuities of glass and its failure stress. In particular, the "flaws", as he called them, with large dimensions compared to the molecular structure of glass, are the cause of the weak performance of isotropic solids. The high theoretical strength of materials, can be obtained only when these flaws are eliminated. On these grounds, a smaller flaw is accompanied by a higher strength and vice versa. Therefore, it is essential to detect and characterise the flaws in the glass to gain an impression about its actual strength.

The origin of the flaws is usually the production process of glass. From the melting and the formation till the cooling processes, glass is prone to many types of defects. Even the raw materials themselves can introduce inclusions in the volume or in the surface of glass. The flaws which are developed during the formation of the glass are called "intrinsic" (Quinn, 2020). During the manufacturing, the application and the use phase of glass, new flaws are introduced on its edges and its surface, the so called "extrinsic" flaws. Finally, due to the chemical reaction between the glass surface and the humidity in the natural environment to which it is exposed, these defects are forced to expand.

The defects in glass have been categorized by many researchers, based on their location, shape, size, origin and other parameters. The influence of them on the performance of glass varies per type of defect. For instance, some types of defects are responsible for significant strength reduction whereas some others affect the visual quality of it. Some of the glass defects that have been reported in literature are the following (Müller et al., 2001; Agrawal, 2011; Ai and Zhu, 2002):

- Knots and striae: they are often found together, as inclusions of glass of different composition. They may originate from the inhomogeneities on the surface of glass that are caused during the evaporation of glass.
- Scratches and spots: they are patches, marks or flaws on the surface of glass which reduce the visual quality of glass. They may occur during handling, transportation or they can be formed

<sup>1</sup>This phenomenon is explained in Section 3.4.2

as a reaction to different types of applied stresses (localized shear stresses, thermally induced stresses etc.).

- Pit defects: the air bubbles that are close to the surface of glass might be cut during the polishing process, resulting in small open holes with particular depth that are sensitive to contamination. Pit defects could be developed also solely due to corrosion or oxidation.
- Digs: they are found on the surface and they are caused by grinding, impact or contact damage.
- Foreign material: opaque material that cannot melt can be found embedded in the glass in the form of lump.
- Metallic inclusions: they are introduced by metals during the production process (i.e. in the melting units), due to contamination etc.
- Crystals: they have crystalline characteristics, such as dendritic or hexagonal growth, plates etc.
- Stones: they are developed during the crystallization of the glass or by crystal formation from reactions with other materials or contamination. They are crystalline large inclusions.
- Bubbles: they are the most common type of defect in glass. They are hollow spaces in the form of bubbles, filled with gas such as oxygen, carbon monoxide and hydrogen. Bubbles can also contain small crystals or other solids. They are developed by the decomposition of raw material and contamination.

Figure 3.1 illustrates several volume and surface defects of glass, as they were identified under observations with microscopes by several researchers.

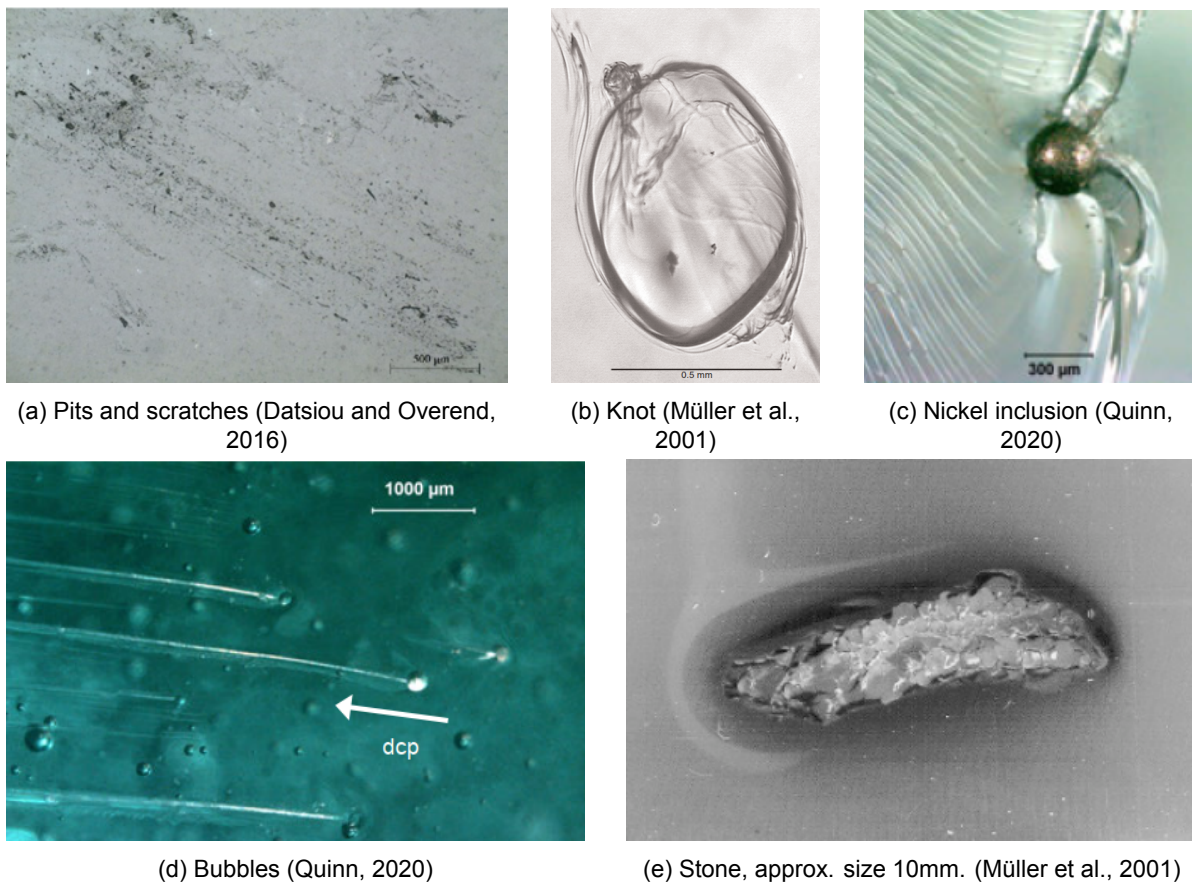


Figure 3.1: Images of several types of defects in glass.

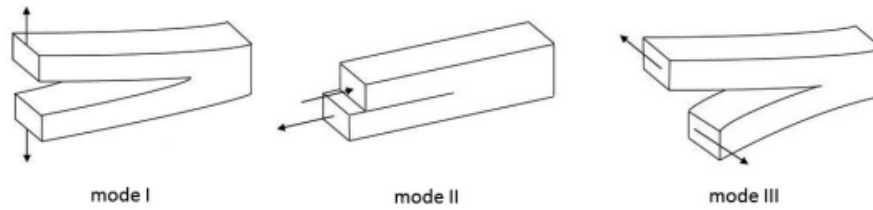


Figure 3.2: Three failure modes, mode I (opening mode), mode II (sliding mode) and mode III (tearing mode) (LINDQVIST, 2013).

## 3.4. Fracture mechanics

The surface condition of glass, and particularly its surface flaws, as well as its low fracture toughness are responsible for the significant drop from the theoretical to the practical strength. The almost ideally linear elastic and brittle behavior of glass allows researchers to implement the theory of Linear Elastic Fracture Mechanics (LEFM) for the assessment of its performance.

### 3.4.1. Stress Intensity Factor

Lawn (1993) described the influence of the flaws on the strength of glass, based on theory of LEFM and through the definition of a new material property, the stress intensity factor (SIF). The SIF is described by the formula 3.1.

$$K_I = \sigma \cdot Y \cdot \sqrt{\pi \cdot c} \quad (3.1)$$

Where,

$K_I$  is the stress intensity factor for mode I crack propagation,  
 $\sigma$  is the tensile stress, normal to the crack's plane,  
 $Y$  is the shape correction factor of the flaw and  
 $c$  is the flaw size in meters.

Depending on the direction of the force acting on the crack's plane, the failure mode can appear in three different ways (see Figure 3.2). The mode I crack propagation, for which the formula 3.1 applies, occurs when the crack is subjected to tensile stresses perpendicular to its plane. Shear stresses parallel to the crack's plane lead to mode II crack propagation. Finally, out-of-plane shear stresses result in the failure mode III. Since the SIF is a function of the field of stresses, for each failure mode, it has different value ( $K_I$ ,  $K_{II}$ ,  $K_{III}$ ). However, the SIF for mode I is always larger than that for modes II and III, and therefore, it normally dominates in the crack propagation (Wang and Hadfield, 2004).

When  $K_I = K_{IC}$ , where  $K_{IC}$  is the critical stress intensity factor for mode I crack propagation, fracture occurs and the  $\sigma$  becomes  $\sigma_f$ , the fracture strength of glass. Figure 3.3 shows the decrease of the glass strength as a function of the flaw depth, for constant  $K_{IC}$  and  $Y$  (Haldimann, 2006). If the characteristics of the crack (size, geometry factor) and the  $K_{IC}$  are known, formula 3.1 can be used for the estimation of the failure stress of this crack.

### 3.4.2. Static fatigue

The actual strength of glass exposed to the natural environment is reduced over the years, in a non-predictable manner, due to the growth of its surface flaws. The phenomenon that describes the time-dependency of the strength of glass to the environment, is known as static fatigue. According to this phenomenon, the humidity in the air reacts chemically with the glass, enhancing the growth of cracks and leading to a delayed failure under constant load. This phenomenon is also called "stress corrosion". The chemical reaction rate determines the failure time, namely the time that is required for a sub-critical

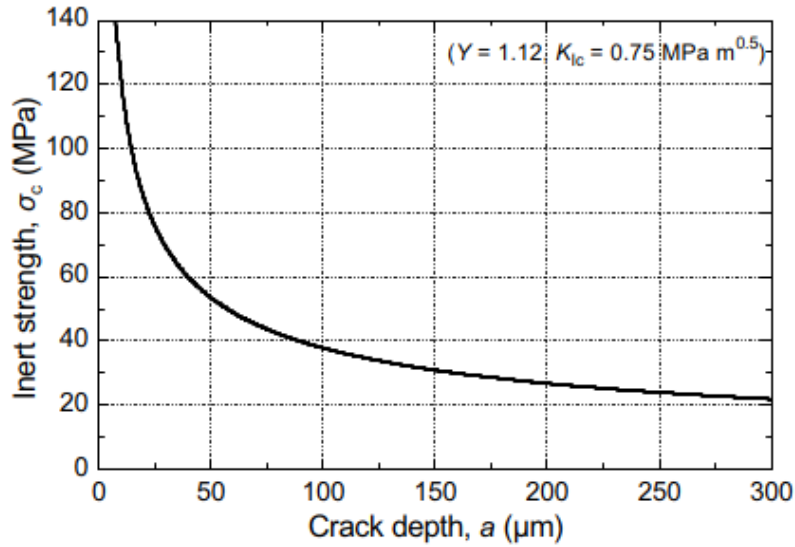


Figure 3.3: Inert strength of a single crack as a function of its depth by Haldimann, 2006.

crack to become critical and cause the fracture (Evans and Wiederhorn, 1974). It was revealed that the chemical composition of glass has a considerable influence on the crack growth velocity, with silica glass having the greatest resistance against crack growth (S. Wiederhorn and Bolz, 1970). In literature, the time-dependent growth of cracks in glass is described by the power function in formula 3.2 (Overend and Zammit, 2012).

$$\frac{da}{dt} = v_o \cdot \left( \frac{K_I}{K_{IC}} \right)^n \quad (3.2)$$

Where,

$v$  is the crack velocity,

$K_I$  is the mode I stress intensity factor,

$n$  and  $v_o$  are crack velocity parameters which depend on the material, the environment and the humidity,

$a$  is the crack length and

$K_{IC}$  is the mode I fracture toughness.

The phenomenon of stress corrosion could become a matter of concern during the testing process of glass. In particular, if the tests are conducted with low stress rates, the fracture is reached at longer load duration and strength degradation occurs due to sub-critical crack growth. On the contrary, if the stress rate is high, the fracture occurs sufficiently early, namely within 10s - 15s (ASTMC1499-09, 2013), and the effect of stress corrosion is considered negligible. Even when testing at constant stress rate, specimens which seem identical are likely to reach fracture at different times. To tackle the influence of the load duration of experimental results, the tests can be conducted in vacuumed conditions, where the environment is not influential. Alternatively, the failure stresses can be normalised to an equivalent stress  $\sigma_{f,eq}$ , usually for a reference period of 60 seconds, according to the cumulative damage criterion of Brown (1972), which is described by the equation (3.3).

$$\sigma_{f,eq} = \sigma_f \left[ \frac{t_f}{t_{ref} \cdot (n + 1)} \right]^{1/n} \quad (3.3)$$

Where,

$t_f$  is the failure time of each specimen in seconds,

$t_{ref}$  is the equivalent reference time of each specimen in seconds and

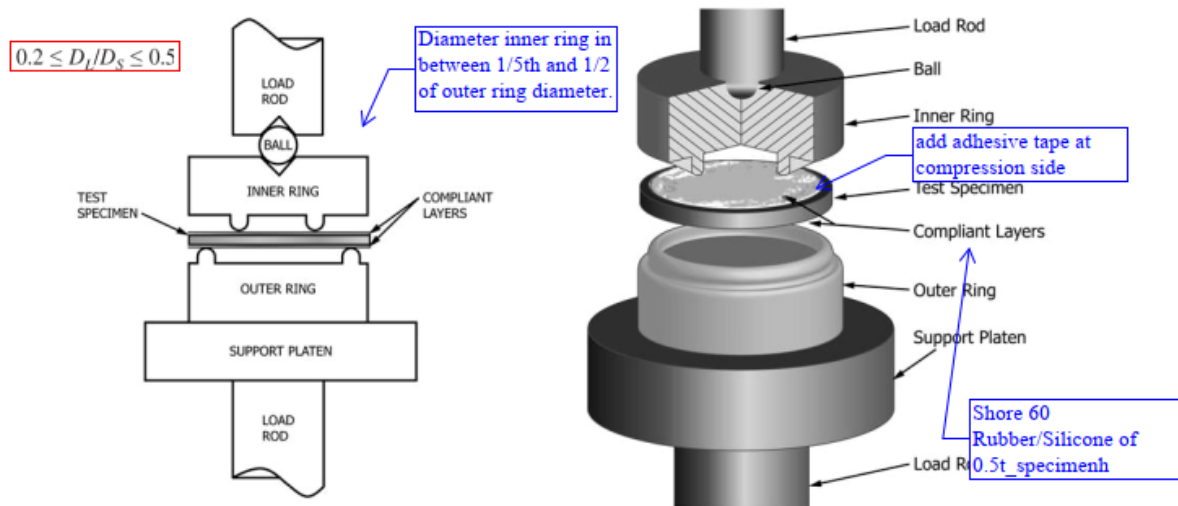


Figure 3.4: Section View and Perspective View of Basic Fixturing and Test Specimen for Equibiaxial Testing (ASTMC1499-09, 2013).

$n$  is the stress corrosion constant. For soda-lime silica glass and temperatures below  $150^{\circ}\text{C}$ , a value of 16 can be used (Charles, 1958).

### 3.5. Experimental methods for determining the strength of glass

As mentioned in Section 3.2, the actual strength of glass is orders of magnitude smaller than the theoretical strength. The crack growth on the glass surface is the detrimental factor for the reduction of its actual strength, which varies even for glass panels manufactured in identical conditions. The extrinsic strength of glass can be predicted in two ways. The first way presupposes that the critical flaw, namely the flaw that will cause the fracture, and its characteristics are known. In this case, the strength of glass can be predicted explicitly based on that information. The second way is useful when the critical flaw characteristics are unknown. Then, a stochastic approach is followed for the prediction of the fracture strength of glass. In both cases, destructive tests on glass are performed for the validation of the outcomes of these two approaches.

#### 3.5.1. Destructive tests on glass

According to ISO1288-1 (2016), the bending strength of flat glass can be determined based on:

1. Coaxial Double Ring (CDR) test on flat specimens with large test surface areas (see Figure 3.4).
2. Test with specimen supported at two points.
3. Coaxial Double Ring test on flat specimens with small test surface areas.

Among these three experimental setups, the most commonly used one for measuring the surface bending strength of glass is the CDR setup with small test surface areas. The advantage of cutting a glass panel into smaller pieces, and testing those instead of the complete panel, lies on the increased number of specimens that are obtained. The increased number of specimens leads to statistically significant results<sup>2</sup>. The CDR testing method is described in both the European NEN-EN1288-5 (2000) and the American ASTMC1499-09 (2013) standards. In both standards, the sample size, which in this case is the number of the glass specimens, is determined by the desired reliability of the results.

The principle of this testing method is the application of homogeneous tensile stress on the glass surface and more specifically, within the loading or "inner" ring, as illustrated in Figure 3.4). In this way,

<sup>2</sup>The effects of the panel size and the sample size on the statistical processing of the experimental results are discussed in Section 3.6



Figure 3.5: Front view of dynamic glass testing rig showing the 2.35m diameter piston behind the opening where the glass will be installed (Dalgliesh and Taylor, 1990).

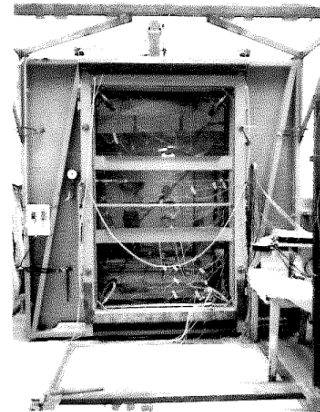


Figure 3.6: Front view with tempered glass panel in place (All the wires are from the strain gages). (Johar, 1981).

the maximum tensile stress is in the center of the specimen and thus, the failure is expected to initiate in this area. According to ASTM C1499-09 (2013), a failure whose origin is outside the loading ring, is considered invalid. Therefore, a post-failure analysis is usually undertaken after the ring-on-ring tests to determine the origin of the failure and evaluate the validity of the results.

The main difference between the two standards which describe the CDR tests, NEN-EN1288-5 (2000) and ASTM C1499-09 (2013), lies on the loading method. The European standards suggest the application of load via gas pressure, which increases over the course of the test in order to maintain uniform stress in the area of the loading ring. The method proposed by the American standards is simpler since the specimens are subjected to constant stress rate without gas.

### 3.5.2. Tests on large glass panels

For applications of glass in buildings, where normally larger elements are used, ISO 1288-1 (2016) suggests the use of the testing methods 1 and 2 (see Section 3.5.1). These methods test larger elements and thus, it is likely that the emerged strength will represent more accurately the actual strength of a glass window or facade element. To this extent, the ASTM C1499-09 (2013) standards clarify that the testing of a particular component of a larger element may not provide representative strength results for the entire-size element.

In literature, only few studies were found that conducted tests on full-size windows or facades. Some of them were the studies of Johar (1981) and Dalgliesh and Taylor (1990). In both cases, a unique apparatus was manufactured which led to a time consuming and expensive experimental procedure. Additionally, such tests required at least twenty large glass specimens available for testing, which are more difficult to find compared to the specimens required in small-scale tests. Therefore, the strength of larger glass elements is until now extrapolated from the strength data of smaller specimens by means of statistics, as it is explained in Section 3.6.2.2.

## 3.6. Fracture statistics

The tests on macroscopically identical glass specimens result in strength values which range significantly. These results are not sufficient for the determination of the characteristic strength of glass and the development of design guidelines for this material. Therefore, engineers aim to tackle these uncertainties in the strength of glass by implementing a probabilistic approach and statistics in the processing of experimental data.

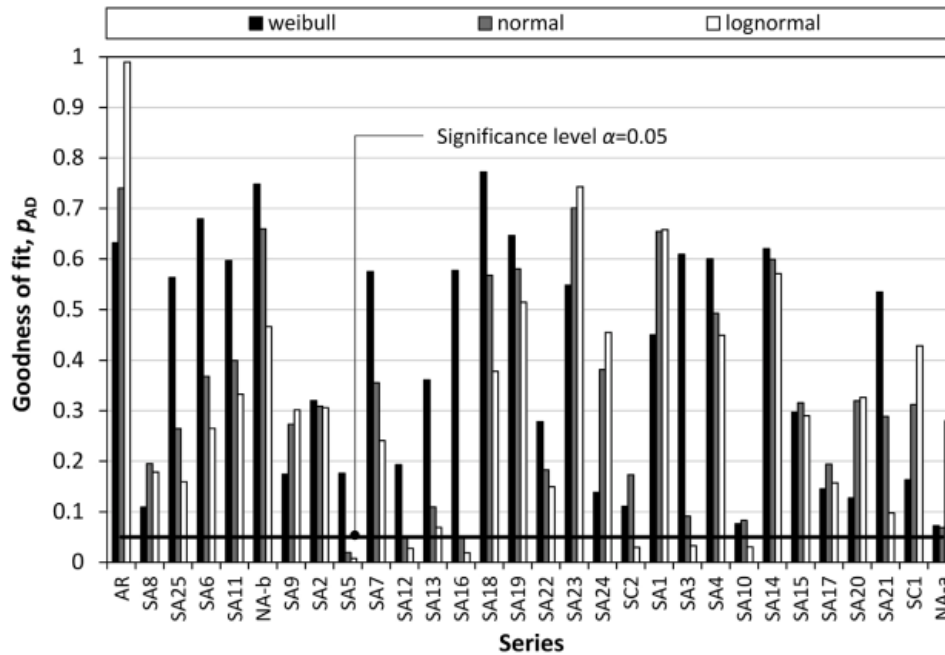


Figure 3.7: Goodness of fit for all data series fitted to a Weibull, a Normal and a Lognormal distribution (Datsiou and Overend, 2018).

### 3.6.1. Probability distribution functions

The two-parameter Weibull probability distribution has been widely used for the statistical interpretation of the strength of glass. This distribution is based on the Weakest-Link-Theory, according to which a stressed brittle material fails when one of its flaws fail (Schula et al., 2013). The Weibull distribution revealed to approach the experimental data of glass at an acceptable level, apart from the area of the lower probabilities of failure. A recent study of Pisano et al. (2019), showed that the left-truncated Weibull distribution fitted better the variable data of the glass strength, including the lower values.

The Lognormal distribution is another established probability distribution for the statistical evaluation of the strength of glass. It is described by the two parameters  $\mu$  and  $\sigma^2$ , which are the mean and the variance of the sample, respectively (Schula et al., 2013). However, this distribution turned out to be less conservative than the two-parameter Weibull distribution (Datsiou and Overend, 2018). Veer (2007) studied the applicability of the normal statistical distribution and he concluded that this distribution could approach well the strength data of glass only in rare cases. An example of the goodness of fit of the three probability distributions of thirty testing series is shown in Figure 3.7, while an extensive comparison of these methods is available in (Datsiou and Overend, 2018).

Overall, although Weibull distribution does not describe well the strength data for lower probabilities of failure, it is the most commonly used because it is the only one with a physical background. Furthermore, the conservative results of this distribution are preferred especially for engineering design purposes. The Weibull distribution is also the established method for describing the glass strength in the European (NEN-EN12603, 2002) and American (ASTMC1239-13, 2018) standards. Therefore, the strength results of this research will be processed with this method but the goodness of fit of the test data to the Normal and the Lognormal probability distributions will be evaluated as well.

### 3.6.2. Weibull probability distribution function

The Weibull distribution function is described by the equation 3.4 (Weibull et al., 1951). As mentioned above, this distribution is based on the Weakest-Link-Theory, according to which a chain as a whole fails, when one of its links fail (Weibull et al., 1951). In case of a stressed brittle material such as glass,

the failure occurs when one of the material's flaws fail.

$$F(x) = 1 - \exp(-\phi(x)) \quad (3.4)$$

The two-parameter Weibull distribution function is expressed in the form of the formula in 3.5 (Overend et al., 2007). The scale and shape parameters  $\theta$  and  $\beta$ , respectively, or the so called "surface flaw parameters", aim to model the influence of the surface flaw characteristics on strength.

$$P_f = 1 - \exp(-\beta A \sigma_f^\theta) \quad (3.5)$$

Where,  $P_f$  is the probability of failure of the glass element,  
 $A$  is the surface area,  
 $\sigma_f$  is the strength of glass and  
 $\theta$  and  $\beta$  are the scale and shape parameters, respectively (also called surface strength parameters).

### 3.6.2.1. Sample size

Since the experimental strength of glass is mostly analysed by means of statistics, the sample size becomes crucial. More specifically, the number of the testing specimens will determine whether the obtained results are statistically significant or not. A small sample size might not be sufficient to overcome the uncertainties that the highly variable strength of glass imposes.

The American standards ASTM C1499, which describe the coaxial double ring tests on glass, specify that a minimum number of 10 valid <sup>3</sup> tests are required for the derivation of the mean biaxial flexural strength of the tested series. When it comes to the estimation of the Weibull parameters though, a sample consisting of at least 30 specimens is required (ASTMC1499-09, 2013). On the other hand, the International Standard ISO1288-1 expresses the uncertainty in glass strength in terms of confidence limit. As long as a sample results in "fairly narrow" confidence limits, it is considered acceptable. Therefore, the desired accuracy of the results determines the optimum sample size or confidence level.

Pisano and Carfagni (2015) examined the resulted failure stresses of thirty series of tests. Each one of the thirty samples included approximately 25 glass plates. The great variation that they observed among the results of individual samples, lead them to the conclusion that 25 specimens are not sufficient for determining the allowable stress of glass. In the study of Kinsella and Persson (2018), an overview of 16 test series on new annealed glass is available. The sample size of those experiments ranged from 10 to 113 specimens. Hence, no clear conclusions can be made about the optimum sample size, based on previous experiments nor based on the existing standards.

### 3.6.2.2. Size effect

The formula (3.5) is sensitive to the duration of the load, the surface area, the orientation of the surface flaws, the humidity and the magnitude of the tensile stresses. A visual representation of the influence of the surface area on the strength, as derived by several researchers, is presented in Figure 3.8. These plots indicate that as the loaded surface area increases the strength of glass reduces, due to the increased probability of encountering a larger flaw in this area.

In literature, this phenomenon is called "size effect" and it is expressed as function of the failure stress and the shape factor of the Weibull distribution, according to (3.6) (Schula et al., 2013). The opportunity to relate a specimen's property, such as its size, to a statistical parameter, is another reason for the engineers to prefer this probability distribution over others.

$$\frac{\sigma_{f,A1}}{\sigma_{f,A2}} = \left( \frac{A_1}{A_2} \right)^{(1/\beta)} \quad (3.6)$$

<sup>3</sup>A test is considered valid when it complies with all the requirements of the testing method described in ASTM C1499 and its fracture origin is not at the specimen's edge

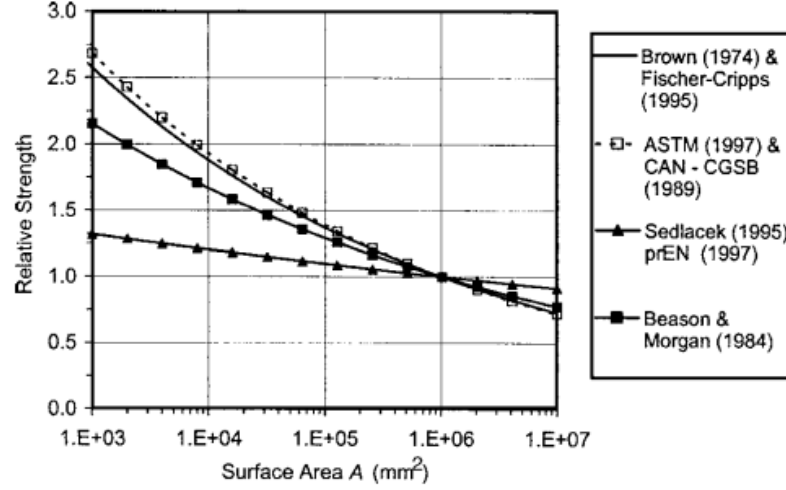


Figure 3.8: Relative strength of annealed glass with variation in surface area (dotted lines represent weathered glass) from Overend et al. (2007).

Where,

$\sigma_{f,A_i}$  is the failure stress of the panel with surface area  $A_i$  and  $\beta$  is the estimated shape factor of the Weibull distribution.

### 3.6.2.3. The size effect in the design standards

According to the Dutch design standards NEN2608 (2014) for structural glass, the design strength of new annealed float glass can be derived from the formula (3.7). The most recent draft European Standard (prCEN/TC250-1, 2018) defines the design strength of new annealed glass as described in formula (3.8). Furthermore, an informative part of this standard provides a more detailed design method, based on the formula (3.9).

$$f_{mt,u,d} = k_e \cdot k_a \cdot k_{mod} \cdot k_{sp} \cdot \frac{f_{g,k}}{\gamma_{M,A}} \quad (3.7)$$

$$R_d = k_{ed} \cdot k_{sp} \cdot k_{mod} \cdot \frac{f_{g,k}}{R_M \cdot \gamma_M} \quad (3.8)$$

$$R_d = k_{ed} \cdot k_{sp} \cdot k_{mod} \cdot \lambda_A \cdot \lambda_1 \cdot \frac{f_{g,k}}{R_M \cdot \gamma_M} \quad (3.9)$$

All the aforementioned standards implement several parameters in the calculation of the design strength of glass, which influence this value. In Table 3.1, the parameters of the three design methods are explained and typical values for them are presented<sup>4</sup>. It can be seen that one of these parameters, the  $k_a$  or  $\lambda_a$ , accounts for the influence of the loaded area on the strength of glass. This parameter is calculated through the formula (3.10) and (3.11) for the Dutch and European standards, respectively. In both norms, the increase of the size of the loaded area leads to smaller size-effect parameters and as a consequence, to lower strength. The informative part of the European standards states that this parameter must always be within the limits  $0,75 \leq \lambda_A \leq 1,0$ .

$$k_a = 1,644 \cdot A^{-\frac{1}{25}} \quad (3.10)$$

<sup>4</sup>These values correspond to a four-sided supported window, subjected to wind load for 5 seconds (Consequence Class 2). New annealed float glass with as cut edges is considered.

Table 3.1: Overview of the design methods for the calculation of the design strength of glass

Factor	Purpose	NEN2608 2014	CEN/TC250 2018	CEN/TC250 (Informative) 2018
$k_{ed}, k_e$	Edge quality	0,8	0,7	0,7
$k_{sp}$	Surface treatment	1,0	1,0	1,0
$k_{mod}$	Load duration	1,0	0,85	0,88
$\gamma_{m,A}$	Material factor	1,6	1,8	1,8
$k_a, \lambda_a$	Size-effect (area)	<i>variable</i>	-	<i>variable</i>
$\lambda_1$	Size-effect (edge, hole)	-	-	1,0
$R_m$	Consequence class	-	1,0	1,0

Where,  $A$  is the load area in  $mm^2$ .

$$\lambda_A = \left( \frac{0,24m^2}{k \cdot A} \right)^{1/7} \quad (3.11)$$

Where,  $A$  is the tensile area in  $m^2$ , and  $k$  is the effective area for bending under out-of-plane loads.

Figure 3.9 illustrates the design strength as a function of the loaded area. According to the normative European standards, the size effect does not influence the design strength of glass. However, the informative methodology of the same standards accounts for that effect, especially within the limits of  $0,75 \leq \lambda_A \leq 1,0$ . Beyond these limits, the design strength is constant with a difference between the upper and lower limit of approximately 33%. If these limits were not imposed, the design strength would have the exponential behavior indicated as "theoretical" in Figure 3.9. On the contrary, the design strength according to the Dutch standards accounts always for the size of the loaded area. The difference in the strength due to the size effect is considerable for areas up to  $1 m^2$  and lower for areas larger than  $12 m^2$ .

Overall, the Dutch norms result to considerably higher value for then design strength of glass, than the European norms. Apart from the size effect, few other parameters are responsible for this difference. For instance, both methods take into account the duration of the load applied on the glass through the modification factor,  $k_{mod}$ . However, the Dutch standards are normalised to the duration of the wind load (5 seconds), leading to a  $k_{mod}=1,0$  for that load, while Eurocode leads to  $k_{mod}=0,88$ . Furthermore, the effect of the edge quality is more conservative in the European norm, in which a value of  $k_{mod}=0,7$  is recommended, while the Dutch norms imply  $k_{mod}=0,8$  for as cut edges.

Nevertheless, none of the existing design standards provide information about the characteristic nor the design strength of weathered glass. Thus, it is still unknown which of these parameters must be applied when estimating the design strength of this type of glass. This research will investigate one of these parameters, the size-effect, but when it comes to the re-use of glass, further research on all these parameters is required.

### 3.6.3. Prediction of glass strength

A complete process for the prediction of glass strength must incorporate two subsequent steps, the detection of the flaws on its surface in a non-destructive way and the correlation of these flaws to the strength. None of these two processes is simple and many challenges are incorporated in them.

On the one hand, for the flaw detection and characterization, a suitable scanning equipment must be found. A previous study revealed that the strength of glass is not influenced by the length of the cracks but by its depth (Kašiarová et al., 2005). The accuracy of the depth measurements, which depends on both the equipment and the operator, is of major importance for reliable strength predictions. A recent study showed that same flaws measured with different devices led to considerably different strength

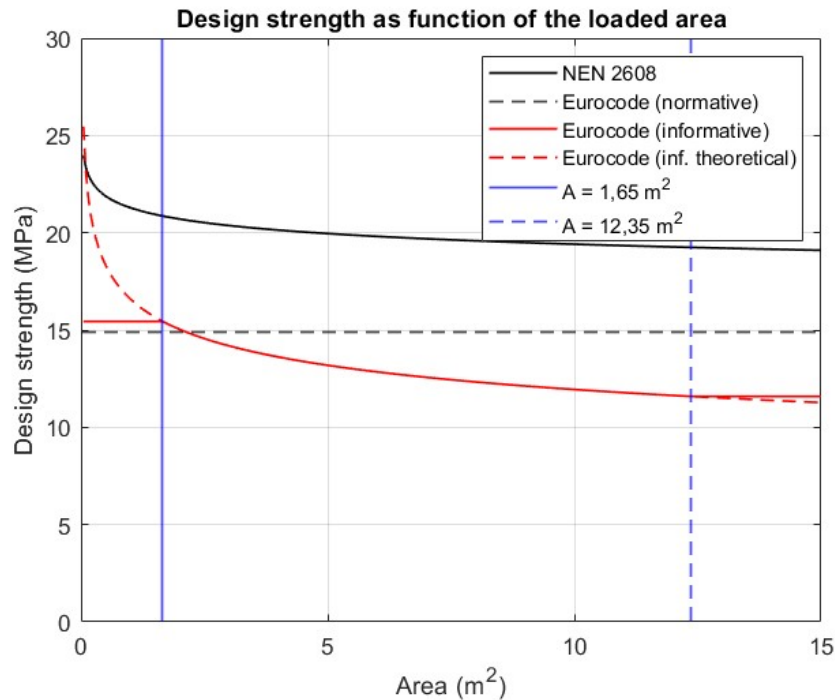


Figure 3.9: Design strength as a function of the loaded area, according to the European and Dutch standards, for a four-sided supported plate under wind load with duration 5 seconds (For annealed float glass with as cut edges).

predictions (Kwan, n.d.). Therefore, the selection of scanning equipment has an essential contribution to the prediction of the strength.

On the other hand, the correlation of the glass strength to the flaw size is another challenging task which has not been attempted yet a lot by researchers. One way to evaluate the glass strength according to the Canadian standards (Board, 2017) is based on visual inspection. Although this method is simple and low-budget since no equipment is incorporated, its efficiency is doubted. More specifically, it is doubted whether the human eye can identify flaws with dimensions of several micro meters. A second way for assessing the strength of glass non-destructively is by using the theory of LEM, which relates the strength of a brittle material to its flaws. The formula 3.1 has been previously used for this purpose by Kwan (n.d.). However, this formula was simplified by several researchers in the past, who introduced uncertainties in each one of its parameters which cannot be neglected<sup>5</sup>. As a consequence, these uncertainties in combination with the error of the optical method used, affect the accuracy of the predictions. Therefore, the predicted failure stresses should be verified with the actual ones, as derived from destructive tests, until a sound method for the prediction of the glass strength is established.

### 3.7. Non-Destructive Tests

A Non-Destructive Test (NDT) aims to identify and characterize the damage (defects) on the surface or the interior of a material, without altering the sample Dwivedi et al., 2018. Usually, such tests take place in the production line of several materials, such as composites, metal, ceramic etc., as quality control systems. Since in this project the re-use of glass is considered, its surface damage must be assessed without harming the examined specimen. Some of the techniques which have been used for NDT in composite and ceramic materials are the following (Zhao, 2021; Gholizadeh, 2016; Kwan, n.d.):

- Visual testing or visual inspection

<sup>5</sup>The parameters which synthesized this formula are elaborated in Section 6.3

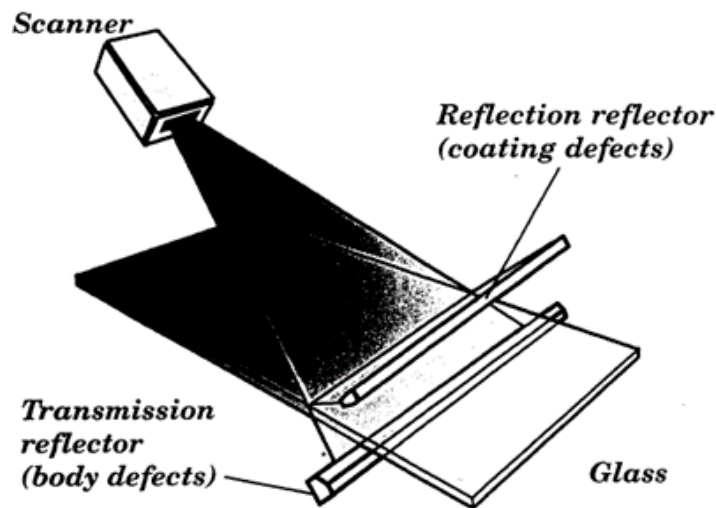


Figure 3.10: Configuration of retroreflective scanner for simultaneous detection of body glass defects and coating defects (Holmes, 1997).

- Radiographic testing
- Ultrasonic testing
- Thermographic testing
- Infrared thermography testing
- Acoustic emission testing
- Acoustic-ultrasonic testing
- Electromagnetic testing
- Machine vision
- Laser ultrasonic testing
- X-Ray tomography
- Electrified particle testing

Among these techniques, the visual inspection, the ultrasonic testing, the machine vision and the electrified-particle testing, have been already used for testing glass. The drawbacks of a NDT depend highly on the chosen method. The main disadvantage of most of these methods, except from the visual inspection, is the significant cost associated with the equipment and the well-qualified staff which is required for their implementation.

### 3.7.1. Equipment used in research

The defects on the glass surface have dimensions that range between several nanometers to millimeters. Usually, the natural flaws on glass range from  $20\mu\text{m}$  to  $200\mu\text{m}$  (Schula et al., 2013). Defects with dimensions of nano or micro meters are not visible by human's eye and thus, optical magnification devices are required to obtain images of the surface condition of glass. Through these images, the surface flaws can be characterised, which is an essential part of the NDT techniques for predicting the strength of glass.

The easiest way to detect the larger defects on a surface is with visual inspection. This method has minimal cost since no equipment is required apart from the inspector's eye. However, the reliability of visual inspection is low because it is prone to human's error. Furthermore, it is time consuming to examine large panels manually. Therefore, in the production process of glass, where a non-destructive

and qualified method is required, automatic inspections are performed. In this case, laser, or line, scanners and moiré deflectometers are normally used for the quality control of the end product (Holmes, 1997; Rasouli and Tavassoly, 2005). With this type of equipment, large glass surfaces can be scanned uninterrupted and with high speed (see Figure 3.10).

In the field of research, the scanning methods that are used differ from those used in the production line of glass. This is attributed to the high resolution which is required in a scientific study, compare to the massive quality control that takes place during production. Over the years, many researchers tried to detect the flaws on the glass surface with equipment that is normally used in material sciences or even in other sectors, such as in automotive and in medicine. A review of the equipment that has been used to scan the glass in several previous studies is presented in Table 3.2. Unsurprisingly, it can be seen that the most commonly used scanning equipment is the optical microscope and in particular, the convectional light microscopy, the polarized or the confocal one. The microscopes have been consistently chosen by researchers perhaps because they can be found in almost every laboratory, due to their wide range of applications.

Figures 3.11 and 3.12 show the external surface of weathered glass as emerged out of examination

Table 3.2: Overview of the equipment used in research for defect detection in glass.

Equipment	Study
Optical (Light) Microscope	Vandebroek et al. (2013) Datsiou and Overend (2017b) Ronchetti et al. (2013) Kwan (n.d.) Zammit and Overend (2010)
Optical Polarized Microscope	Overend and Zammit (2012) Speranzini and Agnetti (2014)
Optical Confocal Microscope	Haldimann (2006) LINDQvIST (2013) Kašiarová et al. (2005)
Surface Profilometer	Kwan (n.d.) LINDQvIST (2013)
Scanning Electron Microscope	LINDQvIST (2013) Varner and Oel (1975)
Electrone Probe Microanalysis	Müller et al. (2001)
Atomic Force Microscope	Müller et al. (2001) Zammit and Overend (2010)
Digital Holography Microscope	LINDQvIST (2013)
Optical Coherence Tomography	Chen et al. (2015)
Laser Scanning Microscope	Schneider et al. (2012)
Digital Image Correlation - Digital Camera	Speranzini and Agnetti (2014)
Ultrasonic testing with non-linear acoustic waves	Karlsson et al. (2018) Persson et al. (2020)

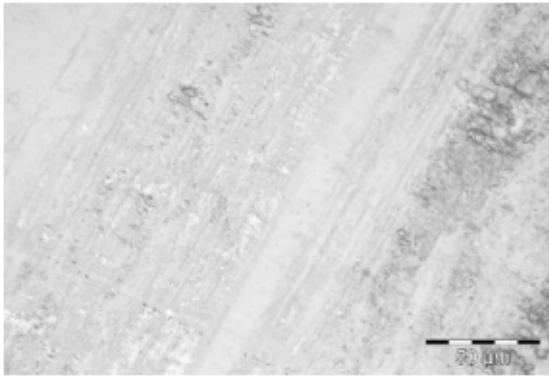


Figure 3.11: Optical microscope image of the external surface of weathered glass (Zammit and Overend, 2010).

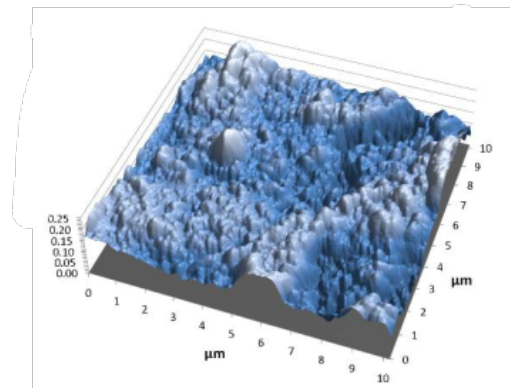


Figure 3.12: 3D surface map of the external surface of weathered glass (Zammit and Overend, 2010).

with optical microscope and with atomic force microscope, respectively. The small size of the area that can be scanned with an atomic force microscope, makes it difficult to assess quantitatively the flaws on weathered glass since it is likely that only a part of a flaw will be visible (Overend and Zammit, 2012).

Two researchers used several devices in order to compare and evaluate their efficiency according to different criteria. First, LINDQVIST (2013) conducted tests using the following equipment:

- A confocal microscope (Zeiss LSM710)
- A scanning electron microscope (SEM, FEI XLF30-FEG)
- A digital holographic microscope (DHM, Lyncée Tec SA)
- A mechanical profilometer (Bruker)

LINDQVIST (2013) reported that the confocal microscope is a proper method for visual estimations, rough measurements and quick results. It provides a two-dimensional image of the glass surface and the only preparation that the specimen needs prior the measurement is cleaning. The SEM resulted in more illustrative depiction of the glass surface but the whole process could become time consuming due to the sample preparation that is required, namely the application of a conductive coating on the glass surface. On the other hand, the DHM and the profilometer can provide a three-dimensional profile of the glass but only in a considerably small area compared to the other methods. Therefore, a limitation of this method is that only small defects were detected since larger or deeper ones were not in the capabilities of the equipment. Finally, LINDQVIST (2013) concluded that the confocal microscope prevailed over the other methods due to the minimal preparation and time that was required to obtain measurements and the size of glass that can be tested.

In the second study, Kwan (n.d.) examined the surface of new, artificially aged and naturally aged glass, in order to predict its glass strength, with the following methods:

- Visual inspection
- Optical microscope
- Innowep's Traceit<sup>®</sup> mobile 3D optical profilometer
- Nanovea's Chromatic Confocal profilometer

Kwan reported that the visual inspection was not a reliable method for detecting flaws on artificially aged glass but its efficiency increased when silvering was applied to the glass surface. Visual inspection without silvering was proved unreliable for naturally aged glass, whose flaws were smaller. The measurements made with optical microscope gave accurate strength predictions as long as the found flaws were large. When the flaw had a relatively small depth, the predicted failure strength was considerably overestimated. Furthermore, the small flaws on naturally aged glass were not detectable



Figure 3.13: The influence of the viewpoint on visual detectability: inwards view, high viewpoint (top); inwards view, low viewpoint (bottom) (Haldimann, 2006).

with optical microscope. Finally, between the two profilometers that he used, the measurements with Innowep's Traceit<sup>®</sup> resulted in strength predictions close to the actual strength of glass and he recommended the use of this equipment in future research on weathered glass.

Kwan recommended also the investigation of the effectiveness of visual inspection for flaw detection on large glass panels, such as windows. In this case, the flaws are likely to be sufficiently large and thus visible, in contrast with those on the small glass samples used in his experiments. The Canadian Glass standard Board (2017) provides a guide directed mainly to the glass suppliers, for defect detection. According to those standards the observer must examine the glass specimens from a distance of 3 meters. A list of acceptable defects is then provided in order to approve or discard the examined specimens. Haldimann (2006) conducted such tests with four different inspectors evaluating the surface condition of several specimens (see Figure 3.13). In that research, a threshold for the visual detectability was reported which is translated into a depth of 40 micrometers.

### 3.7.2. Selection of equipment

Each one of the devices mentioned in Table 3.2 has different characteristics and it gives different results. The field of view, the magnification, the resolution of the given image and the duration of the scanning process are only few of the parameters that are considered when choosing equipment for non-destructive tests. Therefore, it is of major importance for each researcher to develop a list of requirements for the scanning device before selecting the most appropriate one.

The most important selection criteria for the scanning equipment of this project are:

- **Availability:** The most crucial selection criterion is the availability of the equipment. The equipment considered in this project is based on what is available in the laboratories of TU Delft. In addition, equipment which was recommended in previous studies is also examined in case its use is feasible.
- **Scanning duration:** The duration of the scanning process is important either when the surface area is large or when the surface area is small but a large number of panels is about to be tested.
- **Scanning area:** The aim is to obtain an impression of the surface condition of a glass panel.

Table 3.3: Matrix for scanning equipment selection based on multiple criteria.

Equipment \Criteria	Availability	Time	Resolution	Area	Output
Keyence VHX5000 digital microscope	+ <sup>1</sup>	+	++	-+	+
Keyence VHX7000 digital microscope	+	+	++	-+	+
Nanovea ST500 Ultrafast Large Area Profilometer	-	+	+	++	-+
Traceit® Profilometer	+	+	+	+	+
LEXT OLS3100 Confocal laser scanning microscope	+	+	++	-	-+

<sup>1</sup> (+) = sufficient, (-) = insufficient, (-+) = neutral

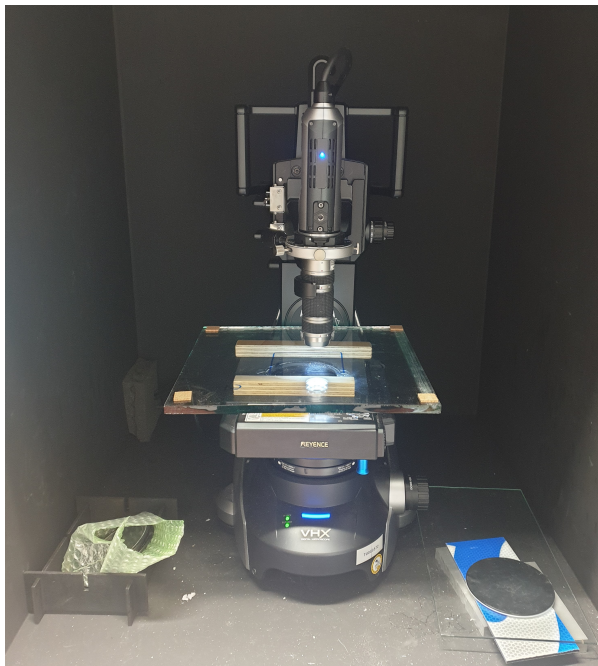


Figure 3.14: Digital Microscope Keyence VHX7000 (Faculty of Architecture, TU Delft)

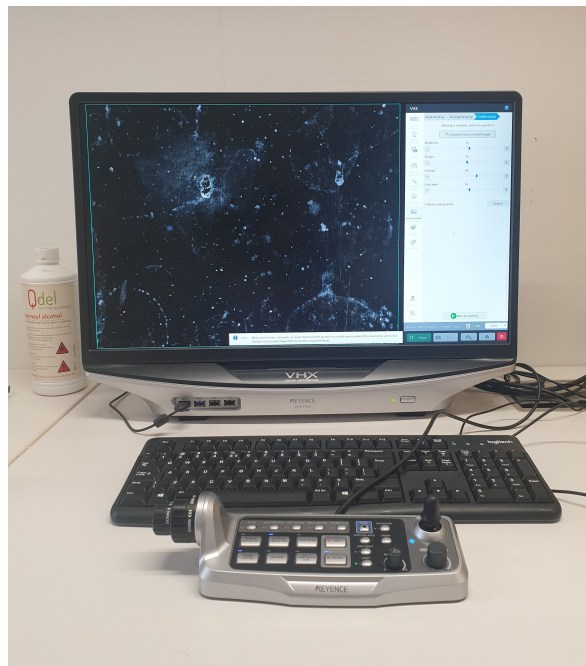


Figure 3.15: The monitor of the digital microscope Keyence VHX700

However, it is almost impossible to scan a complete panel at high resolution. Therefore, only the locations of interest will be scanned. The size of the field of view must be at least in the order of magnitude of millimeters.

- Precision: Since the field of view must have dimensions of several millimeters, a precision of  $\pm$ few microns is considered acceptable.
- Outputs: The output of the scanning process could be an image, from which the measurements must be taken by the operator. Alternatively, the size of the defect could be measured automatically and the result is given as a number to the user. Both cases are acceptable but the preference of the researcher lies on the second one. In this way, the human error is excluded from the measurements and the results can be imported directly in a calculation sheet or software for further processing.

Based on the defined set of selection criteria, the Table 3.3 was created to compare the several scanning devices. Most of these devices are available in the TU Delft and the rest are recommended in previous research (Kwan, n.d.). Among this equipment, the digital microscope from Keyence VHX7000 was chosen for the initial defect detection. This microscope is available at the Faculty of Architecture of TU Delft and it has been used before for similar purposes (see Figures 3.14 and 3.15). It provides two-

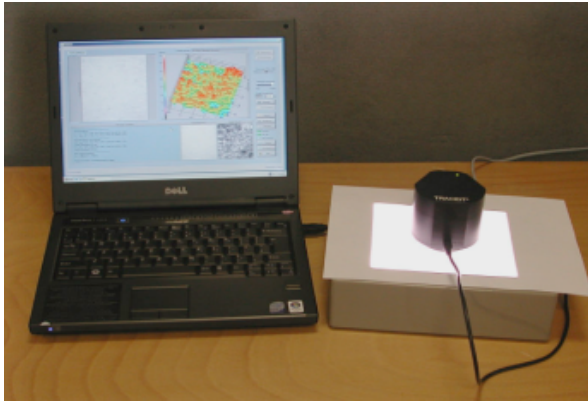


Figure 3.16: Traceit<sup>®</sup> mobile 3D profilometer (Innowep GmbH, n.d.).

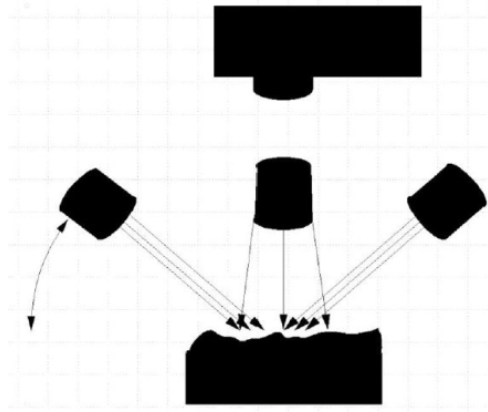


Figure 3.17: Working principle: measuring head with three white lights (Innowep GmbH, n.d.).

dimensional images of the glass surface in an acceptable period of time. The main limitation that this device imposes regards the maximum size of the tested specimen, which must fit on the stage under the microscopic lens.

The mobile 3D optical profilometer Traceit<sup>®</sup> was provided by Innowep GmbH for use in this project. After a training program given by Innowep's specialists, the researcher became able to use Traceit<sup>®</sup>. The device was brought to TU Delft for use in the non-destructive tests. The most important features of this equipment which made it attractive for this project are the following:

1. Mobile design: Its design allows its use for measurements both on-site and in the laboratory.
2. Specimen's size: It does not have any limitation regarding the size of the tested specimen since it can be placed directly on the examined surface and at the location of interest.
3. 3D measurements: The measuring head with three white lights makes topology measurements feasible. Therefore, it was examined whether it is possible to measure also the depth of the defects apart from their length and width (see Figures 3.16 and 3.17).

### 3.8. Conclusions

In this chapter, the basic knowledge about the strength of glass, its defects and their correlation through the theory of LEFM was introduced. The detrimental effect that the surface flaws have on the strength of glass was underlined, since they can cause the fracture at locations which do not coincide with the locations of maximum stress. Strength predictions can be obtained based on the stress intensity factor but such attempts are rarely found in the existing literature.

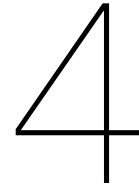
The experimental methods for determining the strength of glass were also described. The most commonly used testing method is the Coaxial Double Ring test. Between the two standards which describe that methodology, the American ASTM C1499-09 (2013) and the European NEN-EN1288-5 (2000), the former is mostly followed due to the simpler equipment that it requires. Thus, this method is chosen for this research as well. The phenomenon of stress corrosion could have significant influence on the experimental strength data if the testing conditions are not controlled (loading rate and the humidity).

The large uncertainties in the experimental strength data of glass are tackled with statistical processing of the results. The existing literature suggests that the Weibull distribution fits usually better the test data, compared to other distributions. However, for each testing series, the most suitable probability distribution function should be found, based on the goodness of fit of the strength data. The Weibull theory can be used also for the extrapolation of the strength of large glass elements from that of small specimens, since the destructive testing of them is neither practical nor economical.

Furthermore, this chapter reviewed the scanning equipment used in previous studies, with the optical microscopy prevailing among others. This is attributed to the simplicity of its use and its existence in almost all the laboratories rather than to the high accuracy of its measurements. Even though with other scanning devices more detailed results can be obtained, their performance is usually limited by the small size of the area that can be scanned or the time consuming sample preparation that they require.

Overall, it was revealed that the correlation between the bending strength of glass and its surface condition lacks experimental investigation. Therefore, this research will examine the strength of naturally aged annealed glass, with defects introduced over the service life of a facade panel, through both non-destructive and destructive tests. Finally, the influence of the "size effect" on the strength of weathered glass will be investigated, since no recent relevant research exists in this field.





# Experimental investigation

## 4.1. Introduction

This chapter presents the experimental investigation carried out on new and weathered soda-lime silica annealed glass specimens of two different dimensions. The study includes non-destructive tests with a digital microscope and a mobile optical profilometer on a 55-year-old glass, and destructive Coaxial Double Ring (CDR) tests. The experimental study aimed to investigate the following:

1. The surface damage on weathered glass: With equipment suitable for studying the geometry and the size of the surface defects, the damage on the internal and the external surfaces of weathered glass was assessed and the possible "critical" flaw was investigated.
2. The effect of weathering on the strength of glass: As stated in Section 3.4, the strength of glass is governed by its defects and thus the external surface, which theoretically is more damaged than the internal, was expected to have lower strength. Through CDR tests, the surface strength of both surfaces of weathered glass was calculated and compared to that of new glass.
3. The size effect on the strength of weathered glass: According to previous observations on new glass, the strength of glass reduces as the loaded area increases (Section 3.6.2.2). Thus, specimens of two different dimensions were tested, with two different sets of loading and supporting rings.

The tested specimens are described in Section 4.2 and the methods for the non-destructive and destructive tests in Section 4.3. A summary of the results of all the tests is presented in Section 4.4. In Section 4.4.3, images of the defects found on the internal and on the external surface of the 55-year-old glass, along with an indication of their size as measured with Traceit<sup>®</sup>, is provided. The flaw characterization on weathered glass is a valuable outcome of this research, since such data is rare in the existing literature. The dimensions of all the specimens and the test results are presented analytically in the Appendices B and D, respectively.

## 4.2. Test specimens

The examined glass was taken from the interactive, curtain wall facade of the office building at Koningskade 4 in The Hague, in the Netherlands (see Figures 4.1 and 4.2). The building was originally designed in 1967, so the age of the glass elements is approximately 55 years. The tested specimens of uncoated annealed glass were cut from the single outer panes of the double skin facade, which is illustrated in the detail in Figure 4.3, provided by Scheldebouw B.V.<sup>1</sup> These glass elements, exposed to environmental influences (temperature, humidity, abrasion etc.) for 55 years, were expected to give an impression of the damage that a glass facade panel undergoes during its service life.

<sup>1</sup>Scheldebouw B.V. is the manufacturer of the examined facade.



Figure 4.1: Location of the building from which the examined glass was removed.



Figure 4.2: The office building at Koningskade 4, the Hauge.

According to Scheldebouw B.V., the facade was made from "ordinary float glass", so it was produced on a tin bath. However, it was not possible to distinguish the air from the tin side of this glass with the tin detector. An X-Ray Fluorescence (XRF) analysis indicated that the composition of this glass is aligned with that of float glass, but no traces of tin were found. Perhaps the damage induced over the service life of the facade, removed any tin residues from its surface. Such phenomenon was previously observed in the research of Datsiou and Overend (2016), where the extensive weathering prevented the characterization of the tin side. The results of the XRF analysis are presented in Appedindix A.

Among the several types of glass elements which are used in the building industry, facade panels were chosen since they are the most commonly found. Currently, during building renovations, many windows and facade panels made of soda-lime silica annealed float glass are discarded. Therefore, only this type and composition of glass are in the scope of this research.

The size of the tested specimens was limited by the requirements of ASTM C1499-09 (2013) about the Coaxial Double Ring (CDR) tests. In particular, they were chosen to be large enough to exclude the influence of the edges on the glass strength, but also small enough to comply with the aforementioned standards. Thus, the large facade panels were divided into square elements of 250mm x 250mm x 10mm and 450mm x 450mm x 10mm. The specimens were manually cut by Hermans Groep, as illustrated in Figure 4.4. New, as-received glass with the same thickness and dimensions, provided by Versteeg Zichtbaar in Glas, was tested as well for comparison with the old glass.<sup>2</sup> It is stressed out that the microscopy examination implied another crucial size limitation, since the specimens must fit on the microscope stage. In this project though, that problem was eliminated by using the mobile profilometer Traceit<sup>®</sup>.

Each testing series included at least 20 specimens in order to tackle the great variability in the strength data of glass. In this way, even if some of the tests were invalid, there would be still sufficient test results for statistical processing. Thus, eight series of tests were performed, with 171 specimens tested in total. An overview of the testing series is presented in Table 4.1. For the weathered glass, the "external" surface is the one which was exposed to the natural environment while the "internal" surface was facing the inside of the building during the service life of the facade panel. For the testing series with the new glass, the air and the tin sides were distinguished using a tin-side detector. The thickness at the mid-points of the four edges of each specimen was measured with a caliper and the thickness at the middle of the specimen was calculated as the average of these four measurements. The exact dimensions and the thickness measurements of each specimen can be found in Appendix B.

<sup>2</sup>An XRF analysis was performed on that glass as well and the results are presented in Appendix A.



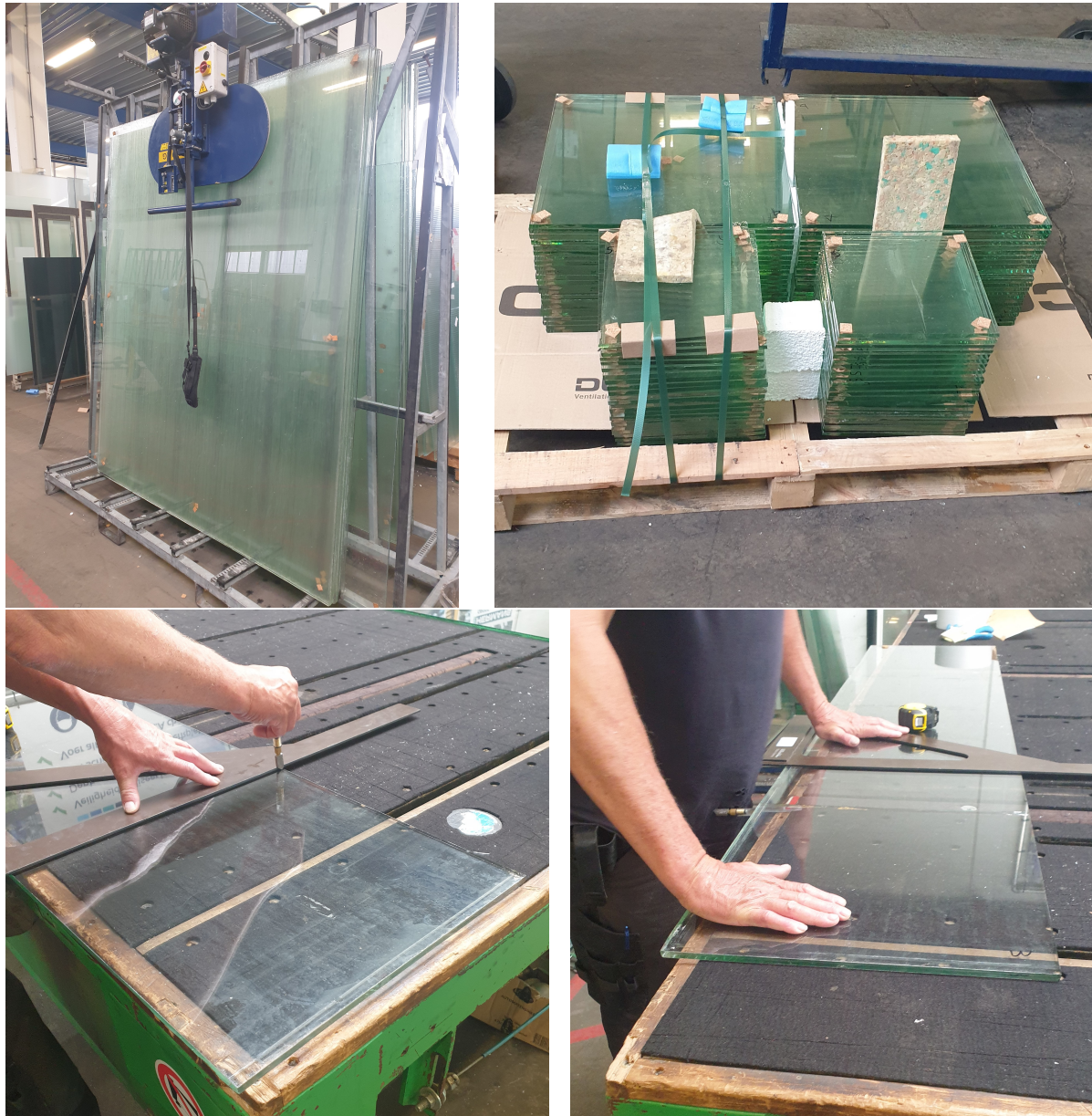


Figure 4.4: Cutting process of the large specimens at Hermans factory.

Table 4.1: Overview of the specimens number and dimensions of each testing series.

Series name	Type of glass	Dimensions (mm)	Surface in tension	Amount of spec.
NA - 1a	Weathered	250x250x10	External	21
NA - 1b	Weathered	250x250x10	Internal	23
NA - 2a	Weathered	450x450x10	Internal	24
NA - 2b	Weathered	450x450x10	External	22
AR - 1a	New	250x250x10	Tin side	20
AR - 1b	New	250x250x10	Air side	20
AR - 2a	New	450x450x10	Tin side	20
AR - 2b	New	450x450x10	Air side	21

## 4.3. Test methods

### 4.3.1. Microscopy examination before the CDR tests

An initial microscopy examination was performed to obtain information about the surface condition of the weathered annealed glass, after fifty-five years of exposure to the natural environment. More specifically, the main goals of this investigation were:

1. To find appropriate equipment for examining the surface of naturally aged glass.
2. To study the type and amount of damage on the surface of naturally aged glass.
3. To distinguish the external and the internal side of the specimens.
4. To assess the effect of weathering on glass by comparing the amount and type of damage on the two sides of the specimens.
5. To identify and measure the critical flaw in the tested area in order to correlate it later on to its strength, through the theory of LEFM.

An overview of the scanning equipment which was previously used for flaw detection on glass by other researchers was already presented in Section 3.7.1. As explained in the same Section, the equipment chosen for this project is limited to the following two devices:

- Keyence digital microscope VHX7000
- Innovep's Traceit<sup>®</sup> mobile 3D optical profilometer

It is worth to mention here that during this investigation, only the area inside the loading ring was examined, instead of the entire surface of the specimens. In a CDR test, the maximum stress is developed in that area and the testing standards provide a formula for the calculation of the stress in that area. The fracture of glass though, does not always coincide with the location of maximum stress. In particular, even if the stresses are maximum inside the loading ring, a larger flaw outside that ring can cause failure at stress lower than the maximum. However, the state of stress outside the loading ring is unknown. Therefore, fractures in that area are considered invalid because they cannot be interpreted directly. Usually, in such cases a finite element model is created for the estimation of the fracture stress outside the loading ring. Nevertheless, in this project, only the surface area inside the loading ring was studied, since only for that area direct conclusions can be made.

#### 4.3.1.1. Scanning process with the digital microscope

For the microscopy examination, the specimens were cleaned and placed under the microscopic lens on the horizontal stage. In particular, the common alcoholic cleanser was not sufficient to remove all the residues from the glass surface (see Figure 4.5) and thus a cleaning detergent suitable for glass was used. The stage was then moved in the x and y direction to observe as larger as possible part of the specimen at magnifications from 50x to 200x. Finally, at the locations of interest, namely the ones which included larger scratches or digs, images of the examined surface were taken. These images were local, focused on a part of a defect, or wider, created through the stitching of many smaller images.

After the examination of the first surface of the specimen, the other surface was examined under the microscopic lens. The examination of that surface was performed according to the same procedure. Based on the amount and type of damage that was found on the two surfaces, the internal and the external sides of the specimens were distinguished. The results of this process can be found in Section 4.4.1.

#### 4.3.1.2. Scanning process with Traceit<sup>®</sup>

The scanning process with Traceit<sup>®</sup> was simpler than that with the digital microscope. The profilometer was connected to a laptop, on which the required software was already installed and it was ready for use (see Figure 4.6). The software is user friendly, with simple interface, as illustrated in Figure 4.7.

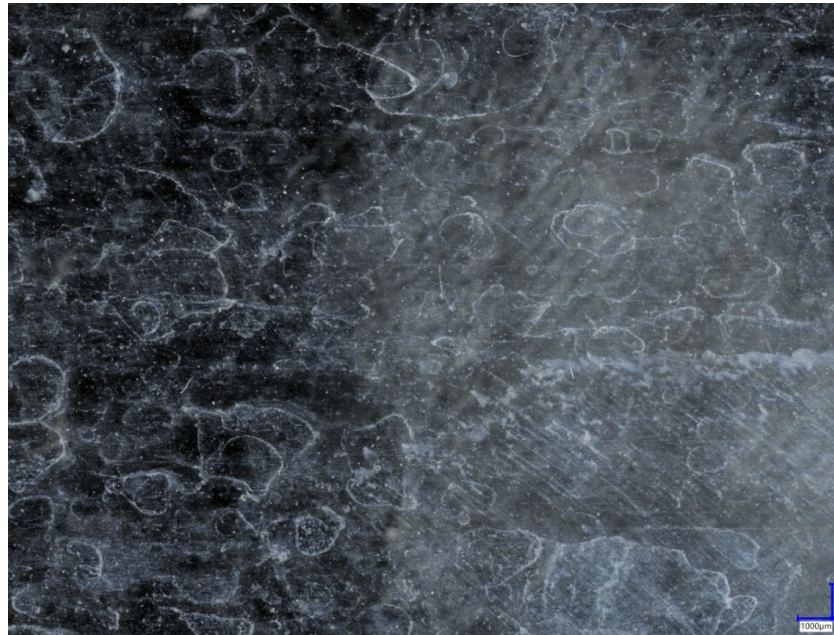


Figure 4.5: Image of the glass specimen cleaned with alcohol (left part) and uncleaned (right part), as captured with Keyence VHX7000.

The greatest advantage of Traceit<sup>®</sup> lies on its design itself, since it is a small and light device (it can fit in the user's hand) and it can be placed directly on the specimen. The user has more control over the scanning process since he/she can move the profilometer directly from one position to another, without changing any settings.

To increase the efficiency of Traceit<sup>®</sup> in the scanning process of glass, the "transparency unit" provided also by Innowep GmbH, was used. That unit functioned as an additional light source which was positioned below the specimen. In this way, images with both top lighting (from the Traceit<sup>®</sup>) and bottom lighting (from the transparency unit) were taken.

#### 4.3.1.3. Measurements with Traceit<sup>®</sup>

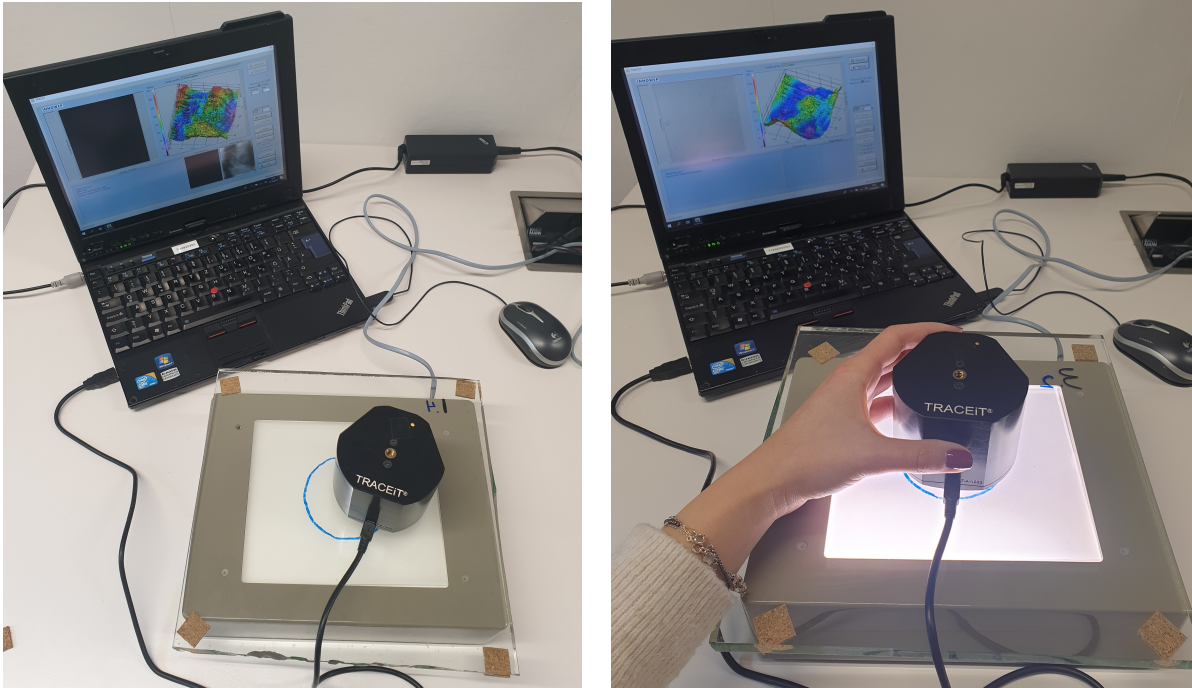
During the non-destructive tests, the cleaned surface of the glass specimens was examined with the live camera of Traceit<sup>®</sup>. When the location of interest was identified, the profilometer was held stable for several seconds and an analysis was performed. The output of this analysis was the surface roughness parameters along with a 3D height map of the surface topography of an area 5mm by 5mm. Furthermore, surface images with top lighting (denoted as "visual impression" in the software), with transmitted lighting, and a 2D height map were obtained.

From these outputs, quantitative data were derived for the surface damage of glass. In particular, from the "visual impression" images, the area of the defect was identified and then from the 2D height map, the height variation within that area was measured. In this way, depth and width measurements of the larger defects were taken, as illustrated in Figure 4.8. The results from the experimental investigation with Traceit<sup>®</sup> are reported in Section 4.4.1. In the same Section, a study on the reliability of the depth measurements with Traceit<sup>®</sup> is presented.

#### 4.3.2. Coaxial Double Ring tests

After the microscopy examination on the weathered glass, the specimens of new and old glass were prepared for the CDR tests, according to the American standards, ASTM C1499-09 (2013)<sup>3</sup>. In particular, both sides of the glass specimens were covered with a thin adhesive layer, so as to retain the

<sup>3</sup>The principles of this testing method are described in Section 3.5.1.



(a) The transparency unit is off, analysis only with top lighting.

(b) The transparency unit is on, analysis with transmitted light.

Figure 4.6: Experimental setup with Traceit®

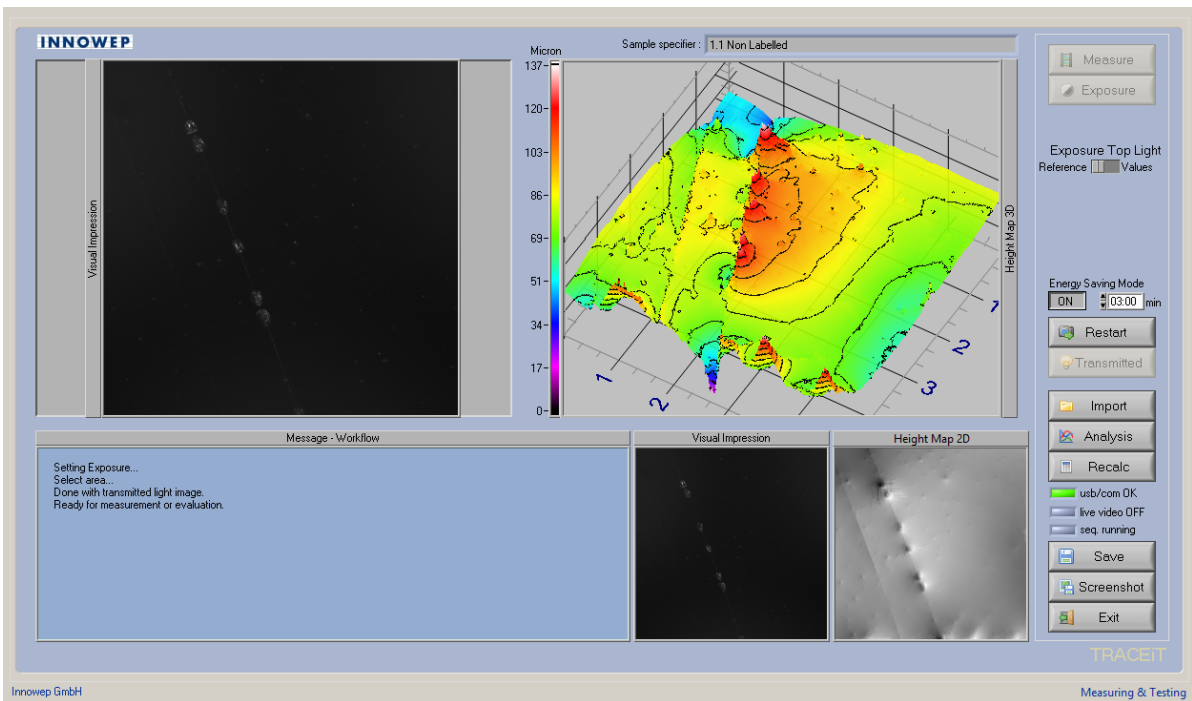
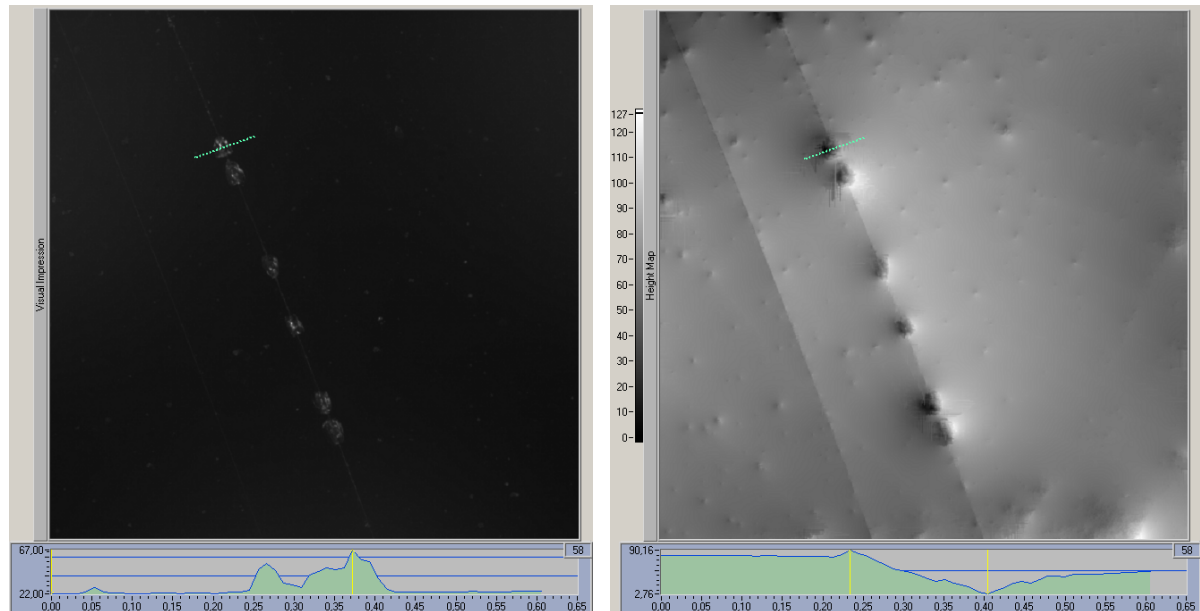
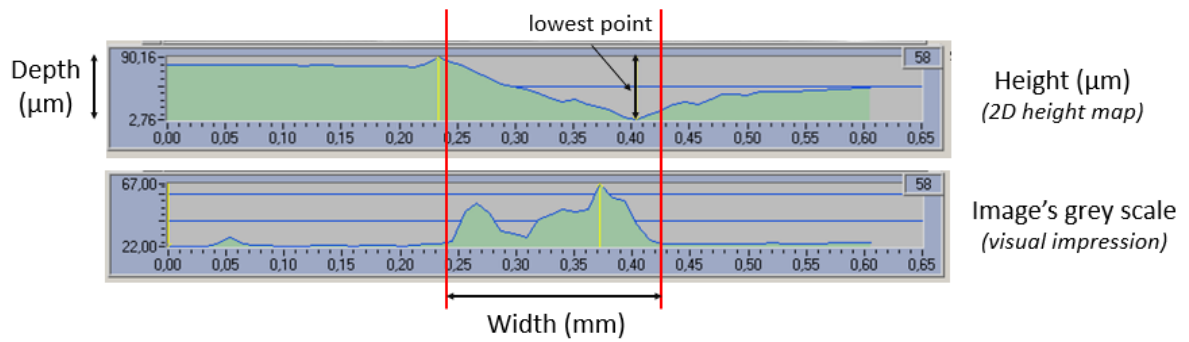


Figure 4.7: Screenshot of the main interface of Traceit® software.



(a) Screenshot of Traceit® software where the "visual impression" is visible.

(b) Screenshot of Traceit® software where the 2D height map is visible.



(c) Manual depth and width measurements.

Figure 4.8: Process of measuring the depth and the width of flaws with Traceit®.

fragments in place after fracture and to aid the post-failure fractography analysis. Figure 4.9 illustrates a sketch of the testing setup for the small and large specimens.

The CDR tests were performed with the materials testing machine Zwick Z100, which is available at the Faculty of Mechanical, Maritime and Materials Engineering of TU Delft. The test software testXpert® III was used. The output of that software was a force-displacement diagram, based on which the equibiaxial strength inside the loading ring was calculated, according to the formula (4.1). The specimens of all the testing series were subjected to load with a displacement rate 5mm/min. It is stressed out that the loading and the supporting rings were positioned in a way that they were coaxial. Figures 4.11 to 4.13 illustrate the testing machine and the testing setup for the small and large specimens.

$$\sigma_f = \frac{3F}{2\pi h^2} \left[ (1 - \nu) \frac{D_s^2 - D_L^2}{2D^2} + (1 + \nu) \ln \frac{D_s}{D_L} \right] \quad (4.1)$$

Where,

$F$  is the breaking load in N,

$h$  is the thickness at the middle of the specimen,

$\nu$  is the poisson's ratio (for soda-lime silicate glass,  $\nu=0,23$  (ISO1288-1, 2016)),

$D_s$  is the diameter of the supporting ring,

$D_L$  is the diameter of the loading ring and

$D$  is the diameter of a circle that expresses the characteristic size of the plate and it is calculated as follows:

$$D = \frac{l}{0.90961 + 0.12652 \frac{h}{D_s} + 0.00168 \ln \frac{l - D_s}{h}} \quad (4.2)$$

and,

$$l = 0.5(l_1 + l_2) \quad (4.3)$$

Where,

$l_1$  and  $l_2$  are the lengths of specimen's edges and the other symbols are as defined for Equation (4.1).

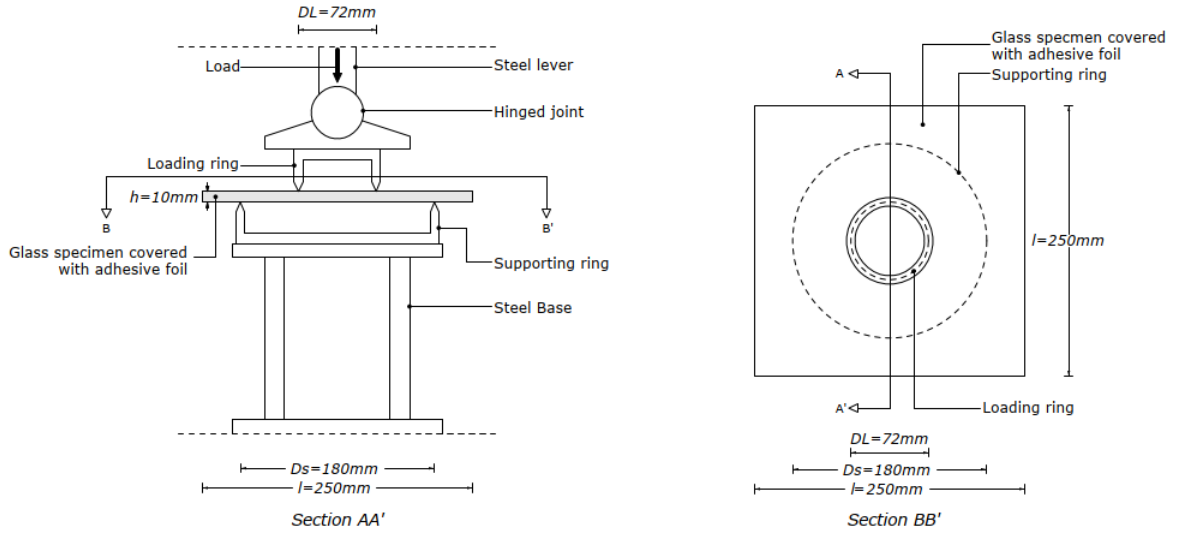
The dimensions of the rings were chosen in accordance to the recommendations of the ASTM C1499-09 (2013), based on the dimensions and the thickness of the specimens, as presented in Table 4.2. It can be seen that in the case of the large specimens, the overhang size and the ring diameter ratio  $D_L/D_s$  do not comply with these recommendations. However, according to the Note 5 of ASTM C1499-09 (2013), the equation (4.1) is valid for non-dimensionalized overhang  $(D/D_s)/h$  up to 24, which is higher than the overhang in this case which is 23,6. In particular, for specimens scored from larger panels with poor edge finishing, a ratio over 12 is recommended. Such large overhangs though, could alter the stress distribution, which might lead to different strength measurements than those in tests with smaller overhangs. Nevertheless, it was decided to proceed with the dimensions indicated in the Table 4.2, since these were the available rings at TU Delft. For the same reason, the false  $D_L/D_s$  ratio was also accepted.

#### Stress corrosion

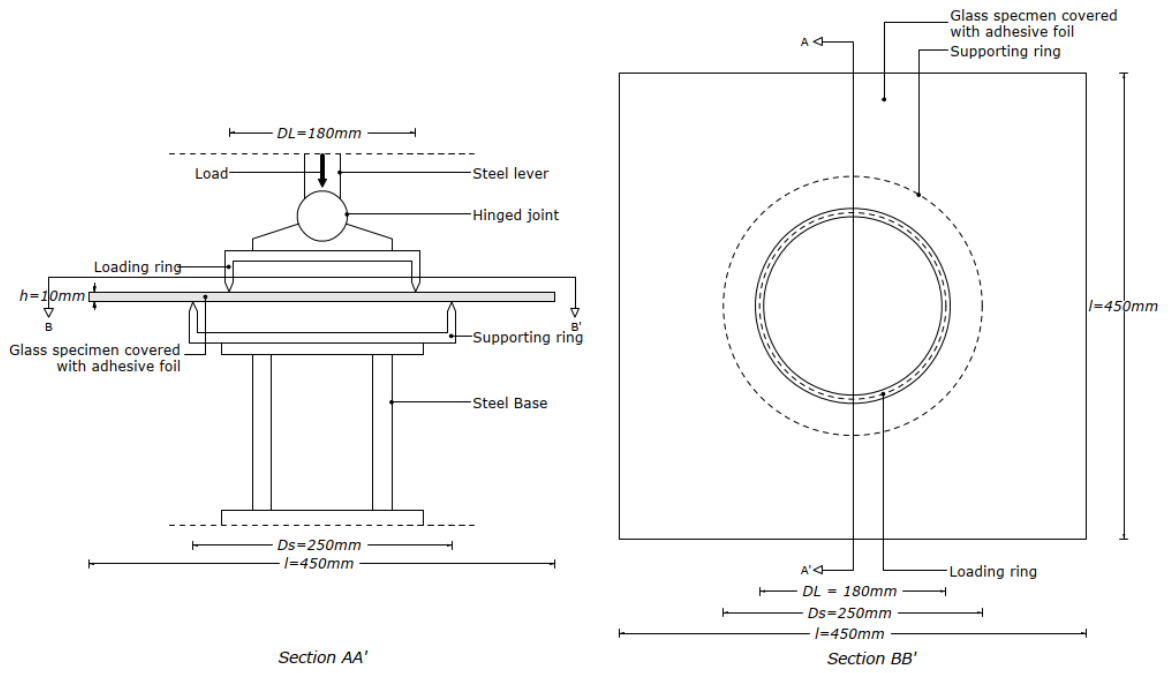
The effect of stress corrosion, which is explained in Section 3.4.2, could become of high influence for the test results, since the specimens failed at different times and consequently, some of them experienced the stress for longer period. To account for that, the calculated failure stresses  $\sigma_f$  with the equation (4.1) were normalised to an equivalent stress  $\sigma_e$  for a reference period of 60 seconds, according to the formula (3.3). Furthermore, the adhesive layer on both sides of the specimens prevented the surface of glass from any interaction with the environment.

### **4.3.3. Microscopy examination after the CDR tests**

After the destructive CDR tests, a post-failure analysis of the specimens was performed. For that analysis, the Keyence VHX700 digital microscope was used, since microscopes are used in principal



(a) Setup for the specimens 250x250x10mm.



(b) Setup for the specimens 450x450x10mm.

Figure 4.9: Sketches of the CDR testing setup.



Figure 4.10: Materials testing machine Zwick Z100 at the Faculty of 3ME, TU Delft.

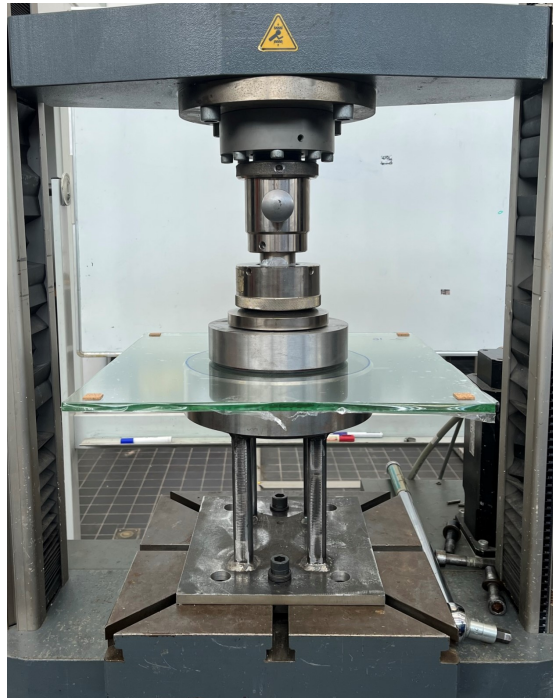


Figure 4.11: Experimental setup for the CDR tests on the large specimens.

for such purposes. The main goals of the post-failure examination were:

1. Identification of the fracture origin, which became known after the CDR tests.
2. Identification and analysis of the size and shape of the "critical flaw", along the fracture origin.<sup>4</sup>

Due to the complexity of the fractured pattern, this process could become very time consuming. For that purpose, only some specimens were further analysed after fracture. These specimens were the ones which broke at the expected "critical flaw", namely the flaw which was detected with Traceit® and was considered critical, or specimens which broke at very low or high stresses. The results of the post-fracture analysis are presented in Section 4.4.5.

## 4.4. Test results

### 4.4.1. Results of Keyence digital microscope VHX7000

The surface of weathered glass was studied with the Keyence VHX7000 digital microscope. Figure 4.14 illustrates an example of the damage observed on the 55-year-old glass, at magnification 200x. Unfortunately, due to the fine dimensions of the defects, it was not possible to measure their depth with the digital microscope. The 3D image composition function was used for that purpose but the depth was still not clearly shown.

By scanning the two sides of the same specimen, the internal and the external surfaces of the glass were distinguished. In particular, the most heavily damaged side was presumed as external while the other as internal. That distinction was easy to make, due to the noticeable difference in the amount of damage found on the two surfaces. An example of a specimen whose two sides were characterised is presented in Figure 4.15. It can be seen that although the presumed as external surface is not heavily damaged, there are clearly more signs of defects on it than on the surface presumed as internal.

<sup>4</sup>These data are used in Chapter 6 for the evaluation of the methodology for detecting the "critical flaw" and predicting the failure strength of glass.

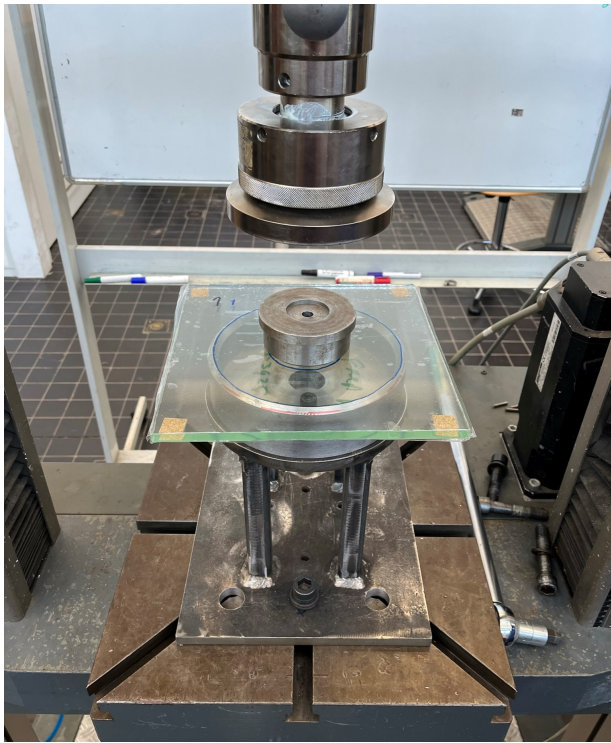


Figure 4.12: Experimental setup for the CDR tests on the small specimens.

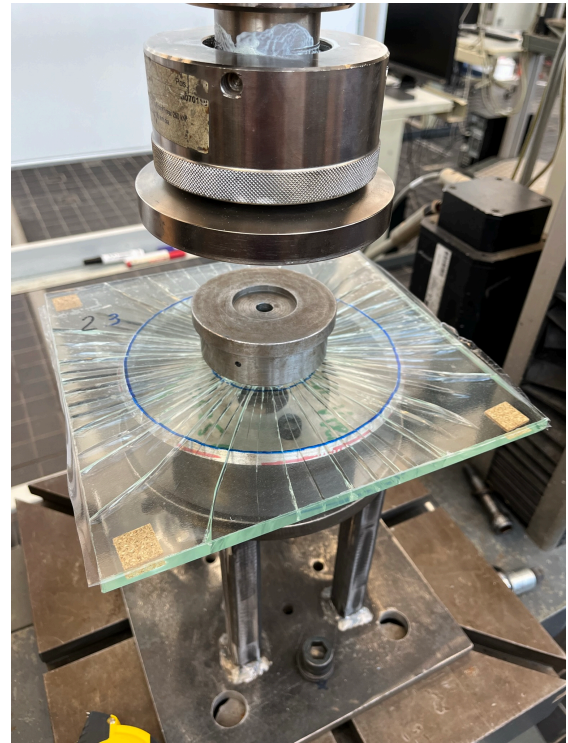


Figure 4.13: Small specimen after fracture in a CDR setup.

#### 4.4.2. Results of Traceit®

To the best of the author's knowledge, this research is the first application of Traceit® for analysing the surface of weathered annealed glass. The greatest challenge of this process was the highly reflective and transparent nature of the material itself. By using the default settings of Traceit® ("visual impression" with only the top lighting on), the larger defects on the surface of glass were observed. On the contrary, with the top light of the digital microscope, much more defects on the glass surface were revealed. That observation generated concerns about the effectiveness of Traceit® in capturing the fine defects on the surface of weathered glass.

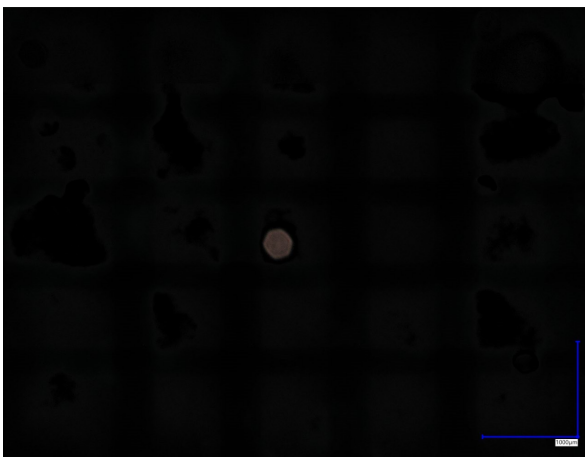
The additional light source provided by the transparency unit (transmitted light), revealed more "pit" type defects on the surface of glass, as the digital microscope did, but not always more scratches. Nevertheless, the external and the internal sides of the specimens were clearly distinguished with Traceit®, even without the transmitted light. Figures 4.16 and 4.17 illustrate a defect as captured by Traceit® with top ("visual impression" option) and transmitted light, respectively.

##### 4.4.2.1. Image processing

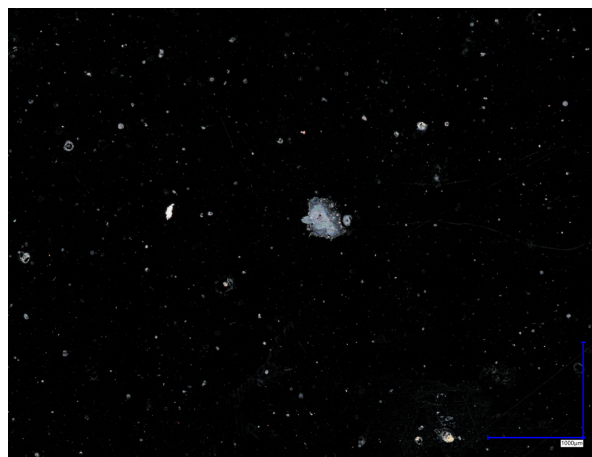
The aforementioned observations led to the hypothesis that probably Traceit® is able to capture the defects on the glass surface with more detail but the output image does not reveal them. To investigate further this hypothesis, the images captured with the default settings of Traceit®, namely the "visual impression" images, were processed for improving their quality. This was initially performed with the "Paint.Net" software, by adjusting the "auto-level", the contrast and the brightness of the images. Figures 4.16 and 4.18 illustrate an image as captured by Traceit® before and after the processing, respectively. Evidently, the results of the image processing confirmed the hypothesis that although the fine defects on the surface of glass were not visible with the live camera, Traceit® can capture them. Therefore, the processed images can provide similar information about the surface damage of glass as the digital microscope, without the need of laboratory conditions and without the size limitation that the microscopy stage imposes.



Figure 4.14: Micrograph of the 50-year-old tested glass, taken with the Keyence VHX7000.



(a) Surface presumed as inner.



(b) Surface presumed as outer.

Figure 4.15: Microscopic images of the two sides of one specimen at a magnification of 200x.

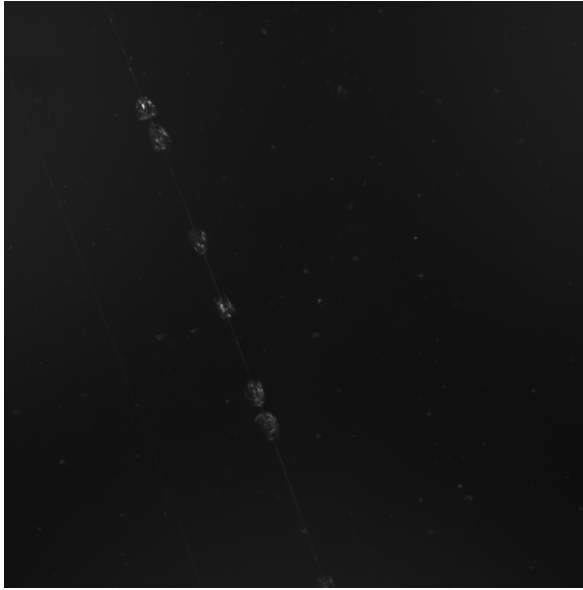


Figure 4.16: Example of an image taken with the default top lighting option of Traceit®

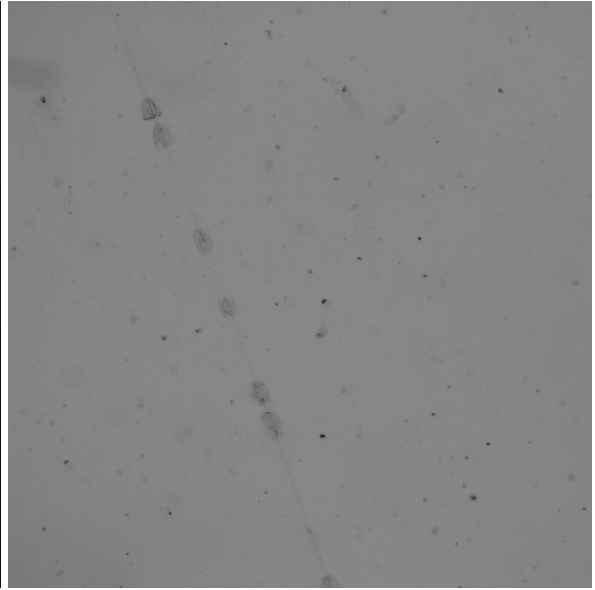


Figure 4.17: Example of an image taken with the transmitted lighting option of Traceit®

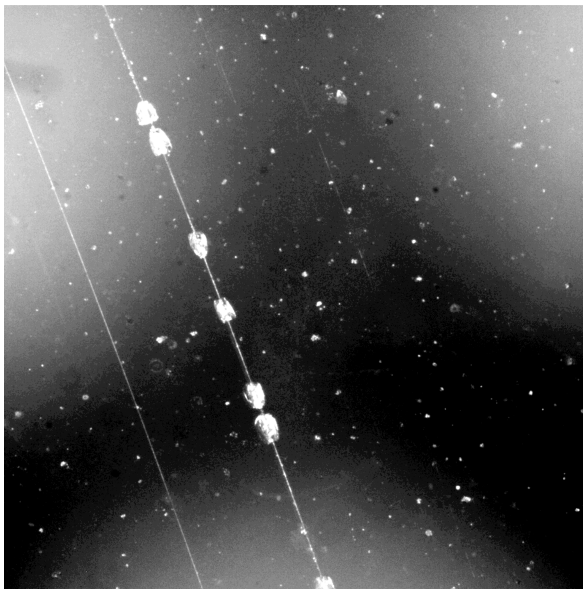


Figure 4.18: The "visual impression" image after the edit in Paint.Net.

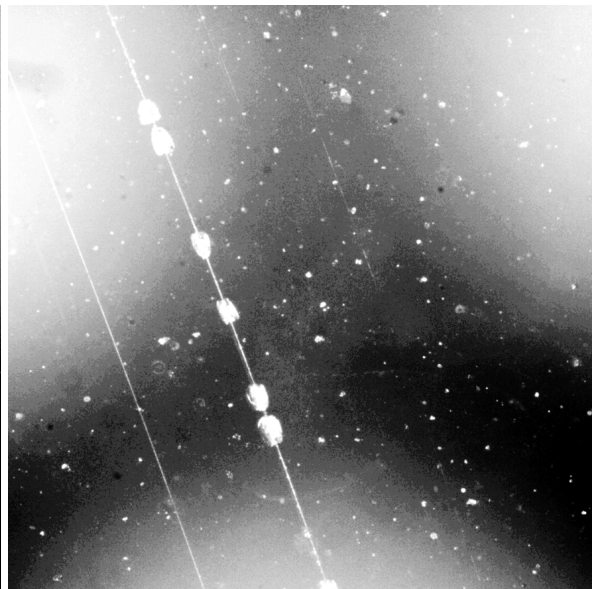


Figure 4.19: The "visual impression" image after histogram equalization.

Table 4.2: Verification of specimen and ring dimensions according to ASTM C1499-09 (2013).

Series		NA-1a, NA-1b	NA-2a, NA-2b
Specimen's thickness	$h$ (mm)	10	10
Width	$l_1$ (mm)	250	450
Length	$l_2$ (mm)	250	450
Equivalent diameter	$D$ (mm)	270	486
Expected eq. biaxial strength	$\sigma_f$ (MPa)	100	100
Young's Modulus	$E$ (Mpa)	70000	70000
Diameter of supporting ring	$D_S$ (mm)	180	250
Diameter of loading ring	$D_L$ (mm)	72	180
Verification			
Max specimen's thickness	$h_{\max}$ (mm)	18	25
Min specimen's thickness	$h_{\min}$ (mm)	6	8
Thickness check		OK	OK
$(D-D_S)/h$		9	23,6
Overhang size check ( $2 < x < 12$ ):		OK	FALSE
$D_L/D_S$		0,40	0,72
Ratio diameter check ( $0,2 < x < 0,5$ ):		OK	FALSE
$l_1/l_2$		1,00	1,00
Ratio edges check ( $0,98 < x < 1,02$ ):		OK	OK

The manual editing process of Traceit<sup>®</sup> images could become very time consuming when dealing with more than forty images, as in this project. Thus, an automated quality improvement of the images was achieved through the Image Processing Toolbox of MATLAB and the function "histeq" (histogram equalization). This function improves automatically the contrast of a grey scale image by using histogram equalization. More specifically, it re-distributes the image pixels in a more uniform way within the intensity spectrum of an image. The result of this processing can be seen in Figure 4.19. It was revealed that the "histeq" function results in an image with slightly less information than the image processed with Paint.Net but in significantly less time. Nevertheless, in both cases the image processing revealed the damage on the surface of glass which was not visible with the default settings of Traceit<sup>®</sup>.

#### 4.4.2.2. Depth measurements and reliability study

The size of the largest defect found on each specimen of weathered glass, as measured with Traceit<sup>®</sup>, along with their type, either scratch or dig, are presented in Table 4.3. The smallest defect had a depth of 19  $\mu\text{m}$  and the largest 161  $\mu\text{m}$ . These depths are aligned with the depths found in literature, which range from 20  $\mu\text{m}$  to 200  $\mu\text{m}$  (Schula et al., 2013). In fact, the majority (67%) of the measured defects, had a depth between 19  $\mu\text{m}$  and 63  $\mu\text{m}$ , 21% of the defects had a depth between 64  $\mu\text{m}$  and 104  $\mu\text{m}$  and the rest were deeper than 104  $\mu\text{m}$ .

Due to the high reflections that the material causes, the 2D height map image of Traceit<sup>®</sup>, from which the depth was derived, was not always clear. Furthermore, it was not possible to verify whether the taken measurements were reliable or not, since no other equipment was used. Therefore, a reliability study was performed in order to examine the precision of consecutive measurements of the same defect.

For the reliability study, a specimen with several defects on its surface, visible by human eye, was chosen. Three of these defects were selected and they were measured 10 times, at as much as possible the same location (See Figure 4.21). For the first five measurements, the Traceit<sup>®</sup> was placed on the specimen at an angle of 0° while for the other five measurements it was rotated by 90° (See

Table 4.3: Depth of the critical defects on each specimen, as measured with Traceit®.

NA-1a					NA-2b				
Spec.	Defect	$d(\mu\text{m})$	$d_{\min}$	$d_{\max}$	Spec.	Defect	$d(\mu\text{m})$	$d_{\min}$	$d_{\max}$
1.1	Scratch	<b>87</b>	82	92	3.1	Dig	<b>78</b>	73	83
1.2	Dig	<b>91</b>	86	96	3.2	Scratch	<b>39</b>	34	44
1.3	Dig	<b>86</b>	81	91	3.3	Scratch	<b>87</b>	82	92
1.4	Scratch	<b>34</b>	29	39	3.4	Dig	<b>104</b>	99	109
1.5	Scratch	<b>45</b>	40	50	3.5	Dig	<b>50</b>	45	55
1.6	Scratch	<b>63</b>	58	68	3.6	Scratch	<b>80</b>	75	85
1.7	Dig	<b>37</b>	32	42	3.7	Dig	<b>19</b>	14	24
2.1	Scratch	<b>25</b>	20	30	3.8	Scratch	<b>52</b>	47	57
2.2	Dig	<b>32</b>	27	37	3.9	Dig	<b>19</b>	14	24
2.3	Dig	<b>19</b>	14	24	3.10	Scratch	<b>59</b>	54	64
2.4	Dig	<b>52</b>	47	57	3.11	Scratch	<b>161</b>	156	166
2.5	Dig	<b>58</b>	53	63	3.12	Dig	<b>33</b>	28	38
2.6	Dig	<b>48</b>	43	53	4.1	Scratch	<b>71</b>	66	76
2.7	Scratch	<b>25</b>	20	30	4.2	Scratch	<b>51</b>	46	56
3.1	Scratch	<b>27</b>	22	32	4.3	Scratch	<b>111</b>	106	116
3.2	Scratch	<b>126</b>	121	131	4.4	Scratch	<b>33</b>	28	38
3.3	Dig	<b>50</b>	45	55	4.5	Dig	<b>50</b>	45	55
3.4	Scratch	<b>77</b>	72	82	4.6	Scratch	<b>41</b>	36	46
3.5	Scratch	<b>55</b>	50	60	4.7	Dig	<b>33</b>	28	38
3.6	Scratch	<b>43</b>	38	48	4.8	Scratch	<b>51</b>	46	56
3.7	Scratch	<b>147</b>	142	152	4.9	Scratch	<b>94</b>	89	99
					4.10	Scratch	<b>59</b>	54	64

Figure 4.20). Since Traceit® creates the surface height map by illuminating light at three different angles, by altering its orientation in relation to the defect, the influence of these lighting angles on the measurements was investigated.

All the measurements of the reliability study can be found in Appendix C. The results of the consecutive measurements for the Defect 1, which was the largest one, vary considerably. Since the measurements were taken manually, as described in Section 4.3.1, it is very likely that the human error contributed to the deviation among the measurements. Especially, the larger the defect, the more difficult it was to take measurements at the exact same location. In the results of the Defects 2 and 3 though, which were smaller, a smaller variation was noticed. In particular, a deviation of approximately  $\pm 5 \mu\text{m}$  for the depth and of around  $\pm 10 \mu\text{m}$  for the width was found. Based on this precision, a maximum and a minimum value for each depth measurement was calculated and it is presented in Table 4.3. It is worth noting that a variation in the width/depth ratios was observed which confirms that the depth is measured physically by Traceit® and that no software interpolation takes place for the derivation of the depths.

Finally, two interesting observations were made during this reliability study. First, the height maps were considerably improved (with less reflections) during the second series of measurements, in which Traceit® was placed at an angle of  $90^\circ\text{C}$ . Thus, when measuring with Traceit®, rotation of the device could improve the results. Secondly, a matte spray coating was applied on the specimen, aiming at reducing the reflections that the material causes. It turned out that due to the significantly small size of the defects, the spray filled them in, and they were not detectable anymore.

#### 4.4.3. Flaw characterization

Images of the naturally aged surface of glass are rarely found in the existing literature. An example of such image, namely a micrograph of a 20-year-old weathered float glass, is presented in Figure 4.22.

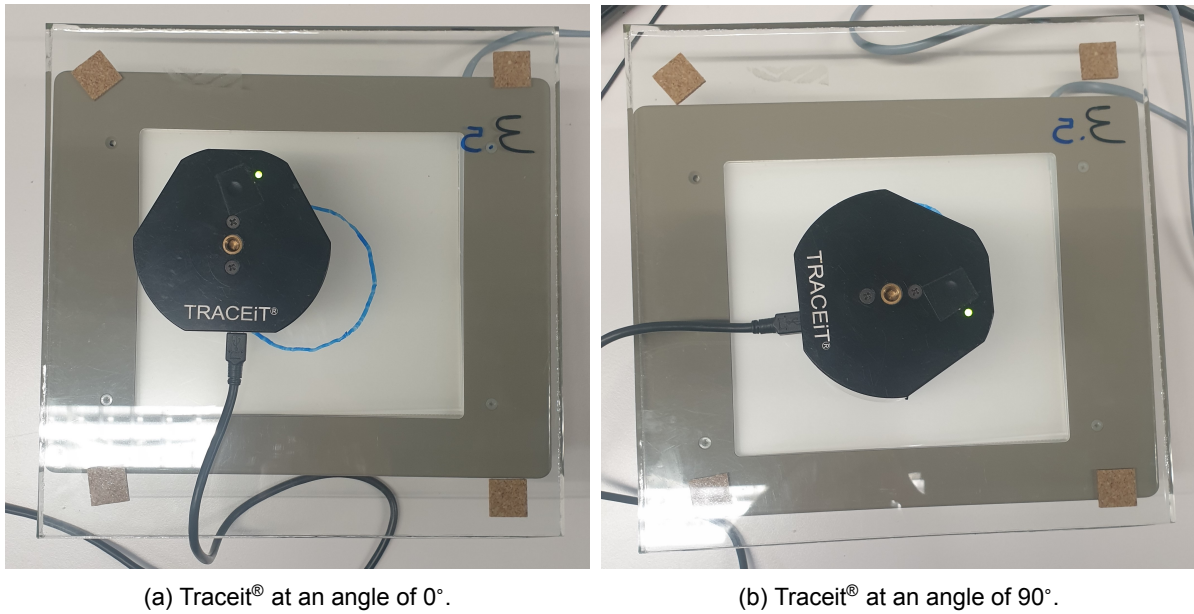


Figure 4.20: Traceit® positions during the reliability study.

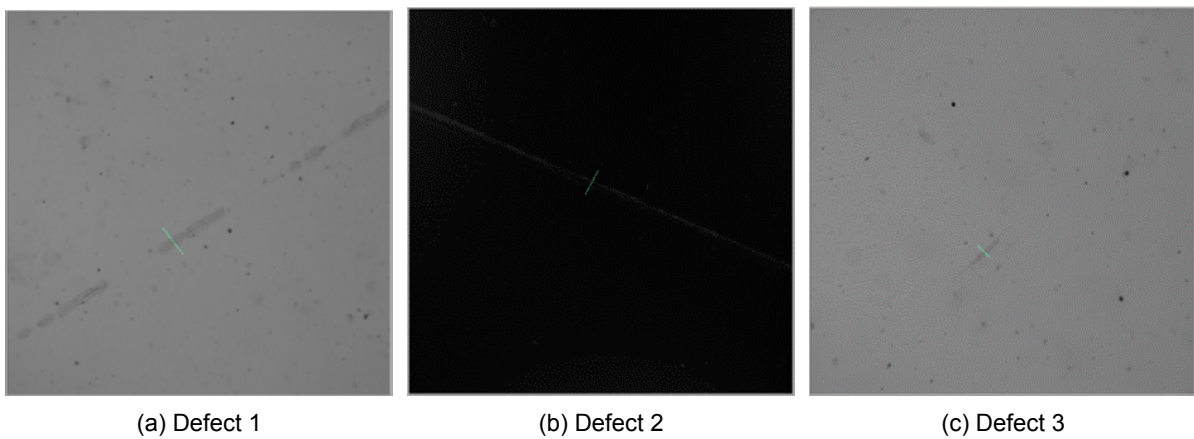


Figure 4.21: The three examined defects on the same specimen, as captured by Traceit®. The green line indicates the location of the measurement along the defects.

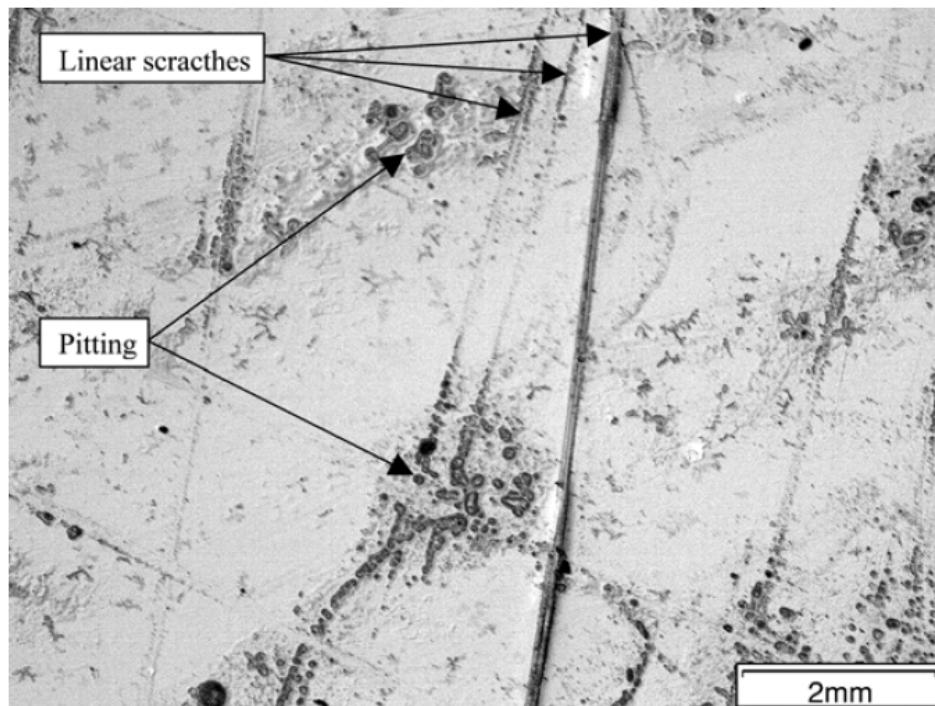


Figure 4.22: Micrograph of 20-year-old weathered float glass. (Overend and Zammit, 2012).

Since this study focuses on this type of glass, the type and size of defects found during the microscopy study are reported here and they are compared to those found in literature.

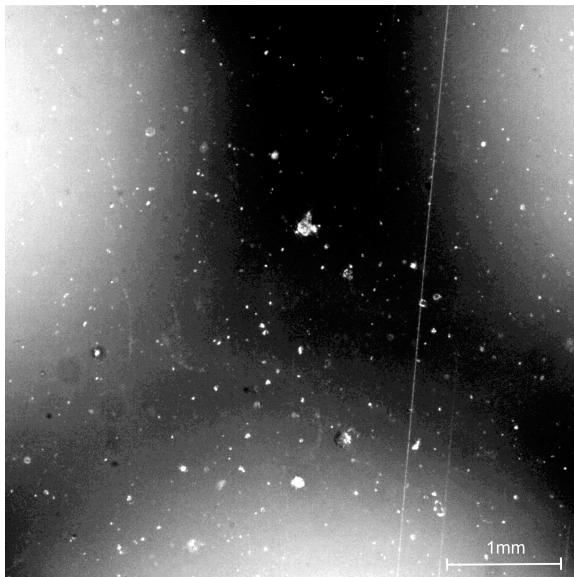
In most of the examined specimens, few fine scratches were visible even with the naked eye, but no significant macroscopic damage was observed (see Figure 4.23a). In all the specimens, many dots ("pits") were observed, which are presumed as corrosion signs, since they were found only on the one side of the glass. These signs formed the basis for the distinction between the internal and the external sides of the glass specimens (see Figure 4.23b).

In few specimens, large and deep linear scratches as well as "digs" were observed<sup>5</sup>. Some of these scratches had a very fine width and they were longer than 10 cm, especially on the larger specimens. As a result, it was not possible to study the complete defect with the microscope or with Traceit<sup>®</sup> and only a part of them was measured. Other scratches were shorter but wider (see Figures 4.23c, 4.23d and 4.23e). The depth and width of those defects, as measured with Traceit<sup>®</sup>, ranged from 19  $\mu\text{m}$  to 161  $\mu\text{m}$ . Although the digs are more localized defects which might not be visible by the human eye (see Figure 4.23f), they were found to be deeper than the scratches in some specimens.

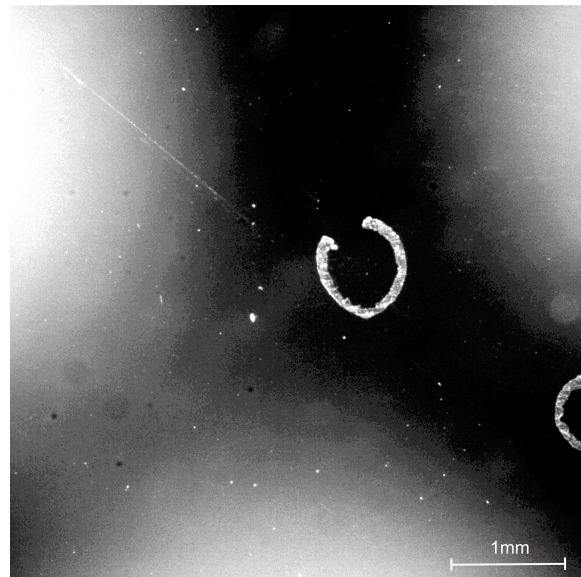
The internal surface of some specimens included also some long and straight scratches which do not resemble the damage that can be naturally induced on a glass panel. On the contrary, it is more likely that these defects were introduced during the service life of glass and especially during the cleaning and maintenance processes. Furthermore, the transportation and processing of the glass panels until the experiments are also possible causes of those scratches. Interestingly, the specimens which had more damage on the internal side were scored from the same facade panel. Perhaps, by tracking back to the location of that panel on the building an explanation for that observation could be found, but unfortunately that was not possible in this research.

Overall, the type of damage on the examined specimens and the specimens found in literature is comparable. In particular, they both contained mainly linear scratches, digs and pits on their surfaces. Their difference though lies on the number and size of the defects. More specifically, the amount of damage on the surfaces of the tested specimens was lower than the expectations from a 55-year-old glass panel and than the 20-year-old glass found in literature. Furthermore, the defects on the tested

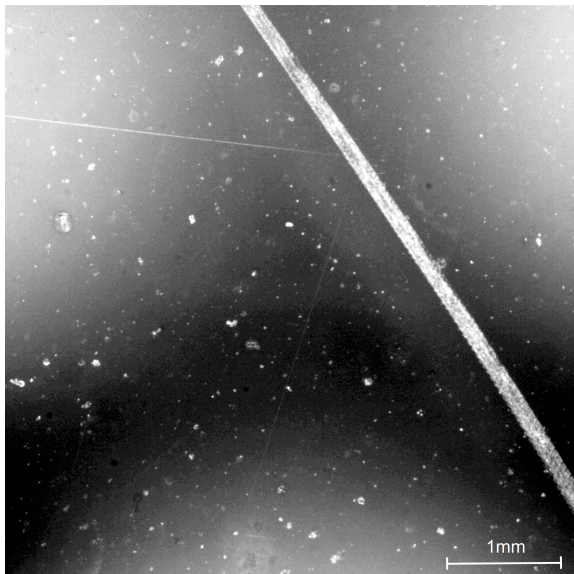
<sup>5</sup>See Section 3.3 for the characterization of several types of defects.



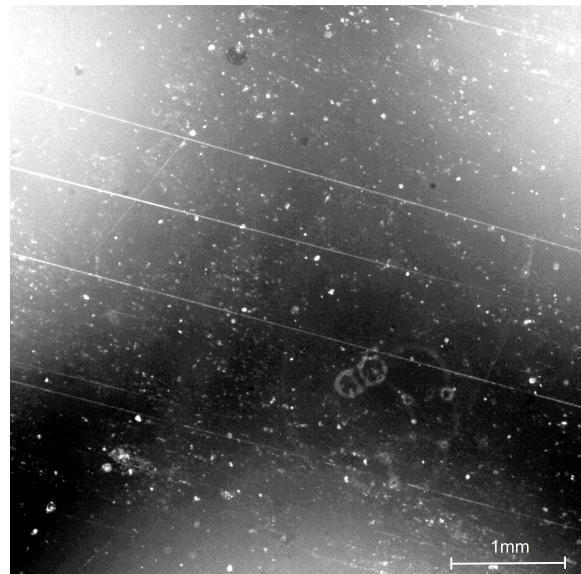
(a) Type of damage on most of the specimens.



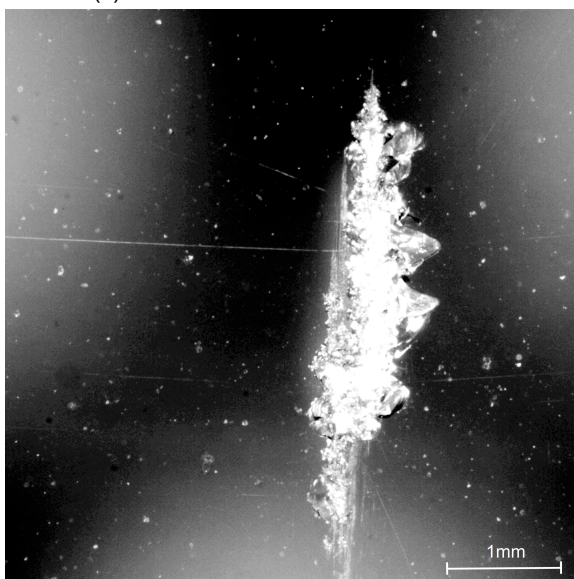
(b) Damage on the internal surface of glass.



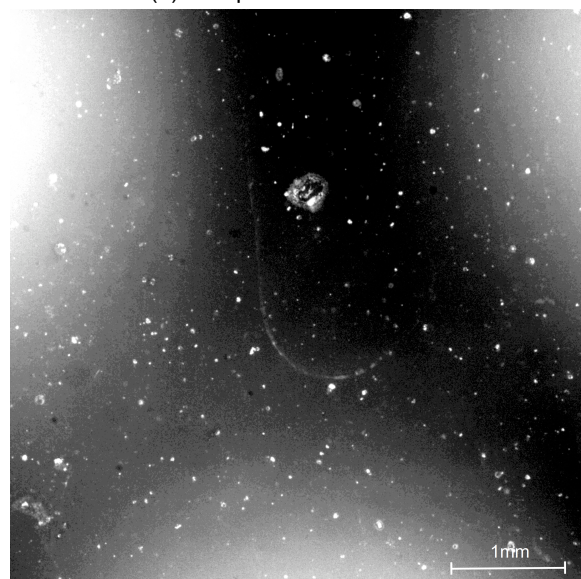
(c) Thick scratch on the external side.



(d) Multiple linear scratches



(e) Short and wide scratch with linear scratches.



(f) "Dig" type defect.

Figure 4.23: Images of several types of defects as captured with Traceit<sup>®</sup>, after processing. The images show an area of 5mm by 5mm of the glass specimens.

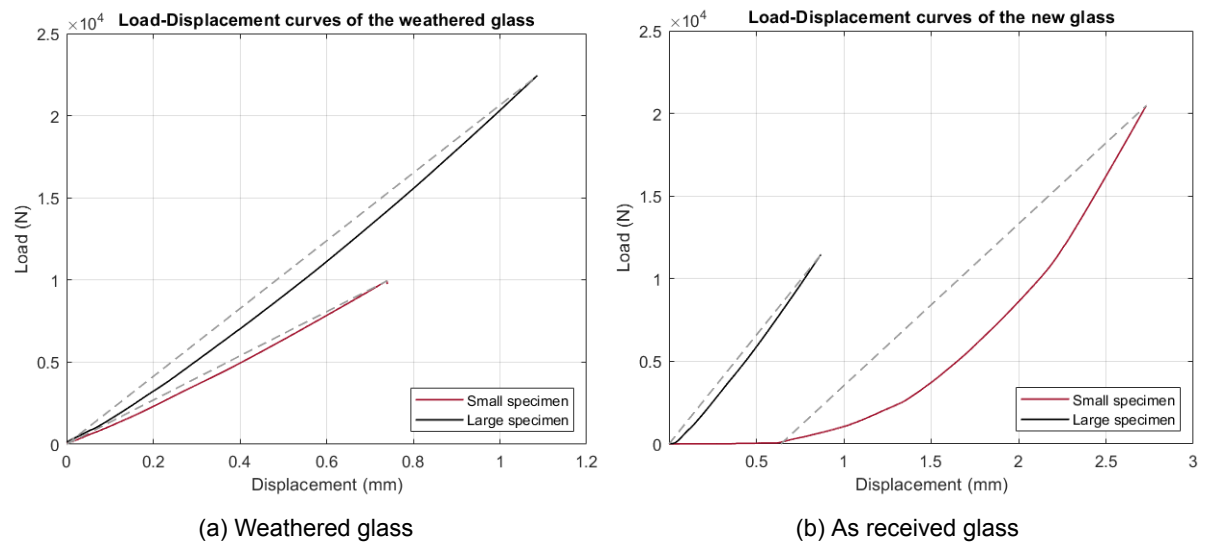


Figure 4.24: Force-Displacement curves of the tested specimens

glass seem smaller than those in Figure 4.22. Nevertheless, it would have been useful to know the location of the examined panels in the building, to see how this relates to its damage. Although it is likely that a panel from a higher floor would be less damaged than a panel from the ground floor, which is accessible by the public, there was no such information available for this research.

#### 4.4.4. Results of the CDR tests

Eight series of tests were conducted, with ninety specimens of weathered glass and eighty-one specimens of new glass tested in equibiaxial bending. The results of the CDR tests of all the specimens are presented analytically in Appendix D.

##### 4.4.4.1. Results of the CDR tests on weathered glass

During the tests, the load-displacement curves of the specimens were recorded for all the specimens. Two examples of the curves of one small and one large specimens of weathered glass are illustrated in Figure 4.24a. It can be seen that the behavior of old glass was almost linear-elastic, according to the expectations. A small deviation from the perfect linearity was observed, especially for the larger specimens. It is likely that the large overhang of those specimens caused that behavior because it alters the stress distribution on the glass plate. Nevertheless, the maximum deflection at failure was always less than 25% of the thickness of the glass, so the simple plate theory was applicable for the calculation of the equibiaxial stress inside the loading ring (ASTMC1499-09, 2013). The slope of each specimen's curve varied, as the failure time and stress for each one of them was highly variable.

Table 4.4 presents a summary of the results of the tests on weathered glass. The maximum, minimum and average failure stresses of the specimens of each testing series are reported in that table, along with the standard deviation. Furthermore, the average time to failure in seconds as well as the average stress rate in MPa/second are reported in the same table. The average temperature during the tests was  $22,2^\circ\text{C}$  and the average humidity 22,3%.

The failure stress values range considerably from 22,9 MPa to 138,2 MPa. The average failure stress of the small specimens of the series NA-1b is 53% higher than that of the series NA-1a, indicating a higher strength for the internal surface compared to the external one. That higher strength resulted also at longer time to failure for the series NA-1b by 45%. The higher strength of the specimens of NA-1b is aligned with the expectations, since the internal surface of weathered glass was found to be less damaged than the external surface. On the contrary, the difference between the failure stress of the series with the large specimens is just above 10%, with the external surface being stronger.

Table 4.4: Summary of the CDR test results on weathered glass.

Dimensions	250x250x10mm		450x450x10mm	
Series	NA-1a (external)	NA-1b (internal)	NA-2a (internal)	NA-2b (external)
$\sigma_{f,max}$ (MPa)	88,9	138,2	76,5	83,5
$\sigma_{f,min}$ (MPa)	37,1	54,1	22,9	32,3
$\sigma_{f,average}$ (MPa)	66,2	101,4	54,6	60,3
Standard deviation	15,0	21,4	13,8	14,0
$t_{f,average}$ (s)	8,8	12,8	13,0	14,1
$Rate_{average}$ (MPa/s)	7,5	7,9	4,2	4,2

Table 4.5: Average failure stresses of specimens scored from the same panel.

Panel	$\sigma_{f,average}$ (MPa)	St. dev.	Panel	$\sigma_{f,average}$ (MPa)	St. dev.
NA-1a (250x250x10, external)			NA-2a (450x450x10, internal)		
1	74,4	17,6	1	64,5	10,9
2	61,4	12,7	2	49,6	13,0
3	62,6	13,9			
all	66,2	15,0	all	54,6	13,8
NA-1b (250x250x10, internal)			NA-2b (450x450x10, external)		
4	92,3	28,4	3	64,0	14,5
5	106,2	16,7	4	55,8	13,5
all	101,4	21,4	all	60,3	14,0

By comparing specimens of two different dimensions, a difference of 86% is observed between the series NA-1b and NA-2a, tested with the internal surface in tension. The size effect seems to have great influence on the strength of these specimens, which is in accordance to the expectation for lower strength of the larger specimens. However, this is not the case for the series NA-1a and NA-2b, tested with the external surface in tension, where a difference of 10% is observed. The effects of size and weathering are elaborated further in Chapter 5 by means of statistics.

The variation in the strength results of the weathered glass is not observed only among specimens of different testing series but also among specimens within the same series, with the same characteristics, which macroscopically were identical. Each testing series included specimens scored out of 2 or 3 different facade panels. As the non-destructive tests revealed, the damage on these panels was not similar. Consequently, the different type and amount of damage led to great variations in the failure stresses within the same testing series. Analytically the average failure stresses for the specimens scored from the same panel are presented in Table 4.5.

#### 4.4.4.2. Results of the CDR tests on new glass

##### Finite Element Analysis

In the experimental series of the new specimens, a non-linear behavior was noticed in the load-displacement curves of the small specimens tested with the air side in tension, as illustrated in Figure 4.24b. The high stresses reached at the fracture of those specimens forced them to deflect more than the 25% of their thickness. The load-displacement curves of the large specimens are almost linear, even though their deflections exceeded the 25% of their thickness too. In both cases, this phenomenon is not accounted by the formula (4.1) of the ASTM C1499-09 (2013) standards for the linear stress calculation. Therefore, two finite element models were developed in Abaqus SIMULIA (2022) to assist the failure analysis of the specimens which cannot be analysed with the linear theory.

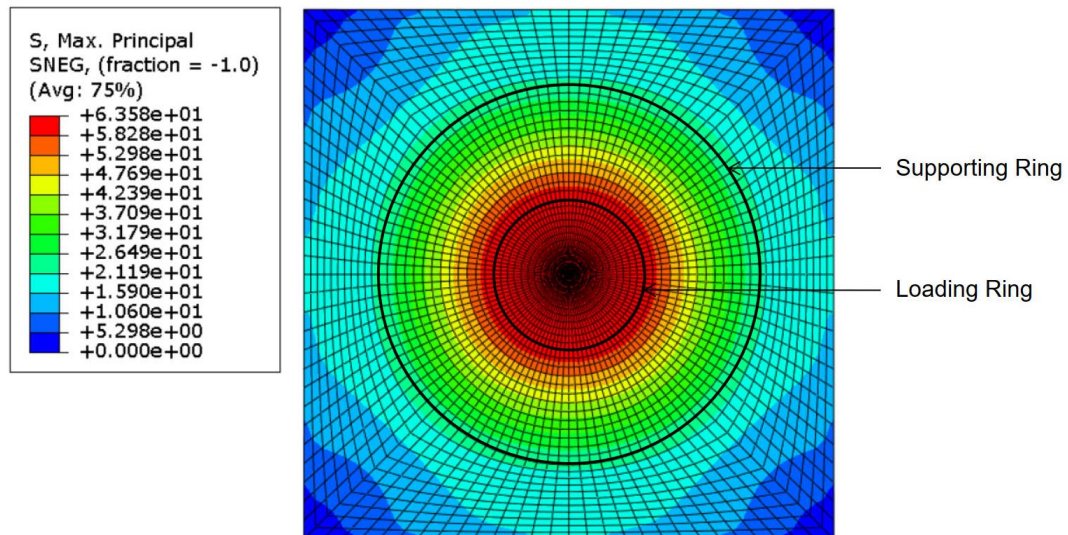


Figure 4.25: Finite element model of the small specimens in Abaqus SIMULIA (2022).

The failure stresses of the specimens whose deflection exceeded the 25% of their thickness and whose fracture origin was within the loading ring, were corrected with the Finite Element Models (FEM). The failures of the rest specimens required an even more elaborated analysis which was not performed since the main focus of this research lies on the strength of weathered glass. Thus, the CDR tests on new glass (Young's modulus  $E=70000$  MPa and Poisson's ratio  $\nu=0.23$ ) were simulated and an analysis which accounts for geometric non-linearities was performed. The models of the small and the large specimens consisted of 3920 and 4736 quadratic quadrilateral shell elements (S8R), respectively.

Since the FEM were constructed after the completion of the CDR tests, it was not possible to calibrate them with the experimental data. Thus, both models were developed based on the assumptions made in the paper of Datsiou and Overend (2016), in which the same loading and supporting rings were used. As in that paper, two scenarios were considered for each model, one with full friction between the glass and the rings and one without friction. The experimental data of Datsiou and Overend (2016) indicated that the full-friction model was more accurate and thus, these models were used to derive the failure stresses of the examined specimens.

In the FEM of the small specimens, equal tensile stresses were developed inside the loading ring, as illustrated in Figure 4.25. Thus, for several failure loads the maximum stress of the FEA model was reported and the failure stresses of the specimens were derived with linear interpolation from the curve shown in Figure 4.27a. In the model of the large specimen though, the stresses were not everywhere equal and more specifically, the maximum stress was developed below the loading ring ("point A" in Figure 4.26) instead of the middle, as shown in Figure 4.26. Considering that the fracture origin of the large specimens was somewhere between the loading ring and the middle of the specimen, the stresses at an intermediate point ("point B" in Figure 4.26) were used as failure stresses for these specimens. The maximum tensile stress, at the point "A", and the stress at the point "B" were plotted as a function of the failure load in Figure 4.27b.

### Results

A summary of the results of the tests on the new glass is presented in Table 4.6. For the data of the air side, the corrected values derived from the FEM were used. The average temperature during the tests was  $24^{\circ}\text{C}$  and the average humidity 57%.

The failure stress of the as received glass, as emerged from the linear and non-linear calculation, ranges from 38,3 MPa to 219,2 MPa. Both values are considerably higher than the corresponding values of weathered glass. Furthermore, these high failure stresses were reached at longer load duration compared to the old specimens. In particular, the average time to failure of the new glass ranges from 20,7 to 32,5 seconds whereas that of the weathered glass is less than 15 seconds. Nevertheless, to

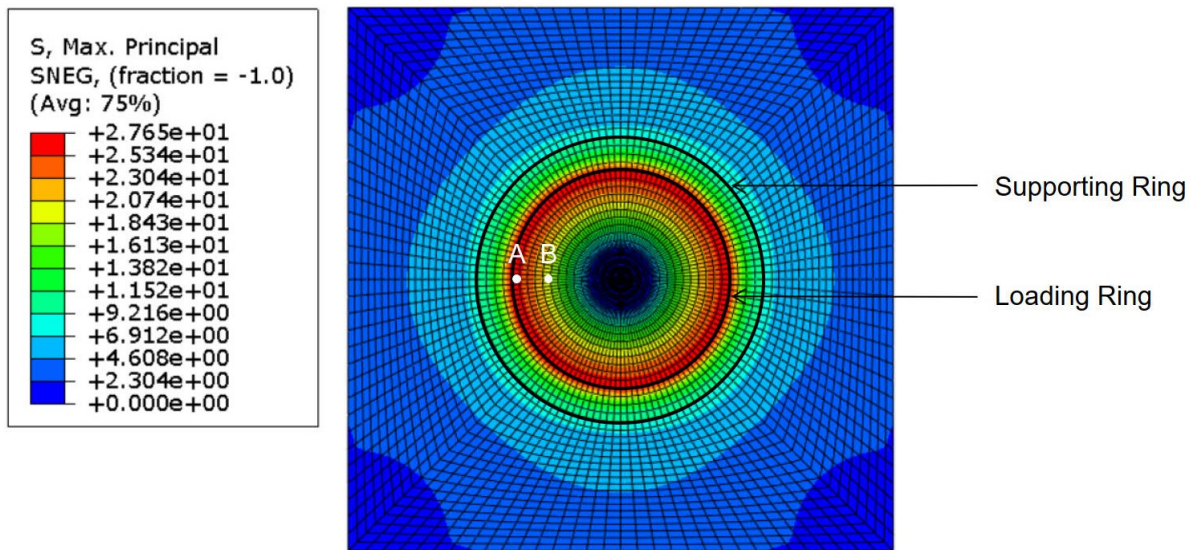


Figure 4.26: Finite element model of the large specimens in Abaqus SIMULIA (2022).

Table 4.6: Summary of the CDR test results on new glass.

Dimensions	250x250x10mm		450x450x10mm	
Series	AR-1a (Tin side)	AR-1b (Air side)	AR-2a (Tin side)	AR-2b (Air side)
$\sigma_{f,max}$ (MPa)	155,6	219,2	116,2	179,8
$\sigma_{f,min}$ (MPa)	57,9	64,1	38,3	84,1
$\sigma_{f,average}$ (MPa)	109,4	159,1	83,3	121,7
Standard deviation	29,7	50,1	18,1	26,2
$t_{f,average}$ (s)	22,5	27,9	20,7	32,5
$Rate_{average}$ (MPa/s)	4,8	5,5	4,0	3,7

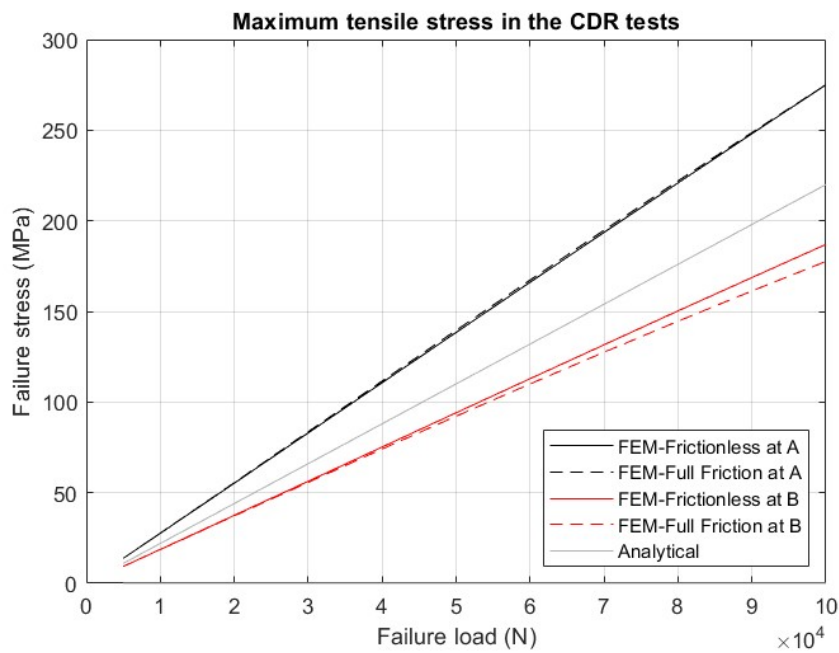
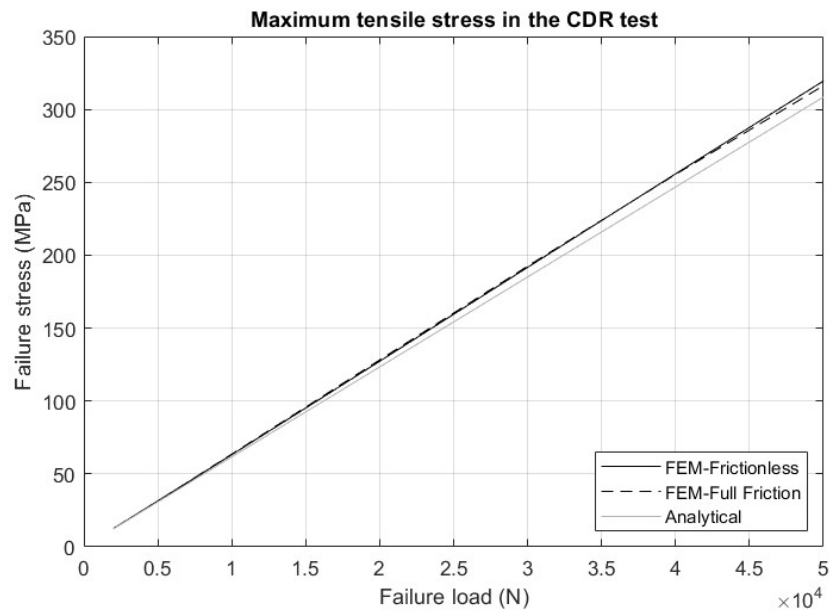
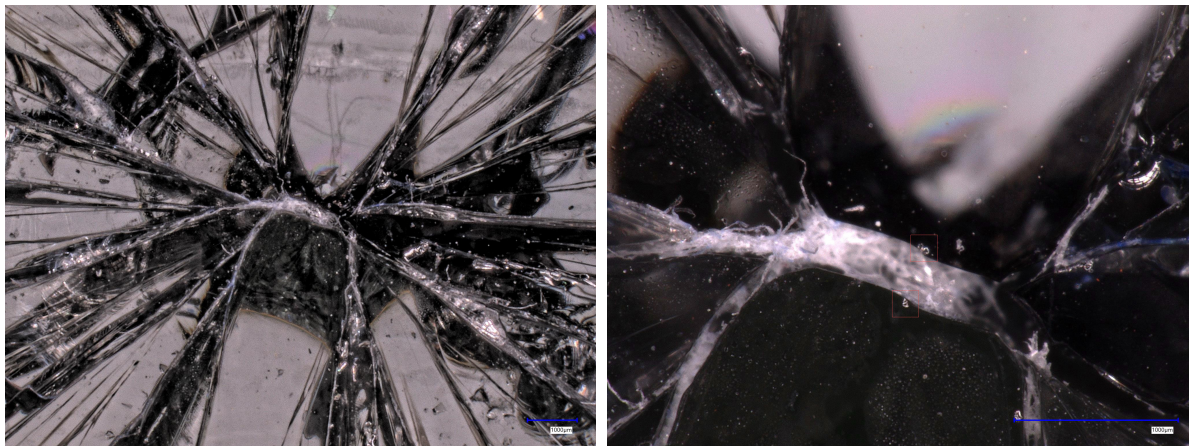


Figure 4.27: Maximum principal tensile stresses according to ASTM C1499-09 (2013) ("Analytical") and to the FEA models for the non-linear calculation.



(a) Fracture pattern at magnification x30.

(b) Butterfly type of fracture at magnification x100.

Figure 4.28: Microscopic images of the fracture pattern of specimen 1.2 (NA-1a).

exclude this variable from the results, the failure stresses of all the testing series were normalised to an equivalent failure time, equal for all of them.

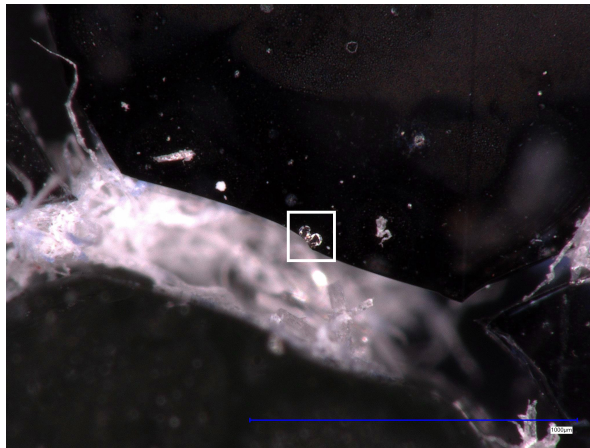
Interestingly, the average strength of the air side is 45% and 46% higher than that of the tin side for the small and the large specimens, respectively. Furthermore, the size effect, namely the influence of the loaded area on the strength of glass, seems to apply here. In particular, the average failure stress of the smaller specimens is 31% higher than that of the larger specimens tested with the tin and air side in tension. The influence of the tin on the strength of glass as well as the size effect on new glass are analysed in Chapter 5.

#### 4.4.5. Results of the microscopy examination after the CDR tests

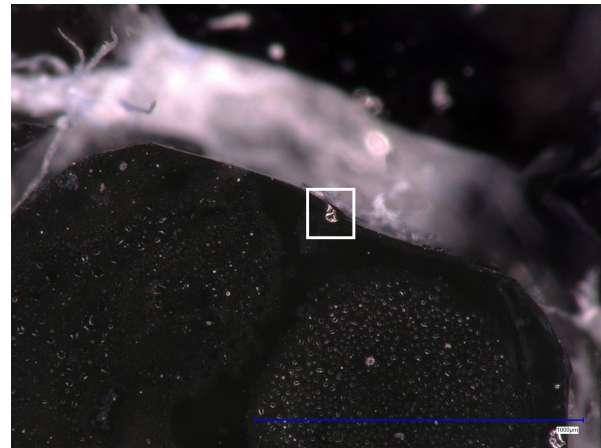
Although the fracture origin became known after the destructive tests, the exact critical defect which caused that fracture was visible only with the microscope at high magnifications. For instance, Figure 4.28 illustrates the crack branching of the specimen 1.2 (from series NA-1a) at magnifications of 30x and 100x. The "butterfly" shape of the fragments is a commonly found pattern for annealed glass subjected to biaxial tensile stresses. In general, the crack branching is an indication of the direction of the crack propagation as well as of the direction of the local maximum principle tensile stresses (Quinn, 2020). Although the fracture origin was identified for that specimen, the exact "critical" defect from where the fracture was more likely originated is still unknown. A more elaborated examination with the microscope revealed that critical location and it is presented in Figure 4.29. These figures illustrate a defect along the fracture origin, which is split. In particular, half of the defect lies on the one side of the butterfly and the remaining part is on the other side. On these grounds, this defect could be the critical one for that specimen and it is probably the deepest location along the fracture origin.

Specimen 1.1 (from series NA-1a) showed an interesting and not expected fracture origin. Although it failed along the largest defect which was expected to be the critical one, Figure 4.30 shows that it did not break at the deepest location of that defect. More specifically, it did not break at the linear scratch in the middle of the defect but at the surrounding part. This failure indicates that inside the defect there is no uniform stress concentration but there is a gradient stress. As a consequence, a small part of the defect was sufficient to cause the fracture at a location which was not the deepest. Unfortunately, the depth measurement for that defect taken before the CDR test, was at different location than the location of the critical defect, so no comparison could be made.

Finally, signs like "beach marks" were found in all the fracture patterns, as illustrated in Figure 4.31. These lines indicate the 3D nature of the crack propagation since this phenomenon was observed at levels below the surface of glass. Therefore, such a crack below the surface could also be the reason for the fracture of the specimen 1.1 at that location or for the fracture of the specimens with no visible defects.

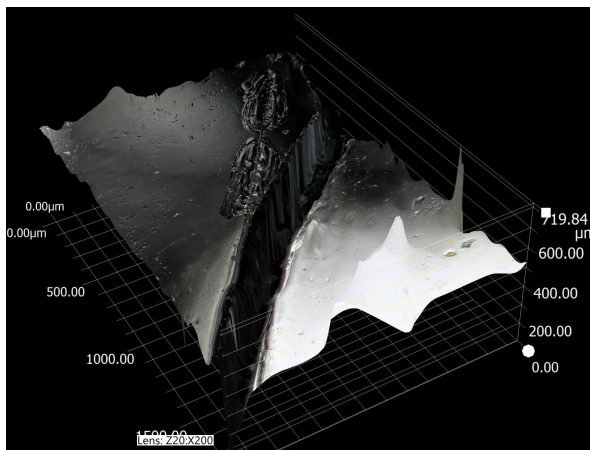


(a) Part of the probably critical flaw along the "butterfly".

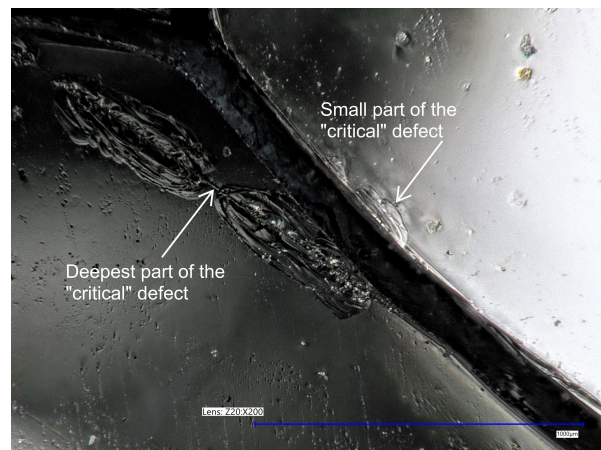


(b) The remaining part of the flaw.

Figure 4.29: Microscopic images of the probably critical flaw of specimen 1.2 at magnification x200.



(a) 3D illustration of the critical flaw.



(b) 2D image of the critical flaw.

Figure 4.30: Microscopic images of the probably critical flaw of specimen 1.1 at magnification x200.



(a) "Beach marks" at magnification x20.



(b) "Beach marks" at magnification x150.

Figure 4.31: Microscopic images of "beach marks", below the surface of glass

## 4.5. Correlation of flaw size and failure stress

This research aims to examine the link between the flaw size and the failure stress of glass. According to LEFM, the larger the flaw size, the lower the failure stress of glass. This theory was investigated here by performing a post-failure analysis on the small specimens of series NA-1a, which failed at the highest and lowest stresses, to examine whether the critical defect was small or large, respectively. The large specimens were not further analysed because they could not fit under the microscope. Thus, the defects found along the middle of the butterfly of these two specimens were measured and compared to the actual failure stress of the specimens, as emerged from the CDR tests. It is important to mention that the critical defect was not always detectable due to the complexity of the fracture pattern, especially in the specimens which failed at high stresses.

For the specimens with visible defects along the fracture origin, the hypothesis that these defects have a half-penny shape was made and used for the measurements (see Figure 4.32). In particular, the length of the defects was measured and the depth was calculated as the half-length. Figure 4.33 illustrates the critical flaw found on the specimen 3.4, which failed at the lowest stress (from the series NA-1a). It can be observed that along the fracture line there are two large defects. It is likely that the failure originated from that location, as a result of the interaction between the stress concentrations around these two defects. Alternatively, the second defect, which is the largest one, could also initiate the fracture. Furthermore, it seems that the small part of that defect on the lower fragment was sufficient for the specimen to fail at only 37,1 MPa. On the other hand, Figure 4.34 illustrates the critical defect of the specimen which failed at the highest stress, 88,9 MPa. The length of the defect in this case is much smaller, which is aligned with the theory of LEFM mentioned above.

The defect measurements shown in Figures 4.33 and 4.34 were used for the estimation of the failure stress, according to the formula (3.1). The geometry factor which corresponds to half-penny cracks ( $Y=0,713$ ) was used in both cases. The calculated failure stress for the weakest specimen was found to be equal to 39,6 MPa, which is 7% higher than the actual value (37,1 MPa). Similarly, for the strongest specimen, the calculated failure stress was equal to 95,3 MPa, 7% higher than the actual stress (88,9 MPa). It can be seen that the calculated failure stresses based on the measured length of the defect are very close to the actual stresses. This indicates that the hypothesis made about the half-penny shape of the defect is probably correct and it suggests that indeed, the larger defects lead to lower failure stresses. However, only an analysis of the fracture surface could indicate whether this is actually true, but such time consuming analysis could not fit in the schedule of this project.

It is stressed out that the aforementioned theory does not apply to all the specimens. For instance, specimens which failed at low stresses did not have any large defect. Finally, some of the specimens which failed at higher stresses did not have any visible defect at all along the fracture origin. For these specimens a more elaborate analysis with the microscope was performed which revealed that in most of the cases, a defect in the sub-surface of glass existed. It is believed that this defect in the volume of the glass caused the fracture of these specimens, even if there was not any visible damage on their surface.

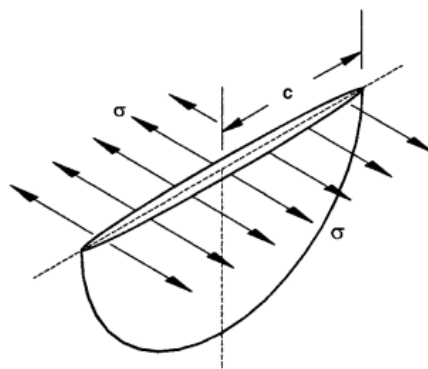


Figure 4.32: Half-penny crack (Overend et al., 2007).

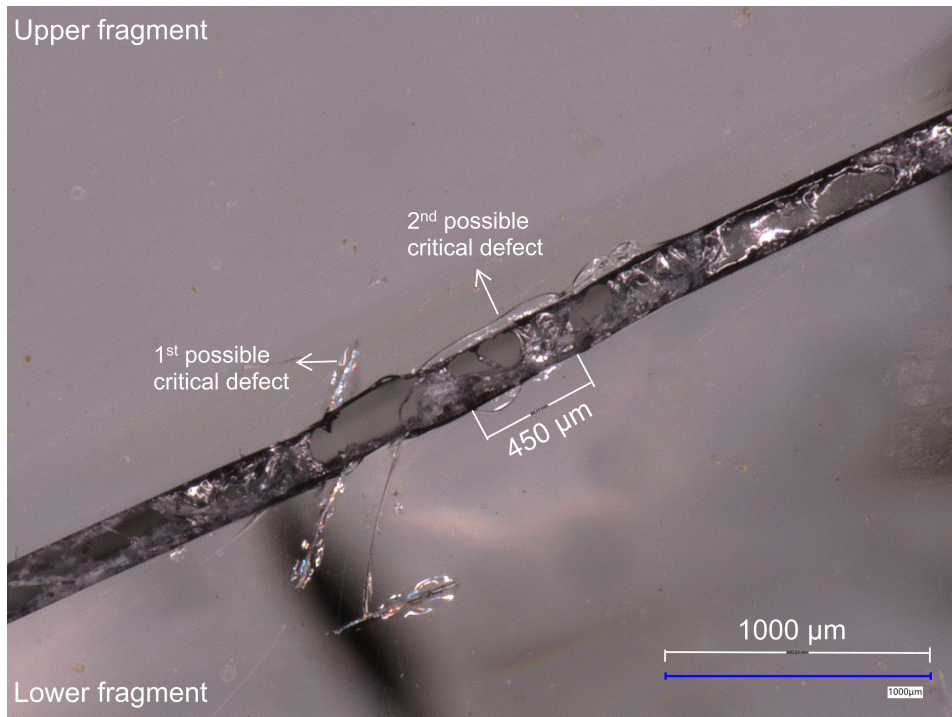


Figure 4.33: Critical defect of the specimen of series NA-1a which failed at the lower stress ( $\sigma_f=37,1$  MPa).

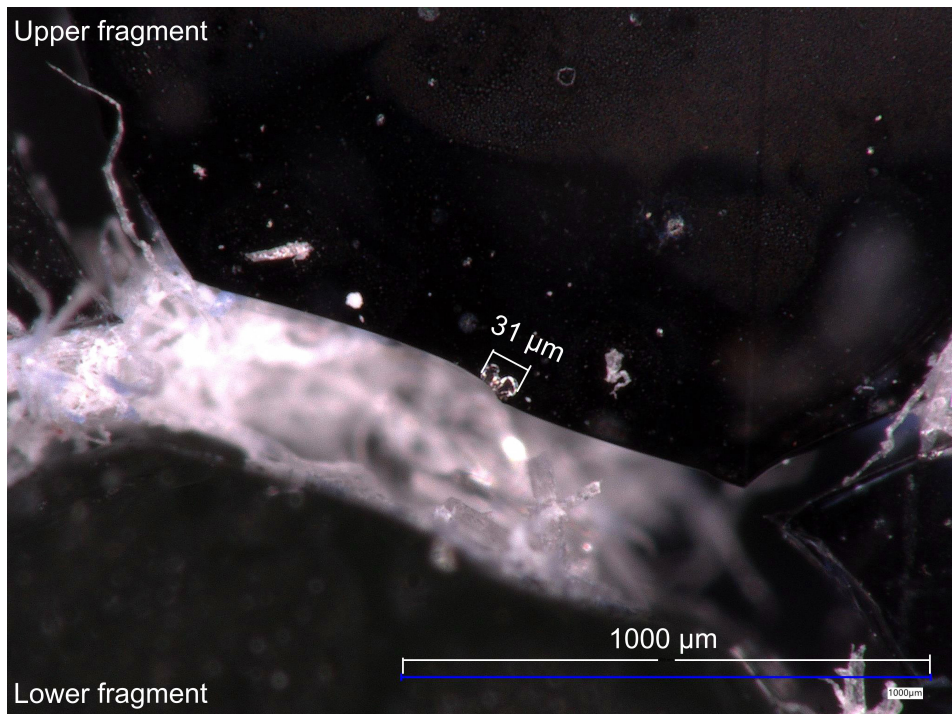


Figure 4.34: Critical defect of the specimen of series NA-1a which failed at the highest stress ( $\sigma_f=88,9$  MPa).

## 4.6. Discussion

One of the main goals of this experimental investigation was to detect and analyse the defects on the surface of weathered glass. The two equipment used for this purpose, the Traceit<sup>®</sup> profilometer and the Keyence VHX 7000 digital microscope, succeeded in distinguishing the external from the internal surfaces of the specimens and with Traceit<sup>®</sup>, it was possible also to take depth measurements of the found defects. Although the latter is normally used in different applications, it showed a great potential for capturing and measuring the defects on the surface of a transparent material such as glass.

New information regarding the type of damage induced by weathering was presented. It was revealed that the majority of the specimens had uniform damage, with mainly dense pits and some deeper digs on their external surface. Some fine linear scratches were also found occasionally. These defects seem representative of the type of damage that wind storms, sand abrasion and other physical phenomena could induce on the surface of glass. However, in some specimens defects possibly caused by other factors were found, such as the maintenance or transportation processes of the glass panels. These were in most of the cases the deepest or widest defects, with perfectly straight or curved shape. Even if these large defects were rare and they did not resemble the effect of weathering, they were important for this research because they were critical for the specimens that included them. Thus, when the effect of weathering is assessed, apart from the defects which are induced naturally, the man-made defects which are inevitably introduced into the glass surface over its service life should also be considered.

The failure stresses of the weathered specimens range from 22,9 MPa to 138,2 MPa. As mentioned at the beginning of this thesis, the strength of glass is governed by its surface flaws. Since the depth of these flaws also ranges considerably from 19  $\mu\text{m}$  to 161  $\mu\text{m}$ , a wide range in the failure stresses was expected. Apart from the depth size, the strength of glass is influenced also by the size of the loaded area. In the cases of both old and new glass, the highest strength value corresponds to a small specimen and the lowest to a large, suggesting that probably the size effect applies here.

The tests on weathered glass revealed that sometimes, higher failure stresses are associated with smaller defects or even no visible defects and vice versa. However, this was not always the case since for some specimens the failure could not be explained by the existence of surface or subsurface defects. For these specimens, an elaborated study of the fracture surface would probably give some answers but due to the complexity of that analysis, it was not feasible to perform it as a part of this research.

The strength of new, as received glass, without any visible damage, also ranges considerably, namely from 38,3 to 219,2 MPa. The results obtained from the tests on the air side were considerably high and associated with non-linear effects which make their reliability questionable. Even though some of these data was corrected with FEA, the model used for that analysis was not calibrated, so its accuracy was not proven. This should be considered in the statistical processing of the results in the Chapter 5.3. Nevertheless, considering that the aim of this project is not to investigate the strength of new glass, it was decided not to proceed with a more detailed FEA, since the obtained failure loads already gave an indication of the performance of this glass compared to the tested weathered glass.

Overall, the goals of the destructive tests were to derive the surface strength of weathered glass and to assess the influence of the phenomena of size effect and weathering on that strength. In the meantime, the experiments on new glass revealed another oddity which needed further analysis, the great difference between the strength of the tin and the air side. Therefore, all these phenomena are investigated further in Chapter 5.3 by means of fracture statistics. Finally, the flaw depth measurements are used in Chapter 6 for the prediction of the failure stress of glass, which is compared to the actual failure stresses of the CDR tests.



# 5

## Failure analysis

### 5.1. Introduction

This chapter analyzes the results obtained from the CDR tests, on weathered and new glass, presented in Chapter 4. In Section 5.2, a fractographic analysis is presented which indicates whether the fracture origin was inside the loading ring. The several fracture patterns observed during the tests are elaborated in that section.

Fracture statistics are used to describe the strength data of weathered and new glass based on three different probability functions. The main focus though is on the Weibull distribution, which is the most commonly used distribution function for glass strength data. More specifically, two methods for estimating the Weibull parameters, a manual and a computational one, are presented and compared in Section 5.3. Then, based on the Weibull plots of the testing series, the influence of the tin and air-side and the effect of weathering on the strength of glass are assessed in Sections 5.4 and 5.5, respectively. Furthermore, the size effect on weathered and new glass is discussed in Section 5.6, and the strength of the large specimens is extrapolated from that of the small specimens, according to the Weibull theory. Finally, the design strength of the examined specimens is compared to the provisions of the existing European and Dutch design standards in Section 5.6.2.

### 5.2. Fractographic analysis

A fractographic analysis was performed to determine whether the test results are valid or not. The distinction was made based on the location of the fracture origin in relation to the loading ring, as indicated in Figure 5.1. These three specimens are representative examples of the three possible locations of the fracture origin, namely inside, just below and outside the loading ring. The locations of the loading and the supporting rings are indicated with blue circles on all the specimens.

The number of specimens which broke at each location is presented in Table 5.1. In the four series of weathered glass (NA-series) with 90 specimens tested in total, 8 of them broke outside the loading ring. The location of the fracture origin of those specimens does not follow any pattern, indicating that the cause for those failures was not the testing setup or any other systematic fault (see Figure 5.2). In the four series of new glass (AR-series) with 81 specimens, 15 of them broke outside the loading ring, almost double than the corresponding specimens of the old glass (NA-series). Since the old glass had almost uniform damage on its surface, the probability of finding a critical defect inside the loading ring was higher than that in the new glass, which did not have any visible damage. Similarly with the NA-series, neither in these series any systematic error was observed in the fracture pattern of the invalid tests.

The fracture pattern of the specimens reflects also the significant strength differences among them. In particular, the higher the failure load, the higher the amount of the stress released during fracture and

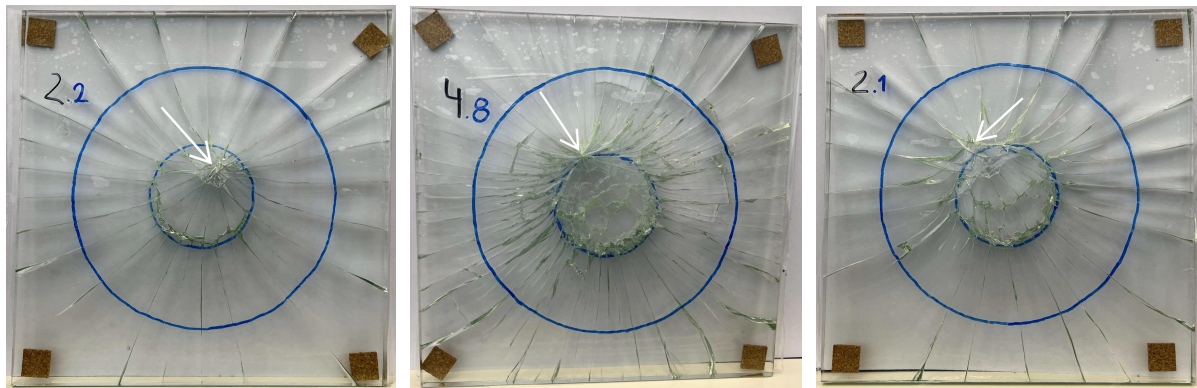


Figure 5.1: Examples of specimens which broke inside, just below and outside the loading ring.

Table 5.1: Number of valid and invalid tests based on the location of the fracture origin.

Dimensions	250x250x10mm		450x450x10mm	
Series	NA-1a (external)	NA-1b (internal)	NA-2a (internal)	NA-2b (external)
Inside the ring (IR)	15	16	22	19
At the ring (LR)	3	4	2	1
Outside the ring (OR)	3	3	0	2
Series	AR-1a (tin)	AR-1b (air)	AR-2a (tin)	AR-2b (air)
Inside the ring (IR)	12	9	16	12
At the ring (LR)	3	0	1	5
Outside the ring (OR)	5	4	3	3

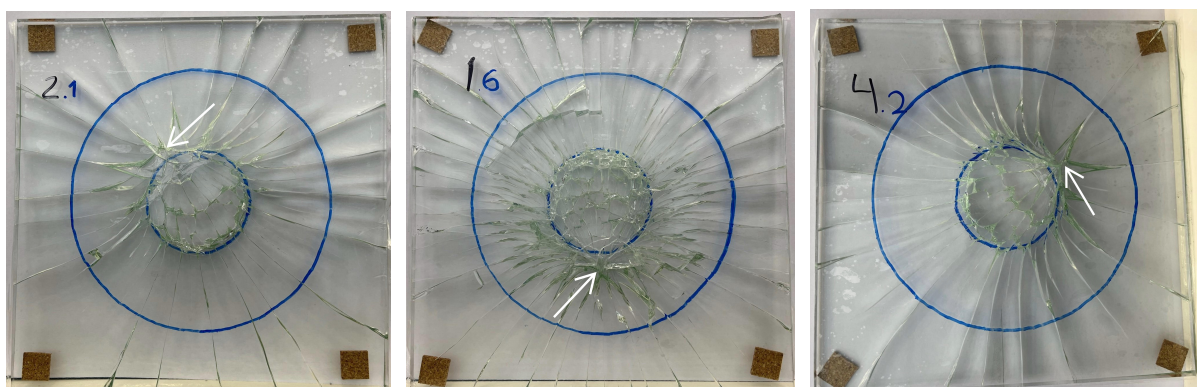
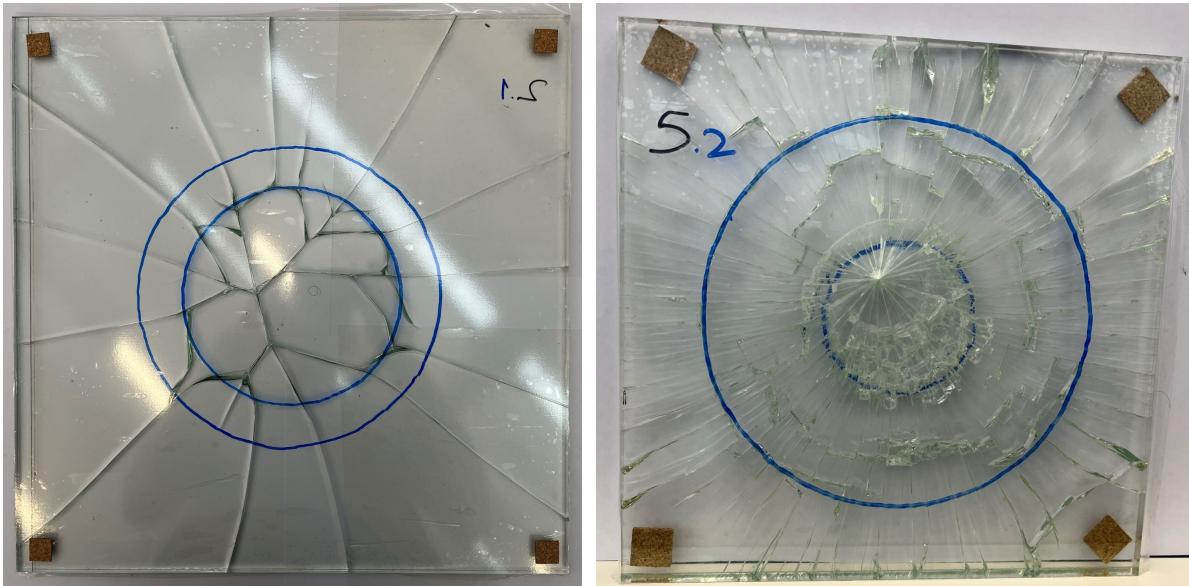


Figure 5.2: Examples of specimens which broke outside the loading ring - invalid tests.



(a) Specimen failed at the lowest strength (22,9 MPa) - Large specimen with internal surface in tension. (b) Specimen failed at the highest strength (138,2 MPa) - Small specimen with internal surface in tension.

Figure 5.3: Fracture patterns of specimens

thus, the denser the fragmentation pattern of glass. A representative example of that is presented in Figure 5.3. The left picture corresponds to the specimen which broke at the lowest stress and the right picture corresponds to the one which broke at the highest stress, both from the series of weathered glass. The failure stresses of these specimens were equal to 22,9 and 138,2 MPa, respectively. In the series of new small specimens with the air side in tension (AR-1b), some of the specimens reached considerably high failure stresses and thus, their fragmentation pattern resembles more the pattern which is expected from toughened glass than from annealed (see Figure 5.4). In particular, in 6 specimens, the fracture origin was not detectable or there were probably more than one critical flaws, which simultaneously initiated the fracture as illustrated in Figure 5.5.

### 5.3. Statistical processing of the results

The strength data of the experimental investigation were fitted to a two-parameter Weibull distribution, since it is the most commonly used method for describing such data, as discussed in Section 3.6. The Weibull Cumulative Distribution function (CDF) is described by the formula (5.1). That formula is also called the "three-parameter Weibull" distribution since apart from the shape and scale parameters, it includes also the location parameter  $\sigma_u$ . This parameter represents a threshold for the stress applied on the material, below of which failure never occurs. The two-parameter Weibull distribution emerges when the  $\sigma_u$  is set equal to zero (see formula (5.2)), which leads to more conservative results. Therefore, for annealed glass this threshold can be set equal to zero for safety reasons in design applications. Finally, the two-parameter Weibull distribution formula in (5.2) can be linearized in the form of (5.3).

$$P_f(\sigma_{f,eq}) = 1 - \exp \left[ - \left( \frac{\sigma_{f,eq} - \sigma_u}{\theta} \right)^\beta \right] \quad (5.1)$$

$$P_f(\sigma_{f,eq}) = 1 - \exp \left[ - \left( \frac{\sigma_{f,eq}}{\theta} \right)^\beta \right] \quad (5.2)$$

$$\ln \left[ \ln \left( \frac{1}{1 - P_f} \right) \right] = \beta \cdot \ln \sigma_{f,eq} - \beta \cdot \ln \theta \quad (5.3)$$

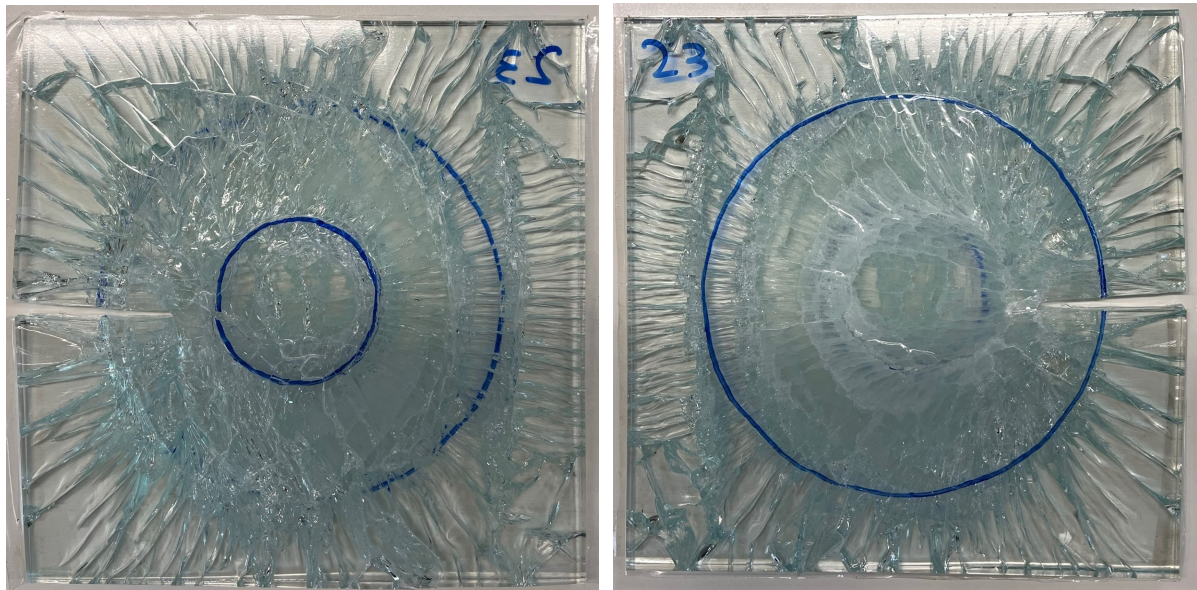


Figure 5.4: Specimen with not detectable fracture origin ( $F_{break}=36960\text{N}$ ).

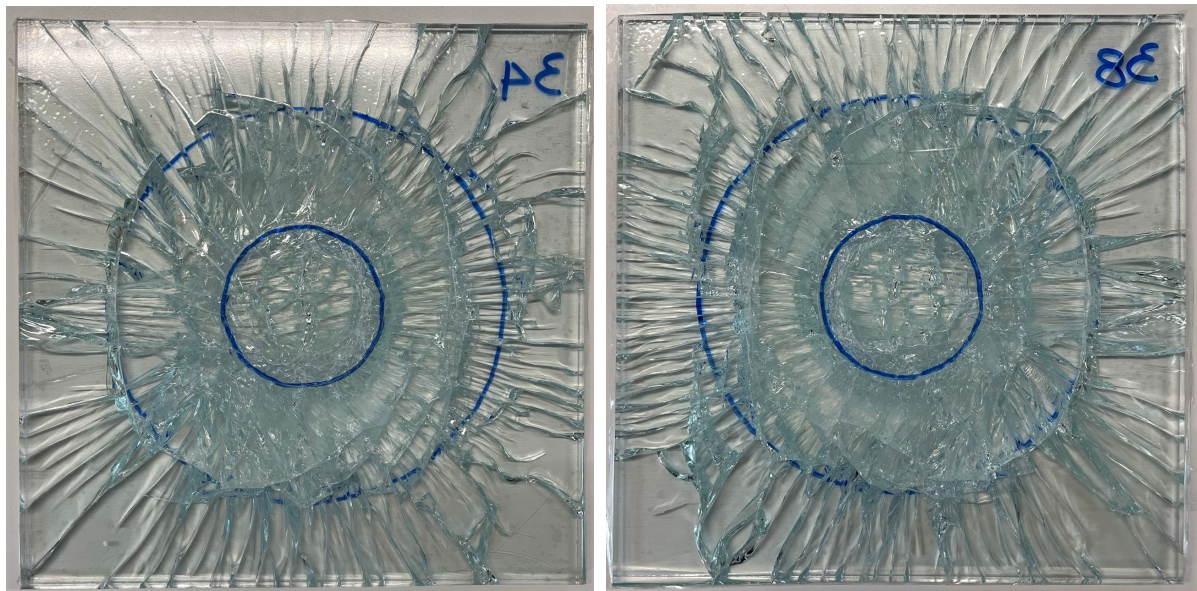


Figure 5.5: Specimens with probably more than one fracture origins ( $F_{break}=27080\text{N}$  and  $30047\text{N}$ , respectively).

Where,

$\sigma_{f,eq}$  is the equivalent failure stress for a reference load duration, as calculated from formula (3.3),

$\beta$  is the shape parameter which describes the scattering of the strength data,

$\theta$  is the scale parameter which indicates the stress below of which the 63.2% of the specimens fail and

$\sigma_u$  is the location parameter.

### 5.3.1. Weibull parameter estimation

The Weibull parameters can be estimated either with manual or with on computational methods. In this research, these parameters were estimated according to both methods and the effectiveness of each method in describing the data of weathered glass was evaluated. In particular, for the manual calculation, the Weighted Least squares Regression (WLR) method was implemented while for the computational method, the Maximum Likelihood Estimation (MLE) approach was followed.

#### 5.3.1.1. Manual Calculation

For the manual calculation of the Weibull parameters, an excel sheet developed by Dr. Kyriaki Corinna Datsiou in the context of her thesis (Datsiou, 2017) was used. The steps which were followed for that calculation according to the WLR method are the following:

1. The strength data were ranked in ascending order ( $i = 1$  to  $k$ ).
2. Equal probabilities of failure were assigned to these data in cumulative form, according to Hazen's estimator:

$$E_i = \frac{i - 0.5}{k} \quad (5.4)$$

3. The Weibull CDF was calculated as a function of the parameters  $\beta$  and  $\theta$  with the excel function "WEIBULL".
4. The weights  $W_i$  for each strength data were calculated according to the formula proposed by Faucher and Tyson (1988):

$$W_i = 3.3 \cdot P_i - 27.5 \cdot \left[ 1 - (1 - P_f)^{0.025} \right] \quad (5.5)$$

5. The shape and scale parameters were calculated according to the Weighted Least Squares Regression method as follows (Bergman, 1986):

$$\beta = \frac{\sum_{i=1}^k W_i \cdot \sum_{i=1}^k [\ln(\sigma_i) \cdot y_i \cdot W_i] - \sum_{i=1}^k [\ln(\sigma_i) \cdot W_i] \cdot \sum_{i=1}^k (y_i \cdot W_i)}{\sum_{i=1}^k W_i \cdot \sum_{i=1}^k [( \ln \sigma_i )^2 \cdot W_i] - \left[ \sum_{i=1}^k (\ln \sigma_i) \cdot W_i \right]^2} \quad (5.6)$$

$$-\beta \cdot \ln \theta = \frac{\sum_{i=1}^k (y_i \cdot W_i) - \beta \cdot \sum_{i=1}^k [\ln(\sigma_i) \cdot W_i]}{\sum_{i=1}^k W_i} \quad (5.7)$$

#### 5.3.1.2. Computational method

For the computational method, a MATLAB script was developed, since MATLAB uses by default the Maximum Likelihood Estimation (MLE) method for the estimation of the Weibull parameters. Then, the parameters were derived from the solution of the simultaneous equations (5.8) and (5.9).

$$\hat{\theta} = \left[ \left( \frac{1}{k} \right) \sum_{i=1}^k \sigma_i^{\hat{\beta}} \right]^{\frac{1}{\hat{\beta}}} \quad (5.8)$$

Table 5.2: Comparison of computational and manual Weibull parameter estimation methods for weathered glass.

Method	Computational (MLE)				Manual (WLR)			
	NA-1a	NA-1b	NA-2a	NA-2b	NA-1a	NA-1b	NA-2a	NA-2b
shape $\beta$	4,6	5,4	4,3	4,8	3,9	4,8	4,0	4,1
scale $\theta$	51,4	85,7	45,3	50,4	51,6	85,8	45,5	50,4
mean $\mu$	46,9	79,0	41,3	46,1	46,7	78,6	41,3	45,8
std $\sigma$	11,7	16,8	10,8	11,1	13,3	18,7	11,5	12,5
$\sigma_{f,0.008}$ <sup>1</sup>	17,9	35,2	14,9	18,2	15,2	31,4	13,7	15,6
$\sigma_{f,0.05}$ <sup>1</sup>	26,8	49,5	22,9	27,0	24,3	46,3	21,7	24,5
$\sigma_{f,0.5}$ <sup>1</sup>	47,4	80,1	41,6	46,7	47,0	79,5	41,5	46,1
$P_{AD}$	0,40	0,58	0,95	0,31	0,46	0,61	0,86	0,41

<sup>1</sup> The failure stresses of all the testing series are normalised to an equivalent load duration of 60 seconds.

$$\hat{\beta} = \frac{k}{\left(\frac{1}{\hat{\theta}}\right) \sum_{i=1}^k \sigma_i^{\hat{\beta}} \log \sigma_i - \sum_{i=1}^k \log \sigma_i} \quad (5.9)$$

Where  $\hat{\theta}$  and  $\hat{\beta}$  are the unbiased estimators of  $\theta$  and  $\beta$ , respectively.

### 5.3.1.3. Comparison of the two results of the methods

In all the statistical analyses presented in this Section, the normalised stress data (for  $t_{eq}=60$  sec) was used, instead of the failure stresses calculated directly after the CDR tests. By using this data, the failure time as variable is excluded from the probability plots and the only variable is the flaw size. Furthermore, the specimens with unclear fracture origin or with origin outside and just below the loading ring were excluded from the analysis, as recommended by ASTM E1499-09 (2013). For the specimens of new glass, whose displacement exceeded the allowable limits for the linear stress calculation, the corrected with the FEA stress values were used, also normalised for  $t_{eq}=60$  sec.

Tables 5.2 and 5.3 present the Weibull parameters, for the testing series of weathered and new glass, respectively, along with the mean and the standard deviation of the Weibull distribution, as derived manually and computationally. The design strength  $\sigma_{f,0.008}$  according to the American standards (ASTM-E1300, 1997), the characteristic  $\sigma_{f,0.05}$  and the mean  $\sigma_{f,0.5}$  strengths and the goodness of fit of the test data to the Weibull distribution (Anderson-Darling test) are also included in these tables.

Tables 5.2 and 5.3 indicate some differences among the results of the two methods. In particular, the difference in the mean failure stresses calculated with the two methods is marginal, namely less than 2%. However, for the lower probabilities of failure, which are used for design purposes, this difference increases. More specifically, the characteristic strength values  $\sigma_{f,0.05}$ , as calculated manually, are up to 15% lower than the corresponding computational values. Likewise, the design values  $\sigma_{f,0.008}$  differ by maximum 26% with the manual method providing the more conservative results. In general, the strength data fit slightly better to the Weibull distribution as derived manually, especially for the testing series of weathered glass. Therefore, it is concluded that the manual method describes slightly better the strength data of weathered glass, in terms of conservativeness and goodness of fit.

The Weibull plots of the normalised strength data are presented in Figures 5.6 and 5.7 for the series of weathered and new glass, respectively<sup>1</sup>. After a closer look at the probability plot of the series NA-2b

<sup>1</sup>The Weibull plots of the strength data of new glass before the correction with the FEA can be found in Appendix F

Table 5.3: Comparison of computational and manual Weibull parameter estimation methods for new glass.

Method	Computational (MLE)				Manual (WLR)			
	AR-1a	AR-1b	AR-2a	AR-2b	AR-1a	AR-1b	AR-2a	AR-2b
shape $\beta$	5,3	3,7	3,6	4,6	4,4	3,1	6,1	4,4
scale $\theta$	104,3	141,7	72,5	107,2	105,3	144,3	72,4	105,6
mean $\mu$	96,0	127,9	67,5	97,9	96,0	129,0	67,2	96,2
std $\sigma$	21,0	38,8	12,4	24,2	24,6	45,8	12,7	24,9
$\sigma_{f,0.008}^1$	41,8	38,0	33,9	37,6	35,4	30,2	33,0	35,1
$\sigma_{f,0.05}^1$	59,4	63,1	45,4	56,2	53,8	55,0	44,6	53,6
$\sigma_{f,0.5}^1$	97,3	128,3	68,5	99,0	96,9	128,1	68,2	97,1
$P_{AD}$	0,42	0,45	0,51	0,37	0,54	0,54	0,44	0,34

<sup>1</sup> The failure stresses of all the testing series are normalised to an equivalent load duration of 60 seconds.

(large specimens of weathered glass), it can be seen that this data might followed a bimodal Weibull distribution. This suggests that the strength of these specimens was governed by two different types of defects, perhaps digs and scratches. A post-fracture analysis would reveal whether this hypothesis is correct. Unfortunately, the specimens of this series were large and they could not fit under the microscope for such examination. A solution would have been to take the fragments apart and study only the fracture surface but this is a time consuming process which was not feasible within the time-frame of this project.

As mentioned in Section 3.6, the Weibull distribution does not describe well the strength data at lower probabilities of failure. This characteristic could lead to very conservative stress estimations for these low probabilities of failure. In this experimental investigation, this phenomenon was observed in the series NA-1a and NA-2b of weathered glass and in the series AR-1a and AR-2b of new glass. Thus, the reliability of the design stresses, which were extrapolated from the Weibull distribution of these series for low probabilities of failure, is questioned.

Finally, it is stressed out that the data of the valid tests from the series AR-1b (small specimens of new glass, air side) are less than 10. According to ASTM C1499-09 (2013), in this case the statistical analysis does not give statistically significant results. Nevertheless, these data were used for further analysis but the reliability of the results from this series is doubted.

### 5.3.2. Normal and Lognormal probability distributions

The normalised failure stress data were fitted also to the Normal and Lognormal distributions, since these distributions were previously used for describing the strength data of glass (see Section 3.6). The Normal and Lognormal probability plots for the eight testing series can be found in Appendix E.

### 5.3.3. Goodness of fit of the three probability distribution functions

The three probability distribution functions, Weibull, Normal and Lognormal, were compared in terms of goodness of fit of the strength data to them. The parameters of each one of these distributions were derived based on the null hypothesis that the equivalent strength data follows that particular distribution function. Therefore, this hypothesis needs to be verified after the statistical analysis.

For the evaluation of the three functions, the Anderson Darling (AD) goodness of fit test was applied. The AD method uses a weight function to apply more weight to the data of the upper and lower tail of the CDF (Datsiou and Overend, 2018). Since the strength data which are used in design applications

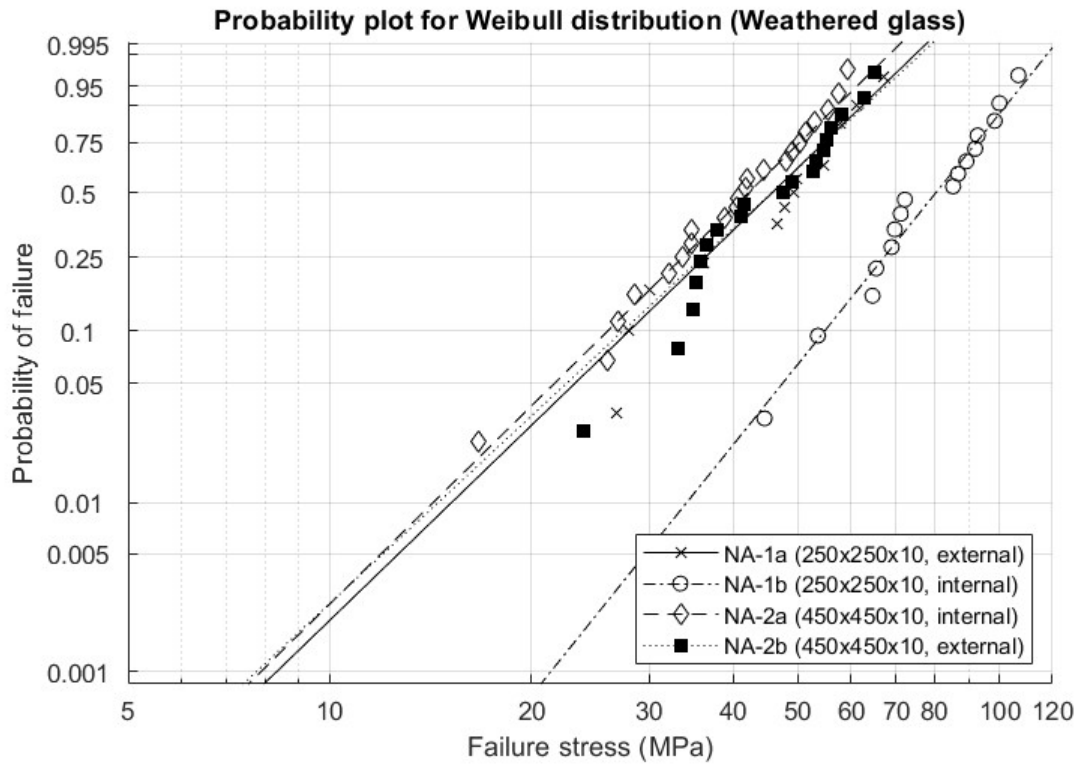


Figure 5.6: Normalised strength data of weathered glass fitted to the Weibull probability distribution function.

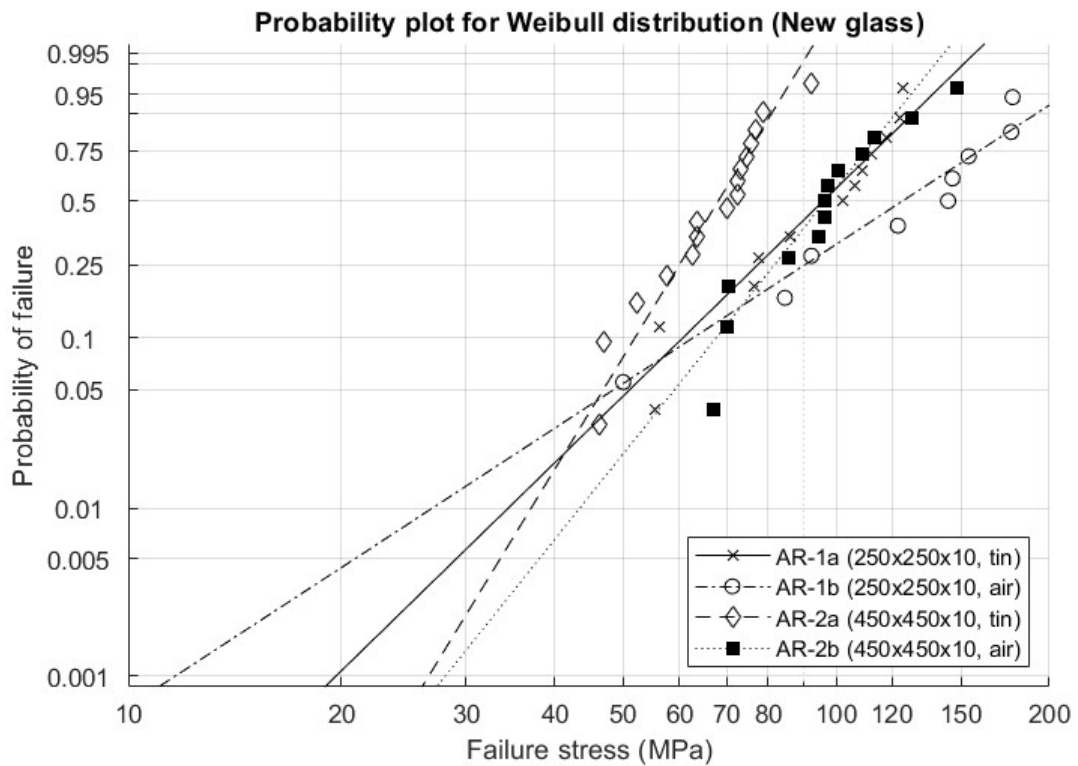


Figure 5.7: Normalised strength data of as received glass fitted to the Weibull probability distribution function.

corresponds to lower probabilities of failure, this method was chosen for the assessment of the statistical analysis. The AD test indicates whether sufficient data exist for rejecting the aforementioned null hypothesis. If this test fails to reject the hypothesis, it is assumed that the data follows that particular distribution function.

The probability of rejecting a good fit is chosen before the statistical analysis, and it is called level  $\alpha$ . In this project, a value of 0,05 was chosen for the  $\alpha$ . This significance level is compared with the observed significance level  $p_{AD}$  of the strength data sets, which is calculated with formula (5.10). If  $p_{AD} > \alpha=0,05$ , there are not adequate data to reject the null hypothesis and thus it is assumed that the data fits to the chosen distribution at an acceptable level. Otherwise, if  $p_{AD} < \alpha=0,05$ , the data do not follow the chosen distribution function.

The goodness of fit of all the testing series to the three probability distributions was calculated and it is illustrated in Figure 5.8, along with the chosen significance level  $\alpha=0,05$  (horizontal red line). It can be seen that the strength data of weathered glass fits better to the Weibull distribution than the other two distributions. The goodness of fit of this data to the Normal distribution is also sufficient but slightly lower than that of the Weibull. On the other hand, the Lognormal distribution has relatively low goodness of fit but always higher than the chosen level of significance. Therefore, the Weibull distribution, which was widely used to described data from as received glass, seems to have the best fit to the strength data of weathered glass as well, among the tested distributions.

The data of the tin side of the as received glass fits also better to the Weibull distribution than the other two distributions. Although the corrected data of the series with the air side of glass have an acceptable goodness of fit to the Weibull distribution, they fit better to the Normal distribution. As mentioned before though, the specimens whose fracture origin was inside the loading ring for the series AR-1b were less than 10 and thus, no sufficient data exists to derive clear conclusions about the best fit for them.

$$p_{AD} = \frac{1}{1 + \exp(-0.1 + 1.24 \cdot \ln(AD^*) + 4.48 \cdot AD^*)} \quad (5.10)$$

Where,

$$AD^* = \left(1 + \frac{0.2}{\sqrt{k}}\right) \cdot AD^2 \quad (5.11)$$

and

$$AD^2 = -k - \sum_{i=1}^k \frac{(2i-1)}{k} \cdot [\ln(P_f(\sigma_i)) + \ln(1 - P_f(\sigma_{k+1-i}))] \quad (5.12)$$

## 5.4. The tin-air side effect

During the production process of float glass, the molten glass is poured into a pool of tin oxide and floats onto steel rollers, where it cools down (annealing) and forms its intended thickness. The side of glass which is in contact with the tin oxide is called the "tin side" and the other side, which is exposed to the air is called the "air side". The tin side of the specimens of new glass was detected with the help of ultraviolet radiation and the specimens were tested consistently either with the tin or with the air side in tension to measure the strength of both sides. This distinction was important to made since the properties of the two sides are different. In addition to the tin residue mainly present on the tin side, this side is also expected to have more defects than the air side, and therefore, lower strength. These defects are induced into the surface of new glass during the annealing process, in which the same side of glass which was in the tin bath, is in contact with the steel rollers.

In the existing literature, the difference between the two sides of glass in terms of strength was characterised as marginal. As shown in Figure 5.10 though, in this experimental investigation this difference was greater. In particular, the mean failure stress of the air side is approximately 32% and 45% higher

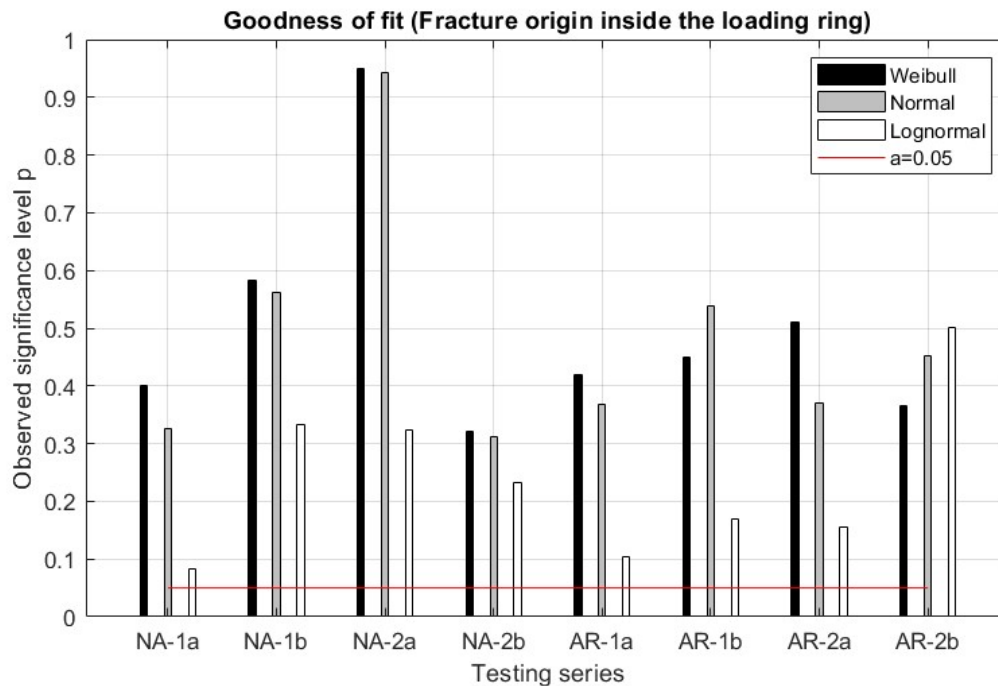


Figure 5.8: Goodness of fit of the test data to the three probability distributions, compared to the chosen level of significance  $\alpha=0,05$ .

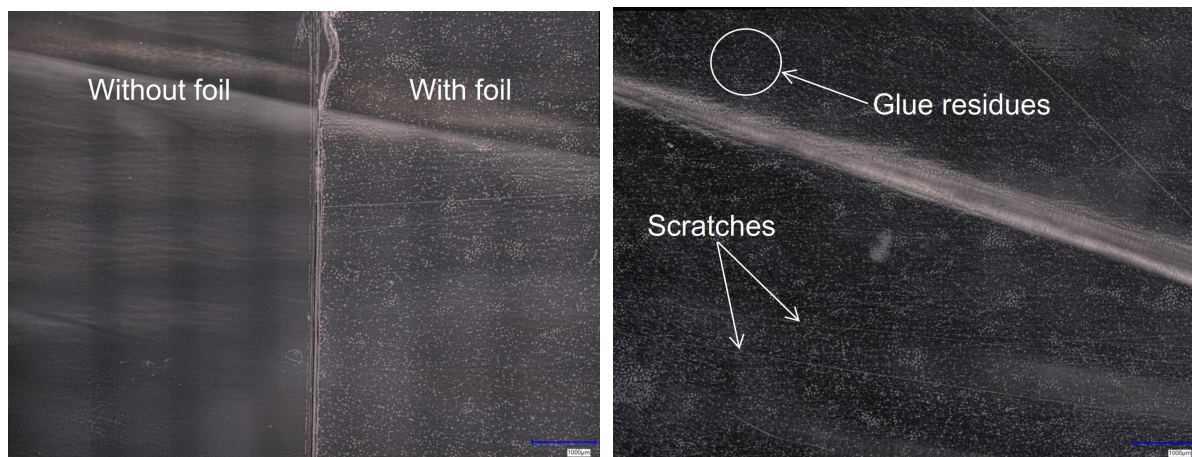
than that of the tin side, for the small and large specimens, respectively. This suggests that probably the tin side has indeed some invisible defects which do not exist on the air side. Nevertheless, by comparing the design strength of the series with air and tin side, the difference between them decreases.

A microscopy examination was performed, so as to investigate the hypothesis regarding the damage on the tin side of new glass. Unfortunately, this examination was performed on the specimens which were covered with the adhesive foil and thus, many glue residues were found on the surface of glass. Apart from these residues though, a small difference in the amount of damage between the tin and the air side was observed, as illustrated in Figure 5.9. In particular, few very fine linear scratches exist on the tin side which resemble the damage induced probably by the steel rollers. Nevertheless, it is recommended to perform such examination before altering the specimens and more specifically on specimens cut and transported in completely protected conditions to prevent new defects on their surface.

## 5.5. The effect of weathering

The non-destructive tests with Traceit® and the microscope indicated a clear difference in the amount of damage on the external and on the internal surfaces of weathered glass. That difference was investigated also in terms of strength, by testing half of the specimens with the internal surface in tension (series NA-1b and NA-2a) and half of them with the external surface in tension (series NA-1a and NA-2b). In this way, the strength of both sides was measured and the effect of weathering on that strength was studied.

Figure 5.11a illustrates the Weibull plots of the small specimens of new and weathered glass. The effect of weathering is clearly reflected on these plots since the strength of the weathered small specimens tested with the internal surface in tension (NA-1b) is considerably higher than that of the external surface (NA-1a). More specifically, the mean strength of the internal surface is around 69% higher than the mean strength of the external surface. By comparing this data to the strength of new glass panels, it is observed that the internal surface is weaker than the tin-side of new glass by 20%. As discussed in Section 5.4, the tin side of glass has some defects which are induced during the annealing process.



(a) Air side of new glass specimens, with and without the adhesive foil.

(b) Damage on tin side of new glass (the adhesive foil was removed).

Figure 5.9: Micrographs of the air and tin sides of new glass at magnification x200.

Therefore, it seems that the the internal surface of weathered glass is more damaged than the tin side of new glass, which also contains some defects.

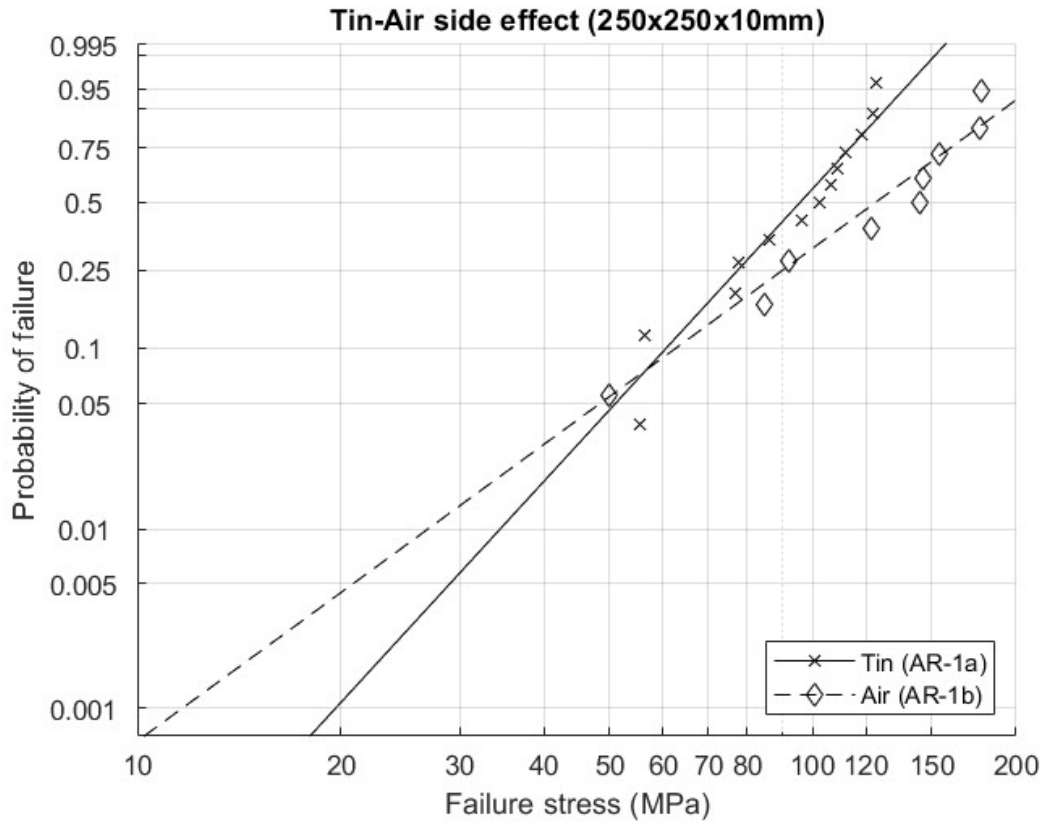
On the contrary, although similar behavior was expected for the larger specimens as well, Figure 5.11b shows no major differences between the strength of the internal and that of the external surfaces of weathered glass. In particular, the mean strength values of the two series differ by 12%. As the same figure implies, the failure stress of the new large specimens is considerably higher than that of the weathered glass. More specifically, the mean strength of the internal surface of weathered glass is 45% lower than that of the tin side of new glass, indicating that the internal surface of the larger specimens was as damaged as the external. Overall, these plots suggest that there is a direct relation between the amount of damage on the glass surface and the strength of it.

## 5.6. The size effect

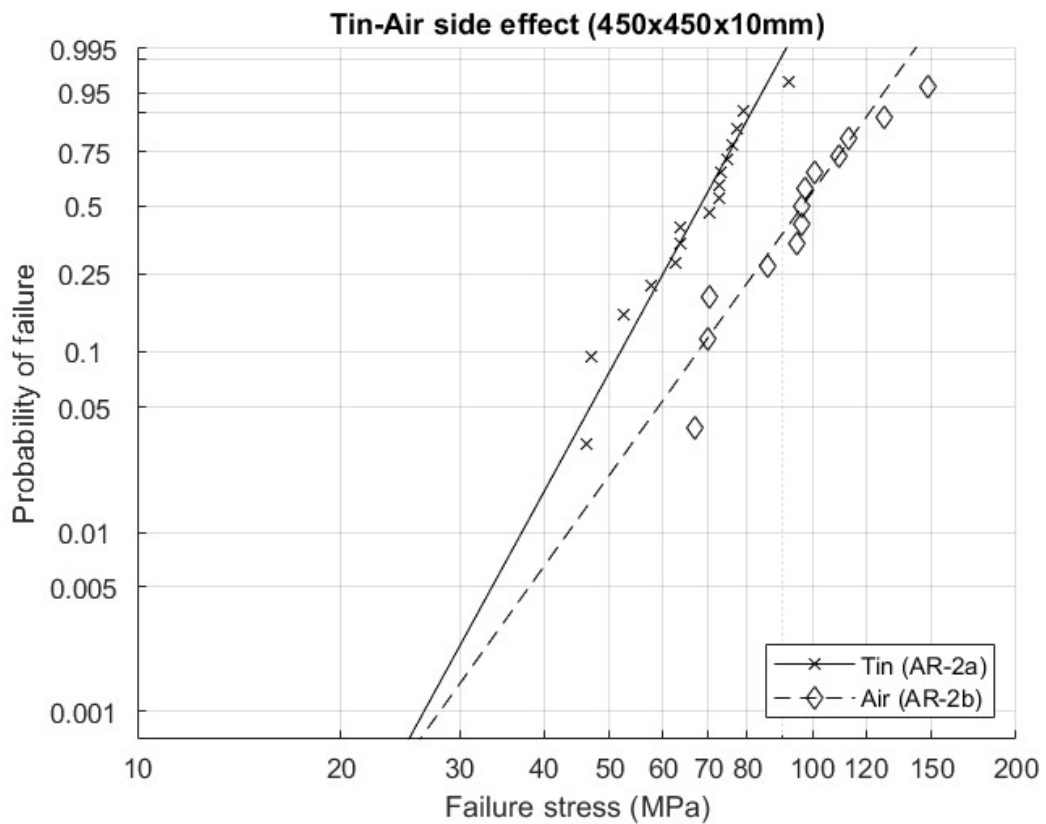
According to the Weibull theory, the strength of glass decreases as the size of the loaded area increases, due to the increased probability of encountering a larger flaw. This phenomenon is called "size effect" and it was already introduced in Section 3.6.2. By testing the specimens with two different loading rings, ("small" with  $D_{LR}=72\text{mm}$  and "large" with  $D_{LR}=180\text{mm}$ ), the influence of the size of the loaded area on the strength of weathered and new glass was investigated. The results of this investigation can be seen in Figures 5.12 and 5.13.

Figure 5.12 indicates that for the specimens of new glass the size of the loaded area influences the strength. In particular, the mean strength of the small specimens is approximately 40% and 30% higher than that of the larger ones, for the air and tin side, respectively. Similar observations were made for the specimens of weathered glass tested with the internal surface in tension. The mean strength of the smaller specimens is approximately 46% higher than the strength of the larger ones. As received glass has occasionally some flaws on its surface, with a random distribution, which are likely to cause the fracture. Therefore, it seems that the internal surface of the examined glass, which did not undergo any weathering, has only these random flaws and it behaves as new glass.

On the contrary, for the specimens tested with the external surface in tension, the size effect does not seem to affect the strength (Figure 5.13b). More specifically, the mean strength of the small specimens is less than 4% higher than that of the large specimens. This behavior suggests that the weathering induced uniformly distributed defects of similar dimensions on the whole surface of glass exposed to the outside environment. As a consequence, after a certain level of damage on the glass surface, the probability of encountering a "critical" defect is equal, regardless the size of the loaded area.

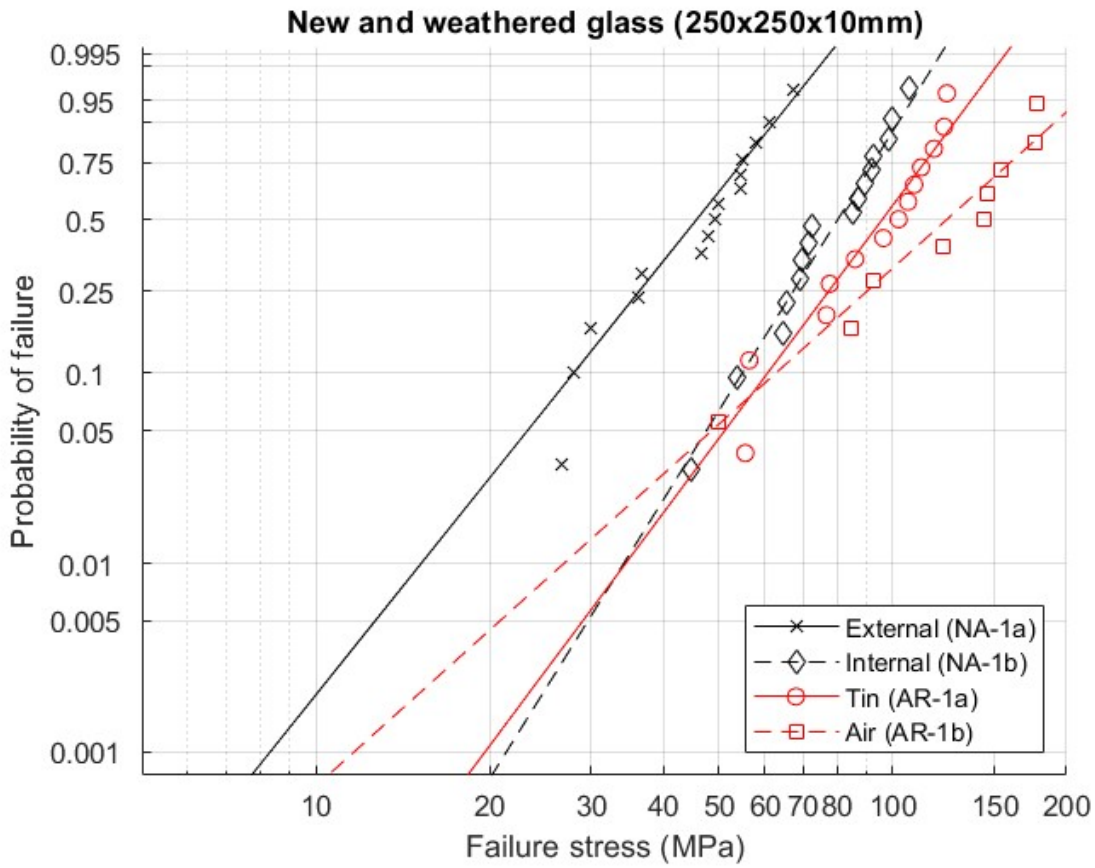


(a) Small specimens (250x250x10mm).

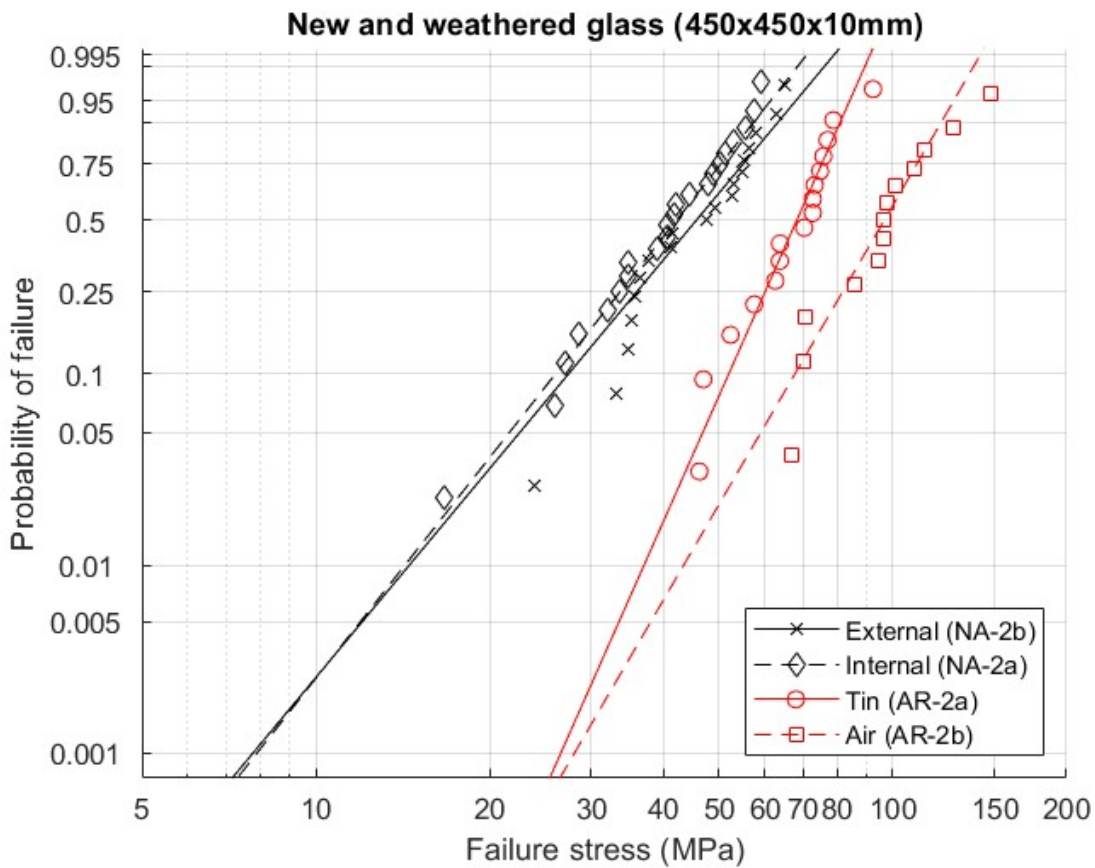


(b) Large specimens (450x450x10mm).

Figure 5.10: The effect of tin side on the strength of the specimens of new, as received glass.

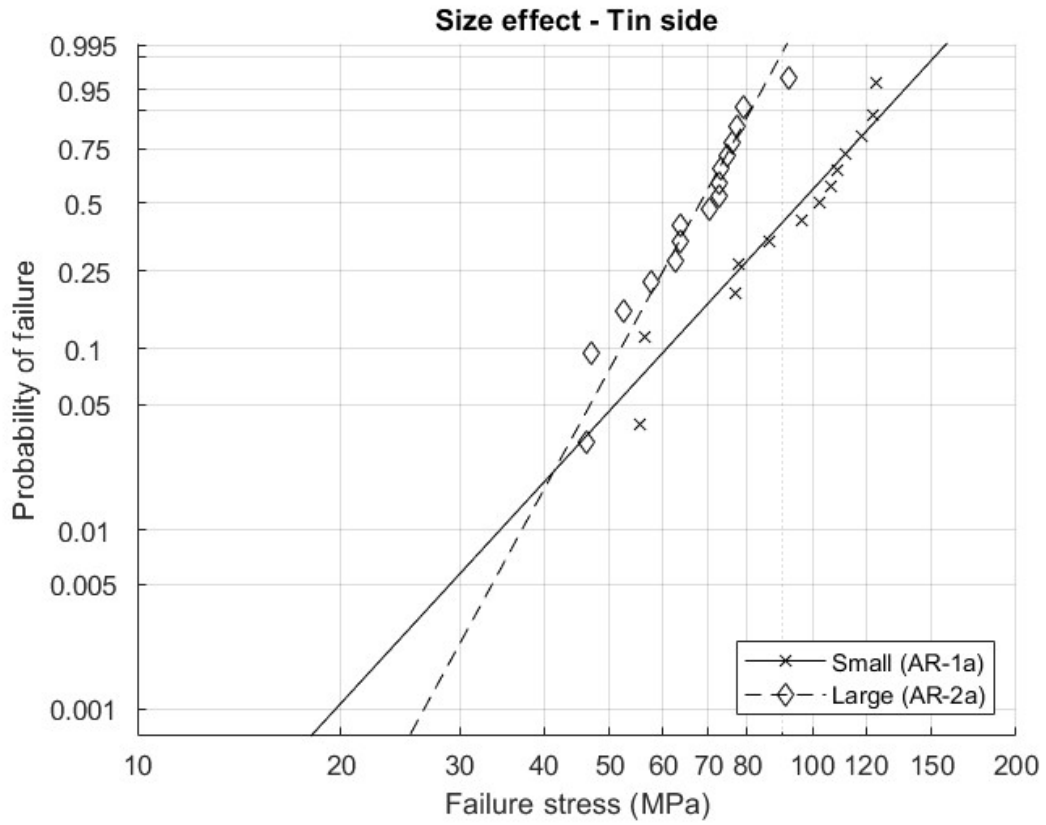


(a) Small specimens (250x250x10mm).

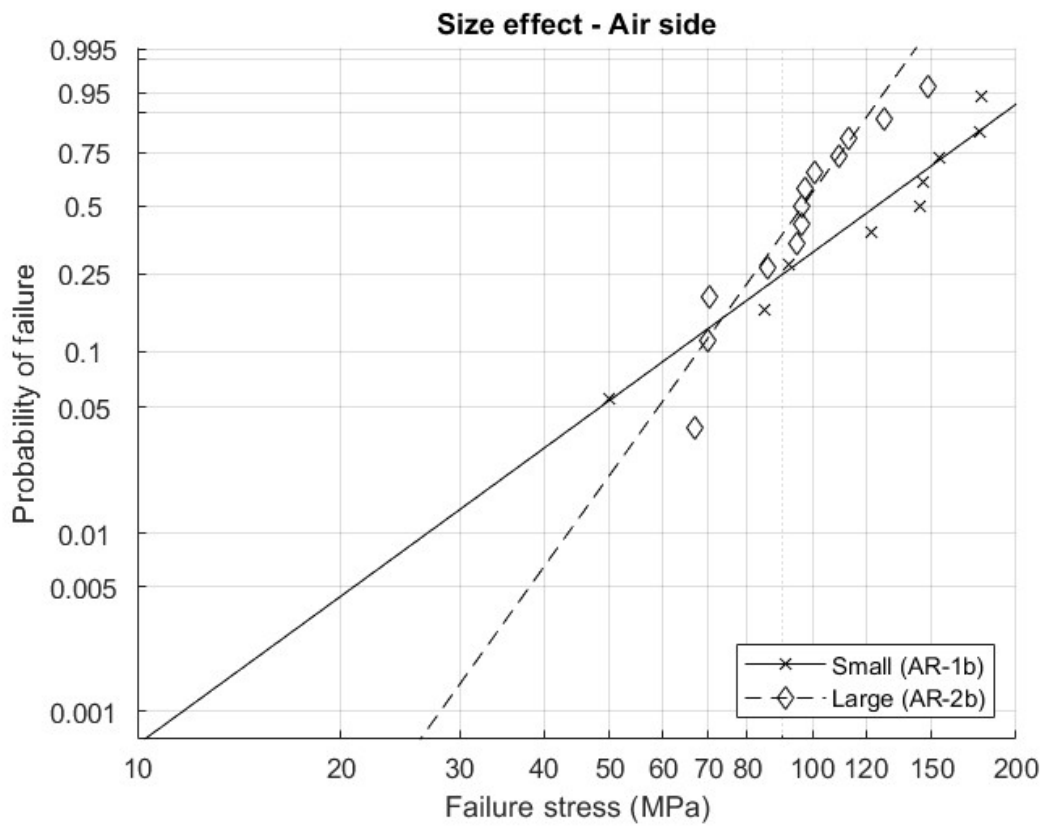


(b) Large specimens (450x450x10mm).

Figure 5.11: Comparison of the strength of weathered and new, as received glass.

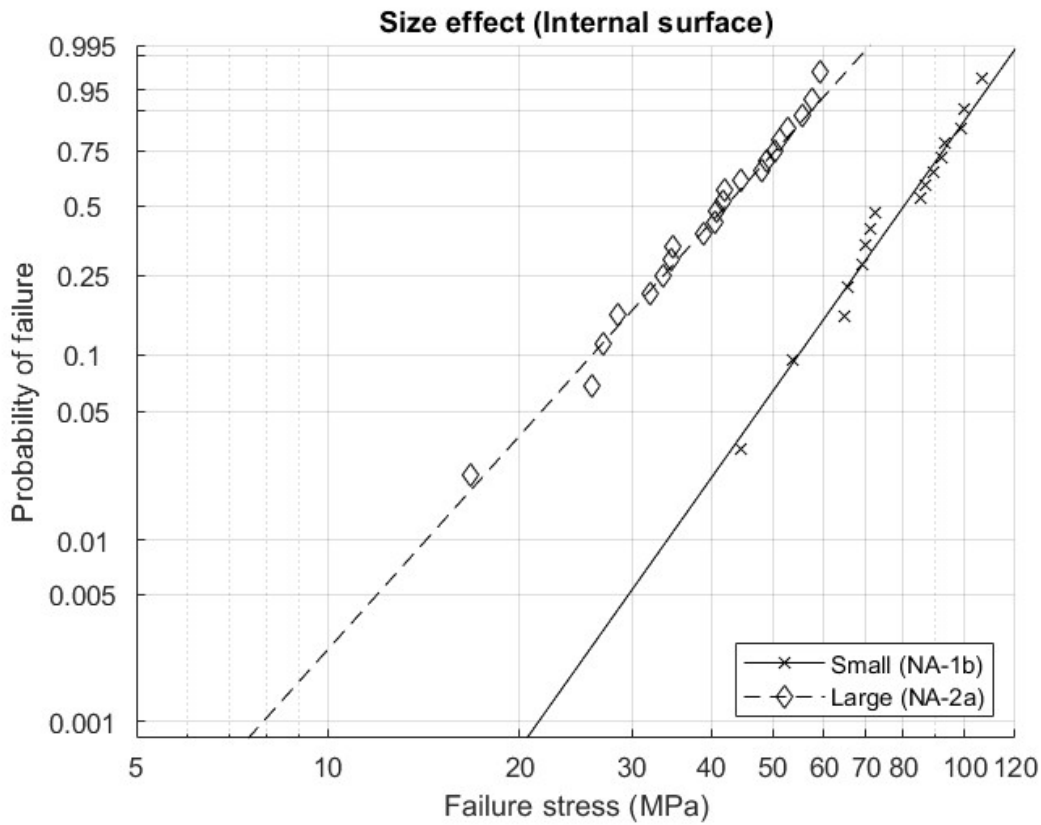


(a) Weibull plots for the small and large specimens tested with the tin side in tension.

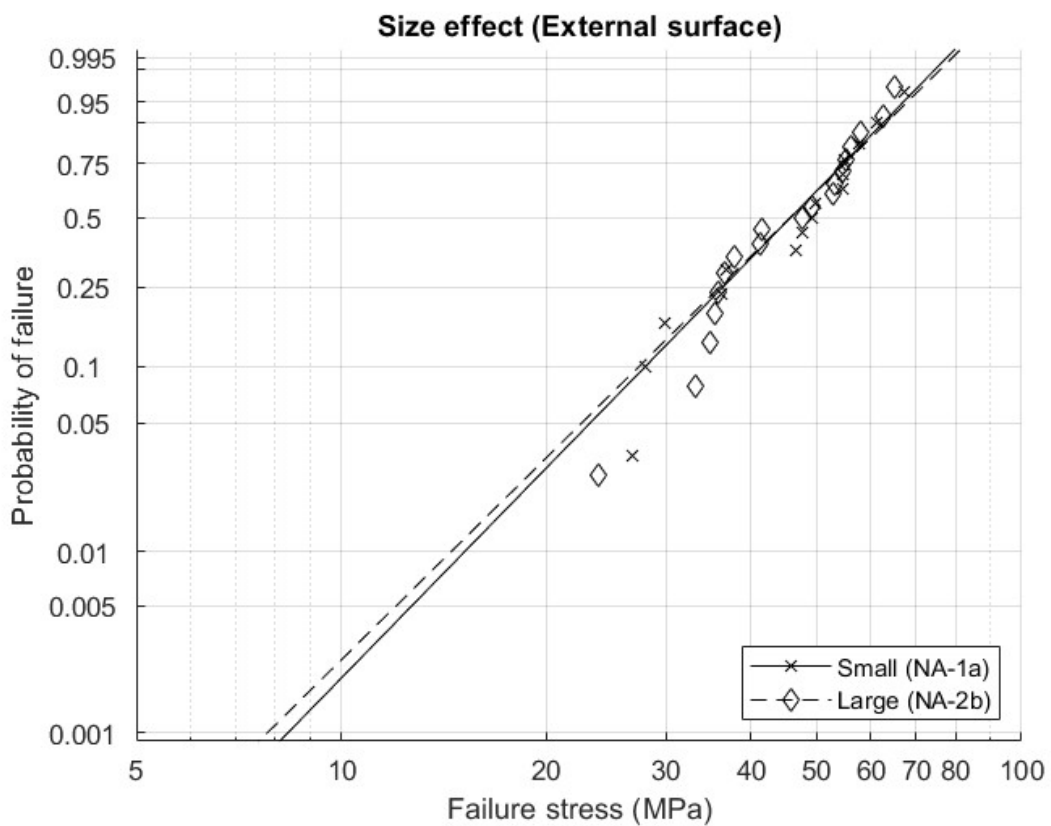


(b) Weibull plots for the small and large specimens tested with the air side in tension.

Figure 5.12: The size effect on the strength of the new glass specimens.



(a) Weibull plots for the small and large specimens tested with the internal surface in tension.



(b) Weibull plots for the small and large specimens tested with the external surface in tension.

Figure 5.13: The size effect on the strength of the weathered glass specimens.

### 5.6.1. The Weibull theory for the size effect

The size effect can be expressed as a function of the surface area and the estimated shape factor  $\beta$  of the Weibull distribution, as described in formula (3.6) (Feldmann et al., 2014). The accuracy of that formula was investigated here by extrapolating the strength of the large specimens from that of the small ones. Then, the estimated values were compared to the actual strength of the large specimens, as emerged from the CDR tests. Figure 5.14 illustrates the Weibull plots of the actual and the estimated failure stresses of the large specimens of weathered glass. For these estimations, the shape factors  $\beta$  of the series with the small specimens, as derived manually and computationally, were used. Furthermore, the value  $\beta = 15$ , proposed by Shen and WÖRMER (1998) for new annealed glass was used. Figure 5.14 shows that formula (3.6) underestimates the strength of the large specimens of weathered glass. In particular, the estimated strength based on the shape factors  $\beta$  is approximately 30% lower than the actual strength for the internal surface and 60% for the external surface. Interestingly, by using the shape factor proposed by Shen and WÖRMER (1998) for new glass, which is almost three times larger than the corresponding factors of weathered glass, the estimated strength values were closer to the actual data.

Figure 5.15 illustrates the Weibull plots of the actual and the estimated failure stresses of the large specimens of new glass. The predicted values were calculated based on the shape factors  $\beta$  of the series with the new small glass specimens. It can be seen that for the series with the tin side in tension, the predicted values are close to the actual ones, especially for the higher probabilities of failure, whereas for lower probabilities of failure the estimations are more conservative. In the plots of the air side, the estimations underestimate significantly the actual values. Thus, although this formula is widely used for the estimation of the strength of new large glass panels, in this research it resulted into very conservative estimations, especially for the weathered glass.

$$\frac{\sigma_{f,A1}}{\sigma_{f,A2}} = \left( \frac{A_1}{A_2} \right)^{(1/\beta)} \quad (3.6)$$

Where,

$\sigma_{f,Ai}$  is the failure stress of the panel with surface area  $A_i$  and  
 $\beta$  is the estimated shape factor of the Weibull distribution.

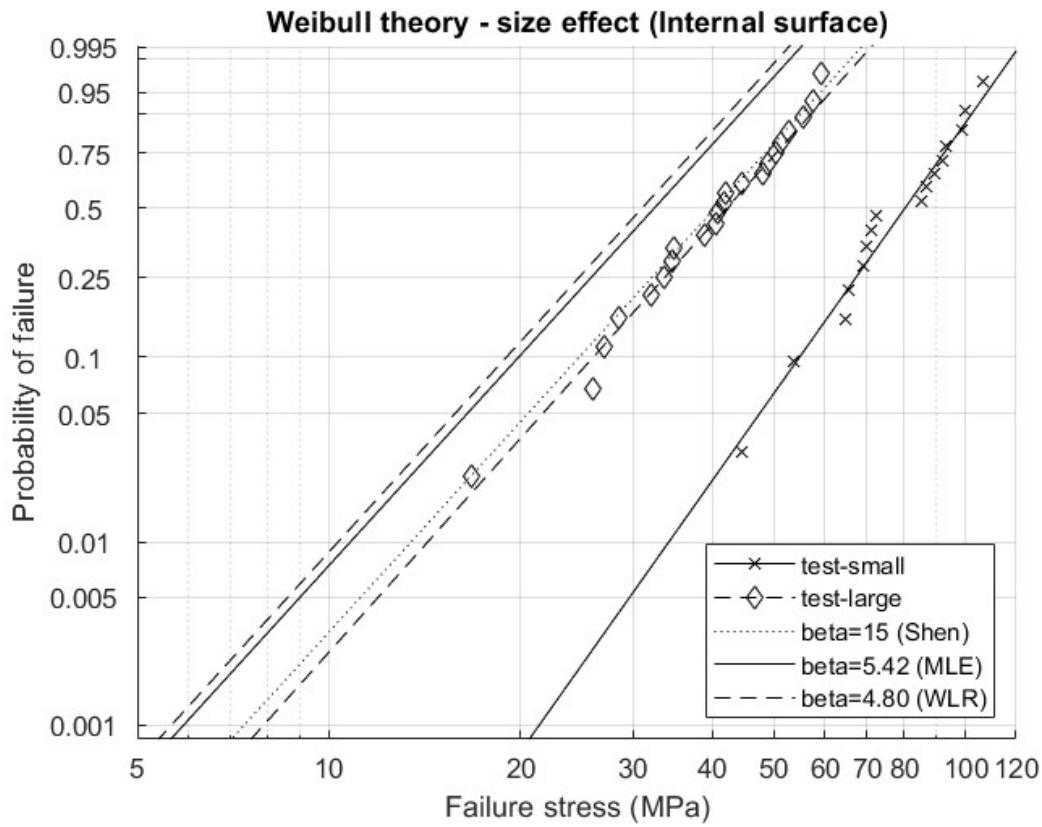
### 5.6.2. Design and characteristic strength of glass

The theoretical design strength of the tested glass specimens was calculated according the Dutch and the European design standards, NEN2608 (2014) and prCEN/TC250-1 (2018), respectively. For this calculation, the area within the supporting ring was considered as the loaded area because although in a CDR setup the load is applied through the loading ring, the area between the loading and the supporting ring is also stressed, as illustrated in the shear and moment diagrams in Figure 5.16. Figure 5.17 indicates that the theoretical strength of the small specimens, (diameter of the loaded area  $D_{SR}=180\text{mm}$ ) according to the Dutch standards is 24,7 MPa, almost 3% higher than that of the large specimens ( $D_{SR}=250\text{mm}$ ) which is 24,0 MPa. Surprisingly, these values according to the European standards are both equal to 15,4 MPa, which is about 37% lower than the Dutch values.

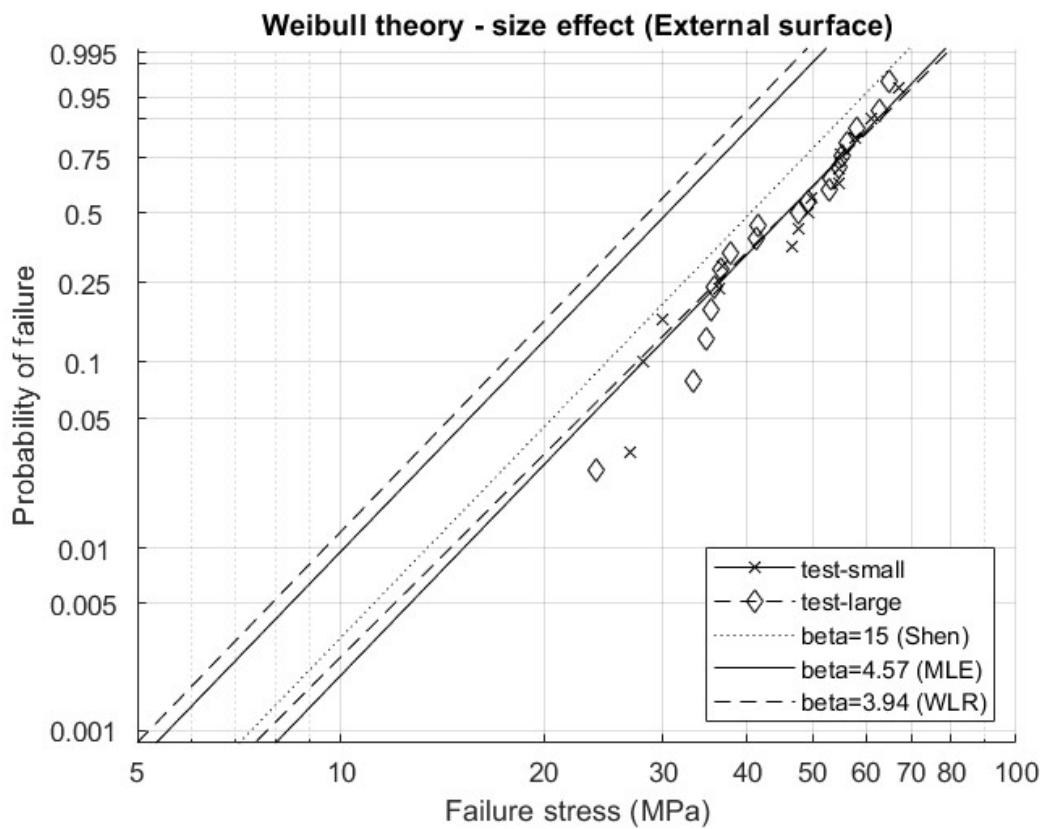
According to EN1990:2002 (2005), the design value of the resistance  $R_d$  equals to the strength which corresponds to probability of failure  $P_f=0,0012^2$ . These values were calculated for the eight testing series of this experimental investigation and they are plotted in Figure 5.17<sup>3</sup>. It can be seen that the design strength of the new glass is higher than the strength proposed by the European standards, and it is closer to that of the Dutch standards. The series AR-1b, with the air side in tension, is an exception, since its design strength higher than that of the European standards but not than that of the Dutch standards. However, there are not sufficient valid experimental data for deriving statistically meaningful conclusions for this series. On the other hand, the design strength of the weathered glass

<sup>2</sup>This value corresponds to buildings with a reference period of 50 years and reliability class 2.

<sup>3</sup>The plotted design values are those emerged from the manual Weibull parameter estimation method, since this method resulted to more conservative values than the computational one.

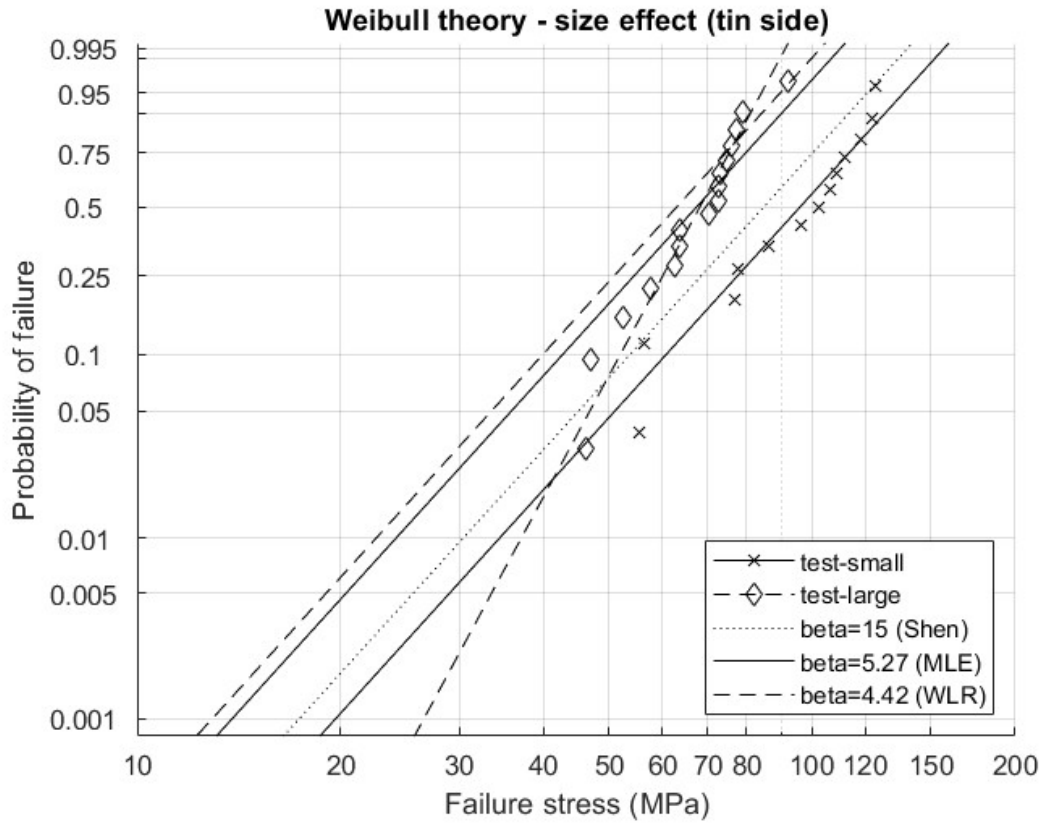


(a) Specimens tested with the internal surface in tension.

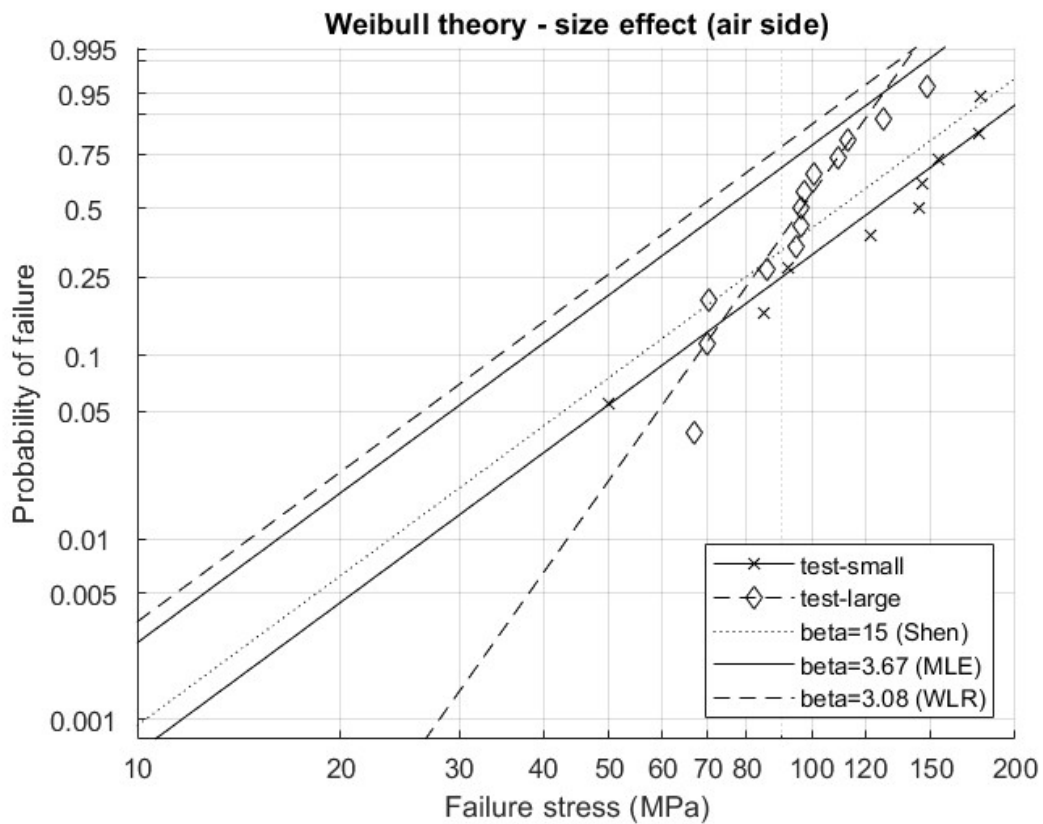


(b) Specimens tested with the external surface in tension.

Figure 5.14: Weibull plots for the actual and the estimated strength of the larger specimens of weathered glass, for several  $\lambda$ .



(a) Specimens tested with the tin side in tension.



(b) Specimens tested with the air side in tension.

Figure 5.15: Weibull plots for the actual and the estimated strength of the larger specimens of new glass, for several  $\lambda$ .

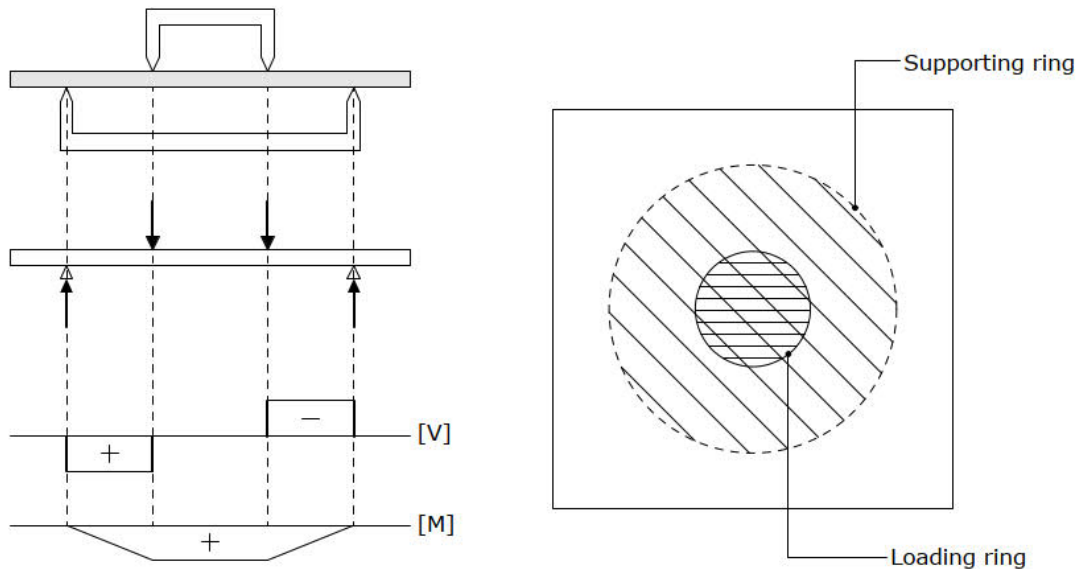


Figure 5.16: Loaded area in the CDR test.

is almost half the strength of the Dutch standards, apart from the strength of the internal surface of the small specimens which is as strong as the new glass.

It is stressed out that the aforementioned values were extrapolated from the Weibull distribution of each testing series. This distribution does not describe well the experimental data at lower probabilities of failure and thus, the found design strength values are probably very conservative. Therefore, the characteristic strength values, which correspond to a higher probability of failure ( $P_f=0,05$ ) are presented in Figure 5.18, since they are expected to be more accurate than the design ones. It can be seen that the found characteristic strength of new glass is approximately 47% higher than that proposed in the European and Dutch design standards. On the other hand, the characteristic strength of weathered glass is almost 30% lower than recommended value, apart from the series NA-1b (tests on internal surface of small specimens), whose strength is 39% higher than the standards.

In Figures 5.17 and 5.18, the presented strength values for the series AR-1b and AR-2b (air side) emerged from the corrected with FEA data. The strength values which correspond to the initial data are presented in Appendix F.

## 5.7. Discussion

At the beginning of Chapter 4, the hypothesis that the external surface of weathered glass is more damaged than the internal one was made, and thus, a lower strength was expected for that surface. This hypothesis was proved correct only in the case of the small specimens, with the internal surface being 68% stronger than the external, whereas in the case of the larger specimens no major difference is observed. The mean strength of the tin-side of the small specimens, which is expected to have occasionally few defects, is 20% higher than that of the internal surface of weathered glass, which also has only few defects. However, the internal surface of the large weathered specimens is 45% weaker than the tin-side of the large new specimens. Thus, it seems that the internal surface of the large specimens is more damaged than that of the small specimens. Since the tested specimens of weathered glass were scored from different panels, some of these panels might be accessible by the users of the building, who introduced more damage to the internal surface, resulting to lower strength values.

A difference between the strength of the tin and the air side of the new glass specimens is noticed.

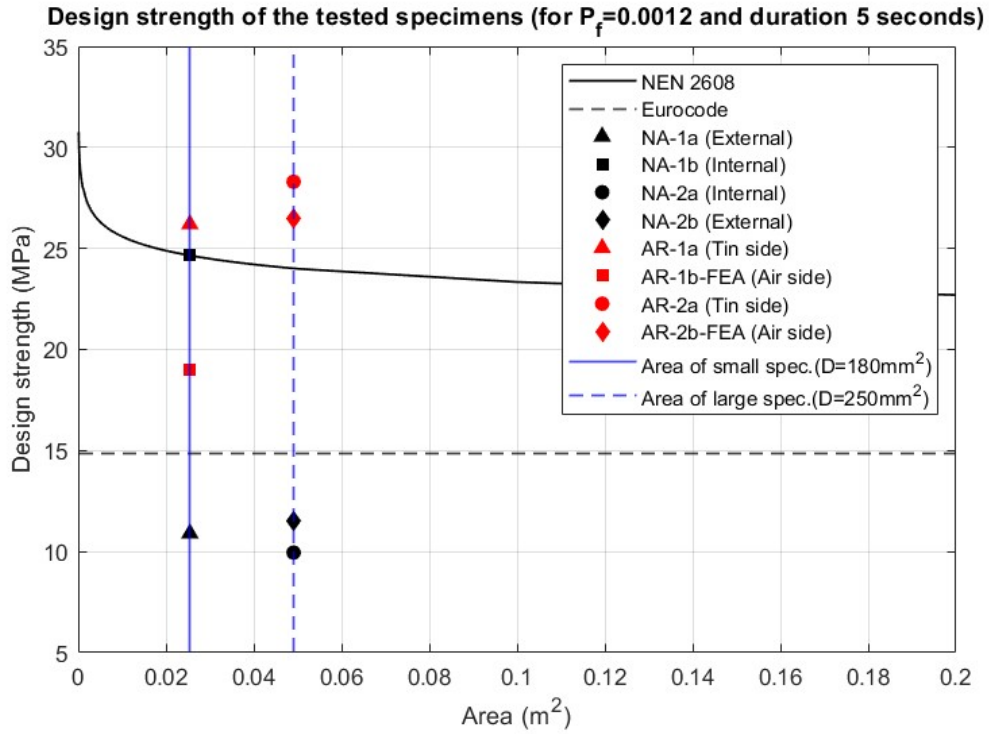


Figure 5.17: Theoretical design strength and design strength according to EN1990:2002 (2005) of the tested specimens (for  $P_f=0,0012$  and load duration 5 seconds).

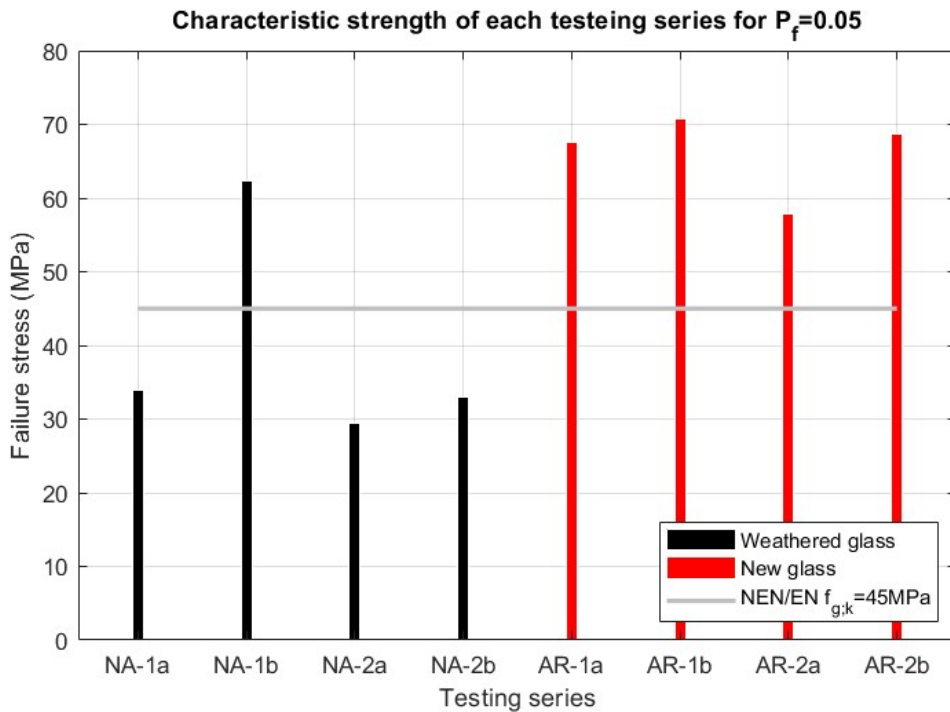


Figure 5.18: Theoretical and experimental characteristic strength of the tested specimens (for  $P_f=0,05$ ).

Although for lower probabilities of failure this difference is small, the mean strength of the air-side is 30-40% higher than that of the tin-side. The microscopy examination of these specimens revealed that the tin-side had more defects than the air-side, and especially some fine linear scratches, which are probably responsible for this difference in terms of strength. However, the reliability of the strength results of the air side is questioned because no sufficient data exist for obtaining statistically meaningful results. The high failure stresses of the air-side were associated with fracture patterns similar to those of toughened glass, and their fracture origin was not detectable, or there were more than one defects which failed simultaneously. Therefore, the valid tests used for the statistical analysis were less than those required according to the ASTM C1499-09 (2013).

The second hypothesis was that the size effect, which applies for new glass, applies also for weathered glass. Regarding the new glass, this phenomenon is widely recognized and it is usually considered in the provisions of the design standards for glass. This phenomenon is also observed in the tests on new glass of this project, since the small specimens failed at approximately 30-40% higher stresses than the large ones. In the case of weathered glass though, the size effect is not always influential. In particular, the mean strength of the internal surface of glass, which was visually less damaged than the external, is 46% higher for the small specimens compared to the large. On the contrary, the strength of the external (weathered) surface is similar, no matter what the size of the tested area is. This behavior suggests that in the surface of naturally aged glass panel, similar defects with uniform density exist. On these grounds, every specimen cut from such panel will have equal probability of encountering a critical flaw, independent of its size. In reality, the defects on the examine glass were not the same but indeed, most of the specimens had defects of similar shape and size (digs and fine scratches) and with similar density.

Finally, the design strength of the weathered specimens is around 25% lower than that of the European (prCEN/TC250-1, 2018) and more than 50% lower than that of the Dutch (NEN2608, 2014) standards. Likewise, the characteristic strength of this glass is approximately 30% lower than that proposed in the two standards. These observations generate concerns regarding the safety that the existing design standards for glass provide. Since the service life of a building is normally 50 years, this must be reflected in the design strength of the materials used. However, in these two standards, it is not clear to which probabilities of failure these design values correspond and thus, the probability of failure which is mentioned in EN1990:2002 (2005) was used in the calculations ( $P_f=0,0012$ ). By using the probability of failure proposed in ASTM-E1300 (1997) though, the design strength of the weathered and new glass specimens would have been higher (See Appendix G for the plots for  $P_f=0,008$ ). In this case, the design strength of weathered glass is slightly higher than that of the European standards but still, it is around 25% lower than that of the Dutch standards.



# 6

## Prediction of glass strength

### 6.1. Introduction

In this chapter, a methodology for the prediction of the strength of weathered glass, based on the theory of Linear Elastic Fracture Mechanics (LEFM) is proposed and tested. The LEFM relate the failure stress of a stressed brittle material to the size of its defects, through the critical Stress Intensity Factor  $K_{IC}$  (SIF) and the geometry factor  $Y$ , as discussed in Section 3.4.

The proposed methodology consists of two parts; the detection of the "critical flaw" and the prediction of the failure stress based on the geometry of that flaw. The "critical flaw" is the one that according to the Weakest-link-theory will initiate the fracture. The steps of the methodology along with the assumptions and simplifications made, are presented in Section 6.2. In Section 6.3, the formula of LEFM used for the predictions is analysed and appropriate values for the factors  $K_{IC}$  and  $Y$  are chosen. Afterwards, the feasibility and effectiveness of the methodology are evaluated in Section 6.4, based on the outcomes of the non-destructive and destructive CDR tests of Chapter 4.

### 6.2. Methodology

The proposed methodology for the prediction of the strength of weathered glass is based on its surface condition. In particular, it aims at finding a link between the size of its defects and its strength. Thus, the methodology consists of two parts with the following steps in each part:

1. Non-destructive flaw detection test: detection of the "critical" defect on the examined surface.
  - (a) Cleaning of the glass surface with cleaning detergent suitable for glass and soft paper. The cleaning must be conducted carefully, so as no more defects are introduced into the glass surface.
  - (b) Manual inspection of the examined surface of glass and detection of visually large defects.
  - (c) Examination of the geometry of the defects found in the previous step with Traceit<sup>®</sup>. Measurements of the depth of these defects with the software of Traceit<sup>®</sup>.
  - (d) Optional: A reliability study can be performed, as explained in Section 4.4.2.2, to derive the random error of the depth values, based on the variation of consecutive measurements.
  - (e) Marking of the deepest defect, which is considered as the "critical" one, namely the flaw that will originate the fracture<sup>1</sup>.
2. Strength prediction based on LEFM: calculation of the failure stress using the depth of the largest defect.

---

<sup>1</sup>This step is not part of the methodology but it is required for the evaluation.

- (a) Selection of values for the critical stress intensity factor and the geometry factor, appropriate for the examined specimen and the presumed as "critical" defect.
- (b) Calculation of the failure stress for the "critical" flaw, according to the formula (3.1). In this case, a reliability study was performed so, a fracture stress interval was calculated, in which the actual strength of glass was likely to be. The upper and lower limits of that interval were determined based on the reliability of the depth measurements. For instance, if a scratch was found to have a depth of  $80 \pm 3 \mu\text{m}$ , the boundaries of that interval will be the  $\sigma_{f,(d=77)}$  and  $\sigma_{f,(d=83)}$ .

The aforementioned steps were followed in this project for the prediction of the strength of the glass specimens. The effectiveness of this methodology was evaluated based on the non-destructive and destructive CDR tests of Chapter 4. Analytically, the steps which were followed for the evaluation are:

1. Evaluation of the non-destructive flaw detection test:

- (a) The location of the fracture origin, which became known after the destructive tests, was compared to the location of the "critical" defect which was detected and marked during the non-destructive tests.
- (b) For the specimens whose fracture origin was successfully detected, further microscopic examination was performed to identify the characteristics (shape and size) of the "critical" defect and evaluate the appropriateness of the chosen geometry factor  $Y$ .

2. Evaluation of the predicted failure stresses:

- (a) The failure stresses of the examined specimens, as derived from the CDR tests, were compared to the predicted failure stresses.
- (b) The predicted strength values were fitted to a Weibull distribution and compared to the Weibull plots of the actual data, to study whether the whole set of the predicted values approaches well that of the actual ones.

### 6.2.1. Assumptions for the development of the methodology

The methodology was developed based on several assumptions and simplifications. To the author's knowledge, no similar predictions were attempted before nor such methodology exists in literature. Therefore, the proposed methodology was kept as simple as possible in order to evaluate its feasibility and effectiveness within the time frame of this project. The assumptions and simplifications made for its development are the following:

1. The external surface of glass was considered more damaged than the internal one and thus a lower strength was expected from that surface. Therefore, the methodology was applied only for that surface.
2. Only the surface area inside the loading ring was examined during the non-destructive flaw detection test.
3. During the CDR tests, all the defects within the examined loaded area were subjected to an ideal equibiaxial field of stresses. Inside the loading ring the stresses were the maximum, compared to other locations of the specimen.
4. The "critical" flaw was the largest defect that can be found within the area of the loading ring. Since there were defects which were visible by human's eye, it was assumed that they would be more critical than the ones which were visible only under the microscope.

### 6.2.2. Examined specimens

The proposed methodology was applied only for the specimens tested with the external surface in tension (series NA-1a with small specimens and NA-2b with large specimens of weathered glass). The microscopy examination before the CDR tests revealed that for most of the specimens, this side was

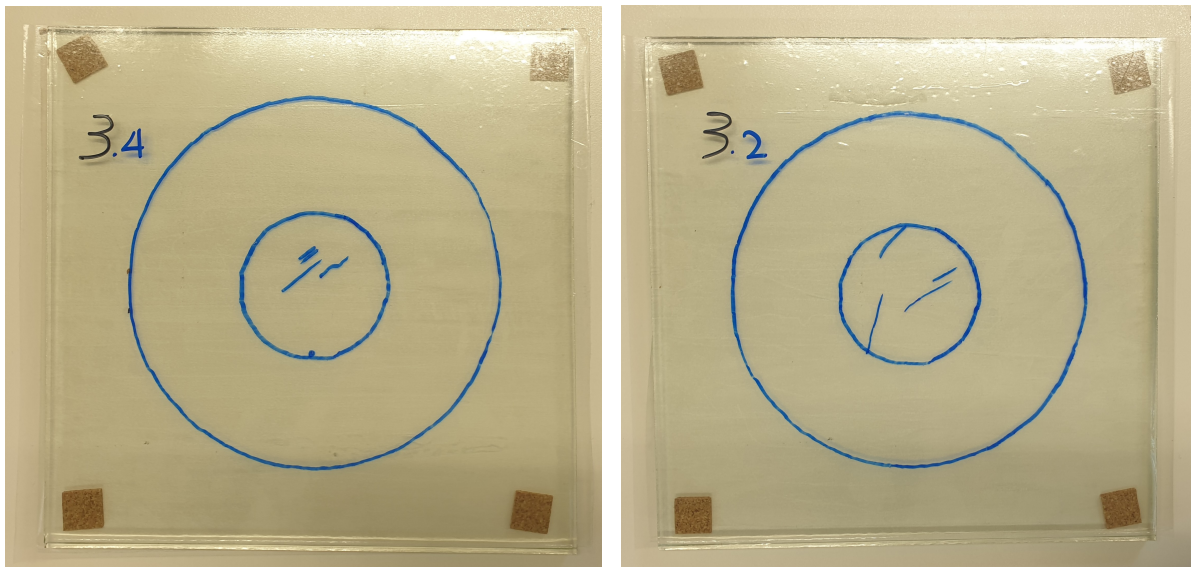


Figure 6.1: Specimens with the deepest defects marked on their surface.

more damaged than the internal one (see Section 4.3.1). Therefore, the 21 specimens of the series NA-1a and the 22 specimens of the series NA-2b, were tested according to the steps of the methodology described in Section 6.2. Figure 6.1 illustrates two of the specimens, on which the larger flaws were marked. The marker was not applied directly on the glass surface but on the adhesive foil to facilitate the post-fracture analysis afterwards.

### 6.3. Stress intensity factor formula

Formula 3.1 seems simple to understand and use but its derivation is based on numerous assumptions, experiments and the experience of researchers. The parameters which synthesize this formula can be derived experimentally or they can be chosen from the existing literature. For this research, in which the second option was followed, the essence of understanding and making the right parameter choice is underlined. Thus, the parameters which compose this formula are discussed in this section to assist its use for the strength predictions.

$$K_I = \sigma \cdot Y \cdot \sqrt{\pi \cdot c} \quad (3.1)$$

Where,

$K_I$  is the stress intensity factor for mode I crack propagation,

$\sigma$  is the tensile stress, normal to the crack's plane,

$Y$  is the shape correction factor of the flaw and,

$c$  is the flaw size in meters.

#### Critical stress intensity factor $K_{IC}$

Although it was defined as a material property, the critical stress intensity factor is not constant for all the glass elements. In practice, this factor, describes the elastic stress intensity close to the crack tip and it is influenced by the geometry of the crack, the geometry of the element and its loading condition (Overend et al., 2007). In addition, for different glass compositions, different values for the fracture toughness were reported (S. Wiederhorn, 1974).

For brittle materials such as glass, several studies revealed that the value of  $K_{IC}$  ranges between 0,6-1,0 MPa  $m^{0,5}$  (S. Wiederhorn, 1974; Lehman, n.d.; Kwan, n.d.; Datsiou and Overend, 2017b). These values were derived experimentally. In short duration bending tests though, values that range from 0,45-0,55 MPa  $m^{0,5}$  were found, while in long duration tests, even lower values were reported (Rodichev

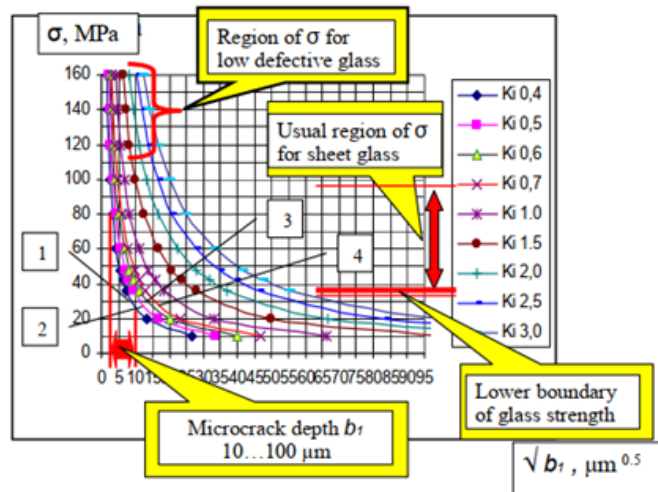


Figure 6.2: The calculated dependencies of the bending strength of glass plates subject to the depth of semi-elliptical surface micro-crack in a fracture focus (Rodichev and Veer, 2010).

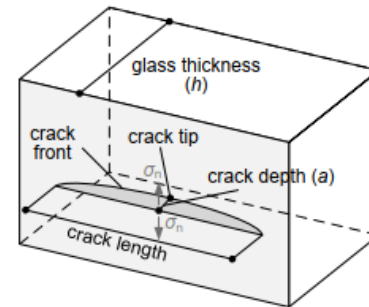


Figure 6.3: Flaw characteristics (Haldimann, 2006).

and Veer, 2010). In the same study, tests performed under controlled environmental conditions and high loading rates led to higher factors up to  $2,0 \text{ MPa } m^{0,5}$ . The dependency of the strength of glass to the fracture toughness is shown in Figure 6.2. In most of the cases, a typical value of  $0,75 \text{ MPa } m^{0,5}$  is used for the fracture toughness of soda lime silica glass.

#### Geometry factor $Y$

The value of the flaw shape factor or geometry factor  $Y$  is also derived experimentally. As its name implies, it is a function of the defect's geometry. This factor depends also on other parameters, such as the stress field, the geometry of the element, the depth and the orientation of the defect. According to Quinn (2020), the shape factor varies even around the perimeter of the flaw, with the fracture initiating at the location with the maximum  $Y$ -value. However, in case of shallow cracks, these dependencies are usually neglected, avoiding many uncertainties in the calculations (Haldimann, 2006). For half-penny shaped flaws in a semi-infinite solid, a value of 0,713 was proposed (Lawn, 1993). Haldimann (2006) suggested a factor of 1,12 for surface cracks away from the edges, that are long enough compared to their depth. An overview of the several geometry factors that can be found in literature is available in his study. The reported experimental values of the geometry factor  $Y$  reached the high value of 2,0 (Rodichev and Veer, 2010).

#### Tensile stress $\sigma_f$

When  $K_I = K_{IC}$ , the tensile stress on the crack tip equals to the inert strength of the crack. In case of annealed glass, it is the stress for which the crack opens and causes the fracture of glass. In case of prestressed glass, this value depends on the residual compressive stresses  $\sigma_r$  on the glass surface. However, this type of glass is out of the scope of this study, so it is not elaborated more.

#### Flaw size $c$

The age of the weathered glass, its previous application and its processing during manufacturing are only few of the parameters that influence the size of the surface flaws in glass. In literature, the parameter flaw size is found to have slightly different definitions. In some cases, this size parameter stands for the flaw length, the half-length of the flaw, or the flaw depth as shown in Figure 6.3 (S. Wiederhorn, 1974; Fischer-Cripps and Collins, 1995; Haldimann, 2006; Zammit and Overend, 2010; LINDQVIST, 2013). This observation can be explained by the slightly different ways in which formula (3.1) was derived. The most elaborated definition was found in the book of Quinn, where this parameter is presented to vary with the location of the flaw (Quinn, 2020).

Table 6.1: Evaluation of critical flaw detection method.

NA-1a (Small specimens)			NA-2b (Large specimens)		
Specimen	Defect type	Evaluation	Specimen	Defect type	Evaluation
1.1	Scratch	Success	3.1	Dig	FF
1.2	Dig	ND	3.2	Scratch	FF
1.3	Dig	ND	3.3	Scratch	FF
1.4	Scratch	Success	3.4	Dig	Success
1.5	Scratch	FF	3.5	Dig	ND
1.6	Scratch	ND	3.6	Scratch	Success
1.7	Dig	FF	3.7	Dig	ND
2.1	Scratch	FF	3.8	Scratch	FF
2.2	Dig	ND	3.9	Dig	ND
2.3	Dig	FF	3.10	Scratch	FF
2.4	Dig	ND	3.11	Scratch	Success
2.5	Dig	ND	3.12	Dig	ND
2.6	Dig	ND	4.1	Scratch	FF
2.7	Scratch	Success	4.2	Scratch	FF
3.1	Scratch	FF	4.3	Scratch	FF
3.2	Scratch	Success	4.4	Scratch	FF
3.3	Dig	ND	4.5	Dig	ND
3.4	Scratch	Success	4.6	Scratch	ND
3.5	Scratch	FF	4.7	Dig	ND
3.6	Scratch	Success	4.8	Scratch	FF
3.7	Scratch	Success	4.9	Scratch	FF
			4.10	Scratch	FF

## Conclusions

The value of each parameter can range significantly, imposing large uncertainties to the formula's outputs. For this project, a value of 0,75 was chosen for the  $K_{IC}$  factor, since it is the most commonly used for soda lime silica glass. For the shape factor  $Y$ , the values 1,12 and 0,713 were used, depending on the different geometries of the found defects. Finally, it is stressed out that an accurate depth measurement is essential for the use of formula (3.1), especially for fine defects, around 20  $\mu\text{m}$  or smaller. As Figure 6.2 implies, the smaller the flaw, the more crucial it becomes to determine the flaw size precisely, due to the exponential relationship between the strength and the flaw depth.

## 6.4. Evaluation of the methodology

The effectiveness of the proposed methodology is evaluated based on the outcomes of the destructive and the non-destructive tests presented in Chapter 4. The evaluation is divided into two parts, in accordance to the parts of the methodology; the feasibility and success of the critical flaw detection test and the accuracy of the predicted failure stresses, compared to the actual values.

### 6.4.1. Non-destructive detection of the critical flaw

Table 6.1 presents the results of the critical flaw detection test. In total 10 out of the 43 specimens of both testing series failed at a defect which was detected before the tests ("Success"). In 19 of the specimens, the critical flaw was not marked ("FF - Fail to Find"), even though on these specimens other defects were marked as critical. Finally, in 14 out of the 43 specimens, it was not possible to detect through manual inspection and mark any visible large defect ("ND - Not Detected").

From the 10 specimens which broke at the detected flaw, 7 of them were small (see Figure 6.4). Thus,

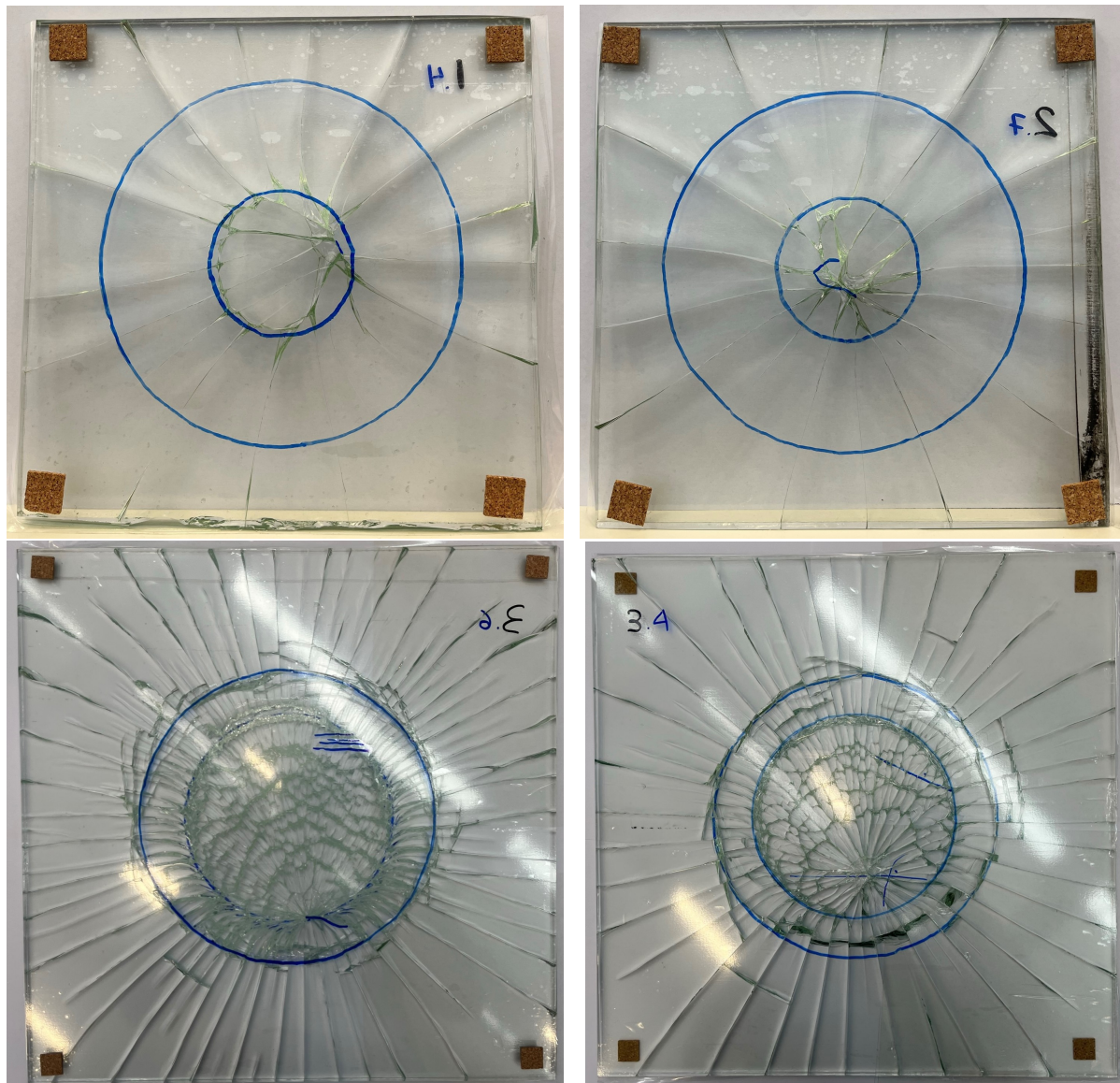


Figure 6.4: Specimens which broke at the detected "critical flaw".

in the 33% of the small specimens, the critical defect was detected successfully. Since the detection method was manual, the smaller the examined area, the higher the effectiveness of the manual inspection. On the contrary, although the larger specimens contained more visible scratches within the examined area, it was not feasible to measure or mark all of them manually. Therefore, only 3 out of the 22 specimens failed at a marked defect.

A post-fracture analysis was performed on the specimens which broke at the detected defect, in order to verify the depth measurements taken with Traceit® before the CDR tests. However, as explained in Section 4.4.5, the specimens did not always break at the deepest location of the defect or at the exact location where the measurement was taken. Therefore, the measurements taken before the tests were not comparable to the results of the post-fracture microscopy analysis.

#### 6.4.2. Prediction of failure stress

For the prediction of the failure stress, the formula (3.1) was used. It is stressed out that this formula does not account for the phenomenon of stress corrosion and the time-dependency of strength. More specifically, the strength derived from that formula is the inert strength of glass, as illustrated in Figure

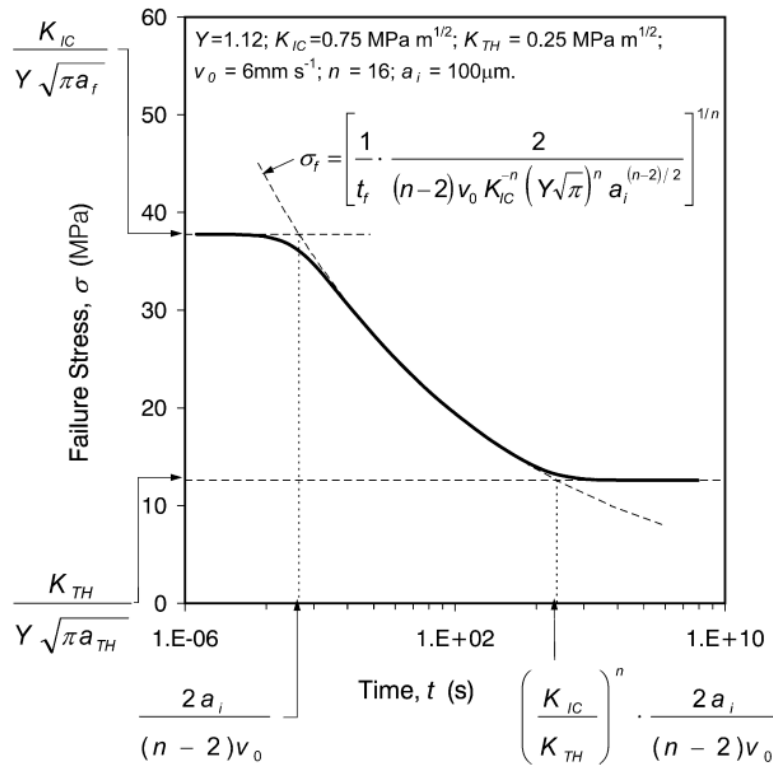


Figure 6.5: Failure stress of a surface crack as a function of stress duration by Overend and Zammit (2012).

6.5. This must be taken into account when comparing the predicted failure stresses to the actual failure stresses. As discussed in Section 4.4, the specimens reached failure at different times and the failure stresses were normalised to an equivalent period of 60 seconds for the statistical analysis. However, for the comparison with the predicted values, the experimental results were normalised to a reference time of 1 second, which is estimated to approach better the predicted inert strength.

The size and the type of the defects, which are required for the predictions, were already presented in Table 4.3. As described in the steps of the methodology, the failure stress for each specimen was predicted not as a single value but as an interval in which the strength was likely to be, based on the scattering of the depth measurements found during the reliability analysis. As mentioned in Section 4.4.2.2, the scattering of the results was larger for the deepest defect and smaller for the smaller defects. This observation is important since the relation between the strength and the size of the defects is exponential (see Figure 6.2). Thus, a great variation in the measurements of large defects (i.e. deeper than 70 μm) does not affect considerably the prediction of the failure stress, whereas an accurate depth measurement is required when it comes to defects smaller than approximately 30 μm. To this extend, the use of the measured defects with a tolerance of ±5 μm is expected to give representative predictions.

Figures 6.6 and 6.7 illustrate the Weibull plots of the actual failure stresses and those of the maximum and minimum predicted values, for the series NA-1a and NA-2b. The critical SIF at both cases was set equal to 0,75 MPa m<sup>0,5</sup>.

In Figure 6.6, the same geometry factor was used for all the defects, equal to 1,12, which corresponds to linear scratches. For that set of parameters, the predictions do not approach well the experimental data. However, since the defects were not always scratches but also digs, with a more circular shape, another geometry factor was used. In particular, the value of 1,12 was used for the linear scratches but for the predictions which corresponded to digs the value 0,713 was chosen, which was proposed for half-penny cracks. The predictions in this case are much closer to the actual values, especially for

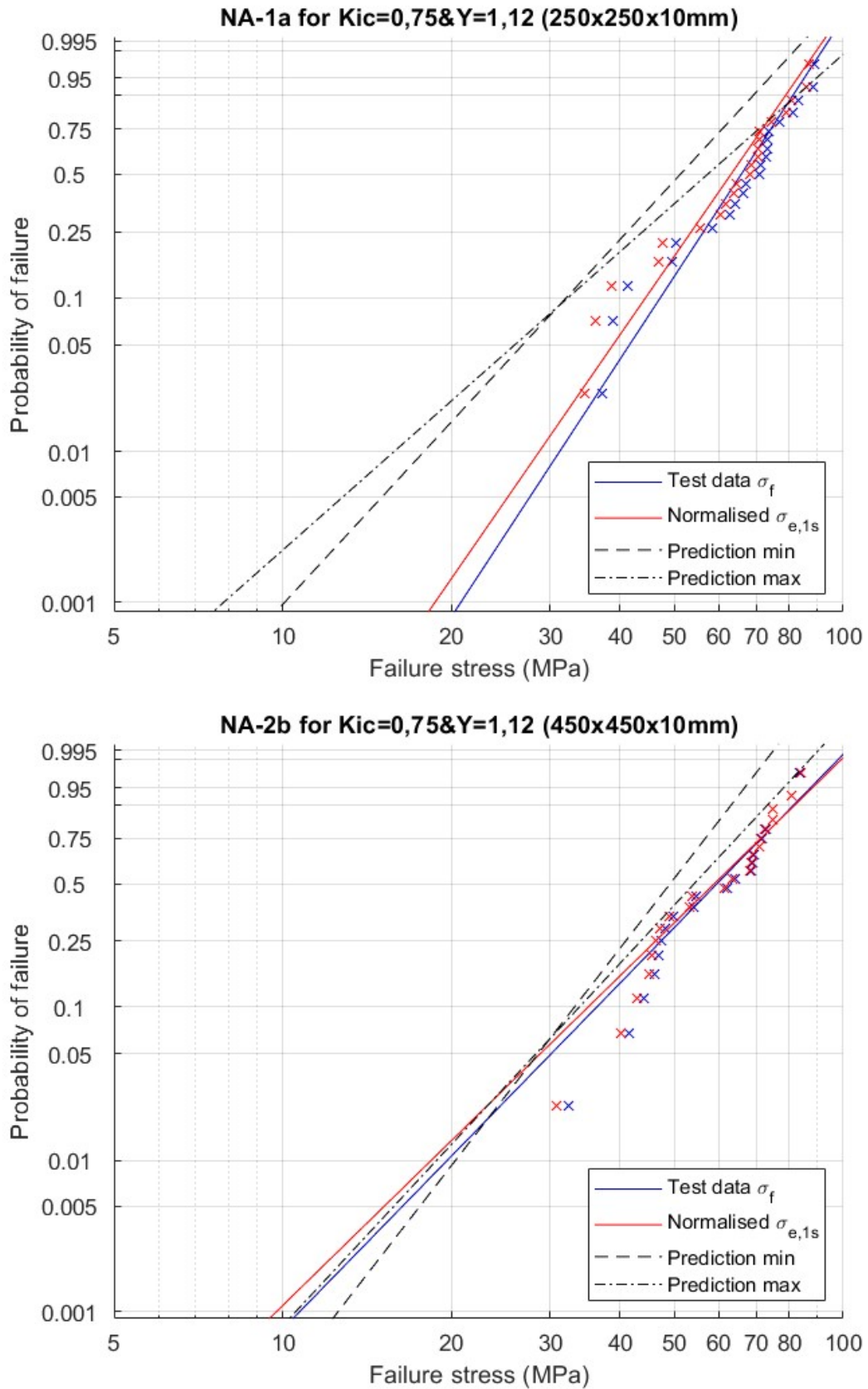


Figure 6.6: Weibull plots of the actual and predicted failure stresses for the specimens tested with the external surface in tension, for  $K_{Ic} = 0,75 \text{ MPa } m^{0,5}$  and  $Y=1,12$ .

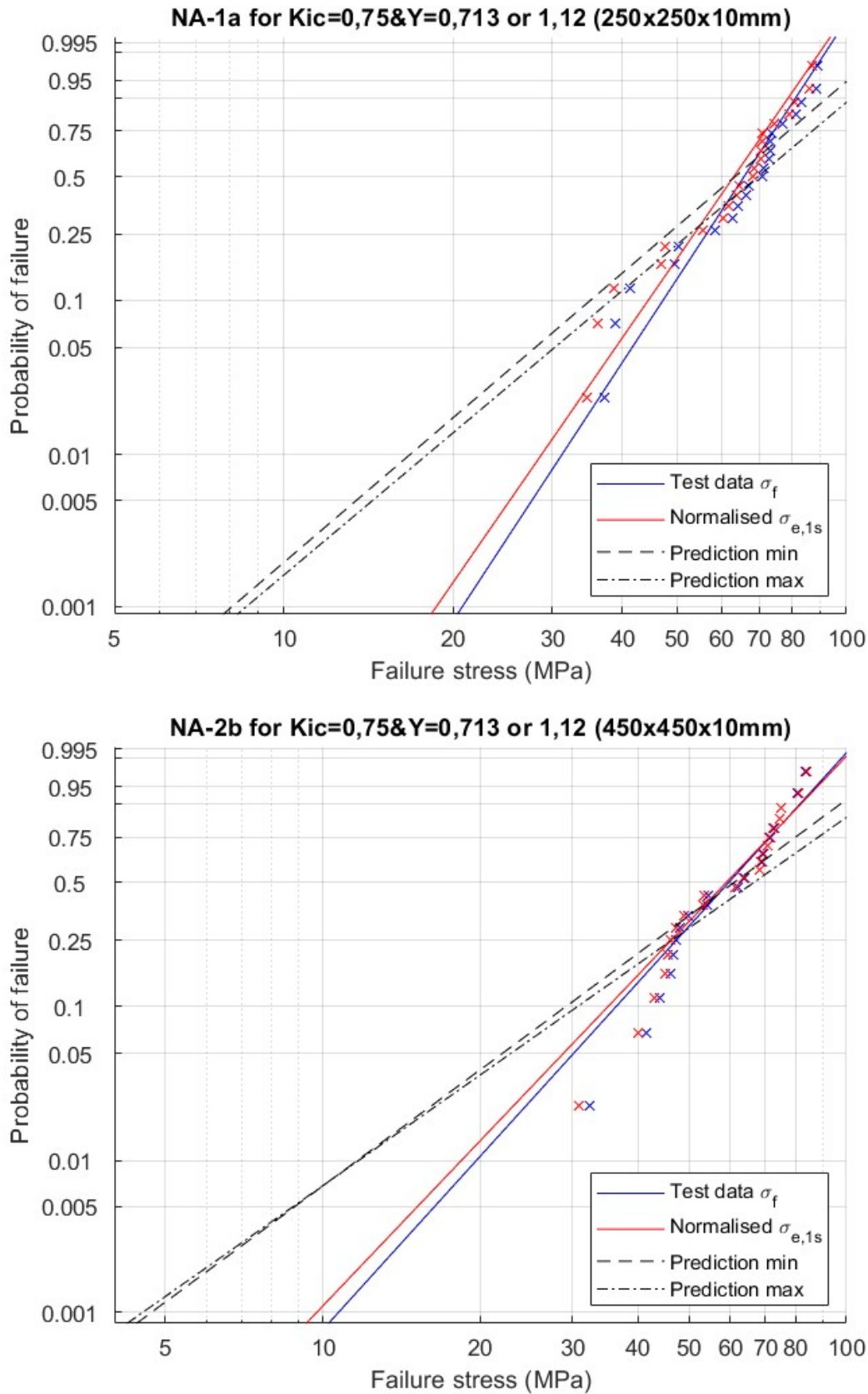


Figure 6.7: Weibull plots of the actual and predicted failure stresses for the specimens tested with the external surface, in tension for  $K_{Ic}$  0,75 MPa  $m^{0,5}$  and  $Y=1,12$  or  $Y=0,713$ .

Table 6.2: Average actual and predicted failure stresses for  $K_{IC}=0,75MPa m^{0,5}$  and  $Y = 1, 12$  or  $0, 713$ .

Series	$d_{mean}$ ( $\mu m$ )	$\sigma_{f,mean}$ (MPa)	$\sigma_{eq,1s,mean}$ (MPa)	$\sigma_{pred,mean}$ (MPa)	Error $\sigma_f$	Error $\sigma_{eq,1s}$
NA-1a	58	66,2	63,6	68,7	8 %	4 %
NA-2b	63	60,3	59,7	65,6	10 %	9 %

probabilities of failure around 50%, as illustrated in Figure 6.7. Thus, a more elaborated selection of geometry factors will probably improve considerably the accuracy of the predictions.

In Figure 6.8, the average actual and predicted failure stresses are presented for  $K_{IC}=0,75 MPa m^{0,5}$  and  $Y=1, 12$  or  $0, 713$ . For the series NA-1a, with the small specimens, the average predicted strength  $\sigma_{pred}$  is 8% higher than the average normalised failure stress  $\sigma_{eq,1s}$  and just 4% higher than the average actual failure stress  $\sigma_f$ . Similar observations can be made for the series NA-2b, with the large specimens. More specifically, the average predicted strength is 10% higher than the average normalised failure stress and 9% higher than the average actual failure stress. The exact values of the average actual and predicted failure stresses are presented in Table 6.2.

Finally, by comparing each prediction to the actual values one by one, instead of the average values, a larger deviation is noticed. In particular, the average error ranges from 30% to 47% for the several sets of  $K_{IC}$  and  $Y$  parameters. In most of the cases, this high error is because the specimens failed at different location than the predicted one. However, even for the specimens which failed at the detected defect, the prediction is not always close to the actual value. This was explained well with the post-fracture analysis, which revealed that the linear scratches were interrupted by circular digs, and the latter were in most of the cases the critical locations. This misinterpretation of the critical defect led to wrong selection of geometry factors which affects considerably the predictions. In other cases, the specimens failed at the detected defect but not at the deepest location, as discussed in Section 4.4.5, which also led to larger errors in the predictions. The predictions for each specimen and their actual failure stresses can be found in Appendix H.

#### 6.4.3. Predicted design and characteristic strength

In Figure 6.10, the design strength values of the examined specimens are plotted, as derived based on the experimental and on the predicted failure stresses. It can be seen that for the series of small specimens (NA-1a), the actual and predicted design strengths differ by approximately 34%, with the actual strength being higher. Furthermore, it is worth mentioning here that the predicted characteristic strength of the series NA-1a differs by 19% from the actual characteristic strength.

For the series with the large specimens, the predicted design strength is not presented here, since its reliability is doubted. In particular, the goodness of fit of the predicted values for the series NA-2b is below the chosen level of significance for the AD goodness-of-fit test (see Figure 6.9). Thus, the appropriateness of the Weibull distribution for the derivation of that particular design strength is questioned.

#### 6.4.4. Reverse prediction process

By reversing the prediction process, the critical flaw depth was calculated based on the actual failure stresses, for  $K_{IC}=0,75 MPa m^{0,5}$  and  $Y=1, 12$  or  $0, 713$ . Table 6.3 presents the maximum, minimum and average flaw depths, as measured with Traceit® and as calculated from the failure stresses of the two testing series. It can be seen that the average measured and calculated (for  $\sigma_f$ ) depths differ by only 4% and 8% for the series NA-1a and NA-2b, respectively. Furthermore, the maximum depths differ by 3% and 13% while the minimum by 5% and 15%. Overall, the range of the depths measured with Traceit® and that of the depths which correspond to the actual failure stresses are very close.

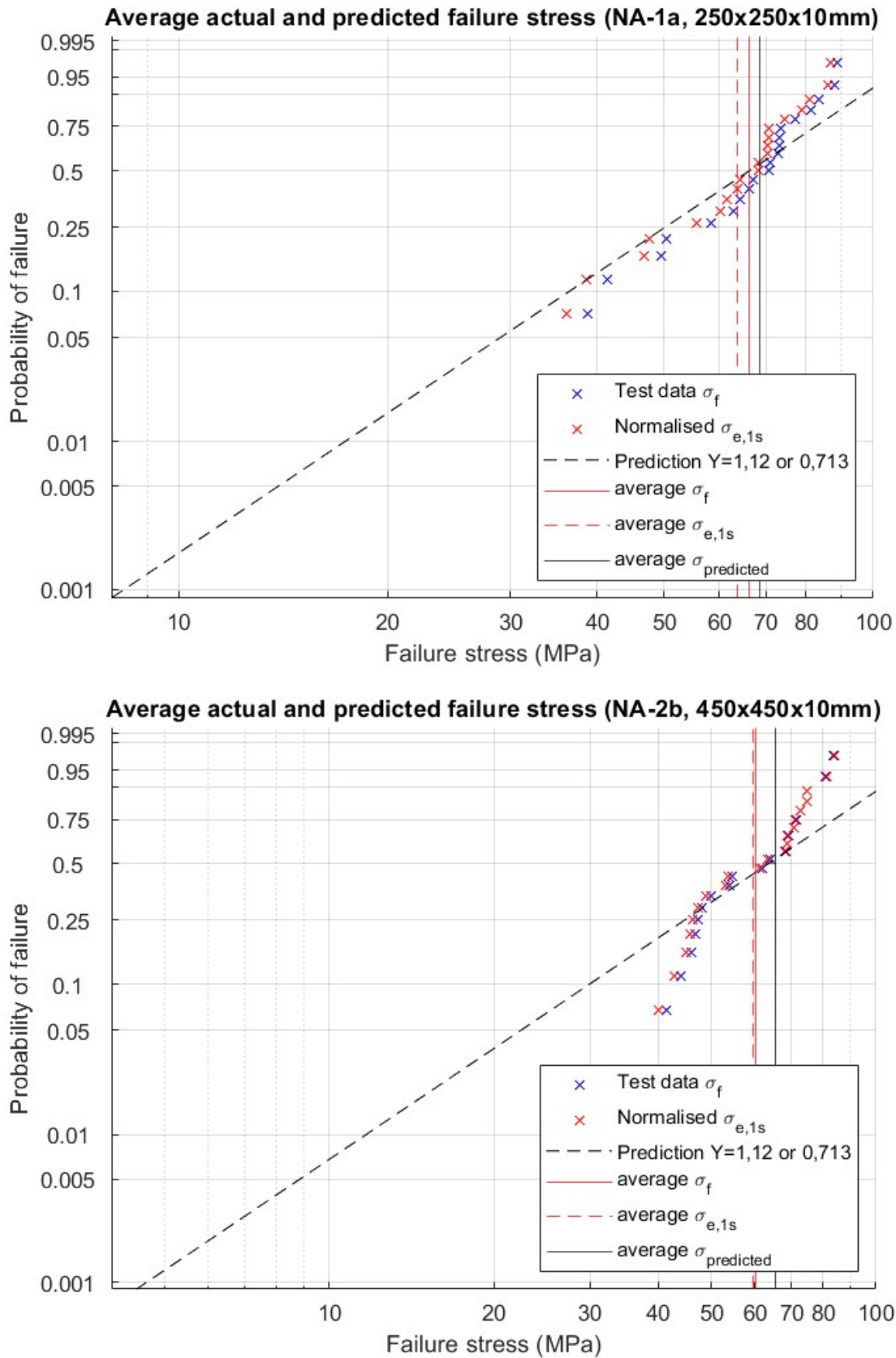


Figure 6.8: Weibull plots of the average actual and predicted failure stresses tested with the external surface in tension.

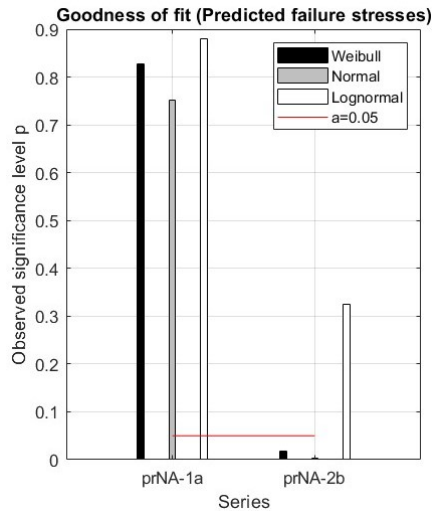


Figure 6.9: Goodness of fit of the predicted failure stresses to the three probability distribution functions.

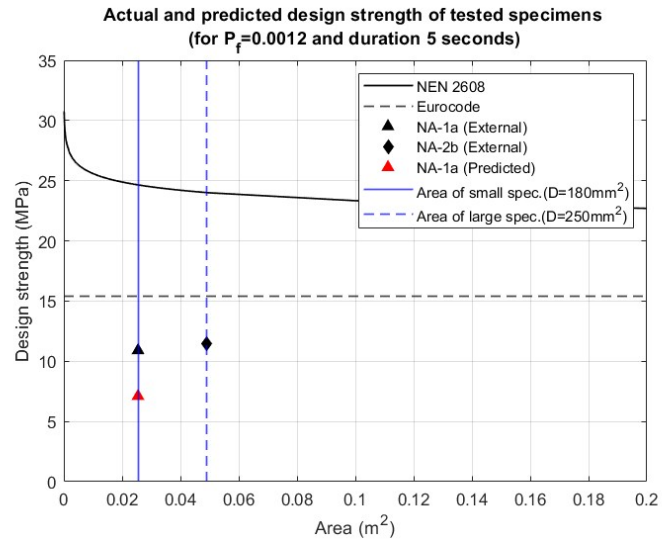


Figure 6.10: Actual and predicted design strength (for  $P_f=0,0012$  and load duration 5 seconds) of the series NA-1a, along with the design strength according to the Dutch and the European standards.

Table 6.3: Comparison of the flaw depths as measured with Traceit<sup>®</sup> and as calculated based on the actual failure stresses.

Series	NA-1a		NA-2b	
	Measured (Traceit <sup>®</sup> )	Calculated (for $\sigma_f$ )	Measured	Calculated
maximum	147	143	161	182
minimum	19	18	19	22
average	58	61	63	68

## 6.5. Discussion

The proposed methodology was developed based on several assumptions which in practice, are not completely correct. In particular, it was assumed that the manual inspection can detect all the large defects in the glass surface. However, depending for example on the light or the angle of observation, the human eye is very likely to overlook some defects. Furthermore, it was assumed that the largest defect within the loaded area would be the critical one. It is known though that the fracture origin does not always coincide with the largest defect or the location of the maximum stress. Moreover, the perfectly equibiaxial state of stresses within the loading ring is achieved only in theory. Usually in the experimental investigations, stress concentrations occur below the loading ring, especially when no other intermediate material is used, as in this case. Additionally, a small misalignment in the testing set-up could also alter the stress distribution in the tests. Nevertheless, no consistent invalid tests or other irregularities were observed which could potentially imply such stress concentrations.

A previous attempt to detect the critical flaw in small specimens of naturally aged glass through manual inspection was proved unsuccessful but the recommendation to evaluate this technique also in larger glass elements was made (Kwan, n.d.). The critical flaw detection test in this project, where the manual inspection was combined with a more elaborated analysis with Traceit<sup>®</sup>, was proved successful for the 33% of the small specimens and only for the 14% of the large specimens. This suggests that indeed, the visually largest defect on a glass panel could be the critical one but in larger elements, which include much more defects, it is not possible to detect the largest one manually. Nevertheless, even though the achieved percentage of success is low, the fact that these results emerged from a methodology

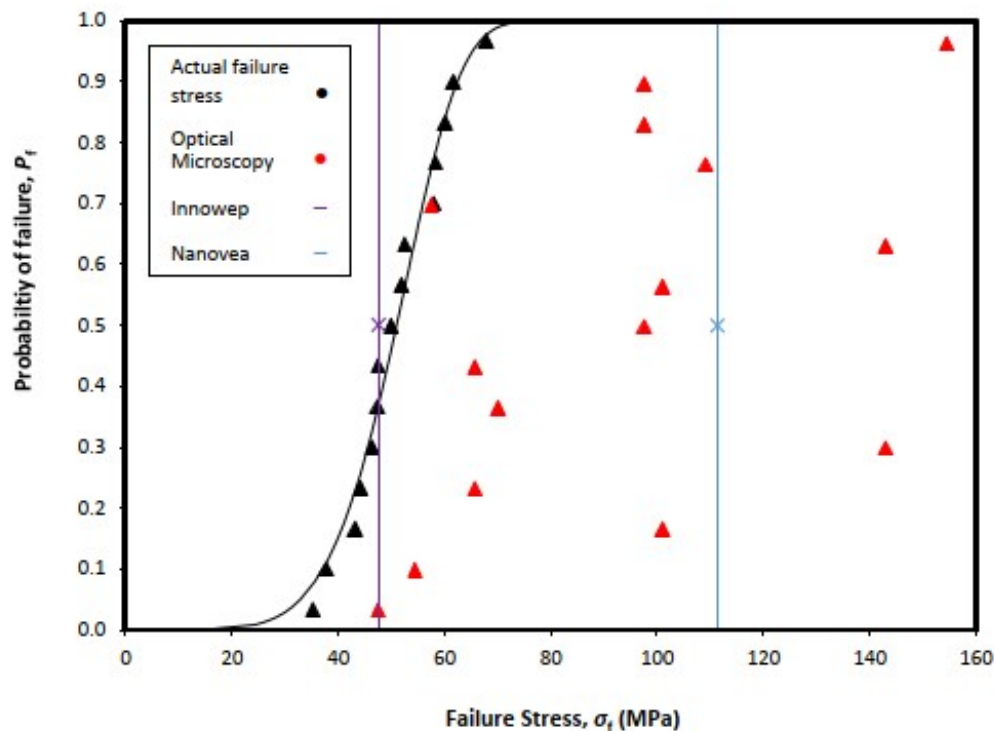


Figure 6.11: Results of previous application of Traceit<sup>®</sup> for the prediction of the strength of artificially scratched glass (Kwan, n.d.)

prone to human error must be considered. It is believed that if the manual inspection was replaced by an automated scanning process, a considerably higher number of successful tests would have been achieved. This idea is elaborated more in Section 7.3.2, as a recommendation for a two-step scanning process.

Although most of the specimens did not fail at the predefined location, the average predicted strength was very close to the actual one (difference of 4% and 9% for the small and the large specimens, respectively). This can be explained by the uniform damage found on the weathered glass surface. In particular, a defect which was identified as critical for one specimen but eventually it was not, it was probably very similar to the critical defect of another specimen. This is aligned with the earlier observation that the size effect might not apply in the case of weathered glass due to the uniform distribution of similar defects on its surface. Thus, even if the comparison of the predictions one by one resulted to high errors, the average of the predictions is very close to the average actual strength.

At this point, it is worth mentioning that in the only previous application of Traceit<sup>®</sup> for predicting the strength of artificially scratched glass, a similar observation was made. In particular, in the research of Kwan (n.d.), the predictions with Traceit<sup>®</sup> approached well the actual failure stress for probabilities of failure around 50%, as illustrated in Figure 6.11. These predictions were much closer to the actual data compared to the predictions made with an optical microscopy and a different profilometer. Therefore, it seems that Traceit<sup>®</sup> is a device which can provide an impression of the damage on glass and a good estimation of its average strength.

Furthermore, Traceit<sup>®</sup> led to conservative predictions of the characteristic and the design strength of the small specimens (error 19% and 34%, respectively), which is essential for safe design applications. However, these conservative values are probably result of the poor goodness of fit of the strength data to the Weibull distribution at lower probabilities of failure. Perhaps a two-parameter Weibull distribution would describe better the predictions, since the predicted values emerged by considering two different types of defects ( $Y=1,12$  and  $Y=0,713$ ). Otherwise, a detailed calculation of the geometry factor based on the shape of each defect is also likely to provide more accurate predictions.

Finally, the reverse prediction process revealed that the flaw depths as measured with Traceit<sup>®</sup> are very close to the depths calculated based on the actual failure stress and the theory of LEFM. This result also highlights the potential for Traceit<sup>®</sup> to give an indication of the size of the defects that exist on the surface of weathered glass. Finally, since the strength prediction process (based on the flaw depth) and the reverse process for the depth calculation (based on the failure stress) are in agreement, the formula of LEFM which was used for the predictions is probably able to describe the behavior of the examined weathered glass.

# 7

## Conclusions

### 7.1. Introduction

In this thesis, a methodology for the prediction of the fracture strength of naturally aged glass, based on its surface flaws, is proposed. The aim was to investigate the link between the surface strength of weathered annealed glass and its surface flaws. Section 7.2 answers the main research question, which was defined at the beginning of the project, and it presents the main findings of this research. In Section 7.3, the new questions which emerged from this thesis are listed as propositions for future work.

### 7.2. Conclusions

#### 7.2.1. Conclusions

The main research question of this thesis is:

*How can the strength of weathered glass be predicted based on its surface flaws and the theory of LEFM?*

This question was answered through the development of a methodology for scanning and predicting the residual strength of glass, using the theory of LEFM. The methodology was applied in this research and it was evaluated through comparisons with actual experimental data from a 55-year-old glass. The first steps of the methodology include manual inspection and surface scanning at high resolution, for the identification of the critical defect. In the subsequent step, the failure stress of the examined glass is calculated, based on the geometry of the defect found during scanning.

The novelty of this methodology lies on the equipment used for the analysis of the weathered glass surface. Although the effectiveness of microscopes was already proven in the existing literature, they cannot be easily used for measurements on-site or on large panels. In order to achieve that with commercial microscopes, modifications of the testing setup or custom made solutions are required. Considering that the ultimate goal of this research is to apply the methodology to windows or facade glass panels, it was developed based on Traceit<sup>®</sup>. The latter is a mobile optical surface profilometer, which is normally used in completely different applications. Traceit<sup>®</sup> showed a potential for further use in this field, since it can provide an impression not only of the type but also of the size of the defects that exist on a transparent material like glass. On the other hand, although the manual inspection was recommended for flaw detection in large elements (Kwan, n.d.), in this case it was proved to be neither an effective nor an efficient method, since it was not possible to examine manually all the defects in a large area.

The methodology resulted to very accurate strength predictions for probabilities of failure around 50%

(deviation of less than 9% from the actual strength), which is aligned with the findings of the only previous application of Traceit<sup>®</sup> for the prediction of the strength of artificially scratched glass (Kwan, n.d.). Furthermore, the predicted characteristic strength (for  $P_f=0,05$ ) of the small specimens was approximately 19% lower than the experimental characteristic strength of the same series. Regarding the design strength (for  $P_f=0,0012$ ), the predicted strength was 34% lower than the experimental one. Overall, these outcomes suggest that the methodology can give an impression of the performance of weathered glass by providing a good estimation of its average strength. Finally, further research is required for the predictions at lower probabilities of failure but the found conservative characteristic and design strength values highlight the potential of the methodology for use in design applications.

As a conclusion, before this research no methodologies for non-destructive evaluation of the surface strength of glass existed and the performance of weathered glass lacked experimental investigation. This research provides valuable scientific data, obtained from a sample of 90 specimens of weathered glass and 81 specimens of new glass, and it can serve as the starting point for an in-depth research in the field of the reuse of glass.

## 7.2.2. Findings

Apart from the proposed methodology, this research provides new information about the performance of weathered glass, the used scanning equipment and the fracture statistics. All these findings are listed in this section, as answers to the sub-questions defined during the design of the research.

- **How can the defects on the surface of glass be identified and measured?**

The literature study revealed that the most commonly used equipment for defect detection in glass is the optical microscope. The digital microscope used in this project was able to identify the defects on the surface of the small specimens, but not on the larger ones, since they could not fit under the microscopic lens. The mobile optical profilometer Traceit<sup>®</sup>, provided by Innowep GmbH, was able to capture the defects on the glass surface but a post-processing of the images was required. The great advantage of Traceit<sup>®</sup> lies on its design as a portable profilometer, since it can provide useful information without the need of laboratory conditions nor the size limitation that the microscope imposes. Nevertheless, both equipment succeeded in distinguishing the internal and the external surface of the examined weathered glass based on the amount of damage.

Due to the fine dimensions of the defects found on the surface of weathered glass, it was not possible to measure their depth with the digital microscope. On the other hand, Traceit<sup>®</sup> provided a 2D height map of the examined surface which gave an indication of the depth of these defects. After the destructive tests on glass, when the failure stresses of the specimens became known, the depths associated with these stresses were calculated based on the theory of LEFM. The average calculated depths and the depths measured with Traceit<sup>®</sup> differed by less than 8%.

- **What type of defects can be found on the surface of naturally aged glass?**

The damage found on the majority of the weathered specimens was uniform, with mainly dense pits and some deeper digs on the external surface. Fine linear scratches were also found occasionally but no significant macroscopic damage was observed. The depths of the defects on the 55-year-old glass ranged from 19  $\mu\text{m}$  to 161  $\mu\text{m}$ . In all the specimens, the pits were found mostly on the one side of the glass, which suggests that this side was exposed to the natural environment and the pits were presumed as signs of corrosion. It is stressed out that apart from the defects induced naturally on the glass surface, also some straight, long and wide scratches were found at both the internal and the external surfaces. These defects were probably man-made defects which were inevitably introduced to the glass surface over its service life. The shape and size of these defects did not resemble the uniform damage of weathering but it is believed that processes like cleaning, maintenance or transportation were responsible for them.

- **Which one of the surface defects will initiate the fracture?**

The non-destructive flaw detection test, based on manual inspection and measurements with Traceit<sup>®</sup>, revealed that the visually largest defect could be the critical one. This was the case for the 23% of the examined specimens. The post-fracture analysis of some specimens showed

that although the critical defect was the largest one, the fracture did not always originate from the deepest part of that defect. This failure behavior indicates that inside the defect there is no uniform stress concentration but a gradient stress.

In some specimens with no visible defects on their surface, the post-fracture analysis revealed that a sub-surface defect existed along the fracture surface which probably caused the failure. Generally, signs like "beach marks" were found in all the fracture patterns, indicating the 3D nature of the crack propagation. This sub-surface cracking is also possible cause of fracture in specimens with no visible surface defects.

- **How does the size of the loaded area influence the strength of weathered glass?**

The phenomenon of size effect was noticeable in the tests of new glass, since the mean strength of the specimens with the small loaded area was 30-40% higher than that of the specimens with the large loaded area. The size of the loaded area had an influence also on the strength of the internal surface of the weathered glass with the large area leading to approximately 46% lower failure stresses. On the contrary, the strength of the external surface was similar, regardless the size of the loaded area. This observation implies that the weathered glass has defects of similar dimensions, uniformly distributed on its surface exposed to the natural environment. Thus, the probability of encountering a critical flaw is equal at every location and it is independent from the loaded area of the weathered surface.

The Weibull theory for the extrapolation of the strength of large specimens from that of small ones was found very conservative in the case of weathered glass. By using a higher shape factor, which was proposed for new glass ( $\beta=15$ ), the calculated failure stresses were closer to the actual ones. In the case of the tin side of the as received glass, the calculated failure stresses of the large specimens were closer to the actual ones but for lower probabilities of failure the theory underestimated the strength. No clear conclusions were made about the air side since no sufficient valid experimental data existed.

- **How do the flaws induced by weathering on the surface of glass affect its strength?**

The effect of weathering on the strength of glass was observed in the tests of small specimens of weathered glass. More specifically, the mean strength of the internal surface, which was not heavily damaged, was 69% higher than that of the external surface, which was exposed to the natural environment. Furthermore, the internal surface was 20% weaker than the tin side of new glass, which occasionally had few defects.

This phenomenon was not observed in the case of the large specimens since the difference between the mean strength of the internal and the external surfaces was 12%. Furthermore, the internal surface was weaker than the tin side of the new glass by 45%. Since the specimens of weathered glass were scored from different facade panels, it is possible that the amount of damage on the internal surface of the large specimens was higher than that on the small specimens, resulting in strength values close to those of the external surface. Overall, a relation between the amount of damage and the surface strength of glass was observed, with the more damaged specimens failing at lower stresses.

- **Additional findings**

- The failure stresses of weathered glass ranged from 22,9 MPa to 138,2 MPa. The variation in the strength results was not only among specimens of different testing series but also among specimens within the same series, with the same characteristics. This is aligned with the great variation observed in the flaw depths.
- The strength data of weathered glass had a better fit to the Weibull distribution than to the other examined distributions. The data had slightly lower goodness of fit to the Normal distribution function and even lower to the Lognormal distribution. The same applies for the tin side of new glass.
- The manual method for the estimation of the Weibull parameters (Weighted Least square Regression) was found to describe slightly better the strength data of weathered glass, com-

pared to the computational method (Maximum Likelihood Estimation), in terms of conservativeness and goodness of fit.

- The elaborated selection of appropriate geometry factor for the predictions of the failure stress had a noticeable influence on the accuracy of the predicted failure stresses.
- The post failure analysis revealed that higher failure stresses were in some cases associated with smaller defects and vice versa, but not always.
- The failure stresses of the specimens of new glass, ranged considerably, from 38,3 MPa to 219,2 MPa, even if they were macroscopically identical.
- The mean strength of the air side of new glass was 32% and 45% higher than that of the tin side, for the small and large specimens, respectively. A microscopy examination revealed that the tin side had some defects, probably induced during the annealing process of glass.

### 7.3. Future work

This research sets the foundations for the development of a methodology for the prediction of the strength of weathered glass. Over the course of this project, a number of questions emerged which were not answered in this thesis. Therefore, this section provides some guidelines for future work in order to develop this methodology at a level which will allow its application in practice. These recommendations are aimed at both engineers and researchers.

#### 7.3.1. Recommendations for practice

- **A characterization system for new glass elements**

Every glass panel has some unique characteristics which are important for its reuse. Among these characteristics are:

- Manufacturer and date of manufacturing
- Chemical composition
- Type (annealed, strengthened)
- Post-processing (lamination, coatings)
- Dimensions and thickness
- Tin and air side (if float glass)
- Application (location, exact position on the building, side exposed to the outside environment)
- Load history (design loads, any extreme or unusual load which occur during its service life)

A characterization system is proposed which will incorporate a barcode or a QR code on every new glass panel. This code will include all the aforementioned information, added by the manufacturer and the architect or the contractor who asked for these panels. Update of this information should be possible in case something changes or new information must be added. The implementation of such system will save considerable time in the future, during the maintenance or repairing of these panels and especially at the end of their intended service life, when the reuse is considered.

- **A database for old glass elements**

The development of a database, accessible to architects and engineers is proposed, in which all the available old glass elements will be included. After the removal of an element from a building, it could be added in the database accompanied by any known information about it, such as dimensions, thickness and previous application. In this way, everyone who is interested in the reuse of glass, he/she will be able to search in the database for elements which match with

his/her requirements. In case the aforementioned characterisation system is implemented too, all the information included in the elements codes could be used to register them in the database.

Undoubtedly, in order to reuse safely an old glass element, further research is required. However, the aforementioned propositions could be already considered by the current manufacturers and engineers in order to enhance the future possibilities for reuse of the new elements.

### 7.3.2. Recommendations for further research

- **Parametric study on the strength of weathered glass**

The strength of new glass depends on several parameters and so does the strength of weathered glass. This research investigated whether the size of the loaded area ("size effect"), which influences the strength of new glass, affects also the strength of weathered glass. Furthermore, the influence of the surface damage on the strength was investigated too. However, other parameters such as the loading history, the chemical composition or the post-processing of the element are also of major interest for the strength of old glass. Therefore, a detailed parametric study is proposed in order to examine which parameters influence the strength of this type of glass. To this extend, a formula for deriving the design strength of weathered glass could emerge. As a starting point, the parameters for which it is already known that they affect the strength on new glass could be investigated.

- **Extend this methodology for other types of glass**

This research studied the simplest version of glass, the annealed glass, but in practice heat strengthened glass is also common. Thus, the relation of the flaw size and the strength of this type of glass should be investigated. A more complicated relation is expected due to the residual stresses on the glass surface which probably alter the crack growth mechanism in this type of glass. A research in this field could extend the applications of this methodology for non-destructive assessment of glass strength from the building industry to other industries as well, such as in automotive. Likewise, a study on the strength of weathered laminated glass should also be carried out. In this case, the interest lies not only on the old glass but also on the weathering of the interlayer. Is the durability of the glass and the interlayer the same? What is the service life of each of these materials and what is that of the laminated glass? The answers of these questions will lead to the development of a more solid methodology for the prediction of the glass strength in general.

- **A two-step scanning process**

The proposed methodology depends largely on manual inspection and the detailed surface analysis comes at a later stage. Due to the limited ability of the human eye to detect all the defects on the glass surface, the effectiveness of the methodology on the large specimens was lower than on the small specimens. Therefore, a two-step scanning process is proposed, in which the manual inspection (first step) will be replaced by a large scanner and the detailed analysis (second step) could be performed in a similar manner as proposed. At the first step, a scanning device such as the line scanners, which are already used in the production line of glass, can be used to examine the complete glass panel at low resolution and reveal the critical locations, namely the largest defects. Afterwards, a second scanner with higher resolution could be used to analyse the geometry of these defects and measure their dimensions. That second scanner should be portable to avoid any cutting or alterations of the specimen, since the ultimate goal is to reuse that element. The mobile optical profilometer Traceit® could be used at that stage, since it showed its potential for measuring the depth of glass defects.

- **Size effect on weathered glass**

In this research, the loaded area of the large specimens was 6 times larger than the loaded area of the small specimens and no significant difference in the strength was noticed. Is this always the case for weathered glass; namely, is the strength of weathered glass independent from the size of the loaded area? In order to scale up the proposed methodology to the prediction of the strength of a normal-size window or facade panel, an extensive study on the size effect and on

the formula which relates the strength of weathered glass to the size of its surface area should be carried out. In the design standards for glass, the strength of large glass elements is extrapolated from that of small elements, according to the Weibull theory and the shape parameter  $\beta$ . In the case of weathered glass though, this formula led to very conservative strength values for the large specimens. Thus, its applicability for this type of glass is doubted and since the phenomenon of "size effect" for weathered glass is also doubted, further investigation in that field is required.

- **Study on the progress of weathering**

This research examined the surface strength of a 55-year-old glass and provided useful information about the influence of the natural environment on that strength. However, there is no information about the strength of that glass at its initial condition, to compare the two states of the material. Similarly, there is no information about the strength of that glass several years ago. In particular, the progress of the effect of weathering on the strength of glass remains unknown. Does this phenomenon have a constant influence on the strength or is there a saturation? Is there a time-limit, beyond that there is no further reduction in the strength of glass? An investigation of the degradation progress of glass over the years should be performed, based on consecutive testing on similar glass specimens.

- **FEA to assist the CDR tests on new glass**

The air side of the new glass was stronger than expected and it resulted into a non-linear behavior. Although a FEM was constructed afterwards to assist the analysis of these specimens, it was not possible to calibrate it based on experimental data. Thus, in case similar glass is tested in the future in a CDR setup, it is recommended to apply strain gauges on the examine surface, in order to collect data (strain measurements) for the calibration of the FEM. To this extend, it will be possible to perform more elaborated non-linear analysis to simulate the exact performance of the particular specimens subjected to an equibiaxial field of stresses.

- **Fractographic analysis**

In this project, only limited specimens were examined after fracture with the microscope. In addition, only the fracture pattern of the specimens was analysed and not the fracture surface of them, due to the complexity of this analysis. However, the fracture pattern did not always reveal the critical defect of the specimens, whereas a careful examination of the fracture surface is expected to give that information. On these grounds, a detailed post-fracture analysis of these specimens will yield more solid conclusions about the relation between the failure stress of glass and the size of the critical defect. Since the 171 specimens tested in this research are still available, an elaborated fractographic examination of them is proposed.

- **Improvements of the proposed methodology**

In case the proposed methodology is investigated more or is tested in the future, several recommendations are made for increasing its effectiveness. First, the exact location of the examined glass panels in the building is useful to be known. In this way, unexpected defects on the external or the internal surface of glass could be probably explained. Furthermore, the predictions were based on geometry factors proposed in literature. As discussed in Section 6.4.2, the selection of appropriate geometry factors could improve considerably the accuracy of the predicted failure stress. Thus, in future applications of the methodology, the geometry factor should be derived experimentally, based on the shape and dimensions of each defect. Finally, it was noticed that even if the glass specimens failed at the visually largest defect, they did not always broke at the deepest location, where the measurement was conducted before the test. Therefore, during the non-destructive defect detection, measurements along the whole length of the estimated as critical defect should be taken. These measurements could be used especially in the evaluation part of the methodology and in combination with post-fracture surface analysis to verify the actual dimensions of the critical defect. To achieve that, a 3D visualization of the defect is required which cannot be obtained manually but with an automated scanning and stitching process of consecutive images.

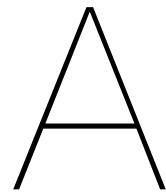
# References

- 16293-1:2008, I. (2018). Glass in building — basic soda lime silicate glass products — part 1: Definitions and general physical and mechanical properties.
- Agrawal, S. (2011). Glass defect detection techniques using digital image processing—a review. *IP Multimedia Communications*, 65–67.
- Ai, J., & Zhu, X. (2002). Analysis and detection of ceramic-glass surface defects based on computer vision. *Proceedings of the 4th World Congress on Intelligent Control and Automation (Cat. No. 02EX527)*, 4, 3014–3018.
- ASTMC1239-13. (2018). Standard practice for reporting uniaxial strength data and estimating weibull distribution parameters for advanced ceramics.
- ASTMC1499-09. (2013). Standard test method for monotonic equibiaxial flexural strength of advanced ceramics at ambient temperature 1.
- ASTM-E1300. (1997). Standard practice for determining load resistance of glass in buildings.
- Bergman, B. (1986). Estimation of weibull parameters using a weight function. *Journal of Materials Science Letters*, 5, 611–614. <https://doi.org/10.1007/BF01731525>
- Board, C. G. S. (2017). *Flat, clear float glass* (tech. rep.). CAN/CGSB-12.3-M91, National Standard of Canada, Canada.
- Brown, W. (1972). A load duration theory for glass design, 75–78.
- Charles, R. (1958). Static fatigue of glass. ii. *Journal of Applied Physics*, 29(11), 1554–1560.
- Chen, Z., Shen, Y., Bao, W., Li, P., Wang, X., & Ding, Z. (2015). Identification of surface defects on glass by parallel spectral domain optical coherence tomography. *Optics express*, 23(18), 23634–23646.
- Commission, E. (2011). Roadmap to a resource efficient europe. *COMMUNICATION FROM THE COMMISSION TO THE COUNCIL, THE EUROPEAN PARLIAMENT, THE EUROPEAN ECONOMIC AND SOCIAL COMMITTEE AND THE COMMITTEE OF THE REGIONS*.
- Dalgliesh, W. A., & Taylor, D. A. (1990). The strength and testing of window glass. *Canadian Journal of Civil Engineering*, 17(5), 752–762. <https://doi.org/10.1139/l90-088>
- Datsiou, K. C. (2017). *Design and performance of cold bent glass* (Doctoral dissertation). University of Cambridge.
- Datsiou, K. C., & Overend, M. (2016). Evaluation of artificial ageing methods for glass. *Challenging Glass Conference Proceedings*, 5, 581–592.
- Datsiou, K. C., & Overend, M. (2017a). Artificial ageing of glass with sand abrasion. *Construction and Building Materials*, 142, 536–551.
- Datsiou, K. C., & Overend, M. (2017b). The strength of aged glass. *Glass Structures and Engineering*, 2, 105–120. <https://doi.org/10.1007/s40940-017-0045-6>
- Datsiou, K. C., & Overend, M. (2018). Weibull parameter estimation and goodness-of-fit for glass strength data. *Structural Safety*, 73, 29–41. <https://doi.org/https://doi.org/10.1016/j.strusafe.2018.02.002>
- Dwivedi, S. K., Vishwakarma, M., & Soni, A. (2018). Advances and researches on non destructive testing: A review. *Materials Today: Proceedings*, 5(2), 3690–3698.
- EN1990:2002. (2005). Eurocode - basis of structural design.
- Evans, A. G., & Wiederhorn, S. M. (1974). Proof testing of ceramic materials—an analytical basis for failure prediction. *International Journal of Fracture*, 10(3), 379–392. <https://doi.org/10.1007/BF00035499>
- Faucher, B., & Tyson, W. R. (1988). On the determination of weibull parameters. *Journal of Materials Science Letters*, 7, 1199–1203. <https://doi.org/10.1007/BF00722337>
- Feldmann, M., Kasper, R., Abeln, B., Cruz, P., Belis, J., Beyer, J., et al. (2014). Guidance for european structural design of glass components. *Publications Office of the European Union*, 1–196.
- Fischer-Cripps, A. C., & Collins, R. E. (1995). Architectural glazings: Design standards and failure models. *Building and Environment*, 30(1), 29–40.

- Gholizadeh, S. (2016). A review of non-destructive testing methods of composite materials. *Procedia structural integrity*, 1, 50–57.
- Haldimann, M. (2006). *Fracture strength of structural glass elements* (tech. rep.). EPFL.
- Holmes, J. D. (1997). Inspection of float glass using a novel retroreflective laser scanning system. *Optical Scanning Systems: Design and Applications*, 3131, 180–190.
- Innowep GmbH. (n.d.). TRACEiT® -. <https://www.innowep.com/traceit/>
- ISO1288-1. (2016). Glass in building — determination of the bending strength of glass — part 1: Fundamentals of testing glass.
- Johar, S. (1981). *Dynamic fatigue of flat glass, phase ii: Final report* (tech. rep.). prepared for National Research Council of Canada. Ontario Research Foundation. <https://doi.org/10.4224/20328096>
- Karlsson, S., Kozłowski, M., Kinsella, D., Haller, K., Andersson, S., Hellman, F., & Persson, K. (2018). Kvalitetshöjning av planglas: Icke-förstörende provning av glasets hållfasthet.
- Kašiarová, M., Rouxel, T., Sangleboeuf, J.-C., & Le Houérou, V. (2005). Fractographic analysis of surface flaws in glass. *Key Engineering Materials*, 290, 300–303.
- Kinsella, D. T., & Persson, K. (2018). A numerical method for analysis of fracture statistics of glass and simulations of a double ring bending test. *Glass Structures & Engineering*, 3(2), 139–152.
- Kwan, A. C. (n.d.). *Evaluation of non-destructive testing techniques for glass* (tech. rep.). Girton College, Cambridge.
- Lawn, B. (1993). *Fracture of brittle solids* (2nd ed.). Cambridge University Press. <https://doi.org/10.1017/CBO9780511623127>
- Lehman, P. R. (n.d.). *The mechanical properties of glass, glass engineering 150:312*. Department of Ceramics and Materials Engineering, Rutgers University, New Brunswick. Retrieved December 6, 2021, from <http://glassproperties.com/references/MechPropHandouts.pdf>
- LINDQVIST, M. (2013). *Structural glass strength prediction based on edge flaw characterization* (tech. rep.). EPFL.
- Müller, H., Strubel, C., & Bange, K. (2001). Characterization and identification of local defects in glass. *Scanning*, 23(1), 14–23.
- NEN2608. (2014). Glass in building - requirements and determination method.
- NEN-EN12603. (2002). Glass in building - procedures for goodness of fit and confidence intervals for weibull distributed glass strength data.
- NEN-EN1288-5. (2000). Glass in building - determination of the bending strength of glass - part 5: Coaxial double ring test on flat specimens with small test surface areas.
- Overend, M., Parke, G., & Buhagiar, D. (2007). Predicting failure in glass—a general crack growth model. *Journal of Structural Engineering*, 133(8), 1146–1155.
- Overend, M., & Zammit, K. (2012). A computer algorithm for determining the tensile strength of float glass. *Engineering structures*, 45, 68–77.
- Persson, K., Haller, K., Karlsson, S., & Kozłowski, M. (2020). Non-destructive testing of the strength of glass by a non-linear ultrasonic method. *Challenging Glass Conference Proceedings*, 7.
- Pisano, G., & Carfagni, G. R. (2015). The statistical interpretation of the strength of float glass for structural applications. *Construction and Building Materials*, 98, 741–756.
- Pisano, G., Carfagni, G. R., & Schneider, J. (2019). Statistical interference of crack healing on the strength of thermally-treated glass. experiments and modelling. *Engineering Fracture Mechanics*, 205, 511–531.
- prCEN/TC250-1. (2018). Structural glass — design and construction rules — part 1: Basis of design and materials.
- Quinn, G. D. (2020). Fractography of ceramics and glasses. *NIST Special Publication*.
- Rasouli, S., & Tavassoly, M. T. (2005). Moiré deflectometer for measuring distortion in sheet glasses. *ICO20: Optical Devices and Instruments*, 6024, 60240E.
- Rodichev, Y., & Veer, F. (2010). Fracture resistance, surface defects and structural strength of glass. *Challenging Glass Conference Proceedings*, 2, 363–374.
- Ronchetti, C., Lindqvist, M., Louter, C., & Salerno, G. (2013). Stress-corrosion failure mechanisms in soda-lime silica glass. *Engineering Failure Analysis*, 35, 427–438.
- Schneider, J., Schula, S., & Weinhold, W. (2012). Characterisation of the scratch resistance of annealed and tempered architectural glass. *Thin Solid Films*, 520(12), 4190–4198.

- Schula, S., Schneider, J., Vandebroek, M., & Belis, J. (2013). Fracture strength of glass, engineering testing methods and estimation of characteristic values. *COST Action TU0905 Mid-term Conference on Structural Glass*, 223–34.
- Shelby, J. E. (2020). *Introduction to glass science and technology*. Royal Society of Chemistry.
- Shen, X., & WÖRMER, J.-D. (1998). Entwicklung eines bemessungs-und sicherheits-konzeptes für den glasbau. *Bauingenieur*, 73(1), 44–52.
- Speranzini, E., & Agnetti, S. (2014). The technique of digital image correlation to identify defects in glass structures. *Structural Control and Health Monitoring*, 21(6), 1015–1029.
- Vandebroek, M., Belis, J., Louter, C., & Molnar, G. (2013). Ratio of mirror zone depth to flaw depth after failure of glass beams. *COST Action TU0905, Mid-term Conference on Structural Glass*, (CONF), 235–241.
- Varner, J., & Oel, H. J. (1975). Surface defects: Their origin, characterization and effects on strength. *Journal of Non-Crystalline Solids*, 19, 321–333.
- Veer, F. (2007). The strength of glass, a nontransparent value. *HERON-ENGLISH EDITION*-, 52(1/2), 87.
- Wang, Y., & Hadfield, M. (2004). Failure modes of ceramic rolling elements with surface crack defects. *Wear*, 256(1-2), 208–219.
- Weibull, W. et al. (1951). A statistical distribution function of wide applicability. *Journal of applied mechanics*, 18(3), 293–297.
- Wiederhorn, S. (1974). *Strength of glass—a fracture mechanics approach* (tech. rep.). NATIONAL BUREAU OF STANDARDS WASHINGTON DC INST FOR MATERIALS RESEARCH.
- Wiederhorn, S., & Bolz, L. (1970). Stress corrosion and static fatigue of glass. *Journal of the American ceramic society*, 53(10), 543–548.
- Zammit, K., & Overend, M. (2010). Increasing the design strength of glass-fractography and stress testing. *Symposium of the International Association for Shell and Spatial Structures (50th. 2009. Valencia). Evolution and Trends in Design, Analysis and Construction of Shell and Spatial Structures: Proceedings*.
- Zhao, Z. (2021). Review of non-destructive testing methods for defect detection of ceramics. *Ceramics International*, 47(4), 4389–4397.



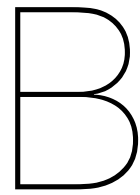


## Chemical analysis

The chemical composition of the examined glass was found through an X-Ray Fluorescence (XRF) analysis, performed at the Faculty of Mechanical, Maritime and Materials Engineering of TU Delft. Two samples were taken from the tested specimens, one from the new glass and one from the weathered glass, and their both sides were analysed by XRF. Table A.1 contains the results of the analysis of the new and the old glass. In the same table, the percent mass fraction of the main compounds of soda-lime silicate glass according to 16293-1:2008 (2018) are presented.

Table A.1: Chemical composition of the examined new and weathered (old) glass (wt%).

Compound	Symbol	ISO 16293-1:20	New Side 1	New Side 2	Old Side 1	Old Side 2
Silica	$SiO_2$	69 to 74	71,705	74,368	73,329	73,894
Soda	$Na_2O$	5 to 14	11,811	11,618	11,864	11,479
Lime	$CaO$	10 to 16	8,902	8,817	9,681	9,443
Magnesium	$MgO$	0 to 6	4,051	4,26	3,588	3,529
Tin oxide	$SnO_2$		2,608	-	-	-
Aluminum	$Al_2O_3$	0 to 3	0,487	0,528	0,404	0,604
Potash	$K_2O$		0,256	0,237	0,066	0,05
Iron	$Fe_2O_3$		0,077	0,062	0,101	0,113
Sulphite	$SO_3$		0,076	0,086	0,721	0,608
Chlorine	$Cl$		0,022	0,02	0,074	0,047
Strontia	$SrO$		0,006	0,005	0,004	0,003
Arsenic oxide	$As_2O_3$		-	-	0,06	0,053
Titanium	$TiO_2$		-	-	0,057	0,049
Phosphorus	$P_2O_5$		-	-	0,035	0,115
Zirconia	$ZrO_2$		-	-	0,01	0,009
Zinc oxide	$ZnO$		-	-	0,007	0,003
Others		0 to 5				



## Specimens dimensions

In the Tables B.1 to B.8, the dimensions of all the tested specimens are presented. The data included in these tables are:

1. The width and the length of each specimen in mm.
2. The thickness at the mid points of the four edges of each specimen, as measured with a caliper, and the average thickness of each specimen in mm.

Table B.1: Dimensions of the specimens of series NA-1a (Weathered glass).

Spec.	Width (mm)	Length (mm)	$d_{\text{edge1}}$	$d_{\text{edge2}}$	$d_{\text{edge3}}$	$d_{\text{edge4}}$	$d_{\text{mean}}$ (mm)
1.1	251	249	9,50	9,48	9,40	9,50	9,47
1.2	251	250	9,52	9,54	9,60	9,42	9,52
1.3	251	249	9,52	9,62	9,52	9,48	9,54
1.4	251	250	9,46	9,40	9,52	9,46	9,46
1.5	251	250	9,50	9,42	9,40	9,44	9,44
1.6	251	250	9,48	9,50	9,52	9,42	9,48
1.7	251	251	9,50	9,50	9,44	9,46	9,48
2.1	251	252	9,48	9,50	9,44	9,52	9,49
2.2	249	251	9,54	9,52	9,52	9,50	9,52
2.3	251	251	9,48	9,48	9,52	9,52	9,50
2.4	251	251	9,52	9,52	9,52	9,58	9,54
2.5	251	250	9,48	9,52	9,50	9,52	9,51
2.6	250	251	9,52	9,50	9,52	9,42	9,49
2.7	251	251	9,54	9,42	9,46	9,58	9,50
3.1	252	248	9,50	9,48	9,50	9,48	9,49
3.2	254	252	9,52	9,52	9,48	9,44	9,49
3.3	250	250	9,50	9,50	9,48	9,50	9,50
3.4	251	248	9,48	9,44	9,42	9,48	9,46
3.5	252	249	9,44	9,44	9,50	9,42	9,45
3.6	252	249	9,50	9,48	9,48	9,46	9,48
3.7	252	251	9,50	9,48	9,60	9,60	9,55

Table B.2: Dimensions of the specimens of series NA-1b (Weathered glass).

Spec.	Width (mm)	Length (mm)	$d_{\text{edge1}}$	$d_{\text{edge2}}$	$d_{\text{edge3}}$	$d_{\text{edge4}}$	$d_{\text{mean}}$ (mm)
4.1	252	253	9,56	9,58	9,56	9,54	9,56
4.2	251	249	9,54	9,50	9,52	9,54	9,53
4.3	252	251	9,58	9,60	9,58	9,58	9,59
4.4	252	249	9,56	9,52	9,56	9,58	9,56
4.5	251	250	9,52	9,50	9,52	9,58	9,53
4.6	252	251	9,52	9,52	9,52	9,54	9,53
4.7	252	249	9,60	9,58	9,52	9,58	9,57
4.8	252	250	9,54	9,50	9,60	9,60	9,56
5.1	248	248	9,58	9,52	9,54	9,56	9,55
5.2	249	248	9,52	9,52	9,50	9,52	9,52
5.3	249	248	9,60	9,60	9,54	9,52	9,57
5.4	249	251	9,52	9,50	9,48	9,54	9,51
5.5	249	249	9,52	9,60	9,52	9,52	9,54
5.6	249	248	9,60	9,52	9,50	9,52	9,54
5.7	250	251	9,60	9,58	9,52	9,52	9,56
5.8	249	251	9,54	9,50	9,52	9,52	9,52
5.9	250	251	9,48	9,52	9,50	9,52	9,51
5.10	249	250	9,54	9,52	9,54	9,50	9,53
5.11	250	249	9,52	9,52	9,54	9,52	9,53
5.12	250	252	9,40	9,48	9,52	9,52	9,48
5.13	249	248	9,52	9,54	9,50	9,50	9,52
5.14	249	249	9,52	9,50	9,50	9,52	9,51
5.15	248	248	9,54	9,50	9,52	9,52	9,52

Table B.3: Dimensions of the specimens of series NA-2a (Weathered glass).

Spec.	Width (mm)	Length (mm)	$d_{\text{edge1}}$	$d_{\text{edge2}}$	$d_{\text{edge3}}$	$d_{\text{edge4}}$	$d_{\text{mean}}$ (mm)
1.1	450	450	9,44	9,42	9,34	9,40	9,40
1.2	450	450	9,40	9,38	9,46	9,38	9,41
1.3	450	450	9,38	9,42	9,40	9,40	9,40
1.4	449	450	9,44	9,42	9,38	9,42	9,42
1.5	449	449	9,42	9,40	9,40	9,40	9,41
1.6	449	449	9,42	9,42	9,42	9,40	9,42
1.7	448	450	9,44	9,40	9,38	9,42	9,41
1.8	449	449	9,42	9,50	9,40	9,40	9,43
2.1	448	450	9,52	9,42	9,50	9,62	9,52
2.2	449	450	9,42	9,42	9,42	9,40	9,42
2.3	450	450	9,70	9,62	9,62	9,52	9,62
2.4	448	449	9,50	9,44	9,50	9,50	9,49
2.5	450	450	9,54	9,58	9,52	9,50	9,54
2.6	450	450	9,50	9,54	9,60	9,70	9,59
2.7	449	450	9,52	9,50	9,52	9,50	9,51
2.8	450	450	9,42	9,44	9,42	9,50	9,45
2.9	450	450	9,40	9,50	9,52	9,60	9,51
2.10	449	451	9,50	9,62	9,50	9,50	9,53
2.11	448	451	9,62	9,60	9,58	9,48	9,57
2.12	448	450	9,50	9,52	9,50	9,54	9,52
2.13	449	450	9,52	9,44	9,50	9,60	9,52
2.14	449	450	9,52	9,50	9,52	9,44	9,50
2.15	449	450	9,50	9,46	9,50	9,60	9,52

Table B.4: Dimensions of the specimens of series NA-2b (Weathered glass).

Spec.	Width (mm)	Length (mm)	$d_{\text{edge1}}$	$d_{\text{edge2}}$	$d_{\text{edge3}}$	$d_{\text{edge4}}$	$d_{\text{mean}}$ (mm)
3.1	450	451	9,42	9,44	9,44	9,48	9,45
3.2	449	448	9,52	9,52	9,54	9,50	9,52
3.3	448	450	9,44	9,46	9,52	9,42	9,46
3.4	449	450	9,42	9,52	9,42	9,50	9,47
3.5	449	449	9,40	9,44	9,42	9,44	9,43
3.6	450	449	9,42	9,46	9,40	9,42	9,43
3.7	449	449	9,42	9,42	9,44	9,42	9,43
3.8	448	450	9,48	9,42	9,42	9,46	9,45
3.9	449	448	9,48	9,50	9,50	9,48	9,49
3.10	450	449	9,46	9,50	9,42	9,42	9,45
3.11	448	449	9,52	9,48	9,44	9,48	9,48
3.12	448	449	9,50	9,52	9,52	9,48	9,51
4.1	450	450	9,48	9,52	9,52	9,50	9,51
4.2	450	449	9,50	9,44	9,50	9,52	9,49
4.3	450	450	9,52	9,54	9,58	9,52	9,54
4.4	449	449	9,56	9,52	9,50	9,58	9,54
4.5	448	449	9,54	9,54	9,50	9,50	9,52
4.6	449	450	9,50	9,52	9,54	9,48	9,51
4.7	449	450	9,50	9,48	9,50	9,50	9,50
4.8	450	450	9,48	9,48	9,46	9,50	9,48
4.9	450	448	9,50	9,52	9,42	9,50	9,49
4.10	450	450	9,50	9,52	9,54	9,46	9,51

Table B.5: Dimensions of the specimens of series AR-1a (As received glass).

Spec.	Width (mm)	Length (mm)	$d_{\text{edge1}}$	$d_{\text{edge2}}$	$d_{\text{edge3}}$	$d_{\text{edge4}}$	$d_{\text{mean}}$ (mm)
1	250	251	9,78	9,80	9,80	9,80	9,80
2	250	251	9,80	9,84	9,82	9,82	9,82
3	250	249	9,90	9,90	9,98	9,92	9,93
4	250	251	9,90	9,98	9,98	9,98	9,96
5	250	251	9,80	9,80	9,90	9,90	9,85
6	250	251	9,80	9,82	9,80	9,80	9,81
7	252	251	9,90	9,82	9,80	9,78	9,83
8	251	250	9,90	9,88	9,90	9,90	9,90
9	249	250	9,98	10,00	9,98	10,00	9,99
10	251	250	9,78	9,84	9,90	9,80	9,83
11	250	251	9,80	9,84	9,90	9,78	9,83
12	252	250	9,82	9,82	9,92	9,90	9,87
13	250	250	9,90	9,92	10,00	9,98	9,95
14	250	252	9,90	9,82	9,90	9,90	9,88
15	251	250	9,90	9,86	9,90	9,90	9,89
16	250	250	9,82	9,90	9,80	9,84	9,84
17	250	251	9,90	9,84	9,90	9,90	9,89
18	251	252	9,92	9,80	9,84	9,84	9,85
19	250	250	9,94	9,90	9,90	9,88	9,91
20	249	250	9,74	9,78	9,78	9,80	9,78

Table B.6: Dimensions of the specimens of series AR-1b (As received glass).

Spec.	Width (mm)	Length (mm)	$d_{\text{edge1}}$	$d_{\text{edge2}}$	$d_{\text{edge3}}$	$d_{\text{edge4}}$	$d_{\text{mean}}$ (mm)
21	250	250	9,88	9,92	9,98	9,98	9,94
22	250	250	9,98	9,98	9,90	9,92	9,95
23	251	251	9,90	9,84	9,84	9,88	9,87
24	250	250	9,90	9,88	9,84	9,92	9,89
25	250	250	9,90	9,96	9,98	9,98	9,96
26	250	251	9,92	9,94	9,94	9,98	9,95
27	250	250	9,90	9,92	10,00	9,94	9,94
28	250	250	9,80	9,84	9,84	9,80	9,82
29	250	250	9,98	9,90	9,94	9,98	9,95
30	251	250	9,88	9,92	10,00	9,98	9,95
31	250	250	9,90	9,86	9,82	9,86	9,86
32	250	250	9,90	9,92	9,96	9,92	9,93
33	249	251	9,98	10,00	9,94	9,92	9,96
34	250	250	9,92	9,82	9,92	9,94	9,90
35	250	249	9,80	9,80	9,78	9,90	9,82
36	251	250	9,90	9,92	9,90	9,84	9,89
37	251	251	9,90	9,84	9,88	9,90	9,88
38	250	250	9,84	9,86	9,90	9,82	9,86
39	252	251	9,94	9,92	9,98	9,98	9,96
40	250	250	9,94	9,90	9,90	9,92	9,92

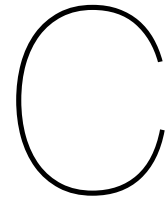
Table B.7: Dimensions of the specimens of series AR-2a (As received glass).

Spec.	Width (mm)	Length (mm)	$d_{\text{edge1}}$	$d_{\text{edge2}}$	$d_{\text{edge3}}$	$d_{\text{edge4}}$	$d_{\text{mean}}$ (mm)
1	450	451	9,98	9,76	9,90	9,98	9,91
2	450	451	9,82	9,90	9,82	9,88	9,86
3	449	450	9,92	10,00	9,98	10,00	9,98
4	450	450	9,94	9,98	10,00	10,00	9,98
5	450	450	9,98	9,92	9,90	9,98	9,95
6	450	450	10,00	9,90	10,00	10,00	9,98
7	450	449	10,00	9,90	10,00	10,10	10,00
8	450	450	10,00	10,00	10,00	10,02	10,01
9	453	450	10,00	9,90	10,00	9,98	9,97
10	450	450	9,98	9,98	9,98	10,10	10,01
11	451	450	9,90	9,80	9,82	9,90	9,86
12	451	449	9,84	9,82	9,82	9,90	9,85
13	451	453	10,00	10,00	9,90	10,00	9,98
14	450	453	10,00	10,00	9,90	9,98	9,97
15	449	453	9,96	9,98	9,90	9,98	9,96
16	450	450	10,00	10,10	9,90	10,10	10,03
17	450	449	9,90	9,82	9,90	9,92	9,89
18	450	452	9,84	9,82	9,90	9,92	9,87
19	450	450	9,82	9,84	9,86	9,90	9,86
20	448	450	9,82	9,84	9,80	9,90	9,84

Table B.8: Dimensions of the specimens of series AR-2b (As received glass).

Spec.	Width (mm)	Length (mm)	$d_{\text{edge1}}$	$d_{\text{edge2}}$	$d_{\text{edge3}}$	$d_{\text{edge4}}$	$d_{\text{mean}}$ (mm)
21	450	450	9,80	9,84	9,84	9,82	9,83
22	448	450	9,84	9,82	9,80	9,84	9,83
23	450	450	9,80	9,80	9,82	9,80	9,81
24	451	450	9,80	9,86	9,80	9,90	9,84
25	450	450	9,80	9,88	9,88	9,82	9,85
26	450	452	9,92	9,86	9,90	9,90	9,90
27	450	450	9,90	9,82	9,84	9,82	9,85
28	450	449	9,80	9,86	9,90	9,90	9,87
29	450	449	9,82	9,82	9,90	9,80	9,84
30	450	450	9,90	10,00	10,00	9,92	9,96
31	450	449	10,02	10,10	9,92	10,10	10,04
32	450	452	10,10	10,02	9,98	10,02	10,03
33	450	450	9,92	10,00	10,02	10,10	10,01
34	450	450	10,02	10,10	10,00	10,00	10,03
35	450	451	10,00	10,02	10,00	9,92	9,99
36	450	450	9,98	10,00	9,98	9,94	9,98
37	449	448	9,98	10,00	10,00	9,90	9,97
38	450	450	9,84	9,86	9,84	9,90	9,86
39	450	452	10,02	10,00	10,00	10,02	10,01
40	453	448	10,02	10,02	10,00	9,92	9,99
41	450	451	9,90	9,98	9,98	9,92	9,95





## Traceit reliability study

In Figure C.1, the results of the reliability study performed with Traceit<sup>®</sup> are illustrated. In particular, each plot includes ten sets of width and depth measurements of the same defect.

The legend "Def.1 ang.0" stands for the measurements of the defect 1 which were taken with Traceit<sup>®</sup> at an angle of 0° to the specimen and "Def.1 ang.90" stands for the measurements taken with Traceit<sup>®</sup> at an angle of 90° to the specimen. Similar legends are used for the defects 2 and 3.

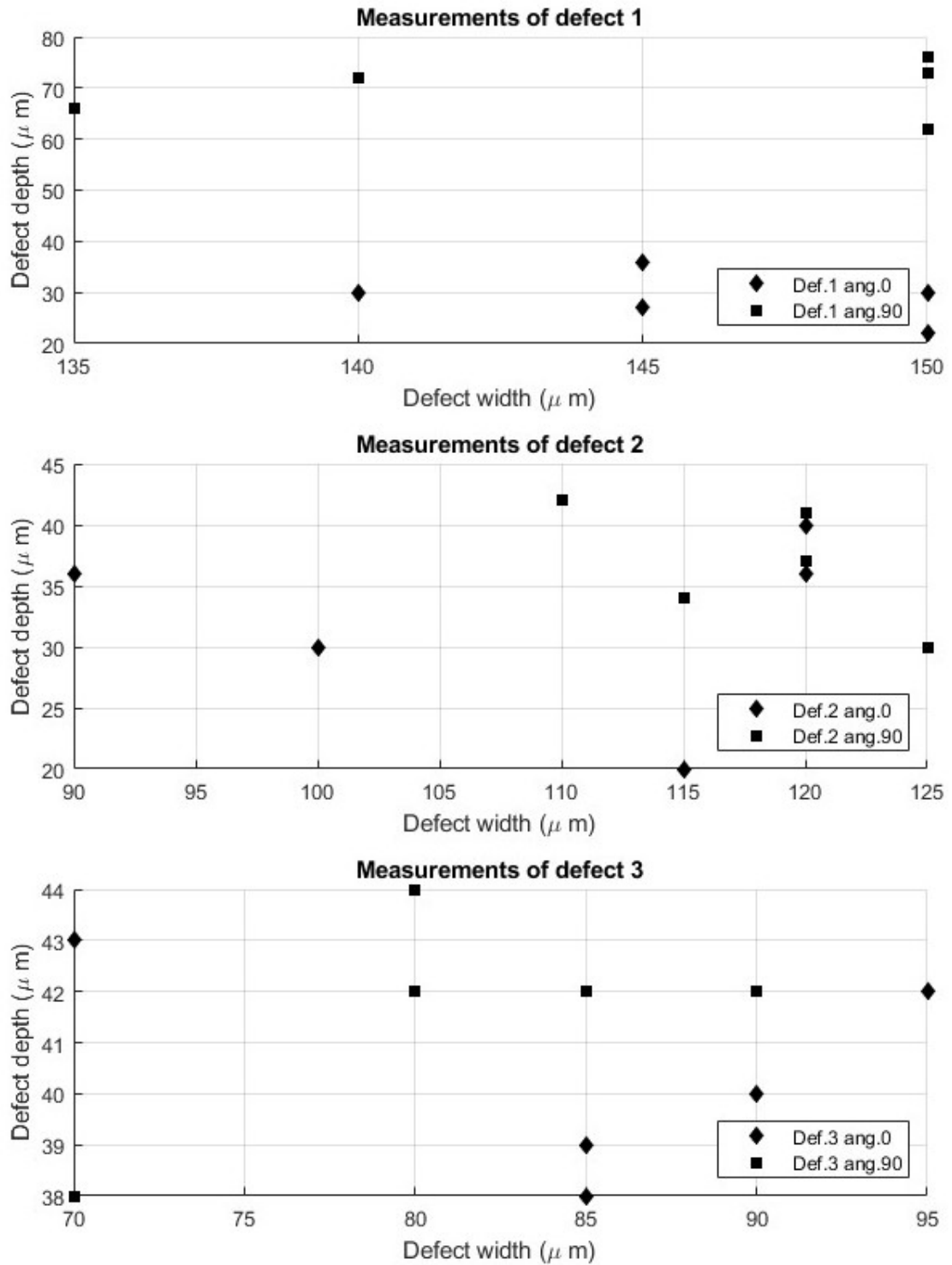
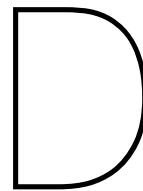


Figure C.1: Plots of the ten measurements for the three examined defects.



## Results of the CDR tests

In the Tables D.1 to D.4, the results of the CDR tests on weathered glass are reported. The displacement rate for all the tests was 5mm/min. The data for each specimen which are included in the tables are:

1. The load at breakage  $F_{\text{break}}$  in N (output of the software testXpert<sup>®</sup> III, used during the tests).
2. The displacement at breakage in mm, as derived from the force-displacement curve (output of the software testXpert<sup>®</sup> III, used during the tests).
3. The failure stress  $\sigma_f$  in MPa, as calculated according to the formula (4.1).
4. The time to failure in seconds, as calculated based on the displacement rate.
5. The stress rate in MPa/s, as calculated after the tests.
6. The normalised failure stress  $\sigma_{e,60s}$  for a reference period of 60 seconds, as calculated based on formula (4.1).
7. The location of the fracture origin in relation to the loading ring, IR (inside), LR (below) or OR (outside).

The same data for the specimens of new, as received glass are included in the Tables D.5 to D.8.

Table D.1: Results of the CDR tests for the series NA-1a (250x250x10mm, external surface).

Specimen	$F_{\text{break}}$ (N)	d (mm)	$\sigma_f$ (Mpa)	$t_{\text{break}}$ (sec)	Rate (MPa/s)	$\sigma_{e,60s}$	Fracture
1.1	9924,8	0,7	67,0	8,9	7,6	49,8	IR
1.2	13299,3	1,0	88,9	11,5	7,7	67,1	IR
1.3	12502,3	0,9	83,3	10,8	7,7	62,7	OR
1.4	5730,5	0,5	38,8	5,4	7,1	28,0	IR
1.5	11987,2	0,9	81,5	10,4	7,8	61,2	IR
1.6	13077,7	0,9	88,1	11,3	7,8	66,5	OR
1.7	10887,1	0,8	73,4	9,6	7,6	54,8	LR
2.1	8679,3	0,6	58,4	7,7	7,5	43,0	OR
2.2	7419,0	0,6	49,6	6,8	7,3	36,2	IR
2.3	10902,7	0,8	73,1	9,5	7,7	54,6	IR
2.4	9955,9	0,7	66,3	8,9	7,5	49,3	IR
2.5	9589,5	0,7	64,3	8,7	7,4	47,7	IR
2.6	11457,1	0,8	77,0	10,1	7,6	57,7	IR
2.7	6165,4	0,5	41,3	5,9	7,0	30,0	IR
3.1	10849,1	0,8	73,0	9,7	7,5	54,6	IR
3.2	10945,0	0,8	73,4	9,6	7,7	54,8	IR
3.3	7481,3	0,6	50,3	7,0	7,2	36,8	IR
3.4	5475,3	0,5	37,1	5,4	6,9	26,8	IR
3.5	10478,4	0,8	71,1	9,2	7,7	53,0	LR
3.6	10513,0	0,8	70,8	9,4	7,5	52,9	LR
3.7	9454,5	0,7	62,8	8,9	7,1	46,7	IR

Table D.2: Results of the CDR tests for the series NA-1b (250x250x10mm, internal surface).

Specimen	$F_{\text{break}}$ (N)	d (mm)	$\sigma_f$ (Mpa)	$t_{\text{break}}$ (sec)	Rate (MPa/s)	$\sigma_{e,60s}$	Fracture
4.1	10849,9	0,8	71,8	9,5	7,6	53,6	IR
4.2	8098,7	0,6	54,1	7,4	7,4	39,7	OR
4.3	9158,9	0,7	60,3	8,1	7,4	44,6	IR
4.4	17775,6	1,2	117,9	14,6	8,1	90,4	LR
4.5	13110,5	1,0	87,4	11,7	7,5	66,1	LR
4.6	19146,6	1,3	127,7	15,7	8,1	98,4	IR
4.7	18142,4	1,2	120,0	14,7	8,2	92,0	IR
4.8	14943,3	1,1	99,0	12,6	7,8	75,2	LR
5.1	13858,9	1,0	92,2	11,7	7,9	69,8	IR
5.2	20620,3	1,4	138,2	16,4	8,4	106,7	IR
5.3	17091,7	1,2	113,3	14,2	8,0	86,8	IR
5.4	18308,7	1,3	122,6	15,1	8,1	94,3	LR
5.5	14113,1	1,0	94,0	12,0	7,8	71,2	IR
5.6	19453,1	1,3	129,8	15,7	8,3	100,0	IR
5.7	17547,9	1,2	116,4	14,6	8,0	89,3	IR
5.8	14029,7	1,0	93,8	11,9	7,9	71,0	OR
5.9	15103,4	1,1	101,2	13,0	7,8	77,1	OR
5.10	12996,1	0,9	86,8	11,1	7,8	65,5	IR
5.11	14260,7	1,0	95,3	12,2	7,8	72,2	IR
5.12	12738,2	0,9	85,8	11,0	7,8	64,6	IR
5.13	16661,8	1,1	111,6	13,7	8,1	85,3	IR
5.14	18046,4	1,2	121,0	14,6	8,3	92,8	IR
5.15	13624,2	1,0	91,2	11,7	7,8	69,0	IR

Table D.3: Results of the CDR tests for the series NA-2a (450x450x10mm, internal surface).

Specimen	$F_{\text{break}}$ (N)	d (mm)	$\sigma_f$ (Mpa)	$t_{\text{break}}$ (sec)	Rate (MPa/s)	$\sigma_{e,60s}$	Fracture
1.1	25548,0	1,2	62,5	14,6	4,3	47,9	IR
1.2	30459,6	1,4	74,4	17,0	4,4	57,6	IR
1.3	31286,6	1,4	76,5	17,1	4,5	59,2	IR
1.4	18329,2	0,9	44,7	11,0	4,0	33,7	IR
1.5	29704,6	1,4	72,6	16,4	4,4	56,1	LR
1.6	27295,0	1,3	66,6	15,5	4,3	51,2	IR
1.7	26854,1	1,3	65,5	15,0	4,4	50,4	IR
1.8	22037,4	1,0	53,6	12,5	4,3	40,7	IR
2.1	9606,4	0,5	22,9	6,4	3,6	16,7	IR
2.2	22514,2	1,1	54,9	13,1	4,2	41,8	IR
2.3	21148,2	1,0	49,4	12,3	4,0	37,5	LR
2.4	19160,4	1,0	46,0	11,4	4,0	34,8	IR
2.5	21581,2	1,0	51,3	12,5	4,1	38,9	IR
2.6	15411,7	0,8	36,2	9,2	3,9	27,0	IR
2.7	17846,2	0,9	42,6	10,5	4,0	32,0	IR
2.8	15773,0	0,8	38,2	9,8	3,9	28,6	IR
2.9	24321,8	1,2	58,2	14,0	4,2	44,5	IR
2.10	28827,3	1,3	68,6	15,8	4,3	52,8	IR
2.11	19468,2	1,0	45,9	11,4	4,0	34,7	IR
2.12	23093,5	1,1	55,1	13,2	4,2	42,0	IR
2.13	26743,4	1,2	63,8	14,7	4,3	49,0	IR
2.14	22254,9	1,1	53,3	12,9	4,1	40,6	IR
2.15	14669,9	0,7	35,0	9,0	3,9	26,0	IR
2.16	30023,1	1,4	72,0	16,3	4,4	55,6	IR

Table D.4: Results of the CDR tests for the series NA-2b (450x450x10mm, external surface).

Specimen	$F_{\text{break}}$ (N)	d (mm)	$\sigma_f$ (Mpa)	$t_{\text{break}}$ (sec)	Rate (MPa/s)	$\sigma_{e,60s}$	Fracture
3.1	29505,4	1,4	71,4	16,4	4,4	55,2	IR
3.2	33855,5	1,5	80,8	18,1	4,5	62,8	IR
3.3	20644,6	1,0	49,9	12,2	4,1	37,8	IR
3.4	22433,2	1,1	54,1	13,0	4,1	41,2	IR
3.5	25523,2	1,2	62,1	14,4	4,3	47,6	IR
3.6	30820,8	1,4	75,0	16,9	4,4	58,0	IR
3.7	26312,9	1,2	64,0	14,8	4,3	49,1	IR
3.8	22502,2	1,1	54,5	13,0	4,2	41,5	IR
3.9	29529,4	1,4	70,9	16,3	4,4	54,7	IR
3.10	28660,5	1,3	69,3	15,8	4,4	53,4	OR
3.11	13417,4	0,7	32,3	8,3	3,9	23,9	IR
3.12	34905,4	1,5	83,5	18,5	4,5	65,0	IR
4.1	20146,2	1,0	48,2	12,2	4,0	36,5	IR
4.2	19477,8	1,0	46,7	11,6	4,0	35,3	IR
4.3	30611,9	1,4	72,7	16,8	4,3	56,2	IR
4.4	19922,6	1,0	47,3	11,9	4,0	35,8	IR
4.5	18455,8	0,9	44,0	11,0	4,0	33,2	IR
4.6	19269,3	1,0	46,0	11,9	3,9	34,9	IR
4.7	28549,3	1,3	68,4	16,0	4,3	52,8	IR
4.8	31101,8	1,4	74,8	17,0	4,4	57,9	LR
4.9	17223,8	0,9	41,4	10,3	4,0	31,1	OR
4.10	28842,0	1,3	69,0	15,8	4,4	53,2	IR

Table D.5: Results of the CDR tests for the series AR-1a (250x250x10mm, tin side).

Specimen	$F_{\text{break}}$ (N)	d (mm)	$\sigma_f$ (Mpa)	$t_{\text{break}}$ (sec)	Rate (MPa/s)	$\sigma_{e,60s}$	Fracture
1	15479,1	1,8	97,7	21,3	4,6	76,7	IR
2	21389,3	2,0	134,3	24,0	5,6	106,2	IR
3	11566,9	1,6	71,2	19,1	3,7	55,5	IR
4	17903,4	1,8	109,3	22,1	5,0	86,0	IR
5	16803,2	1,9	104,9	22,5	4,7	82,6	LR
6	20473,9	2,1	129,0	25,1	5,1	102,3	IR
7	24817,4	2,3	155,6	27,3	5,7	124,0	LR
8	16584,4	1,8	102,6	22,0	4,7	80,7	OR
9	25365,1	2,2	154,1	26,7	5,8	122,7	IR
10	21907,7	2,1	137,3	25,0	5,5	108,9	IR
11	19403,8	2,0	121,6	24,3	5,0	96,3	IR
12	15910,0	1,8	99,0	21,5	4,6	77,7	IR
13	13599,9	1,7	83,2	20,2	4,1	65,1	LR
14	9330,4	1,3	57,9	15,6	3,7	44,6	OR
15	11677,3	1,6	72,3	19,1	3,8	56,4	IR
16	16681,6	1,9	104,4	22,5	4,6	82,2	OR
17	17224,6	1,9	106,8	22,6	4,7	84,1	OR
18	9481,7	1,4	59,1	16,3	3,6	45,7	OR
19	22821,3	2,1	140,9	25,7	5,5	112,0	IR
20	23320,1	2,2	147,9	26,7	5,5	117,8	IR

Table D.6: Results of the CDR tests for the series AR-1b (250x250x10mm, air side).

Specimen	$F_{\text{break}}$ (N)	d (mm)	$\sigma_f$ (Mpa)	$t_{\text{break}}$ (sec)	Rate (MPa/s)	$\sigma_{e,60s}$	Fracture
21	30090,0	2,52	184,5	30,3	6,1	148,1	IR
22	34331,6	2,81	210,3	33,8	6,2	170,0	IR
23	36960,4	2,94	229,9	35,3	6,5	186,3	? <sup>1</sup>
24	28143,5	2,5	174,5	30,3	5,7	140,1	IR
25	33881,1	2,9	207,1	35,0	5,9	167,8	OR
26	19081,4	1,9	116,8	23,2	5,0	92,2	IR
27	37109,1	2,9	227,5	34,4	6,6	184,1	OR
28	32883,7	2,7	206,6	32,9	6,3	166,7	OR
29	30905,5	2,5	189,1	30,2	6,3	151,8	OR
30	24982,9	2,3	153,0	28,1	5,5	122,2	IR
31	10293,5	1,6	64,1	19,0	3,4	50,0	IR
32	45909,9	3,2	282,4	38,3	7,4	230,0	?
33	47826,5	3,9	292,1	46,5	6,3	240,8	?
34	27079,7	2,6	167,4	30,7	5,4	134,5	?
35	25047,0	2,3	157,4	28,0	5,6	125,8	OR
36	17375,3	1,8	107,6	21,9	4,9	84,6	IR
37	35232,7	2,8	218,5	33,3	6,6	176,4	?
38	30046,8	2,5	187,4	30,3	6,2	150,4	?
39	29803,5	2,5	182,0	29,9	6,1	145,9	IR
40	34429,9	2,9	212,2	34,6	6,1	171,7	IR

<sup>1</sup> The fracture origin of these specimens was not detectable due to the dense fracture pattern of the specimen.

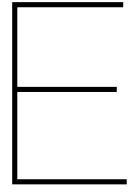
Table D.7: Results of the CDR tests for the series AR-2a (450x450x10mm, tin side).

Specimen	$F_{\text{break}}$ (N)	d (mm)	$\sigma_f$ (Mpa)	$t_{\text{break}}$ (sec)	Rate (MPa/s)	$\sigma_{e,60s}$	Fracture
1	27540,5	1,4	60,6	17,1	3,5	47,0	IR
2	44858,4	2,0	99,8	23,7	4,2	78,9	IR
3	42683,0	1,9	92,7	23,3	4,0	73,2	IR
4	41129,9	1,8	89,2	22,0	4,1	70,2	IR
5	43465,5	1,9	94,9	22,5	4,2	74,8	IR
6	28786,7	1,4	62,5	17,1	3,6	48,4	OR
7	42675,7	1,9	92,2	22,5	4,1	72,6	IR
8	37667,0	1,7	81,3	20,7	3,9	63,7	IR
9	17654,4	1,0	38,3	11,7	3,3	29,0	OR
10	44518,9	2,0	96,0	23,4	4,1	75,8	IR
11	47596,7	2,0	105,8	24,5	4,3	83,8	LR
12	35863,1	1,7	79,9	20,3	3,9	62,6	IR
13	27620,0	1,3	59,9	16,0	3,7	46,2	IR
14	31014,4	1,5	67,4	18,0	3,7	52,3	IR
15	33833,7	1,6	73,7	19,3	3,8	57,5	IR
16	42957,2	1,9	92,3	22,2	4,2	72,7	IR
17	36871,5	1,7	81,5	19,8	4,1	63,7	IR
18	44074,6	1,9	97,7	22,8	4,3	77,0	IR
19	52218,8	2,2	116,2	26,1	4,4	92,4	IR
20	37812,9	1,8	84,4	21,1	4,0	66,2	OR

Table D.8: Results of the CDR tests for the series AR-2b (450x450x10mm, air side).

Specimen	$F_{\text{break}}$ (N)	d (mm)	$\sigma_f$ (Mpa)	$t_{\text{break}}$ (sec)	Rate (MPa/s)	$\sigma_{e,60s}$	Fracture
21	74532,6	3,0	166,8	35,7	4,7	135,3	IR
22	61123,9	2,5	136,9	30,2	4,5	109,8	OR
23	39484,6	1,9	88,7	23,2	3,8	70,0	IR
24	86863,5	3,3	193,8	39,3	4,9	158,1	IR
25	54742,4	2,3	122,0	28,1	4,3	97,5	IR
26	69149,9	2,8	152,5	33,3	4,6	123,1	IR
27	54227,2	2,3	120,9	28,0	4,3	96,5	IR
28	100000,0	3,9	222,0	46,3	4,8	183,0	IR
29	83163,0	3,4	185,8	40,6	4,6	151,9	OR
30	46430,2	2,1	101,2	25,6	4,0	80,4	LR
31	55872,1	2,5	119,9	29,6	4,0	96,1	IR
32	59315,0	2,8	127,3	33,0	3,9	102,8	LR
33	76943,1	3,3	165,9	39,5	4,2	135,4	IR
34	64453,1	2,9	138,4	35,3	3,9	112,2	IR
35	40864,1	2,2	88,5	26,2	3,4	70,4	IR
36	68610,9	3,0	149,0	35,6	4,2	120,8	LR
37	38660,6	2,24	84,1	26,8	3,1	67,0	IR
38	81382,6	3,5	180,8	41,8	4,3	148,1	LR
39	48088,7	2,4	103,6	29,2	3,6	83,0	OR
40	32342,8	1,8	70,0	22,1	3,2	55,1	LR
41	58781,8	2,6	128,4	31,1	4,1	103,2	IR





## Normal and Lognormal probability plots

The Normal and Lognormal probability plots of the testing series of weathered and as received glass are illustrated in Figures E.1 to E.4. Only the data of the specimens which failed inside the loading ring are included in these plots.

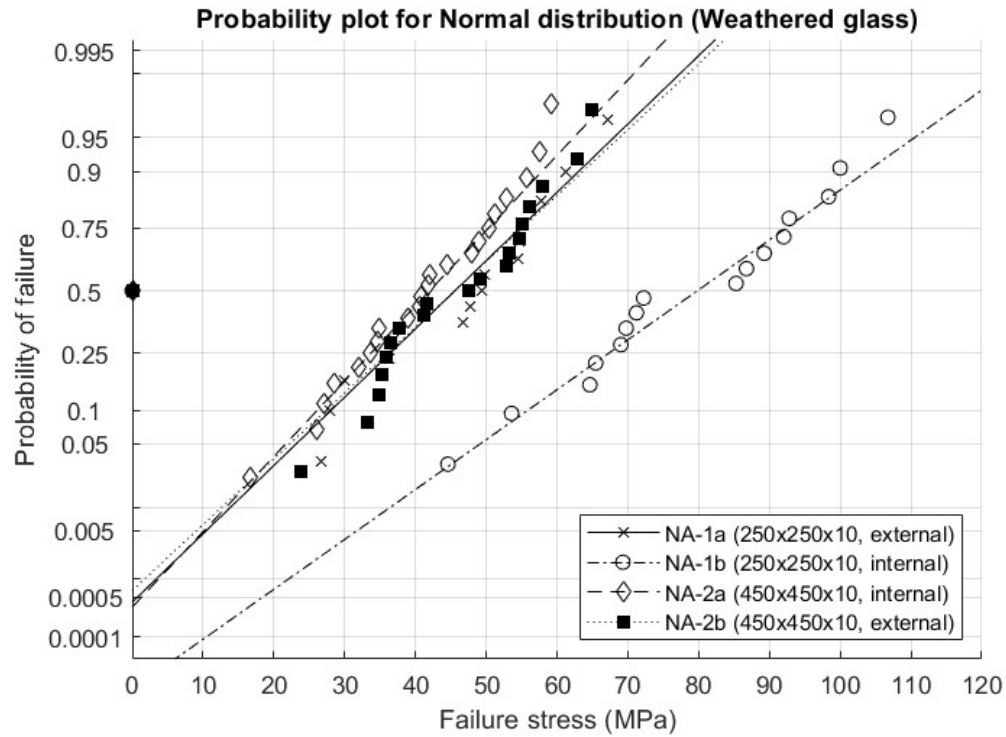


Figure E.1: Normalised strength data of weathered glass fitted to the Normal probability distribution function.

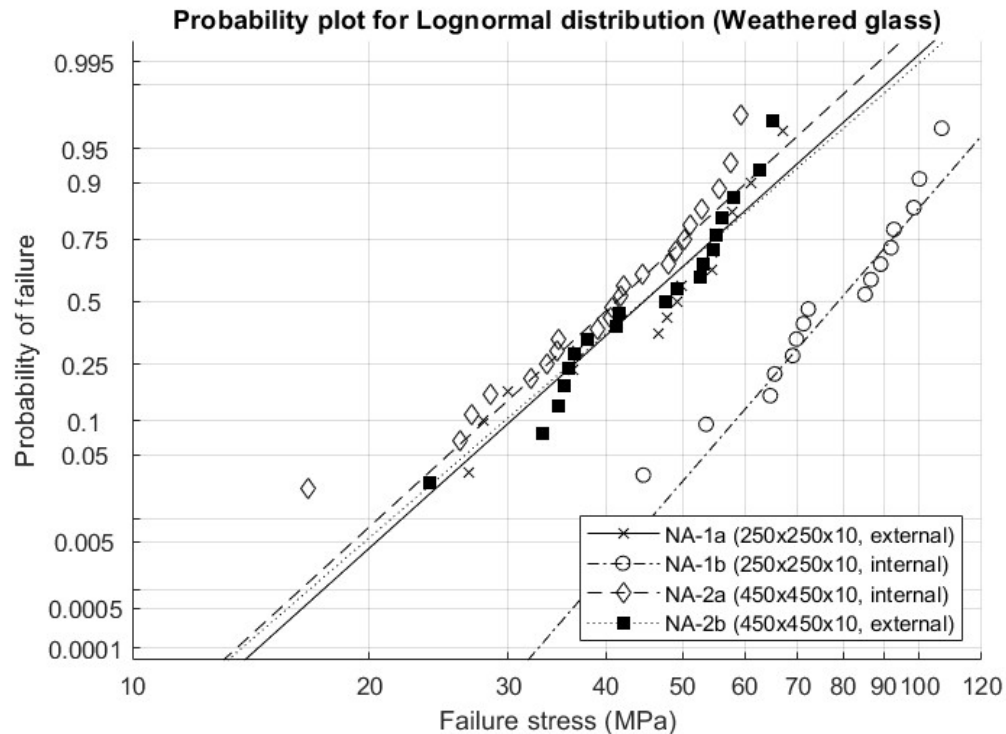


Figure E.2: Normalised strength data of weathered glass fitted to the Lognormal probability distribution function.

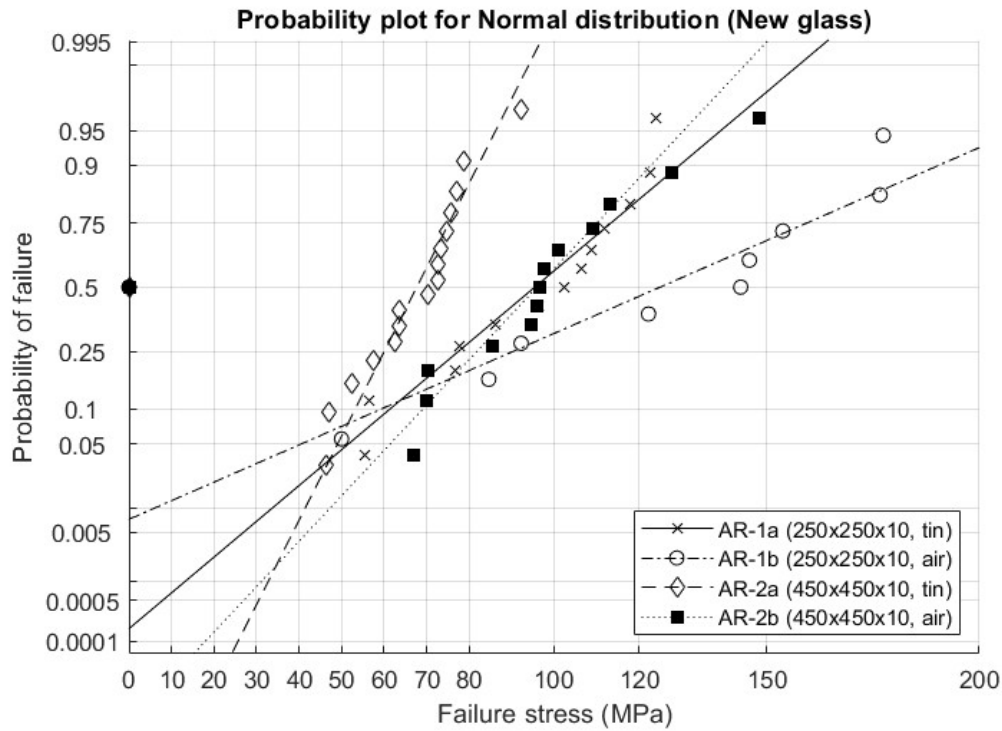


Figure E.3: Normalised strength data of as received glass fitted to the Normal probability distribution function.

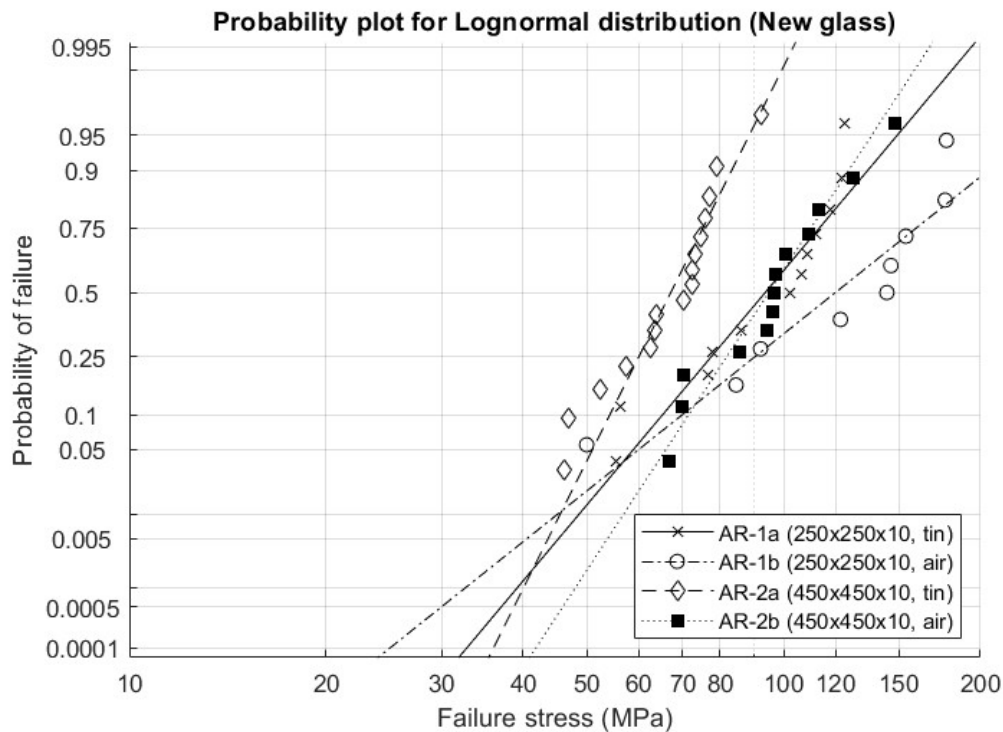
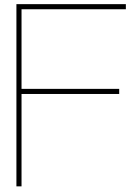


Figure E.4: Normalised strength data of as received glass fitted to the Lognormal probability distribution function.





## Strength data of new glass (without FEA correction)

In this chapter, the results of the tests on new glass, as emerged from the CDR tests are presented. In particular, the data which correspond to the series with the air side in tension (AR-1b and AR-2b) are used, without the correction with the FEA.

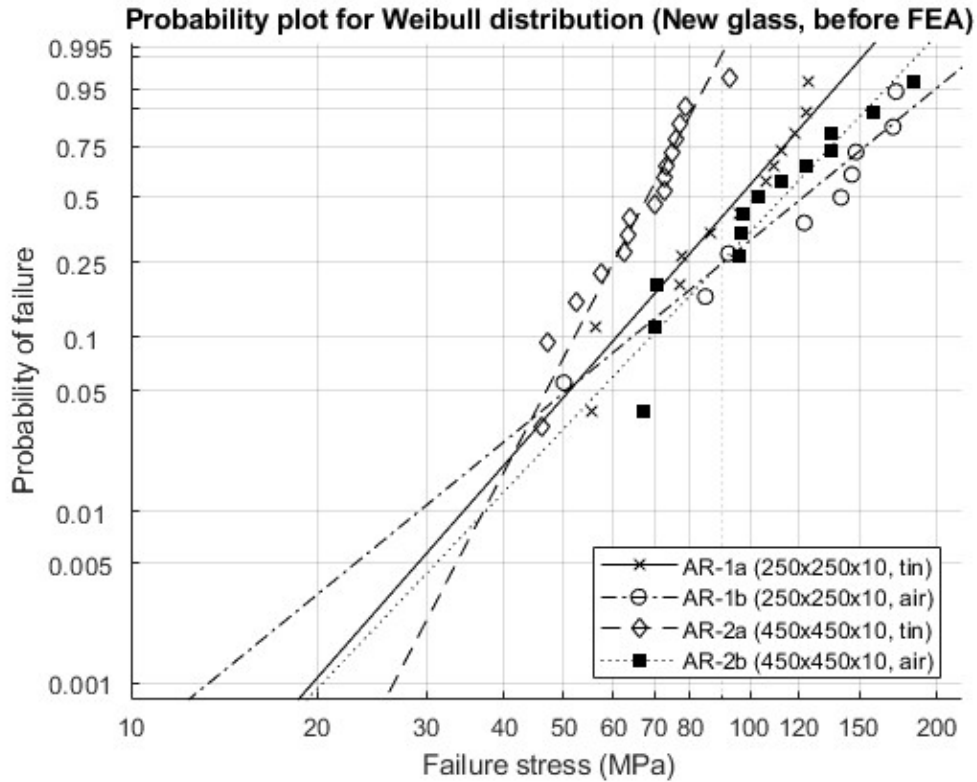


Figure F.1: Normalised strength data of as received glass fitted to the Weibull probability distribution function. - data not corrected with FEA.

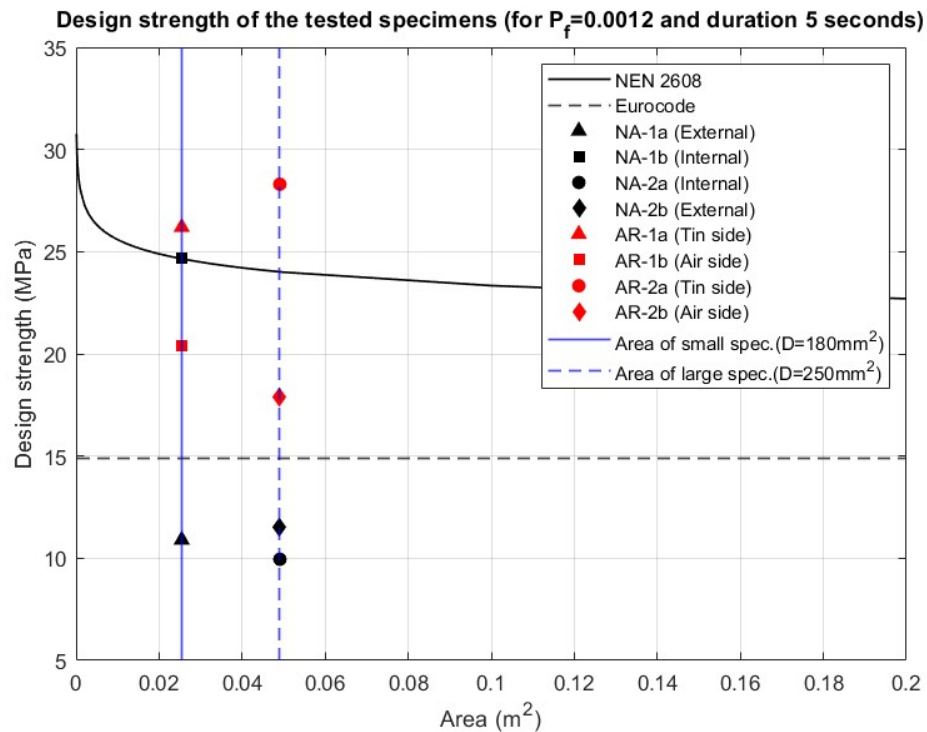


Figure F.2: Theoretical design strength and design strength according to EN1990:2002 (2005) of the tested specimens (for  $P_f=0,0012$  and load duration 5 seconds) - data not corrected with FEA.

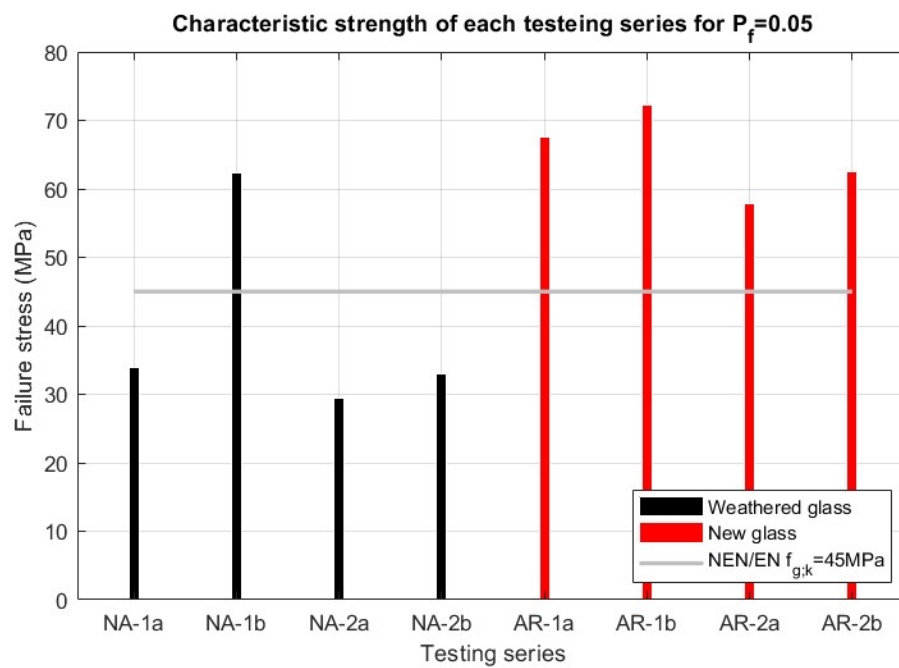


Figure F.3: Theoretical and experimental characteristic strength of the tested specimens (for  $P_f=0,05$ )  
- data not corrected with FEA.





## Design strength according to ASTM

The design strength of the eight testing series was calculated according to the ASTM-E1300 (1997) for probability of failure 0,8%. These values are plotted in Figure G.1. In the same figure, the design strength of glass according to the draft European standard prCEN/TC250-1, 2018) and the Dutch standard (NEN2608, 2014) is plotted, as a function of the loaded surface area.

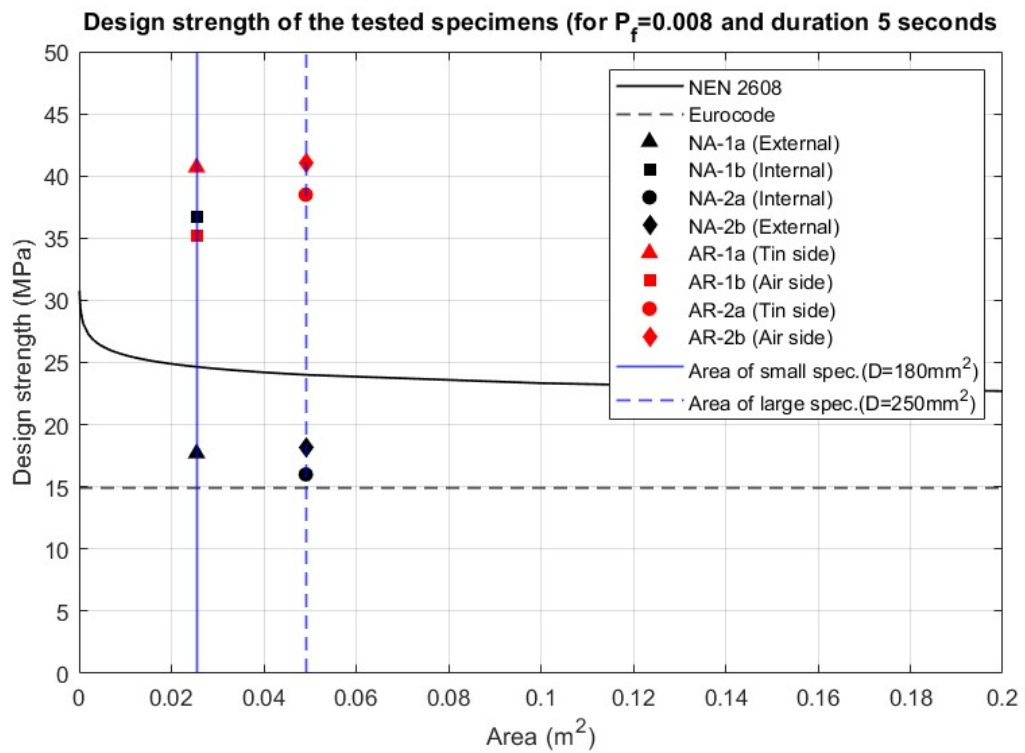
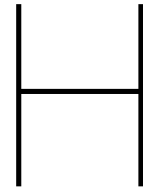


Figure G.1: Theoretical design strength and design strength according to ASTM-E1300 (1997) of the tested specimens (for  $P_f=0,008$  and load duration 5 seconds).



## Error in the predictions

In the tables H.1 to H.4, the error in the predicted strength value for each specimen of the series NA-1a and NA-2b are presented. In particular, the data included in these tables are:

1. The depth of the largest defect in  $\mu\text{m}$ , as measured with Traceit®.
2. The predicted failure stress  $\sigma_{\text{pred}}$  in MPa, for  $K_{\text{IC}}=0,75 \text{ MPa } m^{0,5}$  and  $Y=1,12$  or  $0,713$ .
3. The actual  $\sigma_f$  and normalised  $\sigma_{e,1s}$  failure stress in MPa, of each specimen.
4. The error (%) in the predictions compared to the actual and normalised failure stress.
5. The maximum, minimum and average error (%) for each testing series, for two different sets of parameters  $K_{\text{IC}}$  and  $Y$ .

Table H.1: Error between predicted and actual failure stress for each specimen for series NA-1a (250x250x10mm, external), for  $K_{IC}=0,75 \text{ MPa } m^{0,5}$  and  $Y=1,12$ .

Specimen	Depth ( $\mu\text{m}$ )	$\sigma_{\text{pred}}$ (MPa)	$\sigma_f$ (MPa)	$\sigma_{e,1s}$ (MPa)	Error $\sigma_f$ (%)	Error $\sigma_{e,1s}$ (%)
1.1	87	40,4	67,0	64,4	66	59
1.2	91	39,7	88,9	86,7	124	118
1.3	86	40,8	83,3	81,0	104	98
1.4	34	64,7	38,8	36,1	40	44
1.5	45	56,1	81,5	79,0	45	41
1.6	63	47,5	88,1	85,9	86	81
1.7	37	61,7	73,4	70,8	19	15
2.1	25	76,0	58,4	55,6	23	27
2.2	32	67,1	49,6	46,8	26	30
2.3	19	85,9	73,1	70,5	15	18
2.4	52	52,4	66,3	63,6	27	21
2.5	58	49,7	64,3	61,6	29	24
2.6	48	54,3	77,0	74,6	42	37
2.7	25	76,3	41,3	38,7	46	49
3.1	27	72,8	73,0	70,5	0	3
3.2	126	33,6	73,4	70,8	119	111
3.3	50	53,2	50,3	47,6	6	11
3.4	77	43,0	37,1	34,6	14	20
3.5	55	51,1	71,1	68,4	39	34
3.6	43	57,7	70,8	68,3	23	18
3.7	147	31,2	62,8	60,3	101	93
		Minimum error (%)			0	3
		Maximum error (%)			124	118
		Average error (%)			47	45

Table H.2: Error between predicted and actual failure stress for each specimen for series NA-2b (450x450x10mm, external), for  $K_{IC}=0,75 \text{ MPa } m^{0,5}$  and  $Y=1,12$ .

Specimen	Depth ( $\mu\text{m}$ )	$\sigma_{\text{pred}}$ (MPa)	$\sigma_f$ (MPa)	$\sigma_{e,1s}$ (MPa)	Error $\sigma_f$ (%)	Error $\sigma_{e,1s}$ (%)
3.1	78	42,7	71,4	71,3	67	67
3.2	39	60,3	80,8	81,1	34	35
3.3	87	40,4	49,9	48,8	23	21
3.4	104	37,1	54,1	53,2	46	44
3.5	50	53,5	62,1	61,5	16	15
3.6	80	42,2	75,0	74,9	78	78
3.7	19	86,1	64,0	63,5	26	26
3.8	52	52,4	54,5	53,6	4	2
3.9	19	86,5	70,9	70,7	18	18
3.10	59	49,2	69,3	69,0	41	40
3.11	161	29,8	32,3	30,9	8	4
3.12	33	65,4	83,5	84,0	28	28
4.1	71	44,7	48,2	47,2	8	6
4.2	51	52,8	46,7	45,6	12	14
4.3	111	35,8	72,7	72,6	103	103
4.4	33	65,3	47,3	46,3	28	29
4.5	50	53,4	44,0	42,9	18	20
4.6	41	59,2	46,0	45,0	22	24
4.7	33	66,2	68,4	68,2	3	3
4.8	51	52,8	74,8	74,7	42	42
4.9	94	39,0	41,4	40,1	6	3
4.10	59	49,0	69,0	68,7	41	40
		Minimum error (%)			3	2
		Maximum error (%)			103	103
		Average error (%)			30	30

Table H.3: Error between predicted and actual failure stress for each specimen for series NA-1a (250x250x10mm, external), for  $K_{IC}=0,75 \text{ MPa } m^{0,5}$  and  $Y=1,12$  or  $Y=0,713$ .

Specimen	Depth ( $\mu\text{m}$ )	$\sigma_{\text{pred}}$ (MPa)	$\sigma_f$ (MPa)	$\sigma_{e,1s}$ (MPa)	Error $\sigma_f$ (%)	Error $\sigma_{e,1s}$ (%)
1.1	87	40,4	67,0	64,4	66	59
1.2	91	62,4	88,9	86,7	42	39
1.3	86	64,1	83,3	81,0	30	26
1.4	34	64,7	38,8	36,1	40	44
1.5	45	56,1	81,5	79,0	45	41
1.6	63	47,5	88,1	85,9	86	81
1.7	37	96,9	73,4	70,8	24	27
2.1	25	76,0	58,4	55,6	23	27
2.2	32	105,4	49,6	46,8	53	56
2.3	19	135,0	73,1	70,5	46	48
2.4	52	82,3	66,3	63,6	19	23
2.5	58	78,1	64,3	61,6	18	21
2.6	48	85,4	77,0	74,6	10	13
2.7	25	76,3	41,3	38,7	46	49
3.1	27	72,8	73,0	70,5	0	3
3.2	126	33,6	73,4	70,8	119	111
3.3	50	83,6	50,3	47,6	40	43
3.4	77	43,0	37,1	34,6	14	20
3.5	55	51,1	71,1	68,4	39	34
3.6	43	57,7	70,8	68,3	23	18
3.7	147	31,2	62,8	60,3	101	93
		Minimum error (%)			0	3
		Maximum error (%)			119	111
		Average error (%)			42	42

Table H.4: Error between predicted and actual failure stress for each specimen for series NA-2b (450x450x10mm, external), for  $K_{IC}=0,75 \text{ MPa } m^{0,5}$  and  $Y=1,12$  or  $Y=0,713$ .

Specimen	Depth ( $\mu\text{m}$ )	$\sigma_{\text{pred}}$ (MPa)	$\sigma_f$ (MPa)	$\sigma_{e,1s}$ (MPa)	Error $\sigma_f$ (%)	Error $\sigma_{e,1s}$ (%)
3.1	78	67,0	71,4	71,3	7	6
3.2	39	60,3	80,8	81,1	34	35
3.3	87	40,4	49,9	48,8	23	21
3.4	104	58,2	54,1	53,2	7	9
3.5	50	84,0	62,1	61,5	26	27
3.6	80	42,2	75,0	74,9	78	78
3.7	19	135,2	64,0	63,5	53	53
3.8	52	52,4	54,5	53,6	4	2
3.9	19	135,9	70,9	70,7	48	48
3.10	59	49,2	69,3	69,0	41	40
3.11	161	29,8	32,3	30,9	8	4
3.12	33	102,7	83,5	84,0	19	18
4.1	71	44,7	48,2	47,2	8	6
4.2	51	52,8	46,7	45,6	12	14
4.3	111	35,8	72,7	72,6	103	103
4.4	33	65,3	47,3	46,3	28	29
4.5	50	83,9	44,0	42,9	48	49
4.6	41	59,2	46,0	45,0	22	24
4.7	33	104,0	68,4	68,2	34	34
4.8	51	52,8	74,8	74,7	42	42
4.9	94	39,0	41,4	40,1	6	3
4.10	59	49,0	69,0	68,7	41	40
		Minimum error (%)			4	2
		Maximum error (%)			103	103
		Average error (%)			31	31